DIPLOMARBEIT

Analysis of Mössbauer spectroscopy measurements of $(V_{0.92}Fe_{0.08})_2FeB_2$ at various temperatures and applied magnetic field up to 12 T

zur Erlangung des akademischen Grades

Diplom Ingenieur

im Rahmen des Studiums

Technische Physik

eingereicht von

Manuel MÖRTH, BSc
Matrikelnummer: 01225276

Ausgeführt am

Institut für Festkörperphysik
der Technischen Universität Wien
Wiedner Hauptstrasse 8-10
1040 Wien

unter der Anleitung von

Ao. Univ.Prof. Dipl.-Ing. Dr.techn.
Michael REISSNER

Wien, 18.03.2021

Manuel Mörth

Michael Reissner

Danksagung

Mit diesen Zeilen möchte ich mich bei den Menschen bedanken, die mich während meines Studiums, und im Besonderen bei der Erarbeitung dieses Werkes begleitet und unterstützt haben. In erster Linie möchte ich meinem Betreuer Herrn Ao. Univ.Prof. Dipl.-Ing. Dr.techn. Michael Reissner für die unzähligen Hilfestellungen, Anregungen und die ausgezeichnete Zusammenarbeit, sowohl in dieser aber auch allen früheren Kooperationen, danken. Vielen Dank, dass Sie trotz Ihres vollen Terminkalenders immer Zeit für mich gefunden haben und mich, besonders in den ungewöhnlichen Zeiten, in welchen diese Arbeit erstand, bestens unterstützt und angeleitet haben. Weiters danke ich den Tieftemperaturanlagen der TU Wien, und im speziellen Herrn Amtsdir. Peter Lielacher, die immer mit einer helfenden Hand bereitstanden, wenn diese von nöten war. Ebenso möchte ich meinen geschätzten Bürokollegen, Johannes Kirschner und Robin Kurinjimala, für unsere unzähligen Diskussionen danken. Die neue Ideen und Lösungen welche diese hervorbrachten, haben diese Arbeit oftmals vorangebracht.

Des weiteren möchte ich all meinen Weggefährten und Freunden, die mich während meiner gesamten Studienzeit begleitet haben, danken und hierbei im besonderen meiner besseren Hälfte Dominika Piórkowska, für die unbezahlbare Unterstützung, Motivation und auch Aufmunterung wenn einmal etwas nicht so funktionierte, wie ich es mir erwünscht hatte.

Zu guter Letzt möchte ein riesiges Danke an meine Familie aussprechen. Ohne die unglaubliche Unterstützung, welche ich von euch mein gesamtes Leben erhalten habe, wäre es nie soweit gekommen, dass ich diese Zeilen hier schreiben kann.

Kurzfassung

Da die in [1] publizierte Analyse der Mössbauer Transmissions-Spektroskopie Experimente von $(V_{0.92}Fe_{0.08})_2FeB_2$ offene Fragen hinterließ, wurde diese Arbeit durchgeführt um weitere Informationen über die Eigenschaften des Materials zu sammeln.

Diese Arbeit beinhaltet einen kurzen Exkurs in die theoretischen Hintergründe der Mössbauer Spektroskopie, eine Einführung in den Mössbauer Effekt, eine Beschreibung des untersuchten Probenmaterials sowie eine Interpretation der durchgeführten Messungen. Weiters sind beide experimentellen Aufbauten, welche für die Untersuchung des Materials genutzt wurden, kurz skizziert. Da eine der Anlagen erst reaktiviert und modifiziert werden musste, liegt für dieses Setup eine detaillierte Anleitung zur Einrichtung und Nutzung, im speziellen für alle Modifikationen, im Anhang bei.

$(V_{0.92}Fe_{0.08})_2FeB_2$ Pulver wurde mittels Mössbauer Transmissions-Spektroskopie in einem Temperaturbereich von 4,2K bis zu 294K untersucht. Messungen wurden sowohl mit, als auch ohne, extern angelegten Magnetfeld von bis zu 12T durchgeführt. Die Analyse der Daten mittels magnetischer Hyperfeinaufspaltungsverteilungsanalyse offenbarte paramagnetische Verhalten innerhalb des Temperaturbereiches 100K bis 294K. Unterhalb 100K gibt es Hinweise auf mögliche antiferromagnetische Strukturen.

Die für diese Arbeit erstellten LabView Programme, deren vollständige Dokumentationen, sowie detailierte Reports aller gefitteten Daten, befinden sich ebenfalls im Anhang dieser Arbeit.

Abstract

The not completely satisfying conclusion of the analysis of Mössbauer spectroscopy measurements carried out by Reissner [1] lead to interest in further analysis of the characteristic properties of $(V_{0.92}Fe_{0.08})_2FeB_2$ and thus initiated this work.

This work contains a brief description of the theoretical background of Mössbauer spectroscopy and the theory of the Mössbauer effect, a description of the examined material, $(V_{0.92}Fe_{0.08})_2FeB_2$, as well as an interpretation of the conducted measurements, sketches of the two used experimental setups and a summary of all modifications that had to be made to reactivate one of these used experimental setups. Instructions for setup and operation of the modified can be found in the appendix.

$(V_{0.92}Fe_{0.08})_2FeB_2$ powder has been analysed using transmission Mössbauer spectroscopy in a temperature range of 4.2K to 294K. These measurements have been conducted with and without an applied magnetic field of up to 12 T. Magnetic hyperfine distribution analysis revealed paramagnetic properties between 100 K and 294 K and hints to possible antiferromagnetic structures for temperatures below 100 K.

All LabView programs that have been written to enable this work, including complete documentations can be found in the appendix, as well as detailed informations of the fitted data of the measurements.

Contents

1 Introduction

Mössbauer spectroscopy measurements of $(V_{0.92}Fe_{0.08})_2FeB_2$ conducted at the Institute of Solid State Physics of the TU Wien in 2017 by Rogl et al [1] unveiled an unusual behaviour of the sample material in the temperature range of 20 K to 100 K. This arose questions, that required further investigations, including Mössbauer transmission spectroscopy measurements in external magnetic field. Therefore the task of this thesis was to reactivate the high-field Mössbauer equipment, which was out of order for some time, due to serious errors in the power supply of the superconducting coil. After multiple unsuccessful trials to repair the power supply a new one was installed and integrated into the system from both hard- and software side. New control routines had to be written and the whole system had to be newly calibrated. Measurements of $(V_{0.92}Fe_{0.08})_2FeB_2$ both with and without external field were performed after the successful activation of the system. Two models were developed to analyse the data.

Chapter 2 gives an introduction to the theoretical background and describes the Mössbauer effect, including all concepts that are required to analyse the collected data.

Chapter 3 contains all experimental aspects, a description of the physical properties of the sample material $(V_{0.92}Fe_{0.08})_2$ FeB_2, a brief schematic descriptions of the two experimental setups with a detailed description of the new hard- and software and the two programs for the analysis.

Chapter 4 discusses the created models and the analysis of the collected data, using the model described in chapter 4.2 and gives a short summary.

Detailed reports of all analysed data, in addition to comprehensive instructions for setup and operation of one of the setups can be found in the appendix, alongside with all developed LabView program codes and their detailed descriptions.

2 Theory

The subsequent chapter mainly follows the route given by [2] and [3].

2.1 Essential concepts

The following chapters introduce essential concepts behind the Mössbauer effect.

A Mössbauer experiment consists of a radioactive source that emits gamma quanta onto a target or absorber, which should be analysed, and a detector placed behind that target.

2.1.1 Natural Line Width

Due to the findings of quantum physics, it is known that the energy spectrum is divided in separated energy levels. Usually these levels are indicated as lines of a specific, sharp energy E_0 which is derived from the solution of the Schrödinger equation for a particular problem. However, these lines are not as fine as a single line, but do have a certain width. Because of that is the energy E spread over a certain energy spectrum around the energy E_0. This spectrum can be approximated using the uncertainty relation

$$\Delta E \Delta t \geq \hbar \; . \tag{2.1}$$

Within the equation (2.1) ΔE represents the uncertainty in energy and Δt the available time interval to measure the energy E. Due to the fact that this time frame is in the same order of magnitude as the mean lifetime τ, the measured state will have disappeared, if the experiment will last much longer than the mean lifetime. By setting $\Delta t = \tau$, the approximated width $\mathit{\Gamma}$ of the energy uncertainty ΔE at a specific level equals

$$\Gamma = \frac{\hbar}{\tau} \; . \tag{2.2}$$

Weisskopf and Wigner [4] were able to solve the problem and showed that equation (2.2) expresses the full width at half height of the energy dispersion. To be more precise, the line is forming a Breit-Wigner or Lorentzian shape. This can be described as

$$I(E) = \text{const} \frac{\Gamma}{2\pi} \frac{1}{(E - E_0)^2 + (\Gamma/2)^2} \; . \tag{2.3}$$

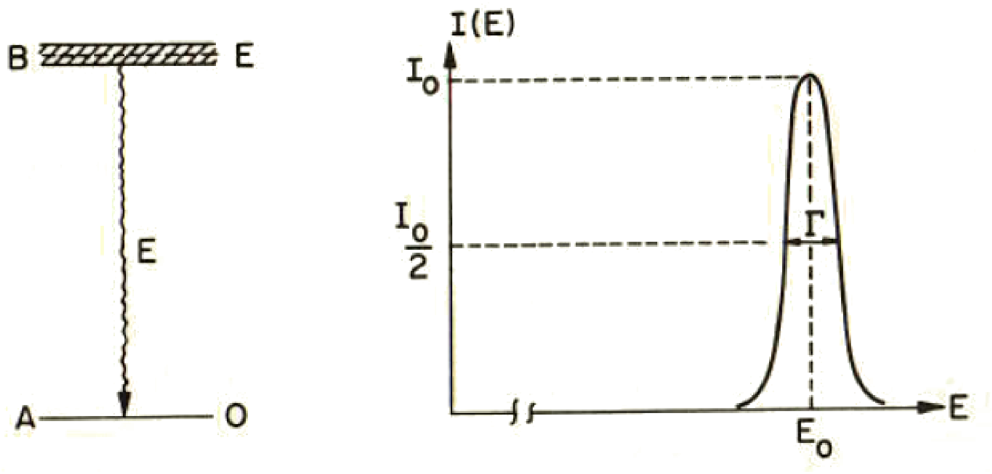

Figure 2.1: Natural line width Γ of an energy E at half height. [2, page 3]

Equation (2.3) illustrates that the ground state is indeed a sharp state, a fact based upon its infinite lifetime, (see figure 2.1 (state A)). Emitted photons of a transmission from an excited state with mean lifetime τ to a stationary ground state, sketched in figure 2.1, have an energy distribution which is also described by equation (2.3).

In practical units and with the mean lifetime τ, equation (2.2) results in a natural line width of the excited state

$$\Gamma(\text{in eV}) = 6.58 \times 10^{-16}/\tau(\text{sec}) \ . \tag{2.4}$$

2.1.2 Recoil Energy Loss

If a photon is emitted during a transmission, as shown in figure 2.1, there will be a recoil energy loss. The momentum conservation leads to the following equation

$$\vec{p}_{\text{nucleus}} = -\vec{p}_{\text{photon}} \ . \tag{2.5}$$

The energy of the photon is connected to the magnitude of the photon momentum and the velocity of light via

$$p_{photon} = E_{photon}/c \ . \tag{2.6}$$

Due to the fact that nuclei are very heavy in comparison to the decay energy, the non-relativistic approximation for the recoil energy

$$R = p^2_{\text{nucleus}}/2M \tag{2.7}$$

can be applied, likewise E_{photon} can be set as E_0 since E_0 is large compared to R. Based on the equations above, the recoil energy can be calculated as

$$R = E_0^2/2Mc \tag{2.8}$$

when using a given nuclear mass M and a given decay energy E_0.

Equation (2.8) can be rewritten in practical units with A the atomic number of decaying nuclei

$$R(\text{in eV}) = 5.37 \times 10^{-4} E_0(\text{in keV})/A \ . \tag{2.9}$$

Therefore, the photon's energy, upon arriving at the target, is only $E_0 - R$, because of the recoil energy it loses after being emitted from the source. To compensate the momentum of the incoming photon its energy has to be $E_0 + R$ in order to excite the energy level of the target. In consequence of the recoil energy R being much larger as the natural line width Γ, no excitation can take place (see figure 2.2).

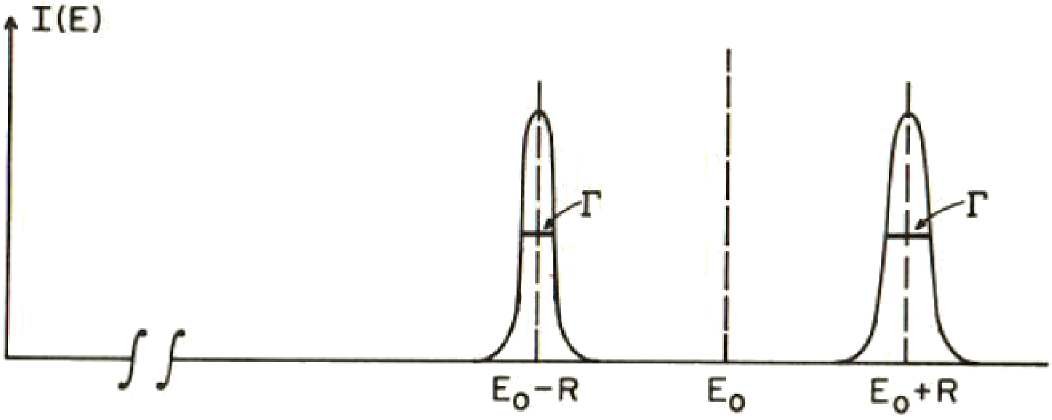

Figure 2.2: E_0 denotes the energy of level B in figure 2.1 left. The photon emitted from a source only possesses the energy $E_0 - R$, but to excite the level B of the target the energy $E_0 + R$ is needed. [2, page 9]

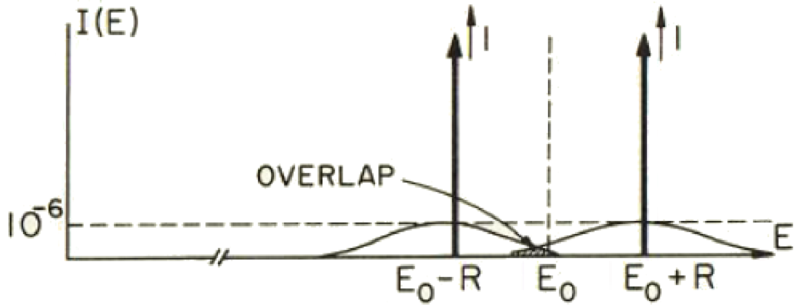

Figure 2.3: Due to the Doppler effect, the emmission and absorbtion lines have lost on intensity, but got broadened. Now they overlap again, and a excitation is possible. [2, page 10]

2.1.3 Doppler Broadening

In contrast to nuclei in rest, which have been looked at in the previous chapter, nuclei in gases can move with quite large velocities. Inside a gas, there velocities can easily be calculated using classical considerations. Using T the temperature in K and k the Bolzmann constant ($k = 8.62 \times 10^{-5}$eV/K) the kinetic energy of a molecule or atom can be calculated by

$$E_{kin} = \frac{Mv_0^2}{2} = \frac{3kT}{2} \ . \tag{2.10}$$

These velocities, which are typically in order of a few hundred meter per second at room temperature, lead to a Doppler broadening. The energy of an emitted gamma ray is shifted by the amount ΔE. This shift occurs along the direction of the movement of the source and its velocity component v_τ. ΔE can be calculated by

$$\Delta E = \frac{v_\tau}{c} E_0 \ . \tag{2.11}$$

In a gas, the emitting atom will move in random directions. Because of this there is a variation in the velocity component in gamma-ray direction of the emitted photons from $-v_\tau$ to $+v_\tau$. Observing a large amount of emitting atoms will lead to a broading of the emission and absorption lines (see figure 2.3). The amount of the broadening is given by

$$\bar{D} = 2\frac{v_\tau}{c} E_0 \ . \tag{2.12}$$

The line height reduces by a factor of $\Gamma/\bar{D}$. The maximum cross section decreases significantly, because of this and therefore also the number of observable photons.

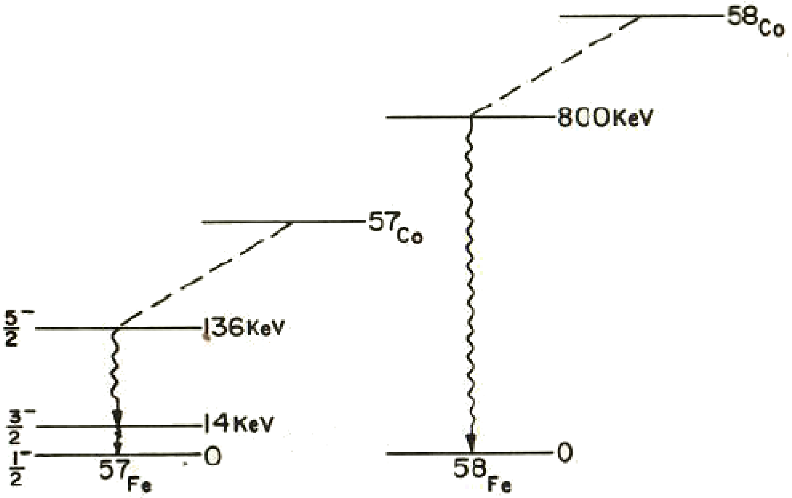

Figure 2.4: Essential aspects of the decay-schemes of ^{57}Fe and ^{58}Fe. [2, page 12]

2.1.4 Recoil-Free emission of gamma rays

The transmission of two iron atoms from first excited to ground state shall be considered next. The values of figure 2.4 are summarized in table 2.1 including the Einstein energy. The Einstein energy E_E is calculated using the sound velocity inside iron v = 5960 m/sec and the lattice constant a = 2.9 Å

$$E_E = \pi\hbar v/a \tag{2.13}$$
$$E_E(\text{iron}) = 0.04 \text{ eV} . \tag{2.14}$$

Table 2.1: Comparison of the recoil and Einstein energy of ^{57}Fe and ^{58}Fe during the emission of a gamma quanta. [2, page 12]

	57Fe	58Fe
Decay Energy	14 kev	800 keV
R	0.002 eV	6 eV
E_E	0.04 eV	0.04 eV

The Einstein energy of iron is smaller than the Recoil energy of the transmission of a ^{57}Fe atom, but larger at a ^{58}Fe atom, which is shown in table 2.1 in tabular and figure 2.5 in graphical form. Because the recoil energy is too low to overcome the Einstein energy, which is the minimum energy necessary to excite vibration modes in the solid, the 14-keV gamma-transmission of ^{57}Fe will be recoilless, if the situation is described semi classically. Even more, as the Doppler broadening is a result of thermal excitation of the solid, there will be no Doppler broadening of the natural line of this transmission. In reality even a transmission with $R \ll E_E$ has a possibility in exciting the solid and therefore to losse energy during a recoil. The probability for a recoilless emission is given by

$$f = e^{-R/E_E} . \tag{2.15}$$

A large fraction of gamma rays are emitted without loosing recoil energy and Doppler broadening, if the ration R/E_E is small. This is the basis for the Mössbauer effect.

Two remarks must be made. A solid will only be predominantly in its ground state for temperatures T much smaller than T_E, otherwise higher states will also be populated to a high degree and eq (2.15) will not give the correct fraction. This fraction would be a lot smaller in that case. It shall also be noted that the Einstein model was used. This model fits the data quite well, but actual frequency spectra are more complicated.

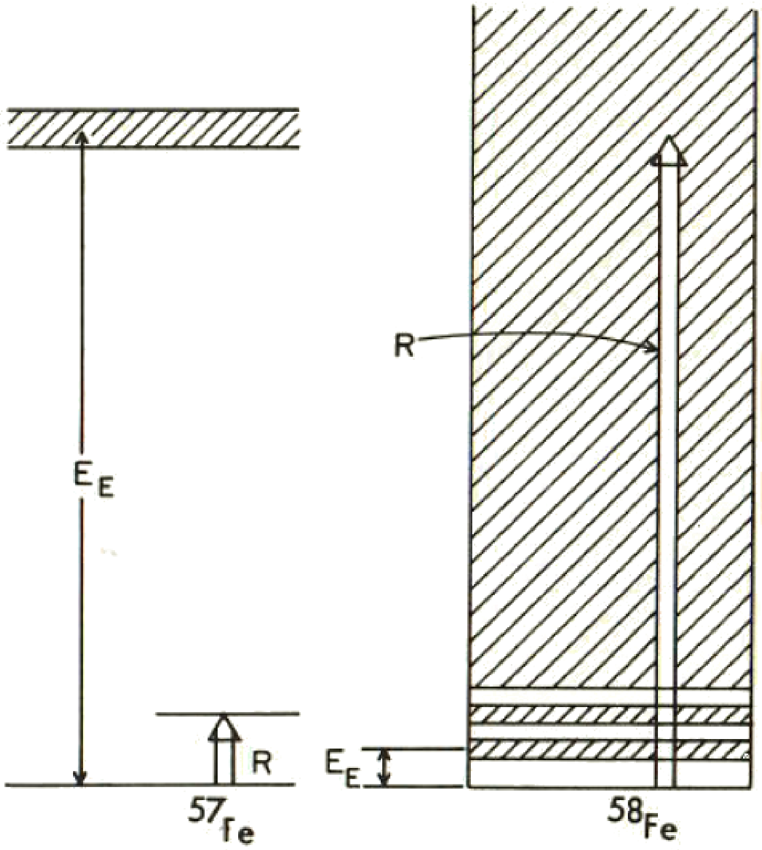

Figure 2.5: Comparison of the Recoil and Einstein energy of ^{57}Fe and ^{58}Fe during the emission of a gamma quant [2, page 13].

2.2 The Mössbauer effect

A short example will be used, to introduce the Mössbauer effect. A source is emitting gamma rays from a ^{57}Fe nucleus, as it was during the experimental work of this thesis. A fraction f, of the emitted gamma rays, is neither loosing energy to a recoil nor gets Doppler broadened. The fraction 1-f, of the 14-keV photons, will be absorbed in the absorber by photo and Compton effect. The nonabsorped part will be counted in the counter behind the absorber. The recoilfree emitted part of the beam undergoes the same absorption, but a fraction of these photons f' will excite ^{57}Fe atoms in the absorber and will therefore be removed from the beam. These excited atoms will decay again later via a 14-keV gamma ray or a conversion electron emission. This fraction can be neglected due to the fact that this re-emission is not focused in one direction, but scattered in all directions. This leads to two effects discovered by Rudolf Mössbauer. First, there are more photons removed from the beam, than were anticipated by the laws of the Compton and the photo effect. Second, by shifting the energy of the emitting photons by a small amount, caused relatively easy by moving the source with a constant velocity, the absorption can be maximized. Using Equation (2.11) and a constant velocity v of the source, gives a new transmission energy $E_0' = E_0(1 + v/c)$. It shall also be noted, that a emission line of width $\mathit{\Gamma}$ and an absorption line, also of width Γ, lead to a transmission line of width $2\mathit{\Gamma}$, as shown in figure 2.6. The observation of the line shape is crucial for most Mössbauer experiments.

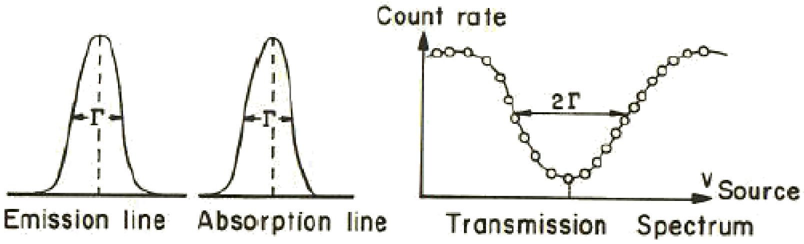

Figure 2.6: Width of the emission, absorption and transmission line. [2, page 16]

2.2.1 Derivation of the Debye Waller factor f

In the previous paragraph it is mentioned that the Mössbauer effect will increase, if the fraction f increases. To reinforce this, the present section shall provide a firmer foundation for this claim by switching from the Einstein to the Debye model, which is a more realistic approximation of the crystal lattice and a derivation of the exact expression of the recoilless fraction f shall be given.

The radioactive nucleus, its atom and the solid, in which it is embedded, shall be considered as one quantum mechanical system. As this system is very complicated, an approximation shall be used. The wave function can be written as

$$\Psi_{\text{total}} = \Psi_{\text{nucleus}} \Psi_{\text{solid}} \tag{2.16}$$

using this approximation. This separation is possible, due to the short range of the nuclear forces. The state of the wave function is not affected by the state of the solid and vice versa. The initial excited state of the nucleus in contrast to the initial stationary state of the solid, denoted as Ψ_i shall be tackled next. An emission of a gamma ray with momentum $\vec{p_0}$ brings the solid to a final state Ψ_f and the nucleus to its ground state. The states Ψ_i and Ψ_f differ in general, because of the recoil acting on the solid during the gamma emission. But there is a certain probability f that an emission will be recoilless and that $\Psi_f = \Psi_i$.

Stationary states of a solid are given by the Schrödinger equation

$$Hu_n = \varepsilon_n u_n \tag{2.17}$$

with u_n the stationary state of the solid with energy ε_n and H the Hamiltonian of the solid. It is assumed that the functions u_n form an orthogonal set. The solid is in a stationary state with energy ε_i before the emission, therefore $\Psi_i = u_i$. Furthermore, as the solid is at rest, u_i has to be an eigenstate of the momentum operator $-i\hbar\nabla$ with eigenvalue 0

$$Hu_i = \varepsilon_i u_i, \qquad -i\hbar\nabla u_i = 0 \ . \tag{2.18}$$

Directly after the emission of a photon with momentum $\vec{p_0} = \hbar\vec{k_0}$, the solid is in the state Ψ_f. Due to the fact that even for very energetic gamma rays the recoil energy is not big enough to eject an atom out of the solid, the entire solid has to pick up the entire recoil momentum $-\vec{p_0}$

$$-i\hbar\nabla\Psi_f = \vec{p_0}\Psi_f \ . \tag{2.19}$$

The wave function of the initial state will be expanded in plane waves, to calculate Ψ_f. The Fourier sum will be used instead of the Fourier integral, as it is general enough for this consideration

$$u_i = \sum_k c_{ki} e^{i\vec{k}*\vec{x}} \ . \tag{2.20}$$

The momentum state of the solid before and after the gamma emission differs only by the recoil moment.The recoil changes each momentum in equation (2.20) from $\vec{k}$ to $\vec{k} - \vec{k_0}$, thus equation (2.20) changes to

$$u_i = \sum_k c_{ki} e^{i(\vec{k}-\vec{k_0})*\vec{x}} \tag{2.21}$$

or after reinserting equation (2.20)

$$\Psi_f = e^{-i\vec{k_0}*\vec{x}} u_i \ . \tag{2.22}$$

This equation represents the solid recoiling with momentum $-\vec{k_0}$ and satisfies equation (2.19). The solid is no longer in an eigenstate of the Hamiltonian H, due to the emission of the photon. Ψ_f shall be expanded in terms of the energy eigenfunctions u_n, to calculate the probability of finding the solid in a given energy state.

$$\Psi_f = \sum_n c_n u_n \tag{2.23}$$

$|c_r|^2$ gives the probability of finding the solid in a state with energy ε_r.

$$|c_r|^2 = \left| \int d^3x u_r^* \Psi_f \right|^2 = \left| \int d^3x u_r^* e^{-i\vec{k_0}*\vec{x}} u_i \right|^2 \tag{2.24}$$

The solid has the same energy as before the emission if $r = i$. This means that the photon must have carried away the full transition energy and therefore was emitted recoilless and without Doppler broadening. Because of this it can be concluded that

$$f = |c_i|^2 = \left| \int d^3x u_i^* e^{-i\vec{k_0}*\vec{x}} u_i \right|^2 \tag{2.25}$$

which is the quantity of the recoil-free fraction and is also called Debye Waller factor.

Equation (2.25) can be rewritten as

$$f = \left| \int d^3 s \rho(\vec{x}) e^{-i\vec{k_0} * \vec{x}} \right|^2 \tag{2.26}$$

using the probability density $\rho(\vec{x}) = u^*(\vec{x})u(\vec{x})$. Equation (2.26) can be interpreted such that the recoil-free fraction is the square of the Fourier transform of the probability density. If $\rho(\vec{x})$ is spread over a large volume, f will become small but on the other hand, if $\rho(\vec{x})$ is concentrated in a small volume, f will be large. The extreme case of this would be if $\rho(\vec{x})$ resembles a delta function. At this point f would become unity. If pictured as waves, these probabilities are easily interpretable. A source nucleus that is moving over a large distance while radiating, emits waves from different points in space. These waves add up to a partially incoherent wave. As a consequence, there will be no well defined frequency and the energy will not be sharp.

As equation (2.25) is quite general, a more detailed model is needed to get a specific expression. The solid shall be represented as a one-dimensional harmonic oscillator. The mass M of the nucleus is bound in this harmonic potential. The sum of the kinetic energy $p^2/2M$ and the potential energy $(M\omega^2/2)x^2$ give the total energy and thus the Hamiltonian of the system is

$$H = \frac{p^2}{2M} + \frac{M\omega^2}{2} x^2 \tag{2.27}$$

It is well known that the energy eigenvalues of this system are [5]

$$\varepsilon_n = \hbar\omega(1/2 + n) \tag{2.28}$$

and its wave functions are u_n. The ground-state wave function is given by

$$u_0(x) = \left(\frac{M\omega}{\pi\hbar}\right)^{\frac{1}{4}} e^{-(M\omega/2\hbar)x^2}, \qquad \varepsilon_0 = \frac{\hbar\omega}{2} \ . \tag{2.29}$$

Using $k_0 = E_0/\hbar c$, $\hbar\omega = E_E$ and inserting this wave function into equation (2.25) leads to

$$f_0 = \left| \int_{-\infty}^{+\infty} dx u_0^*(x) e^{-i(E_0/\hbar c)x} u_0(x) \right|^2 = \exp\left(-\frac{E_0^2}{2Mc^2\hbar\omega}\right) = e^{-R/\hbar\omega} \tag{2.30}$$

which resembles equation (2.15).

Using the average potential energy of a harmonic system $\frac{M\omega^2 \langle x^2 \rangle}{2}$ and the fact that this halves the amount of the total energy of this system $E_n = \hbar\omega(n + 1/2)$, and using $k_0 = E_0/\hbar c$, equation (2.30) can be rewritten for any level as

$$f = e^{-k_0^2 \langle x^2 \rangle} \tag{2.31}$$

Again it is easily seen, that f is large if $\langle x^2 \rangle$, the mean-square displacement along the direction of the photons..

It shall also be shown that the oscillator still gains the average recoil energy $R = \hbar k^2/2M$ as for a free particle. The total energy $\langle E_f \rangle$ of the final state $\Psi_f = e^{-ikx}u_i$ shall be calculated.

$$\langle E_f \rangle = \int dx \Psi_f^* H \Psi_f = \int u_i^* e^{ikx} \left(\frac{p^2}{2M} + \frac{M\omega^2}{2} x^2 \right) e^{-ikx} u_i dx \tag{2.32}$$

$$= \int \left[u_i^* e^{ikx} \left(\frac{\hbar}{2M} \frac{\partial^2}{\partial x^2} \right) e^{-ikx} u_i + u_i^* \frac{M\omega^2}{2} x^2 u_i \right] dx \tag{2.33}$$

$$= \int u_i^* \left[\frac{\hbar^2}{2M} \left(k^2 - \frac{\partial^2}{\partial x^2} \right) + \frac{M\omega^2}{2} x^2 \right] u_i dx = \frac{\hbar^2 k^2}{2M} + E_i \tag{2.34}$$

$$= R + E_{n_i} \tag{2.35}$$

The fact that e^{ikx} commutes with any function of x, particularly ones of the potential energy $(M\omega^2/2)x^2$, but does not commute with the momentum operator $p = (\hbar/i)(\partial/\partial x)$ was used for the calculations.

To describe the behaviour of an actual Mössbauer atom in a crystal a generalisation in two aspects is needed. First an expansion into three dimensions and secondly some 10^{22} modes of vibration in thermal equilibrium have to be considered. The first generalisation is easier. $\langle x^2 \rangle$ of equation (2.31) needs to be interpreted as the mean square displacement along the direction of the photon, but it is important to keep in mind, that $\langle x^2 \rangle$ may be large in one direction and small along others. This can lead to different observations of the recoilless fraction, depending on angle of measurement. The second generalization is more complicated as it is the goal to treat the source nuclei as harmonic oscillators, as done before, but to take a good average over all possible modes of vibration, that can occur at a certain temperature T.

It is known that $\langle x^2 \rangle$ is proportional to the energy, $\langle x^2 \rangle = \varepsilon / M\omega^2$. From statistical mechanics it is known that the average energy $\langle \varepsilon(\omega) \rangle_T$ of a harmonic oscillator at temperature T is

$$\langle \varepsilon(\omega) \rangle_T = \frac{\hbar\omega}{2} + \frac{\hbar\omega}{e^{\hbar\omega/kT} - 1} \ . \tag{2.36}$$

Using this equation the thermal average of $\langle x^2 \rangle$ is given as

$$\ll x^2 \gg_T = \frac{\langle \varepsilon(\omega) \rangle_T}{M\omega^2} \ . \tag{2.37}$$

The calculation of the recoilless fraction f using the Einstein model could be easily done with equation (2.37), but the Einstein model is a quite crude approximation and fails particular in reproducing the low-temperature behaviour of the specific heat. Therefore a switch to the next better model, the Debye model, which allows all frequencies of vibration from $\omega = 0$ to a maximum frequency ω_{max} that is expressed in terms of the Debye temperature Θ_D, shall be made

$$\Theta_D = \frac{\hbar\omega_{\text{max}}}{k} \ . \tag{2.38}$$

Inside the Debye model the number of oscillations $N(\omega)$ of a frequency ω is proportional to ω^2. By normalizing (ω) to unity using

$$\int_{\omega_0}^{\omega_{\text{max}}} N(\omega) \omega d\omega \equiv 1 \tag{2.39}$$

gives

$$N(\omega) = \frac{3\omega^2}{\omega_{\max}^3} \tag{2.40}$$

Combining Equations (2.36) to (2.40) gives the average mean-square displacement

$$\left\langle \overline{x^2} \right\rangle = \frac{3\hbar}{\omega_{\max}^3 M} \int\limits_0^{\omega_{\max}} \left(\frac{1}{2} + \frac{1}{e^{\hbar\omega/kT} - 1} \right) \omega d\omega \tag{2.41}$$

or by using (2.38)

$$\left\langle \overline{x^2} \right\rangle = \frac{3\hbar}{Mk\theta_D} \left[\frac{1}{4} + \left(\frac{T}{\theta_D} \right)^2 \int\limits_0^{\theta_D/T} \frac{xdx}{e^x - 1} \right] , \tag{2.42}$$

which gives the recoilless fraction f

$$f = \exp\left(-k_0^2 \frac{3\hbar}{Mk\theta_D} \left[\frac{1}{4} + \left(\frac{T}{\theta_D} \right)^2 \int\limits_0^{\theta_D/T} \frac{xdx}{e^x - 1} \right] \right) . \tag{2.43}$$

The second term becomes small at very low temperatures, so it is possible to simplify to

$$f_{(T=0)} = \exp\left(\frac{3E_0^2}{4Mc^2 k\theta_D} \right) \tag{2.44}$$

whereas at temperatures above $T = \theta_D/2$ the first term can be ignored and the second one expanded to get

$$f_{(T \geq \theta_D/2)} = \exp\left(-\frac{3E_0^2 (T/\theta_D)}{Mc^2 k\theta_D} \right) \tag{2.45}$$

The values for the Debye temperature scatter depending on the type of measurement method used. This ist not surprising, as even for a simple solid the actual phononen (oscillations) spectrum $N(\omega)$ is more complicated as the Debye spectrum $N(\omega) = \mathrm{const} * \omega^2$. Nevertheless provide the equations (2.44) and (2.45) a reasonable approximation, even for lattices where the Debye model is not strictly applicable like noncubic lattices with different masses.

In conclussion it can be said, that a lower temperature T gives a higher recoilless fraction f and thus an increased possibility for the Mössbauer effect to occur.

2.2.2 Nuclear hyperfine interactions

Up to this point only single line spectra were considered and shown in figures as if nuclei were bare. In reality nuclei are embedded in electric and magnetic fields and interact with them. These interactions lead to perturbation, which can manifest itself as a shift of the nuclear energy levels, as in the case of electric monopole interactions leading to the isomer shift, or splits of degenerated nuclear levels into sub levels, without shifting of the centroid of the multiplet, such as in the electric quadrupole interaction and the magnetic dipole interaction. Only these multipole interactions have to be taken in account, as interactions of higher order are negligible, due to the small energy effects that are too small to be resolved in a Mössbauer spectrum and the electric dipole interaction does not exist, because of symmetry arguments. The following chapters will describe the three phenomena in detail.

A short introduction to electric multipole shall be given, before the deeper look into the Isomer shift.

For a nucleus with charge Ze and its surrounding charges the total energy of the electrostatic interaction is given as [6]

$$E_{el} = \int \rho_n(r) V(r) d\Omega \tag{2.46}$$

with $\rho_n(r)$ the nuclear charge density at a point with coordinates $r = (x_1, x_2, x_3)$, $V(r)$ as the Coulomb potential at point r influenced by all other charges and $d\Omega = dx_1 dx_2 dx_3$. The center of the used coordinate system is the center of symmetry of the nuclear charge. By expanding $V(r)$ at point $r = 0$ using a Taylor series

$$V(r) = V_0 + \sum_{i=1}^{3} \left(\frac{\partial V}{\partial x_i}\right)_0 x_i + \frac{1}{2} \sum_{i,j=1}^{3} \left(\frac{\partial^2 V}{\partial x_i \partial x_j}\right)_0 x_i x_j + ... \tag{2.47}$$

and inserting the equation into (2.46) gives

$$E_{el} = V_0 \int \rho_n(r) d\Omega + \sum_{i=1}^{3} \left(\frac{\partial V}{\partial x_i}\right)_0 \int \rho_n(r) x_i d\Omega + \frac{1}{2} \sum_{i,j=1}^{3} \left(\frac{\partial^2 V}{\partial x_i \partial x_j}\right)_0 \int \rho_n(r) x_i x_j d\Omega + ... \; . \tag{2.48}$$

By using $Ze = \int \rho_n(r) d\Omega$ the first term becomes eZV_0, which is the electrostatic interaction between the nucleus considered as a point and other charges in the material. This term is a contribution to the potential energy as a whole, which is of no further interest for Mössbauer spectroscopy. The second term represents the electrical dipole interaction, which is zero due to symmetry arguments (invariance of nuclear forces against parity transformation and time-reversal invariance). The same applies to all higher odd terms. As it was stated above, all even terms after the third one can be ignored, as their interaction energy is to small too be resolved in Mössbauer spectroscopy. As a result, the only term of interest is the third one.

As $\left(\frac{\partial^2 V}{\partial x_i \partial x_j}\right)_0$ forms a second order tensor V_{ij}, the coordinate system shall be changed in such a way that all non diagonal elements of V_{ij} vanish. The third term of (2.48) can now be rewritten as [6]

$$E = \frac{1}{2} \sum_{i=1}^{3} V_{ii} \int \rho_n(r) x_i^2 d\Omega = \frac{1}{2} \sum_{i=1}^{3} V_{ii} \int \rho_n(r) \left(x_i^2 - \frac{r^2}{3}\right) d\Omega + \frac{1}{6} \sum_{i=1}^{3} V_{ii} \int \rho_n(r) r^2 d\Omega \tag{2.49}$$

with $r^2 = \sum\limits_{i=1}^{3} x_i^2$.

By adding and subtracting $\frac{1}{6}\sum\limits_{i=1}^{3} V_{ii} \int \rho_n(r) r^2 d\Omega$ emerges the definition of the nuclear quadrupole moment in the first term. The diagonal tensor elements are given as $Q_{ii} = \int \rho_n(r)(ex_i^2 - r^2)d\Omega$. Using the Laplace differential equation $\Delta V + 4\pi\rho_e = 0$ at the point r=(0,0,0) gives

$$(\Delta V)_0 = \left(\sum_{i=1}^{3} V_{ii}\right)_0 = 4\pi e\,|\Psi(0)|^2 \tag{2.50}$$

where $\rho_e = -e|\Psi(0)|^2$ is the charge density exerted by the surrounding electrons at the nucleus. Inserting equation (2.50) into (2.49) gives

$$E = \frac{2}{3}\pi e|\Psi(0)|^2 \int \rho_n(r) r^2 d\Omega + \frac{1}{2}\sum_{i=1}^{3} V_{ii} \int \rho_n(r)\left(x_i^2 - \frac{r^2}{3}\right) d\Omega = E_1 + E_Q\ . \tag{2.51}$$

The first term give the electric monopole interaction, which causes a shift of nuclear energy levels and gives rises to the isomer shift δ. The second term represents the quadrupole interaction, that splits degenerated nuclear energy levels and yields the quadrupole splitting ΔE_Q.

2.2.2.1 Isomer Shift δ

Considering the first term of equation (2.51) and substituting $\int \rho_n(r) r^2 d\Omega \equiv \langle r^2 \rangle Ze$ with $\langle r^2 \rangle$ the expectation value of the square of the nuclear radius and $\int \rho_n(r) r^2 d\Omega$ the nuclear charge Ze gives

$$E_1 = \frac{2}{3}\pi Z e^2 |\Psi(0)|^2 \left\langle r^2 \right\rangle \equiv \delta E \tag{2.52}$$

as the interaction energy. This is the energy by which the energy level of a nuclear state is shifted due to Coulomb interactions. This energy change is in the order of 10^{-8} eV. There is a difference in the shift of the ground and the excited state, as it is shown in fig. 2.7 (a).

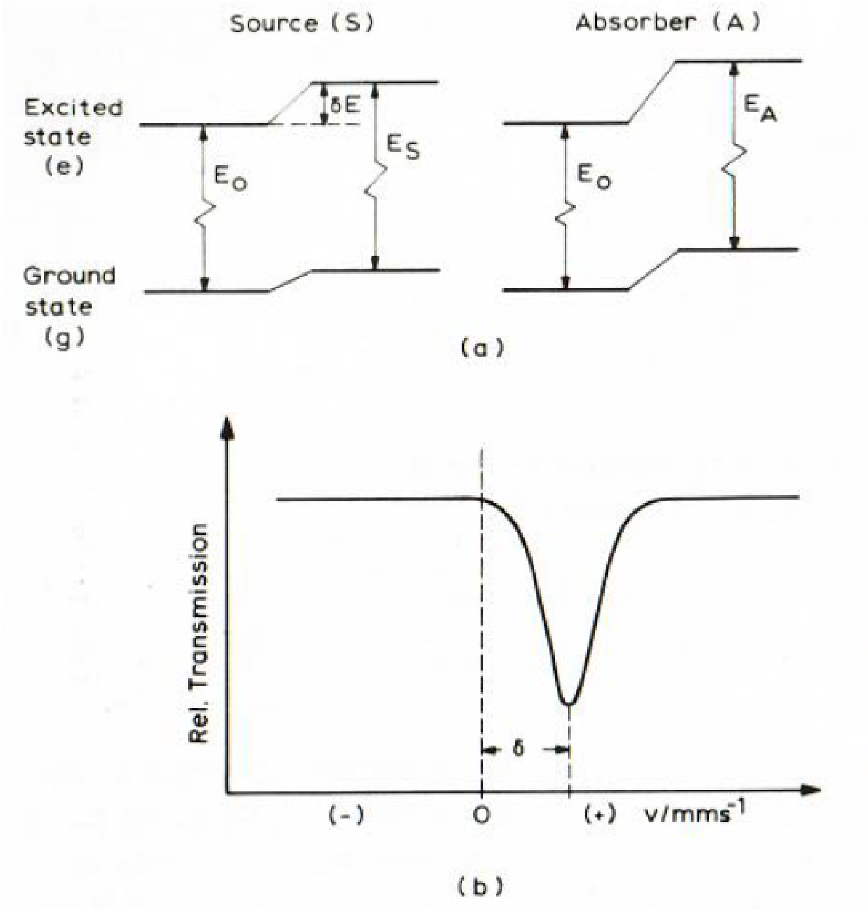

Figure 2.7: (a) Electric monopole interaction shifts nuclear energy levels without degenerating (b) resultant Mössbauer spectrum [3, page 16].

Because of this, the energy change of a gamma ray between a ground and excited state is given by

$$\Delta E = E_S - E_0 = (\delta E)_e - (\delta E)_g = \frac{2}{3}\pi Z e^2 |\Psi(0)|^2 \left[\left\langle r^2 \right\rangle_e - \left\langle r^2 \right\rangle_g \right] \tag{2.53}$$

The emission gamma ray and the absorption line can be put into an optimum overlap by applying a Doppler velocity to either the source or the absorber. This is standard procedure during Mössbauer experiments. It is not possible to observe $(\Delta E)_A$ or $(\Delta E)_S$ separately, only the difference of the electrostatic shift between them. Any difference in electronic configuration, pressure, temperature and similar lead to a change of the electrostatic shift. This difference δ is called isomer shift and is defined as

$$\delta = (\Delta E)_A - (\Delta E)_S = \frac{2}{3}\pi Z e^2 \left[|\Psi(0)|_A^2 - |\Psi(0)|_S^2\right] \left[\left\langle r^2 \right\rangle_e - \left\langle r^2 \right\rangle_g\right] \tag{2.54}$$

Considering atomic nuclei as spherical symmetric with radius R and a constant charge density $\rho_n(r) = 3Ze/4\pi R^3$, defines $\langle r^2 \rangle$ as

$$\left\langle r^2 \right\rangle = \frac{1}{Z_e} \int \rho_n(r) r^2 d\Omega = \frac{3}{4\pi R^3 \int r^2 d\Omega} \, . \tag{2.55}$$

Further replacement of $d\Omega$ with the volume element in spherical coordinates $r^2 dr \sin\theta d\theta d\phi$ leads to

$$\left\langle r^2 \right\rangle = \frac{3}{4\pi R^3} \int_0^R r^4 dr \int_0^\pi \sin\theta d\theta \int_0^{2\pi} d\phi = \frac{3}{5} R^2 \, . \tag{2.56}$$

Inserting this into equation (2.54) gives

$$\delta = \frac{2}{5}\pi Z e^2 \left[|\Psi(0)|_A^2 - |\Psi(0)|_S^2\right] \left(R_e^2 - R_g^2\right) \, . \tag{2.57}$$

The isomer shift δ can be rewritten into the often in literature encountered form by setting $R_e - R_g \equiv \delta R$ and $R_e + R_g \equiv 2R$, which is possible because R_e and R_g differ only a little.

$$\delta = \frac{4}{5}\pi Z e^2 \left[|\Psi(0)|_A^2 - |\Psi(0)|_S^2\right] \left(\frac{\delta R}{R}\right) R^2 \, . \tag{2.58}$$

To restore resonance between source and absorber a certain corresponding Doppler velocity v_D is needed

$$v_D = \left(\frac{4\pi c}{5E_\gamma}\right) Z e^2 R^2 \left(\frac{\delta R}{R}\right) \left[|\Psi(0)|_A^2 - |\Psi(0)|_S^2\right] \, . \tag{2.59}$$

This velocity can be evaluated from a Mössbauer spectrum as the distance between the centroid of a multiplet from zero Doppler velocity. (see figure 2.7 (b))

Up to this point only the nonrelativistic form of the isomershift δ was discussed. For lighter elements up to iron are the errors negligible, in heavier elements however will relativistic forces change the wave function Ψ particular near the nucleus. For example the spin-orbit coupling constant increases with Z^4. Therefore, a modification of the equations above is needed, as the electron density at the nucleus $|\Psi(0)|$ will also be affected and changed. This has been done by Shirley [7] using Dirac wave functions and first order perturbation theory. The calculations show that the relativistic correction is given by a dimensionless factor $S'(Z)$, which he calculated as Z = 1 to 96. With $S'(Z)$ δ changes to

$$\delta = \frac{4}{5}\pi Z e^2 S'(Z) \left[|\Psi(0)|_A^2 - |\Psi(0)|_S^2\right] \left(\frac{\delta R}{R}\right) R^2 \, . \tag{2.60}$$

If only comparisons of compounds of the same Mössbauer nuclide are made during Mössbauer studies, no problem arises concerning relativistic corrections, as the relativistic factor $S'(Z)$ is constant for all compounds of the same nuclide. Additionally, by using one source throughout a study of series of compounds of one nuclide, it is possible to consider $|\Psi(0)|_S^2 = C$ as a constant. This means that the isomer shift δ will become a linear function of the charge density at the absorber $|\Psi(0)|_A^2$

$$\delta = \text{const}\left(\frac{\delta R}{R}\right)\left[|\Psi(0)|_A^2 - C\right] \ . \tag{2.61}$$

The relative change of the nuclear radius going from the excited to the ground state $(\delta R/R)$ is known, though for many Mössbauer nuclides not to any great accuracy. The sign of $(\delta R/R)$ is known for most Mössbauer nuclei and can be positive or negative. If it is positiv, it indicates an increase of the electron density at the nucleus going from the source to the absorber, whereas a negative sign indicates that the energy density at the absorber is lower than at the source.

Isomer shift values must always be reported in reference to a given material. This is a consequence of the fact that Mössbauer spectra of a particular compound may be obtained under identical conditions, but with different sources. As an example the ^{57}Co nuclei used for ^{57}Fe spectroscopy may be embedded in Pd, Pt, Cr or Cu, which lead to different isomer shifts. This becomes obvious, as $|\Psi(0)|_S^2$ in equation (2.60) changes with the chemical environment of the Mössbauer nuclide. In ^{57}Fe spectroscopy, alpha iron and sodium nitroprusside dihydrate (SNP), $Na_2[Fe(CN)_5NO]2H_2O$, are usually used as standard reference material.

The total s-electron density at the atomic nucleus is primarily the cause of the finite electron density at the nucleus. It is composed from a contribution of the filled s-orbitals of the inner electron shells and a contribution from partially filled valence orbitals. The contribution of the valence orbitals is very sensitive to changes of the electronic structure of the valence band, like a change in oxidation, of the spin state or bond properties by electron dislocation. These changes influence the s-electron density at the nucleus in two ways. Firstly, due to direct altering of the population of s-electrons in the valence shell. Any change of the s-electrons in the valence shell will change $|\Psi(0)|^2$ directly and in the same direction. Secondly, indirect by shielding s-electrons by electrons of non zero angular momentum. Any increase of the valence electron density of p-, d- or f-electrons will cause a weaker attraction of the s-electrons by the nuclear charge and thus decrease the quantity $|\Psi(0)|^2$ and vice versa.

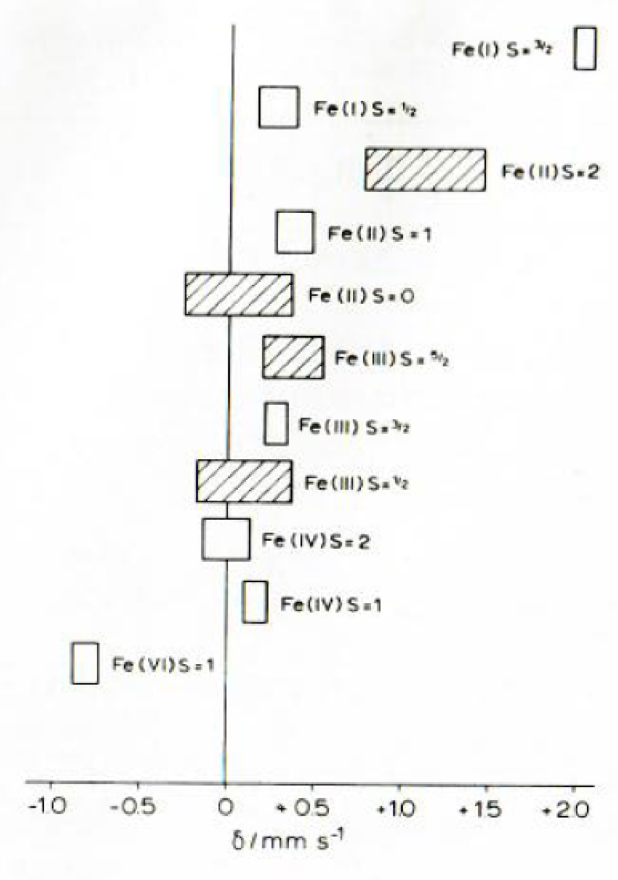

Figure 2.8: Approximate ranges of isomershifts observered in iron compounds.
S refers to the spin quantum number. [3, page 19]

Correlation diagrams, like figure 2.8 for ^{57}Fe, give isomer shift ranges depended on the oxidation state. These diagrams can be very helpful to identify unknown compounds. Figure 2.8 in particular displays the approximate ranges of the isomer shift δ observed in iron compounds with different oxidation and spin states. It can be seen that the δ values for high spin iron compounds rises with decreasing formal oxidation state. This happens due to the shielding discussed in the previous paragraph. It can be noted further that the ranges in high spin compounds with different oxidation states hardly overlap, which makes it relatively easy to identify the oxidation state of a known high spin compound. On the other hand it is shown that the ranges of the isomer shift of low spin iron (II) and iron (III) is quite similar. It is not possible to distinguish one from the other only by measuring isomer shift. Therefore another indicator is needed to separate them from one another. One of these can be the quadrupole splitting ΔE_Q.

2.2.2.2 Quadrupole Splitting ΔE_Q

The nuclear charge distribution was considered uniform and spherically symmetric in the previous section. In that case no nuclear quadrupole moment exists as the second term of equation (2.51) vanishes. This means that the electric quadrupole interaction E_Q becomes zero, if all extranuclear charges, electrons and lattice charges, are arranged in cubic symmetry. In addition, electric quadrupole interaction can only exist if there is an observable nuclear quadrupole moment and simultaneously a non zero electric field gradient (EFG) at the nucleus.

The nuclear charge distribution deviates in many nuclei more or less from spherical symmetry. This deviation may change by switching the level of excitation and is measured by the electric quadrupole moment eQ, with Q being a second rank tensor with elements

$$Q_{ij} = \int \rho_n(r)(x_i x_j - \delta_{ij} r^2) d\Omega \tag{2.62}$$

with x_i, x_j the cartesian coordinates of r, ρ_n the nuclear charge and δ_{ij} the Kronecker symbol.

By choosing x_i, x_j as the coordinates x, y and z of the coordinate system in which all off diagonal elements of Q_{ij} become zero and choosing the z-axis as the axis of preferred orientation, also called the axis of quantization, it is possible to define the quadrupole moment for nuclear charge distribution of cylindrical symmetry as

$$Q \equiv \frac{1}{e} \int \rho_n(r)(3z^2 - r^2) d\Omega = \int \rho_n(r) r^2 (3\cos^2\theta - 1) d\Omega \tag{2.63}$$

with θ the angle between the symmetry axis and $\vec{r}$ and the definition for $z = r\cos\theta$ in spherical coordinates.

Q is negative for a flattened or pancake-shaped nucleus, and positive for an elongated or cigar-shaped nucleus. Nuclei with a spherical charge distribution give Q $= 0$. Due to the fact that nuclear states with spin quantum number $I = 0, \frac{1}{2}$ have no observable quantum moment, only nuclear states with $I > \frac{1}{2}$ are able to interact with inhomogeneous electric field, which is described by the electric field gradient (EFG). As quadrupole splitting is connected with the electric field gradient, a short and basic introduction of the EFG shall be given in the following paragraph.

Electric field gradient

For a nucleus located at the origin of the coordinate system, a point charge q at distance $r = \sqrt{x^2 + y^2 + z^2}$ may cause a potential $V(r) = q/r$. The electric field is defined as the negative gradient of the potential $-\vec{\nabla}V$ and the electric field gradient is defined as

$$\mathrm{EFG} = \vec{\nabla}\vec{E} = -\vec{\nabla}\vec{\nabla}V = \begin{bmatrix} V_{xx} & V_{xy} & V_{xz} \\ V_{yx} & V_{yy} & V_{yz} \\ V_{zx} & V_{zy} & V_{zz} \end{bmatrix} \tag{2.64}$$

with the components defined as (i,j = x,y,z)

$$V_{ij} = \frac{\partial^2 V}{\partial i \partial j} = \frac{q(3ij - r^2\delta_{ij})}{r^5} \tag{2.65}$$

Due to the symmetric form of the tensor only six values can be independent and adding the Laplace equation

$$\sum_i V_{ii} = 0 \qquad i = x, y, z \tag{2.66}$$

which requires the EFG to be traceless, decreases the number of independent values further to five.

Introducing the principal axis system, where all off-diagonal elements vanish, and choosing the order of the remaining elements as

$$|V_{zz}| \geq |V_{yy}| \geq |V_{xx}| \tag{2.67}$$

specifies the EFG with two independent parameters. These parameters are V_{zz} and η the asymmetry parameter, which is defined as

$$\eta = \frac{V_{xx} - V_{yy}}{V_{zz}} \tag{2.68}$$

and is limited between zero and one because of equation (2.67). η becomes 0 if a fourfold or threefold axis of symmetry exists inside the Mössbauer nucleus, as $V_{xx} = V_{yy}$ in that case. The electric field gradient becomes axial symmetric. If two mutually perpendicular axis of threefold or higher symmetry occur in a system, the EFG becomes zero.

To conclude, two possible sources can contribute to the total EFG. On one hand charges on distant ions surrounding the Mössbauer atom in a non cubic symmetry, usually called lattice contribution, and on the other hand anisotropic electron distribution in the valence shell of the Mössbauer atom, which is refered to as valence electron contribution.

The Hamiltonian [8]

$$\hat{H}_Q = \frac{eQV_{zz}}{4I(2I-1)}\left[3\hat{I}_z^2 - \hat{I}^2 + \eta\frac{(\hat{I}_+^2 + \hat{I}_-^2)}{2}\right] \tag{2.69}$$

describes the interaction of the electric quadrupole moment Q, as described in (2.63), in the principal axis system with the z-axis as the axis of quantization and the electric field gradient at the nucleus, described by V_{zz} and η. Using $\hat{I}$ the nuclear spin operator, I the nuclear spin number, $\hat{I}_\pm = \hat{I}_x \pm i\hat{I}_y$ the shift operators and $\hat{I}_x, \hat{I}_y, \hat{I}_z$ the operators of the nuclear spin projections onto the principal axis.
Solving the first order perturbation matrix gives the Eigenvalues E_Q to the perturbation operator $\hat{H}_Q$

$$E_Q = \frac{eQV_{zz}}{4I(2I-1)}\left[3m_I^2 - I(I+1)\right]\sqrt{1+\frac{\eta^2}{3}} \tag{2.70}$$

with the magnetic spin quantum number $m_I = I, I-1, ..., -I$. Wegener has shown that the same expression can be found by starting with the second term of (2.51). [6]

The main effect of the electric quadrupole interaction is the splitting of the $(2I{+}1)$-fold degenerate energy level of a nuclear state with quantum number $I > 1/2$ into substates $|I, \pm m_I >$ without shifting the barycenter of the original level. These substates are described by the magnitude of the magnetic spin number M_I, but due to the power of two in equation (2.70) they remain double degenerated. This twofold degeneration can be removed by magnetic perturbation.

A Mössbauer spectrum, produced by a single line source of an polycrystalline absorber with no magnetic field at the nucleus, will show two resonant lines with equal intensities, usual called a quadrupole doublet, as it can be seen in fig. 2.9 (b). The energy difference ΔE_Q corresponds to the distance Δ between the resonance lines. The quadrupole splitting allows conclusions to be made about molecular and electronic structure problems as well about the bond properties.

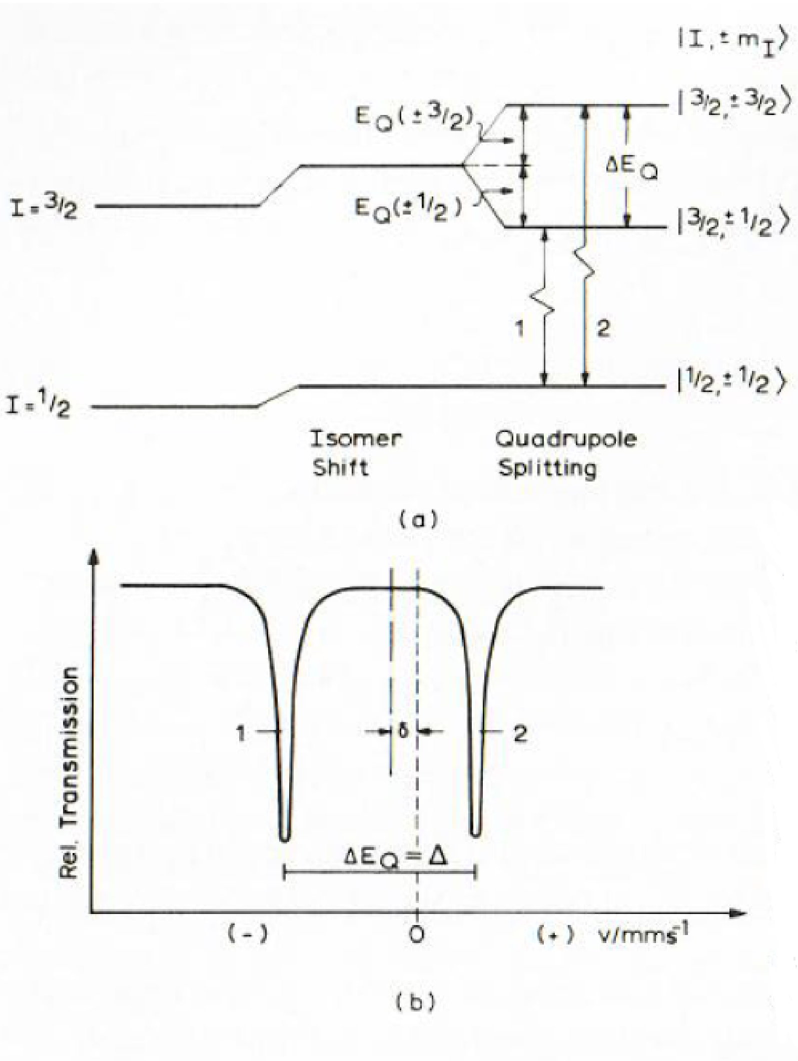

Figure 2.9: (a) The I=3/2 level is split into two sub-levels, the I= 1/2 is not, due to the lack of a spectroscopic quadrupole moment. (b) resultant Mössbauer spectrum [3, page 26]

Figure 2.9 displays the effect of electric quadrupole interaction in ^{57}Fe with $I = 3/2$ in the 14-keV state and $I = 1/2$ in the ground state. The ground state can not split, due to the absence of a quadrupole moment, as discussed above. The excited state splits into the double degenerated substates $|3/2, \pm 3/2 >$ and $|3/2, \pm 1/2 >$. The perturbations energy E_Q can be calculated for the case of an axial symmetry EFG ($\eta = 0$) using (2.70):

$$\begin{aligned} E_Q(\pm 3/2) &= \frac{3eQV_{zz}}{12} = \frac{eQV_{zz}}{4} \quad \text{for} \quad I = 3/2, m_I = \pm 3/2 \\ E_Q(\pm 3/2) &= -\frac{3eQV_{zz}}{12} = -\frac{eQV_{zz}}{4} \quad \text{for} \quad I = 3/2, m_I = \pm 1/2 \end{aligned} \tag{2.71}$$

The magnitude of the perturbation energies are identical, which indicates, that the barycenter of the $I = 3/2$ level is not affected, as predicted above. The energy difference ΔE_Q in this case is

$$\Delta E_Q = E_Q(\pm 3/2) - E_Q(\pm 1/2) = \frac{eQV_{zz}}{2} \tag{2.72}$$

2.2.2.3 Magnetic Hyperfine Interaction

Any nucleus with quantum spin number $I > 0$ and a non zero magnetic dipole moment $\vec{\mu}$ can interact with a magnetic field $\vec{H}$. This interaction is called magnetic dipole interaction or nuclear Zeeman effect, and can be described with the Hamiltonian

$$\hat{H} = -\hat{\vec{\mu}}\hat{\vec{H}} = g_N \beta_N \hat{\vec{I}}\hat{\vec{H}} \tag{2.73}$$

using the nuclear Landé factor g_N and the nuclear magneton $\beta_N = e\hbar/2Mc$, which uses the mass of the nucleus M.

Diagonalization of the first order perturbation matrix gives the Eigenvalues of the Hamiltonian as

$$E_M(m_I) = -\frac{\mu H m_I}{I} = -g_N \beta_N H m_I \tag{2.74}$$

The nuclear state is split into 2I+1 nondegenerated and equally spaced substates $|I, m_I>$. These substates are defined by the sign and the magnitude of the magnetic spin quantum number m_I.

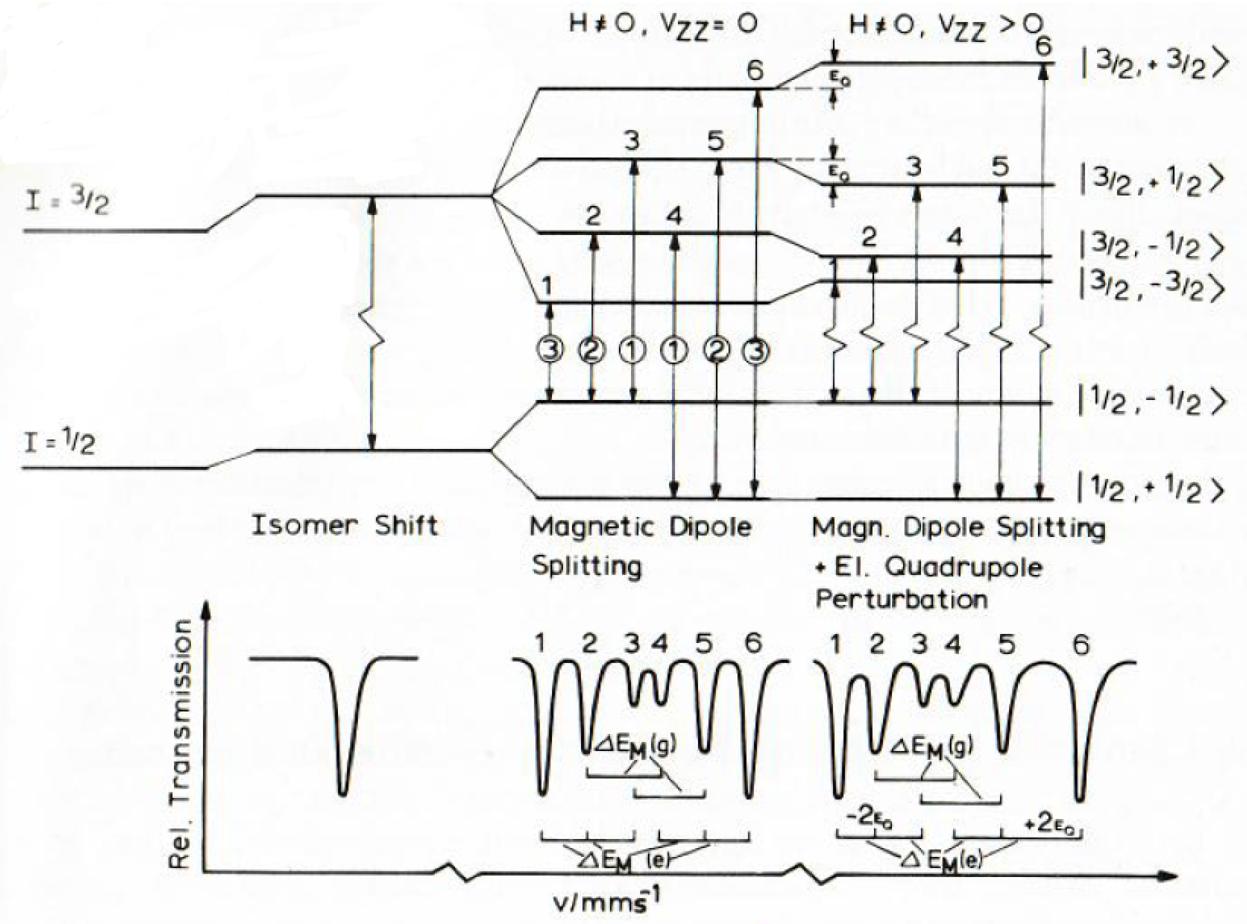

Figure 2.10: Magnetic dipole splitting in ^{57}Fe without $(H \neq 0, V_{ZZ} = 0)$ and with electric quadrupole perturbation$(H \neq, V_{ZZ} > 0)$ and resulant Mössbauer spectra.
$\Delta E_m(g) = g_g \beta_N H$ refers to the splitting of the ground state
$\Delta E_m(e) = g_e \beta_N H$ to the splitting of the excited state. [3, page 27]

Figure 2.10 shows the effect of the magnetic dipole interaction without (in the middle section) and with (the right section) the electric quadrupole interaction. As it can be seen on this example for ^{57}Fe, the $I = 1/2$ level splits into two substates and the $I = 3/2$ state into four substates. Due to the selection rules for magnetic dipole transition

$$\Delta I = 1, \qquad \Delta m = 0, \pm 1 \tag{2.75}$$

only some tranmission are allowed. For ^{57}Fe there are six allowed gamma transitions which are displayed in figure 2.10.

The circled numbers in figure 2.10 correspond to the relative intensities, if isotropic orientation of the magnetic field in respect to the gamma rays is given, which are determined by the squares of the Clebsch-Gordan coefficients [6].

A Mössbauer spectrum, which was generated with a single line source and a magnetically ordered substance as absorber, usually give a resonance sextet. Its center may be shifted due to the isomer shift δ. Using the magnetic hyperfine splitting it is possible to examinate the effective magnetic field acting at the Mössbauer nucleus. This field can have different origins. Most important are the contribution of H^L from the orbital motion of valence electrons with the total momentum spin number L, the contribution H^d, which is called the spin-dipolar field and is arising from the electron spin of the atom under consideration and the Fermi contact field H^C, which arises from a net spin-down or spin-up s-electron density at the nucleus as a consequence of spin-polarisation of inner filled s-electrons by spin polarized filled outer shells.

Due to the chemical applications of the Mössbauer effect, it is not common to find pure magnetic interaction beside the electric monopole action, which is always present due to the fact that $\delta R/R \neq 0$. The nuclear level diagram displays that perturbation treatment can be done for either $E_M \gg E_Q$ or $E_Q \gg E_M$.

For the example in figure 2.10 the latter case was used, as it can be clearly seen, that the electric quadrupole interaction can be treated as a perturbation of the magnetic hyperfine interaction. Because V_{zz} is positive, the sublevels $|3/2, \pm 3/2\rangle$ have been shifted by $E_Q(\pm mI) = \Delta E_Q/2$ to a higher energy and the sublevels $|3/2, \pm 1/2\rangle$ to a lower energy level, where ΔE_Q equals the combined shifts of $E_Q(+mI)$ and $E_Q(-mI)$ If V_{zz} would have a negative sign, the direction of the shifting would be reversed. The sublevels of the state $I = 3/2$ are no longer equally spaced, this results in an asymmetrical magnetic split in the Mössbauer spectrum. Due to the fact that this is directly correlated with the sign of V_{zz}, the sign of the EFG can be extracted from the magnetic splitting in the Mössbauer spectrum for polycrystalline samples. .

2.2.3 Relative Intensities of resonance lines

The line intensities of the hyperfine components are determined by the properties of the nuclear state, like the spin and parity of the excited and ground states but also the geometric configuration, for example the direction of the wave vector $\vec{k}$ of the emitted gamma quanta with respect to the quantisation axis.

Single line Mössbauer sources using ^{57}Fe have an unpolarized magnetic dipole transition (M1) with a negligible electric quadrupole (E2) admixture. The probability of a nuclear transition of multipolarity M1 from a state $|I_1, m_1>$ to a state $|I_2, m_2>$ is given as

$$P(3/2m_{3/2}, 1m|1/2m_{1/2}, \theta, \phi) = | < 3/2m_{3/2}, 1m|1/2m_{1/2} > |^2 F^{1m_{3/2}}_{1m_{1/2}}(\theta, \phi)| < I_1||1||I_2 > |^2 \tag{2.76}$$

with θ, ϕ the polar and azimuthal angle of the z-direction with respect to the direction of the gamma ray emission. (see figure 2.11), $< I_1 m_1, Lm|I_2 m_2 >$ the Clebsch-Gordon coefficients, that are coupling together the three vectors $\vec{I_1}, \vec{I_2}$ and $\vec{L}$, the reduced matrix element $< I_1||1||I_2 >$ which does not depend on the magnetic quantum number and the angular dependent terms $F^{1m_{3/2}}_{1m_{1/2}}$ which are tabulated in [3, page 31]. Tables for the Clebsch-Gordon coefficients can be found in [3, page 30].

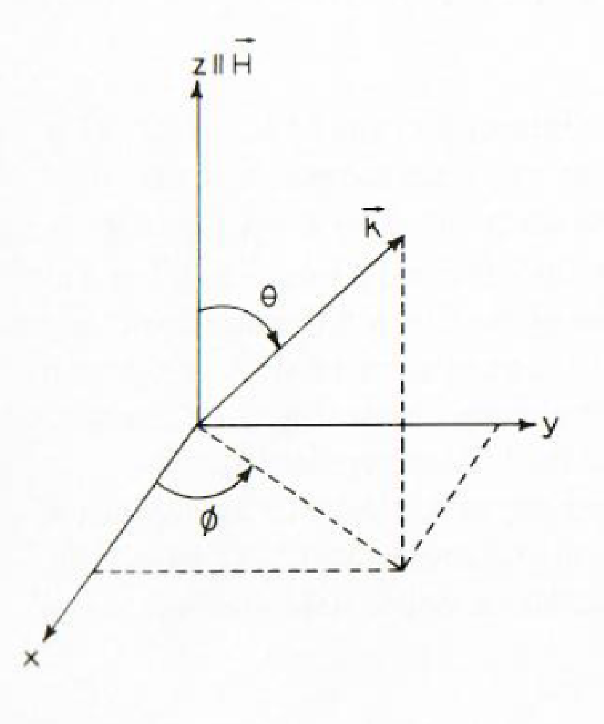

Figure 2.11: Definition of the polar angles θ, ϕ. $\vec{k}$ is the wave vector of the emitted Gamma ray. The z-axis may be defined by the direction of a magnetic field. [3, page 29]

The first case, that shall be discussed, is a magnetically split spectrum derived from powder sample. In that case there are pure m_I states $|I, m_I>$ randomly distributed with the z-axis parallel to the direction of the internal magnetic field. $P(3/2m_{3/2}, 1m|1/2m_{1/2}, \theta, \phi)$ has to be integrated over θ and ϕ, because of this.

$$P(3/2m_{3/2}, 1m|1/2m_{1/2}) = \int_0^{\pi}\int_0^{2\pi} P(3/2m_{3/2}, 1m|1/2m_{1/2}; \theta; \phi) \sin\theta d\theta d\phi \qquad (2.77)$$

or

$$P(3/2m_{3/2}, 1m|1/2m_{1/2}) \propto |< 3/2m_{3/2}, 1m|1/2m_{1/2} >|^2 \qquad (2.78)$$

Using this approximation and the values for the Clebsch-Gordon coefficients give the relative intensity ratio 3:2:1:1:2:3 for the hyperfine components of the powder sample, as decribed in figure 2.10. For the case where $\theta = \theta_0 = 0$, this is the case when the direction of $\vec{k}$ of the gamma rays and of the magnetic field H are parallel, integrating (2.76) over only the azimuthal angle ϕ, leads to a disappearing of the second and the fifth hyperfine component, as it is shown in figure 2.12(c).

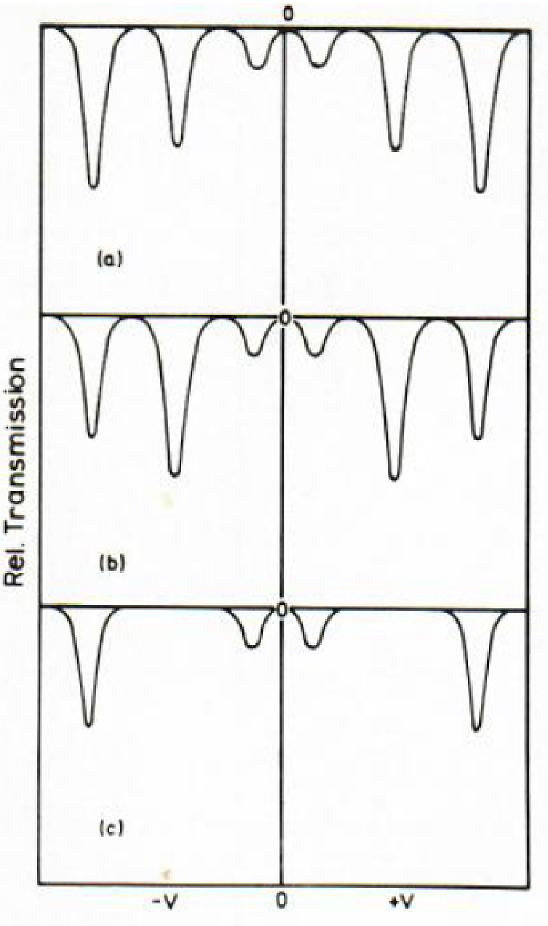

Figure 2.12: Magnetic hyperfine pattern of a powder sample with randomly distributed internal magnetic field (a) and applied magnetic field ($\theta_0 = \pi/2$) (b) and ($\theta_0 = 0$) (c) [3, page 32]

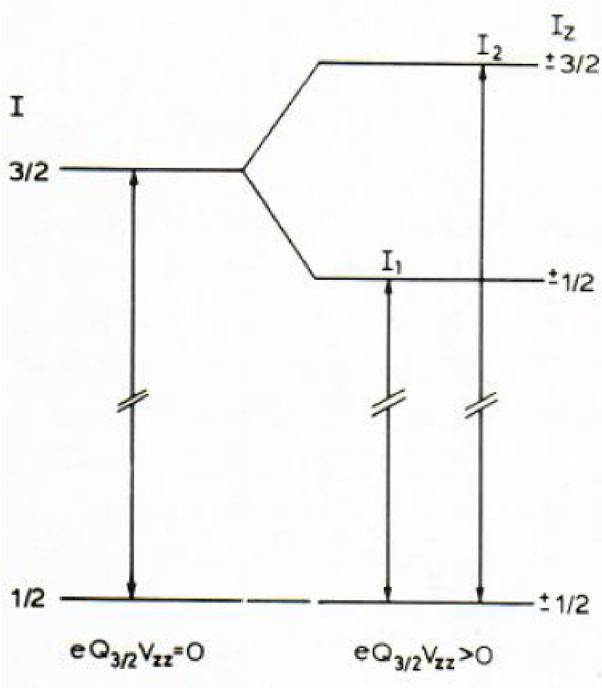

Figure 2.13: Quadrupole hyperfine splitting for ^{57}Fe with $I_e = 3/2$ and $I_g = 1/2$: the quadrupole interaction parameter $eQ_{3/2}V_{zz}$ is assumed to be positive. [3, page 32]

Figure 2.13 shows schematically a pure quadrupole hyperfine splitting. The intensity ratio I_2/I_1 can be obtained for an axially symmetric field gradient using (2.76)

$$\frac{I_2}{I_1} = \frac{\int_0^\pi 3(1+\cos^2\theta)h(\theta)\sin\theta d\theta}{\int_0^\pi (5-3\cos^2\theta)h(\theta)\sin\theta d\theta} \; . \tag{2.79}$$

with $h(\theta)$ being the probability of finding an angle θ between the direction of the z axis and the gamma propagation and only for crystals with an isotropic f-factor.

A random distribution of the principal axis system of the EFG exists in a powder sample and with $h(\theta) = 1$ this leads to a ratio of $I_2/I_1 = 1$. This would describe a symmetric Mössbauer spectrum, in which case it is not possible to determine the sign of the quadrupole coupling constant eQV_{zz}. The intensity ratio of a single crystal, because $h(\theta) = \frac{1}{\sin\theta}\delta(\theta-\theta_0)$, is given as

$$\frac{I_2}{I_1} = \frac{3(1+\cos^2\theta_0)}{5-3\cos^2\theta_0} \; . \tag{2.80}$$

Due to the fact that the ratio ranges from 3 at $\theta_0 = 0$ to 0.6 for $\theta_0 = \pi/2$, it is possible to determine the sign of the quadrupole coupling constant eQV_{zz} in studies on single crystals. For elements where the sign of Q is known, for example for ^{57}Fe, $Q(^{57}Fe) > 0$, this reveals the sign of V_{zz} of the EFG.

If both, magnetic dipole and electric quadrupole interactions, are present, the situation is more complicated. The states are no longer pure m_I states $|I, m_I>$, but linear combinations of these. For ^{57}Fe this lead to:

$$|\Psi_{3/2}i> = \sum_{m_{3/2}=-3/2}^{+3/2} C^{3/2i}_{m_{3/2}} |3/2 m_{3/2}>, \qquad i = 1, 2, 3, 4 \tag{2.81}$$

$$|\Psi_{1/2}j> = \sum_{m_{1/2}=-1/2}^{+1/2} C^{1/2j}_{m_{1/2}} |1/2 m_{1/2}>, \qquad j = 1, 2 \tag{2.82}$$

The strength of magnetic dipole and electric quadrupole interactions have a direct dependency on the coefficients $C^{3/2i}_{m_{3/2}}$,$C^{1/2j}_{m_{1/2}}$ and these can be calculated by diagonalizing the appropriate Hamiltonian $\hat{H} = \hat{H}_M + \hat{H}_Q$. The transition probability arises as [9][10]:

$$\begin{aligned} P(3/2i, 1/2j, \theta, \phi) \propto \sum_{m_{3/2}} \sum_{m'_{3/2}} \sum_{m_{1/2}} \sum_{m'_{1/2}} C^{1/2j}_{m_{1/2}} C^{3/2i}_{m_{3/2}} C^{3/2i}_{m'_{3/2}} C^{1/2j}_{m'_{1/2}} \times \\ < 3/2 m_{3/2}, L = 1 m | 1/2 m_{1/2} >< 3/2 m'_{3/2}, L = 1 m' | 1/2 m'_{1/2} > F^{lm'}_{lm}(\theta, \phi) \end{aligned} \tag{2.83}$$

A mixing parameter ξ (2.85) needs to be used in the cases of nuclear transitions with a mixture of multipolarity M1 and E2. The transition probability is the given as:

$$\begin{aligned} P(3/2i, 1/2, \theta, \phi) \propto (2.83) + \xi^2 * [(2.83)\text{with L=2}] \\ -\xi * \sum_{m_{3/2}} \sum_{m'_{3/2}} \sum_{m_{1/2}} \sum_{m'_{1/2}} C^{1/2j}_{m_{1/2}} C^{3/2i}_{m_{3/2}} C^{3/2i}_{m'_{3/2}} C^{1/2j}_{m'_{1/2}} \times \\ < 3/2 m_{3/2}, L = 1 m | 1/2 m_{1/2} >< 3/2 m'_{3/2}, L = 2 m' | 1/2 m'_{1/2} > F^{2m'}_{lm}(\theta, \phi) \end{aligned} \tag{2.84}$$

with

$$\xi = \frac{< I_1 || E2 || I_2 >}{< I_1 || M1 || I_2 >} \tag{2.85}$$

2.2.4 Experimental line shape and width of resonant absorption

The gamma ray emitted by a Mössbauer source, which is moving with velocity v, has a relative intensity of [11]

$$I_{\mathrm{em}}(v,E) = \frac{f_s \frac{\Gamma}{(2\pi)}}{\left[E - E_0\left(\left(1+\frac{v}{c}\right)\right)\right]^2 + \left(\frac{\Gamma}{2}\right)^2} , \tag{2.86}$$

where f_s is the fraction of the emitted gamma quanta of the source, Γ the natural line width and E_0 the transmission energy at $v = 0$, as described in equation (2.3). The transmission probability $T(E)$ of a gamma quantum with energy E through a resonance absorber is depending on the thickness d, $\sigma(E)$ the absorption cross section and the particle density ρ of the absorber

$$T(E) = \exp\left(-d\rho\sigma(E)\right) . \tag{2.87}$$

As a result of the fact that $\sigma(E)$ can be divided into one part which is nearly energy independent in the energy region defined by the natural line width, and another part that describes the resonance absoption, $\sigma(E)$ can be written as

$$\sigma(E) = \bar{\sigma} + \sigma_r(E) \tag{2.88}$$

with $\bar{\sigma}$ being mainly determined by the cross section of the photo effect and nonresonat scattering.

Using time reversal arguments yield that the cross section for resonant absorption should be proportional to the emission probability. It can be found that $\sigma_r(E)$ is given by [11]

$$\sigma_r = f_{\mathrm{abs}}\beta\sigma_0 \frac{(\Gamma/2)^2}{(E-E_0)^2 + (\Gamma/2)^2} \tag{2.89}$$

with

$$\sigma_0 = \frac{2\pi}{k^2} \frac{1}{1+\alpha} \frac{2I_a+1}{2I_g+1} \tag{2.90}$$

and the relative abundance of the Mössbauer isotope β, the maximum resonant cross section, at $E = E_0$, σ_0 and the internal inversion coefficient α. For ^{57}Fe equation (2.89) gives $\sigma_0 = 2.56 * 10^{-22}$ m^2. The count rate of a transmission Mössbauer experiment, where the absorber is placed between source and counter, is given by the transmission integral

$$C(v) = (1-f_s)\exp(-d\rho\bar{\sigma}) + \int I_{\mathrm{em}}(v,E)T(E)dE \tag{2.91}$$

where $(1-f_s)$ is the nonresonant fraction of the emitted gamma rays.

The off resonance count rate is given by $C(\infty) = \exp(-d\rho\bar{\sigma})$.

The line shape is of Lorentzian form with a half width twice of the nature width, if the natural width of absorber and source are identical. But if the effective absorber thickness (2.92) is not small compared to 1, it is not longer possible to expect a Lorentzian form. It was shown by Margulies and Ehrman [12], that the Mössbauer line shape still can be represented by a Lorentzian form, if the width of the function is a function of the effective absorber thickness.

$$t = f_{\mathrm{abs}} N \sigma_0 = \frac{f_{\mathrm{abs}} \sigma_0 N_L \beta \rho \Delta x}{A} \tag{2.92}$$

with A the atomic weight, $\rho \Delta x$ in g/cm^2 of resonant nuclei and the Loschmidt number N_L.

In many cases is the line broadening, due to the absorber thickness t, much smaller than the broadening of unresolved hyperfine interaction in the source or absorber or from inhomogeneous distribution of hyperfine fields. An improperly working Mössbauer drive can also lead to line broadening due to Doppler broadening or a cosine smearing effect can occur due to inappropriate geometrical arrangements.

Further line width problems can be caused by special physical processes, for example during delayed coincidence experiments, where the Mössbauer spectrum is accumulated at chosen times of order of the lifetime of the excited Mössbauer level after the nuclear transformation. Due to the decay of ^{57}Co(EC,γ)^{57}Fe via electron capture, is it even possible to observe line widths smaller than the natural line width.This is possible due to the Heisenberg uncertainty relation $\Delta E_{\mathrm{exp}} \Delta t_{\mathrm{exp}} \approx \hbar$.[13]

A different example would be thermal spikes, which can occur, due to a nuclear transformation, and which can create long living phonon states, that eventually decay during the lifetime of a Mössbauer level. The Debye-Waller factor would increase with the time the excited nuclear level existed. This means that gamma rays that are contributing to the resonance line would come from excited nuclei with a longer effective lifetime than the mean lifetime. This can also cause a line width smaller than the natural line width due to the Heisenberg uncertainty equation.

3 Experimental

The subsequent chapter describes the sample material, the two experimental setups used, displays the gathered data, explains the theoretical models used for analysis, give a brief description of the analysis software used and discusses the accumulated data and analysis.

3.1 Sample material: $(V_{0.92}Fe_{0.08})_2FeB_2$

The experimental work of this thesis consists of Mössbauer studies of $(V_{0.92}Fe_{0.08})_2FeB_2$ at various temperatures, without and with an external magnetic field. The crystal structure of the studied sample is shown in figures 3.1 to 3.3. Measurements performed by Rogl et al [1] suggest that the sample structure cystallizes in the U_3Si_2 structure type and X-ray analysis revealed that the material is consistent with the centrosymmetric space group P4/mbm. (see table 3.1)
Figure 3.2 displays the two different geometric shapes that form inside the sample. Two connected triangular prisms iterate with tetragonal prisms. Figure 3.3 displays that the blue marked Fe spaces and the red marked B spaces share one plane, as well as the yellow spaces share a separate plane. The distance along the c-axis between this two different planes is always identical. The measurements of Rogl at al [1] also indicates a random distribution of 0.92 V + 0.08 Fe at the yellow marked Vanadium sites. This suggests multiple possible places for ^{57}Fe atoms. On one side there is a fixed position, marked in blue in the figures, and on the other side it can replace vanadium atoms, marked in yellow in the figures. In addition, the red marked B atoms form dumbbells across the rectangular faces of the triangular prisms.

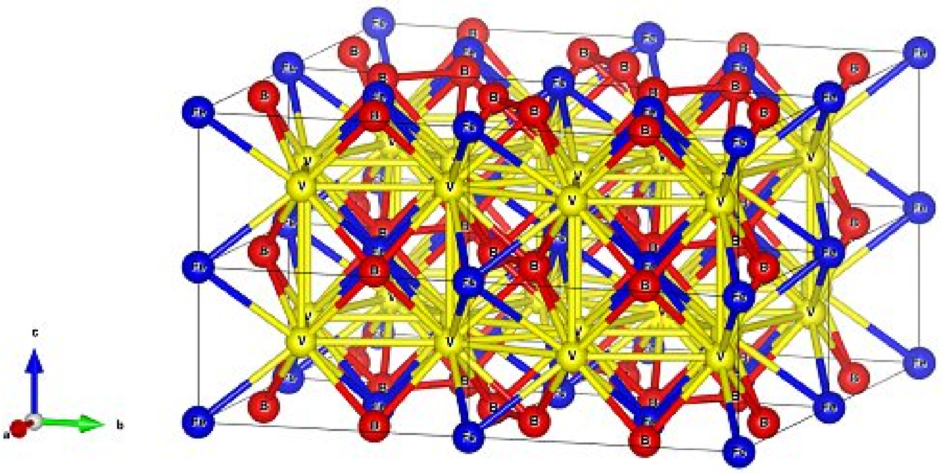

Figure 3.1: Crystal structure of $(V_{0.92}Fe_{0.08})_2FeB_2$ in three-dimensional view.

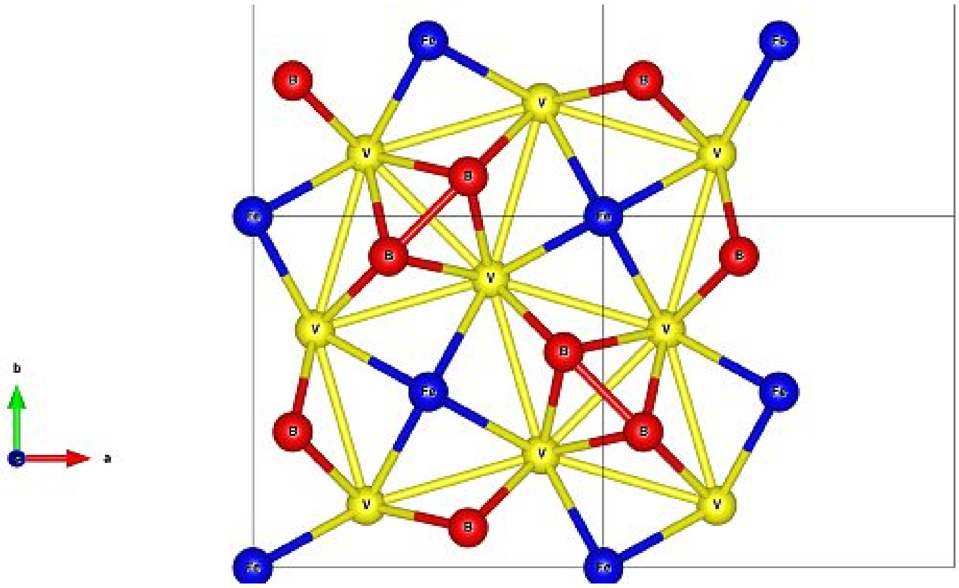

Figure 3.2: Crystal structure of $(V_{0.92}Fe_{0.08})_2FeB_2$ in three-dimensional view, with the c axis pointing outwards the figure.

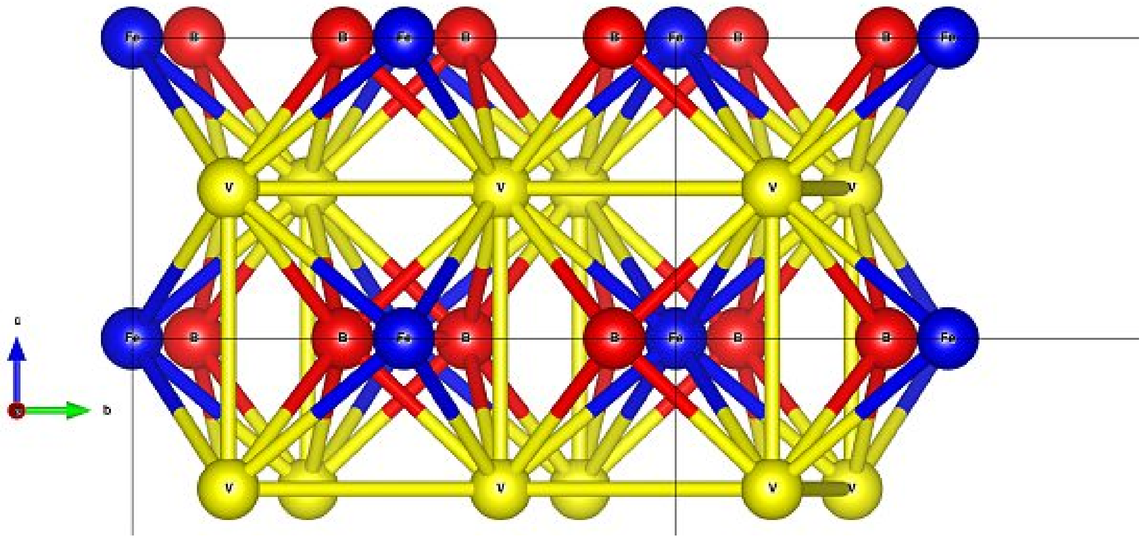

Figure 3.3: Crystal structure of $(V_{0.92}Fe_{0.08})_2FeB_2$ in three-dimensional view, with the b axis pointing outwards the figure.

Table 3.1: Crystallografic data from X-ray single crystal intensity data. Structure standardized with program Structure Tidy [14] [1]

Parameter/compound	Crystal data
Phase composition (EDX, at %)	$V_{36.8}Fe_{23.2}B_{40}$
Refinement composition (at.%)	$V_{1.84}Fe_{1.16}B_2 = V_{2-x}Fe_{1+x}B_2$ (x=0.16)
Structure type	U_3Si_2-type (Mo_2FeB_2-type)
θ range	$2 \leq 2\theta \leq 72.8$
Crystal size	$30 \times 35 \times 50\ \mu m^3$
a,b [nm]	0.555931(9)
c[nm]	0.306781(5)
Reflections in refinement	$146 \geq 4\sigma(F_0)$ of 147
Number of variables	12
Mosaicity	<0.49
$R_{F2} = \sum \vert F_0^2 - F_c^2 \vert / \sum F_a^2$	0.0099
wR2	0.0278
R_{int}	0.056
GOF	1.042
Extinction (Zachariasen)	0.064(8)
M1 in 4h (x,x+1/2,1/2): occ. $U_{11} = U_{22}; U_{33}; U_{12}; U_{23} = U_{13} = 0$	x= 0.17721(3): M1= 0.92 V + 0.08(1) Fe1 0.0031(1);0.0032(1);-.0005(1)
Fe2 in 2a (0,0,0); occ. $U_{11} = U_{22}; U_{33}; U_{23} = U_{13} = U_{12} = 0$	1.00(1) 0.0029(1);0.0070(2)
B1 in 4g (x,x+1/2,0); occ. $U_{11} = U_{22}; U_{33}; U_{23} = U_{13} = 0; U_{12}$	x=0,6135(2); 1,00(1) 0.0040(3); 0.0057(5); -0.0005(4)
Residual electron density: max; min in [electon/nm^3] $\times 10^3$	0.37 (0.05 nm from Fe2); -0.45

3.2 Mössbauer apparatus without external field (Setup A)

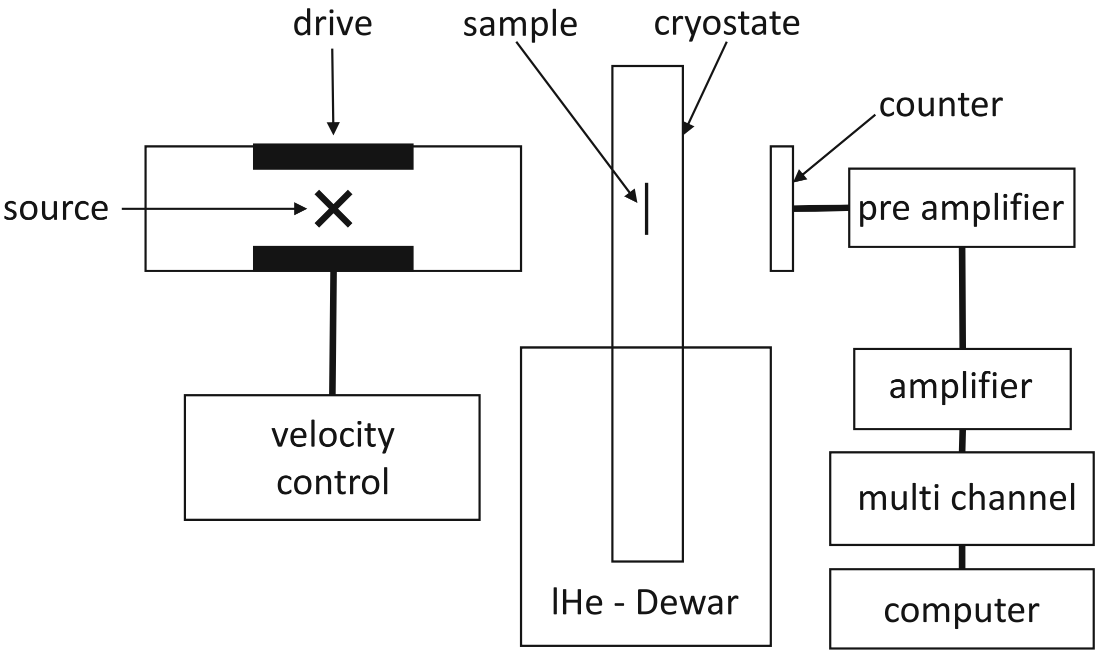

Figure 3.4: Schematic of the experimental setup A.

The experimental setup A consists of a Mössbauer drive, continuous flow cryostat and a detector in line to ensure an unobstructed beam path. A ^{57}Co<u>Rh</u> source is mounted inside the drive. The information gathered by the detector gets boosted by the preamplifier and the amplifier before being inserted into the multichannel analyser. The multichannel analyser is directly connected with a computer for data storage. (See figure 3.4) The cryostat is connected to a temperature controller to ensure a stable temperature during measurements. In depth information about setup A can be found in [15].

3.3 Mössbauer apparatus with external field (Setup B)

The complete setup is outlined in figure 3.5. Setup B differs from Setup A in its ability to apply an external field of up to 15 T at the sample. Several differences occur to accommodate this. The Mössbauer drive moves two sources simultaneous which are connected via a 150 cm rod, which is mounted on springs to ensure a frictionless movement. Source 2 emits gamma rays onto α-Fe-foil, whereas source 2 emits gamma rays onto the sample. The assembly composed of the Mössbauer drive, the two sources and the sample is embedded in the variable temperature controller (VTI). The VTI is inserted into the cryostat, which houses the supra-conducting magnet, the compensation coil mounted around source 1 to compensate any magnetic field at the source, and the internal reservoirs for lHe and lN_2. The counter 2 including its pre-amplifier, sits on top the VTI while counter 1 is located beneath the cryostat. The controls for the Mössbauer drive and the amplifier as well as the multichannel analyser of the two counters are located inside a server rack and connected via wires with the instrument. The following subchapters provide further information about the cryostat and the magnet, as well as more detailed schematics of the VTI and the cryostat.

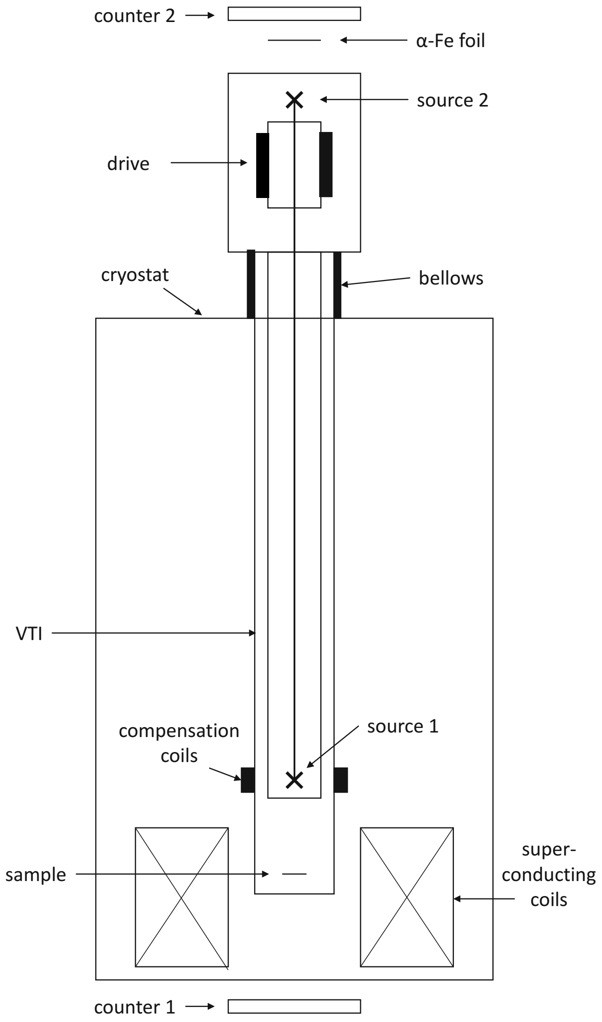

Figure 3.5: Scheme of the experimental setup B.

3.3.1 Hardware

3.3.1.1 Cryostat

The cryostat is a high vacuum insulated vessel featuring a full length liquid nitrogen shield and an additional gas cooled shield surrounding a helium reservoir. (figure 3.6) The outer vacuum case (OVC), liquid nitrogen and liquid helium reservoirs are all welded constructions. The helium reservoir is connected to the neck tube, which is welded into the cryostat top flange. The demountable base flange, which permits access to the magnet, is indium sealed to the reservoir and contains a stainless steel bore tube which itself terminates in an indium seal to which the insert is fitted. The the reservoir is covered with aluminium foil insulation.

The intermediate radiation shield is both supported and cooled by a thermal link to the helium neck tube. It is designed to operate at approximately 20 K. The shield has a copper base flange which is slotted to minimise induced eddy currents in the event of a magnetic quench and has a copper extension tube extending up to the bore of the helium reservoir. The liquid nitrogen reservoir is supported by four filling or vent tubes that are welded into the cryostat top flange and a thermal link to the neck tube. Two of the filling tubes are fitted with pressure relief safety valves. The reservoir extends to the base of the helium reservoir at which point a slotted copper base flange is fitted. An aluminium mylar window in this flange provides experimental access to the absorber. To reduce the emissivity of the reservoir, and therefore the radiated heat load, it is covered with multilayer superinsulation. The nitrogen reservoir has a capacity of 45 litres, the helium reservoir of 30 litres above the magnet. The Variable Temperature Insert (VTI) displayed in figure 3.7 is separated in two chambers and allows measurements at temperatures between 1.5 K and 250 K around the sample. One of these chambers houses source 1, the other one the sample. The temperature can be adjusted individually in both sections. (see also [16])

3.3.1.2 Magnet: Highfield Solenoid C13.6/15.45.13x

The magnet is composed of two sets of concentric solenoids wound on separate formers clamped to a common support flange. The outer sections are wound from $NbTi$ wire whilst the inner section is wound from Nb_3Sn wire. Both types of superconducting wire are of a multifilamentary copper stabilized design. All sections are vacuum impregnated with a potting medium to form a matrix that is both cryogenically and physically stable under the considerable Lorentz forces generated during operation. It shall also be stated that all constituent sections of the magnet are connected to allow serial energization.

The magnet is equipped with a compesation coil, which is necessary to get zero field at the position of the source (Figure 3.5). This compensation coil is also connected in series with the main magnet to ensure that the magnetic field compensation can be retained in the persistent current mode of operation.

A superconducting switch consists of a length of superconducting wire non-inductively wound with a wire electrical heater, which is wound in parallel with entire magnet including the compensation coil. This superconducting wire becomes resistive by raising its temperature using the heater. The switch is then in its open state and current, due to a voltage across the magnet terminals, will flow in the superconducting magnet windings in preference to the resistive switch element. The switch is in its closed state when the heater is turned off and the switch becomes superconducting again. (see also [17])

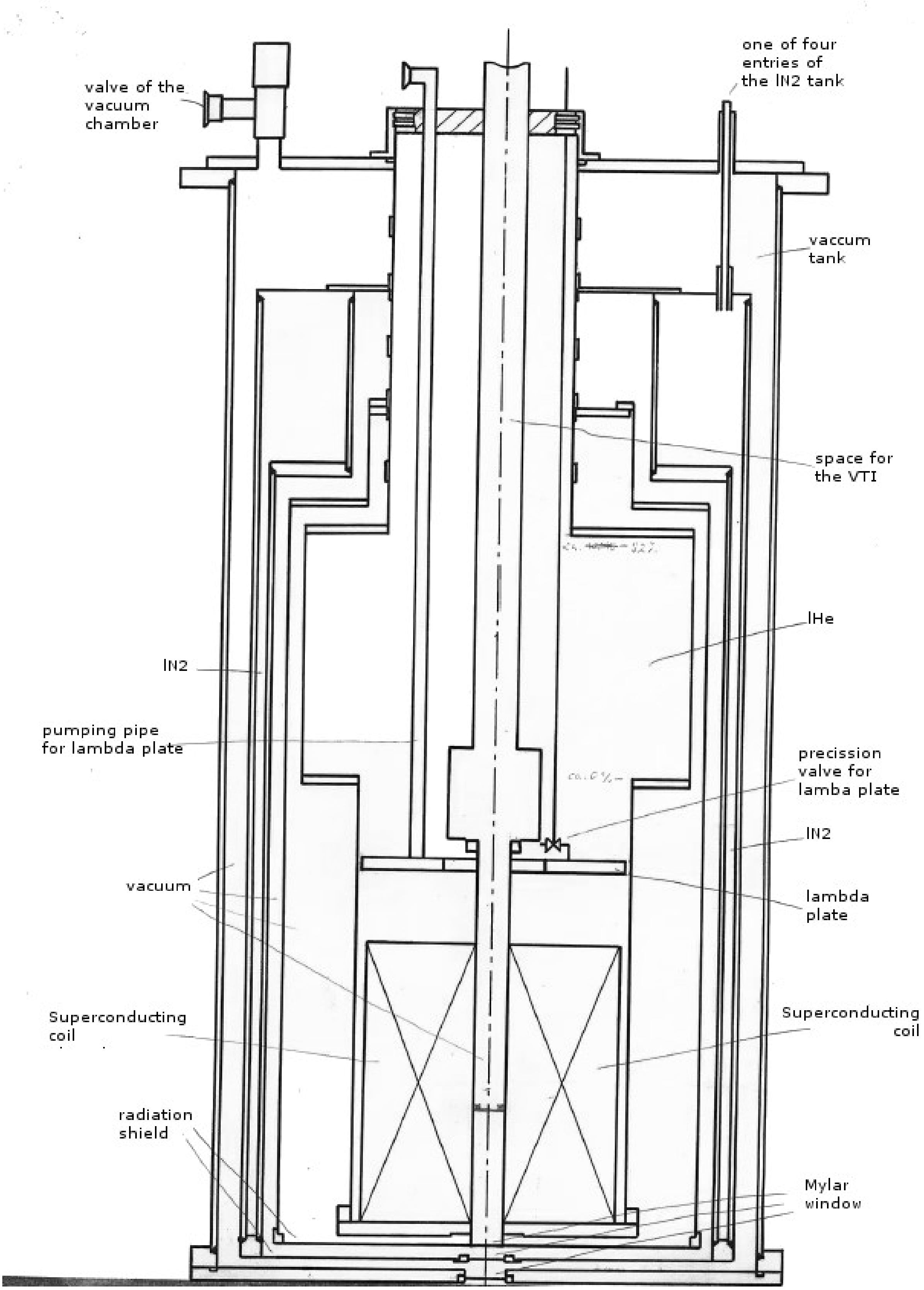

Figure 3.6: Sketch of the cryostat. (setup B)

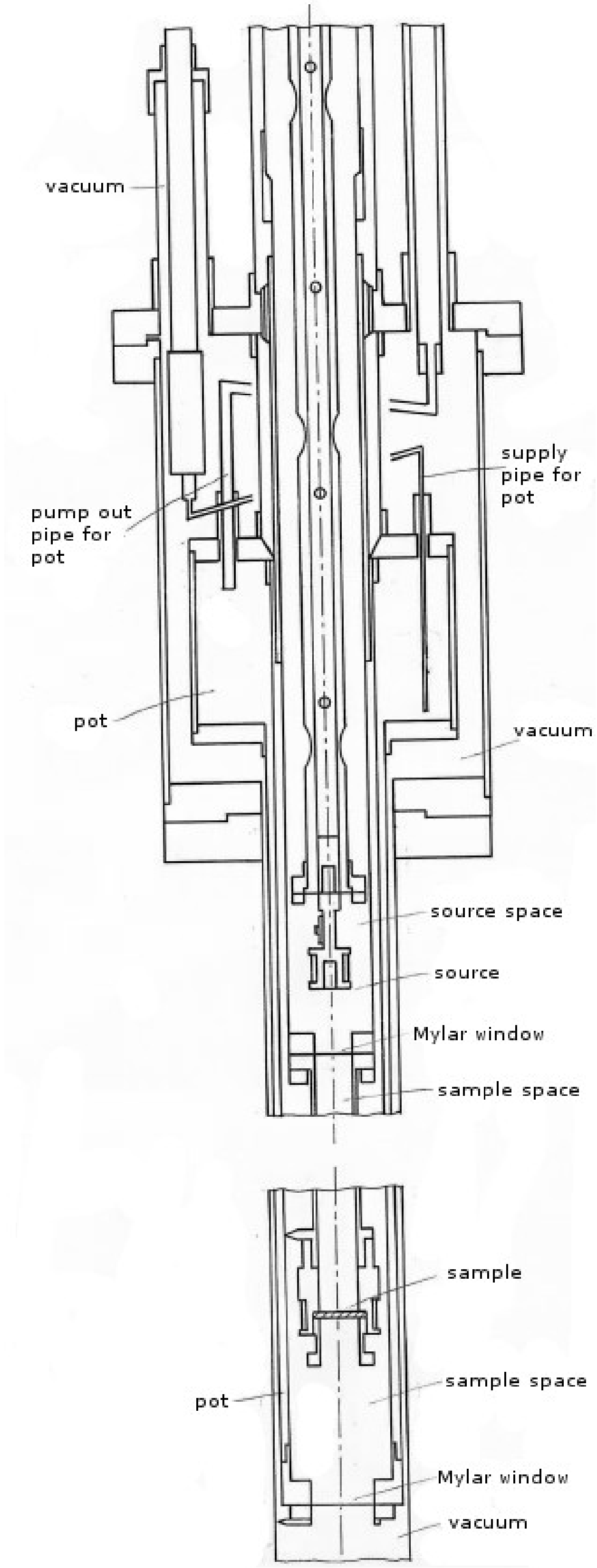

Figure 3.7: Sketch of the Variable Temperature Insert (VTI). (setup B)

3.3.1.3 Power supply MercuryiPS

To get setup B running it was necessary to repair or replace the original power supply, because it didn't work properly. It showed a large drift, which could not be stopped, thus placing the superconducting coil in jeopardy. First a series of efforts to repair the defect unit was undertaken, which had all been unsuccessful. Considerations with the manufacturer about a replacement unit lead to the purchase of a power supply of the type MercuryIPS, which consists of two separate units, working in parallel. This parallel setup is necessary due to the required maximum current of about 78 A, which is essential for the superconducting magnet to reach its maximum field of 15 T, as one single unit is only capable of delivering up to 60 A.
The water cooling of the old power supply was removed from the server rack, in advance to the installation of the power supply, due to the fact that the new power supply is only air-cooled via fans and the gained space inside the server rack allows for optimal airflow and save working conditions for the new power supply. Figure 3.8 displays the new power supply. Instruction on setup and instructions for operation of the power supply MercuryIPS from Oxford Instruments can by found in Appendix A. To run the power supply via computer, a LabView program was developed and integrated into the experimental control software. A description of this program can be found in the following chapter.

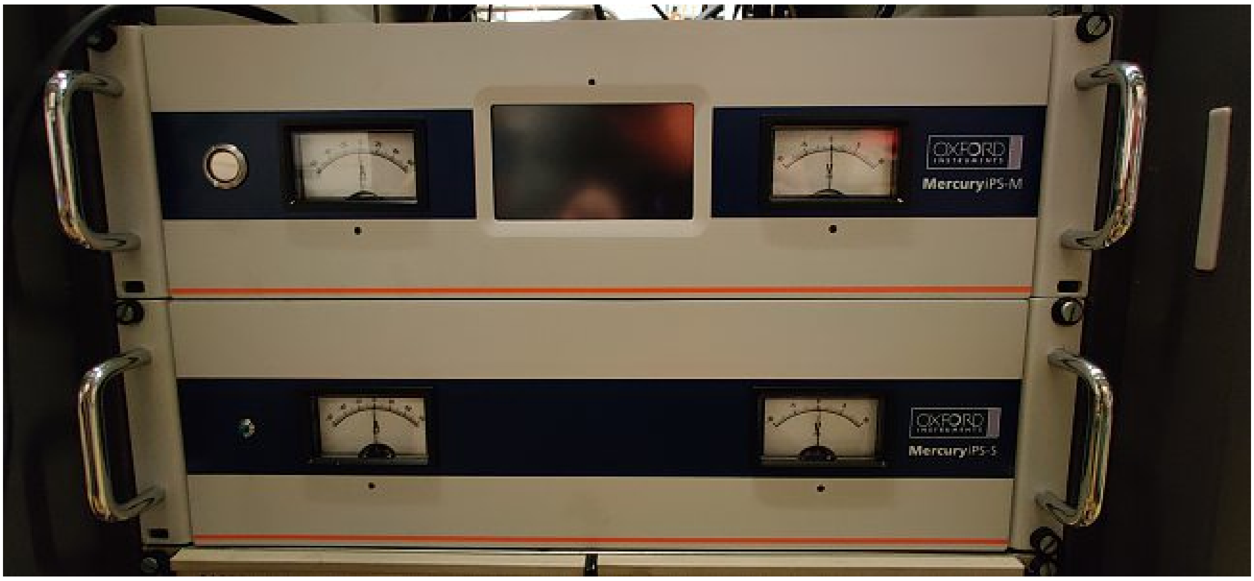

Figure 3.8: Frontpanel of the MercuryIPS Unit.

3.3.2 Software

3.3.2.1 MercuryiPS_Controls

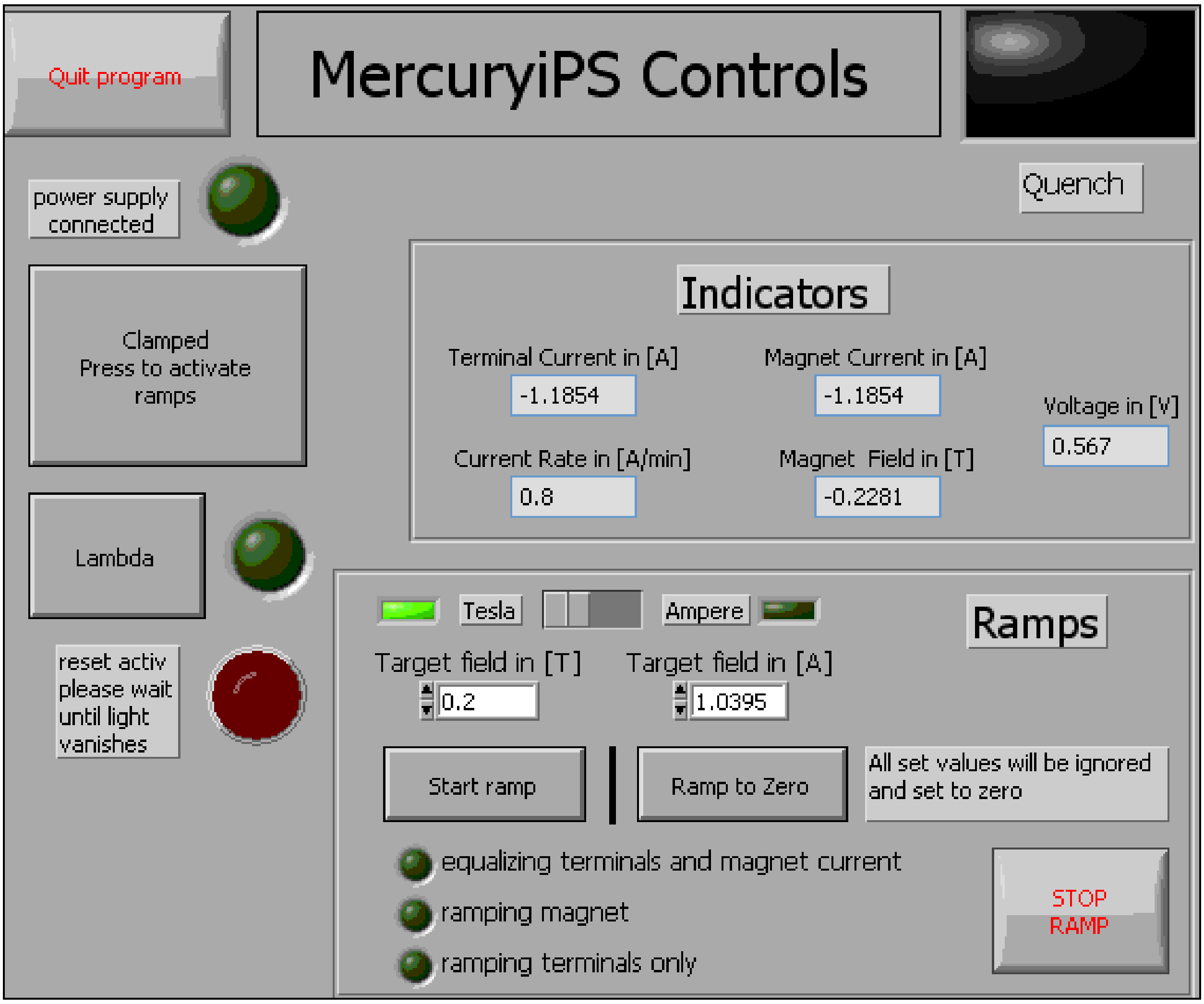

Terminal Current in [A]: -1.1854
Magnet Current in [A]: -1.1854
Voltage in [V]: 0.567
Current Rate in [A/min]: 0.8
Magnet Field in [T]: -0.2281
Target field in [T]: 0.2
Target field in [A]: 1.0395

Figure 3.9: GUI of the implemented MercuryIPS_Controls program.

The program "MercuriPS_Controls", a LabView based control and monitoring software for the power supply "Oxford Instruments MercuryiPS", was written during this work.

The Graphical User Interface consists of the two groups "Indicators" and "Ramps" as well as of several independent buttons and indicators.
The group "Indicator" displays the latest transmitted values of the current and the voltage at the terminals of the power supply, the current and the magnet field inside the magnet and the actual rate used during field change. The units of all values are noted in their descriptions. The group "Ramps" consist of everything that is needed to perform a field ramp of the magnet. The slider between "Tesla" and "Ampere" decides which variable, "Target field in [T]" or "Target field in [A]", shall be used for the ramp. An active LED indicates which mode is active. The other variable will be calculated automatically. A press on the button "Start ramp" will start a ramp of the magnet to the set field value. The controls will be set to zero if "Ramp to Zero" will be pressed, and the magnet will be de-energized. The three indicator lights "equalizing terminals and magnet current", "ramping

magnet" and "ramping terminals only" indicate the actual state of the ramp process. The ramp can be stopped at any moment by pressing the button "STOP RAMP". The program will cancel the current ramp and set the power supply into a safe idle position. The red LED indicator next to the ramp group ignites during this process. A new ramp should not be started until the light extinguishes. The indicator "power supply connected" lights up, if the connection between the computer and the power supply unit is established. The button "Lambda" shall only be pressed if the Lambda fridge mode is in operation and allows to energize the magnet up to 15 T.

The indicator "Quench" in the upper right corner lights up in red if a voltage of more than three Volts is measured at the terminals of the MercuryiPS unit. This leads to an emergency discharge of the magnet. In such case the unit should be checked as soon as possible.

The program can be stopped by pressing the button "Quit program". This will also close the connection between the computer and the power supply.

The program records into a protocol-file, every time "Start Ramp" or "Ramp to Zero" is pressed. The first entry contains the momentary persistent current and the new set point and a second entry is made at the end of a ramp consisting the ending persistent current. The standard path for the protocol file is "C:\MB\MercuryiPS\Protokol.txt".

3.3.2.1.1 Troubleshooting

If the Error code "-1074003951" occurs, check that the USB cable is not bow-taut and restart the MercuryiPS unit.

3.4 Analysis software

Two different programs were used to assist the analysis of the collected data. The following section provide a brief explanation to their mode of operation.

3.4.1 MossWinn 4.0i

MossWinn 4.0i is a Mössbauer spectroscopy analysis program written and sold by Dr. Zoltán Klencsár. All data obtained by setup A were analysed using this software and the model described in chapter 4.1. Each subspectrum was calculated by solving the static Hamiltonian for mixed magnetic and quadrupole interactions, as implemented in MossWinn 4.0i. [18] The z-axis is chosen to be parallel to the hyperfine magnetic field and the Hamiltonian is expressed as in [19]

$$H(I)_{m,m} = -\omega_H \hbar m + \frac{\omega_Q \hbar}{2}\left(3\cos^2\beta - 1 + \eta \sin^2\beta\cos(2\alpha)\right)\left[3m^2 - I(I+1)\right] \tag{3.1}$$

$$\begin{aligned} H(I)_{m,m+1} =& \frac{3\omega_Q\hbar}{2}\sin\beta\left\{\cos\beta - \frac{\eta}{6}\left[(1+cos\beta)\,e^{2\alpha i} - (1-\cos\beta)\,e^{-2\alpha i}\right]\right\}(2m+1)\cdot \\ & \sqrt{(I-m)(I+m+1))} \end{aligned} \tag{3.2}$$

$$\begin{aligned} H(I)_{m,m+2} =& \frac{3\omega_Q\hbar}{4}\left\{\sin^2\beta + \frac{\eta}{6}\left[(1+cos\beta)^2\,e^{2\alpha i} + (1-\cos\beta)^2\,e^{-2\alpha i}\right]\right\}\cdot \\ & \sqrt{(I+m+2)(I+m+1)(I-m)(I-m-1)} \end{aligned} \tag{3.3}$$

$$\omega_H = \frac{g_N(I)B\nu_N}{\hbar} \qquad \omega_Q = \frac{1}{\hbar}\frac{eV_{zz}Q}{4I(2I-1)}$$

with B indicating the flux density of the hyperfine magnetic field, $\eta = \frac{V_{xx}-V_{yy}}{V_{zz}}$ the asymmetry parameter of the electric field gradient, β denotes the angle of rotation around the y-axis that aligns B_{hf} with the direction of the eigensystem of the EFG that is associated with its element having the biggest magnitude (V_{zz}). α is the angle of rotation around the axis of (V_{zz}), which is needed to align the rotated y-axis reference system with the (V_{yy}) axis. I expresses the angular momentum quantum number of the excited or ground state of the Mössbauer nucleus. The value of m is element of the list (-$I, -I+1, ..., I-1, I$). [18]

The thickness of the absorber was considered by using the integrated transmission integral of MossWinn4.0i. The transmission spectrum is calulated via:

$$N(v) = N(\infty)\left((1-b)\frac{T(v)}{T(\infty)} + b\right) \tag{3.4}$$

$$T(v) = 1 - f_s + f_s \int L_s(w-s, \Gamma_s)e^{-\tau A_n(w)}dw \tag{3.5}$$

$$L_s(w-v, \Gamma_s) = \frac{\Gamma_s}{2\pi}\frac{1}{(w-v)^2 + \dfrac{\Gamma_s^2}{4}} \tag{3.6}$$

where $N(v)$ corresponds to the envelope of the fitting curve, $N(\infty)$ is the baseline, b the background fraction of the gamma quanta, τ the effective thickness of the absorber, f_s the Mössbauer Lamb factor of the source and Γ_s the full width at half maximum of the peak emitted by the source.[18]

3.4.2 MGUI

MGUI is the graphical user interface of the Fortran based routine MHAF written and maintained by the Mössbauer group of the Institute of Solid State Physics at the TU Wien. It solves the Hamiltonian

$$H = \frac{eQV_{zz}}{\hbar 4I(2I-1)} \left(3\vec{I}_z^2 - \vec{I}^2 + \frac{\eta}{2} \left(\vec{I}_+^2 - \vec{I}_-^2 \right) \right) - \frac{\mu_N}{\hbar I_N} \vec{H}_0 \vec{I}_z \tag{3.7}$$

using the nuclear magneton μ_N, the nuclear quadrupole moment eQ, the hyperfine field $\vec{H}_0$, the nuclear spin I, the vectorial nuclear spin $\vec{I}$, the asymmetry parameter η and the Plank constant $\hbar$. This is calculated for each subspectrum independently and subsequently added to one cumulative fit.

The program provides a set of parameters for each subspectrum, which allows a fast and easy method of analysing data, collected during Mössbauer spectroscopy experiments. These parameters include the isomer shift δ in mm/s, the hyperfine field in mm/s and kG, the quadrupole splitting parameter $\mathrm{eQV_{zz}}/4$ in mm/s and the line width Gamma/2 in mm/s. The provided possibility of locking these parameters during the fitting procedure, individually for each subspectum or for all subspectra combined, to predetermined values or inside a given range, was of significant importance for the analysis provided in the following chapters. As the fit procedure is defined as the search of the global minimum of the chi-square function, which determines the quality of the fit, it shall be noted that this gives the operator the opportunity to prevent the build-in fit routine on getting captured in local minima. The lack of this possibility in the program MossWinn 4.0i lead to the change to the other analysis program.

The thickness of the sample is taken into account by the Mørup - Both formula [20].

MGUI includes a tool which summarize the gathered information in a compact manner in a report. Examples of these reports can be found in appendix B.

4 Analysis and Discussion

This chapter contains the created models, which were used to analyse the collected data, as well as the discussion of the analysis using model 2.

4.1 Model 1

Due to the structure of the sample discussed in chapter 3.1 and the assumption of a random distribution of Fe and V on vanadium sites, as described by Rogl et al [1], a modified binomial distribution model was created to describe the spectra. Only the possible interaction between nearest neighbour iron atoms, the first shell, was considered. Therefore, an iron atom on a V site, will always have four iron atoms on the fixed Fe site in the nearest neighbour shell. In contrast, an Fe atom sitting on an Fe site has multiple different sets of nearest neighbour atoms. This depends on the possibility of an iron atom switching place with a vanadium one. To account for this, a binomial distribution was calculated using formula (4.1) [21] were p equals 0.08 (the concentration of Fe-atoms on V-sites) and N equals 8 (the number of nearest neighbour (V,Fe) sites to a Fe-site). The results for the different values of n are summarised in table 4.1.

$$P(n|p,N) = \binom{N}{n} p^n (1-p)^{N-n} \tag{4.1}$$

$$\begin{gathered} 0.16\ \mathrm{Fe} + 1\ \mathrm{Fe} = 1.16\ \mathrm{Fe} \\ P_{\text{"Fe"}} = \frac{0.16}{1.16} = 0.1379 \approx 0.14 \qquad P_{\text{"V"}} = \frac{1}{1.16} = 0.8620 \approx 0.86 \end{gathered} \tag{4.2}$$

Owing to the nature of the sample, the ratio between the "Fe" and the "V" place is 86:14, due to its mass ratio as 0.16 Fe located on "V" sites and one Fe on each "Fe" site. This is displayed in equation 4.2. The probability of the Fe on the "Fe" site was multiplied by the fraction $\frac{86}{100}$ and the probability of the Fe on the "V" site was multiplied by $\frac{14}{100}$ to accommodate the ratio. It is also important to consider that it is not possible to measure with infinite accuracy. As a result, possible constellations of iron atoms with a probability below 1.5% after factorisation were cancelled and the remaining ones were renormalised. This results in a model using four subspectra as shown in table 4.2. The names are composed of the respective site and are numbered with decreasing probability.

Table 4.1: Probabilities for specific numbers of Fe atoms in first neigbour shell of Fe on Fe site.

number of Fe atoms in first shell (n)	Probability $P(n\|p, N)$
0	0.51322
1	0.35702
2	0.10866
3	0.018897
4	0.0020540
5	0.00014289
6	0.0000062126
7	0.00000015435
8	0.0000000016777

Table 4.2: Summary of the subspectra and their areas used in the fitting procedure.

Name of the subspectra	Area of given subspectra in % of the complete fit
V1	33.8
Fe1	34.7
Fe2	24.2
Fe3	7.3

Analysis of the collected data using this model was done using the analysis software MossWinn 4.0i (see chapter 3.4.1). It was selected due to its ability to fit multiple data sets in parallel and with interlaced parameters. This analysis revealed physical incorrect results. The temperature dependence of the isomer shift and eQV$_{zz}$ in particular displayed an erratic behaviour for all subspectra, as they did not follow the expected smooth trend, neither for the individual subspectra nor as a whole. This lead to the development of a model (Model 2) using distributions of the magnetic hyperfine field (see chapter 4.2).

4.2 Model 2

In this model the spectra are analysed according to hyperfine field distributions. It was created due to the not satisfying results obtained by the analysis of the collected data, using model 1 (see chapter 4.1)
The model consists of 21 subspectra that share a common value for each of the following parameters, $eQV_{zz}/4$, which describes the quadrupole splitting of the spectrum, CS, describing the center shift, and Gamma/2, which describes the line width. Each subspectrum differs from the rest by its value of the magnetic hyperfine splitting. This value is fixed and in the range from 0 kG to 217,93 kG. It rises in increments of 10,9 kG from one subspectrum to the next. This values were chosen in order to fit all obtained spectra. The broadest splitting was found for the data gathered at 4.3 K and an applied magnetic field of 12 T. (see table 4.3)
The parameters common to all 21 subspectra, $eQV_{zz}/4$, CS and Gamma/2, were not fixed during fitting operations in contrast to the parameter representing the magnetic hyperfine splitting.

This model has the disadvantage of describing only the overall behaviour of the material, in contrast to model 1, which gives the possibility to describe the behaviour at certain fixed sites inside the crystal structure. This is a consequence of the fact that the 21 subspectra in model 2 do not resemble fixed positions inside the material.

The program MGUI was used, due to its better control of fixed parameters during fitting operation compared to MossWinn 4.0i, to analyse the collected data of setup A and B using this model. An additional rule was implied for all measurements without external applied magnetic field.

Table 4.3: Compilation of hyperfine parameters obtained during the analysis of the data obtained in setup A and B using the program MGUI and model 2. B_{ext} is the external applied magnetic field, $\Gamma/2$ represents the line-width at half height and θ is the angle located between the direction of the external and the internal magnetic field.

Setup A							
Temperature	B_{ext}	eQVzz/4	Center shift	$\Gamma/2$	θ	Mean B_{eff}	Figure
[K]	[T]	[mm/s]	[mm/s]	[mm/s]	[◦]	[kG]	
		±0.02	±0.002	±0.002			
4.2	0	-0.09	-0.021	0.218	54.735	89.294	Figure 4.4
20	0	-0.074	-0.033	0.19	54.735	83.66	Figure 4.6
30	0	-0.088	-0.035	0.197	54.735	69.015	Figure 4.8
40	0	-0.099	-0.028	0.192	54.735	61.149	Figure 4.10
50	0	-0.091	-0.024	0.173	54.735	57.553	Figure 4.12
60	0	-0.111	-0.02	0.197	54.735	43.235	Figure 4.14
80	0	-0.121	-0.021	0.256	54.735	24.826	Figure 4.16
100	0	-0.184	-0.022	0.201	54.735	0.322	Figure 4.18
125	0	-0.186	-0.058	0.17	54.735	0.644	Figure 4.19
150	0	-0.181	-0.057	0.158	54.735	0.63	Figure 4.20
175	0	-0.19	-0.084	0.169	54.735	0	Figure 4.21
200	0	-0.187	-0.098	0.163	54.735	0	Figure 4.22
294	0	-0.182	-0.143	0.165	54.735	0	Figure 4.23

Setup B							
Temperature	B_{ext}	eQVzz/4	Center shift	$\Gamma/2$	θ	Mean B_{eff}	Figure
[K]	[T]	[mm/s]	[mm/s]	[mm/s]	[◦]	[kG]	
		±0.02	±0.002	±0.002			
4,3	0	-0.062	-0.18	0.203	54.735	92.931	Figure 4.24
4,3	9	-0.044	-0.174	0.203	67.79414	116.023	Figure 4.26
4,3	12	-0.045	-0.185	0.192	56.38585	131.873	Figure 4.28
20	12	-0.047	-0.174	0.248	46.16108	128.127	Figure 4.30
40	12	-0.046	-0.185	0.196	53.11122	126.207	Figure 4.32
100	12	-0.043	-0.175	0.256	-0.11004	109.712	Figure 4.34
150	12	-0.037	-0.205	0.16	0	115.612	Figure 4.36

4.3 Fitting procedure

This chapter shortly describes how the analysis of the data collected during this work, using model 2, has been conducted.

All analysis displayed in the following chapters and in the tables 4.3 to 4.5, started by applying model 2 to the measurement conducted at 4.2 K and without external applied field. The program MGUI was used as stated above. An additional rule has been applied to the standard fitting process for all measurements without external applied magnetic field. The value of 54.735 was fixed for the angle θ in all subspectra with a non-zero magnetic hyperfine splitting and this value was also fixed for the angle β, if no magnetic hyperfine splitting is present in a given subspectrum, to take into account the polycrystalline nature of the sample.
The result of each fitting procedure was the starting point for the fitting procedure of the measured data at the next higher temperature. This has been done until all data collected in setup A had been analysed.
The starting point of the fitting procedure for data collected in setup B was the final fit of the data of setup A with the corresponding temperature. The handling of θ, the angle between the direction of the external and the internal magnetic field, is the only difference between the fitting procedure of data from the two setups. As stated above the value of θ was fixed for all analysis of setup A, in contrast θ was fitted freely for all subspectra and all measurements conducted within external magnetic fields in setup B. The mean average of these θ values stated in table 4.3 was calculated via equation (4.3), where i is the number of a certain subspectrum and A describes the relative area of that given subspectrum.

$$\text{mean average } \theta = \frac{\sum_{i}^{21} \theta_i \cdot A_i}{\sum_{i}^{21} A_i} \tag{4.3}$$

The analysis of the spread of the magnetic hyperfine field has been done the following way for each measurement. A Gaussian curve was overlaid with each of the columns, which represent the relative area of a given subspectrum (for example see figure 4.5). These curves were added with each other to create one function

$$f(H) = \sum_{i}^{21} \left(y_0 + \frac{A_i e^{\frac{-4\ln(2)\left(H - H_{ci}\right)^2}{w^2}}}{w\sqrt{\frac{\pi}{4\ln(2)}}} \right) \quad , \tag{4.4}$$

using the base line $y_0 = 0$, the center of each Gaussian curve H_{ci} equal to the magnetic hyperfine splitting of a given subspectrum i, the area of that subspectrum A_i and the full width at maximum height w, which was set equal to all 21 Gaussian curves.

The obtained function f(H) was analysed by fitting several Gaussian functions $g_k(H)$ (equation (4.5)), in numerical quantity equal to the number of maxima of f(H), to function f(H).

$$g_k(H) = y_0 + \frac{A_k e^{\frac{-4\ln(2)\left(H - H_{ck}\right)^2}{w_k^2}}}{w_k\sqrt{\frac{\pi}{4\ln(2)}}} \tag{4.5}$$

The parameters in equation (4.5) are the following. A_k represents the area of that curve, H_{ck} the barycenter, w_k the standard deviation sigma and the baseline y_0 was kept at zero.

The resulting areas of the fitted Gaussian peaks were renormalised for each peak using

$$\text{rel.Area}_k = \frac{A_k}{\sum\limits_k A_k} \tag{4.6}$$

The results of this analysis are summarized in table 4.4 and 4.5 and discussed in greater detail in capter 4.4.3.

Table 4.4: Compilation of the analysis of the hyperfine field distribution of the data collected at various temperatures and without external applied magnetic field in setup A using model 2 and the Gauss fuctions described in chapter 4.3.

Setup A									
Measurement		Parameter	Value	Standard deviation	Measurement		Parameter	Value	Standard deviation
4.2 K / 0 T	Peak 1	Barycenter	93.87793	0.0259	50 K / 0 T	Peak1	Barycenter	87.43222	0.02994
Figure: 4.5		rel. Area	0.91736681	0.002575642	Figure: 4.13		rel. Area	0.335481117	0.001854966
		Sigma	8.95792	0.02813			Sigma	8.9293	0.02776
	Peak 2	Barycenter	61.75067	0.22168		Peak2	Barycenter	54.19771	0.0665
		rel. Area	0.08263319	0.002320044			rel. Area	0.453096753	0.002658805
		Sigma	7.49124	0.2347			Sigma	16.98934	0.11491
						Peak3	Barycenter	13.5585	0.04259
20 K / 0 T	Peak1	Barycenter	95.94817	0.05518			rel. Area	0.21142213	0.001195154
Figure: 4.7		rel. Area	0.558967183	0.017392867			Sigma	9.2846	0.04166
		Sigma	8.27741	0.10757					
	Peak2	Barycenter	75.74974	1.0167	60 K / 0 T	Peak1	Barycenter	73.02997	0.02579
		rel. Area	0.379092831	0.020535631	Figure: 4.15		rel. Area	0.379633669	0.000843238
		Sigma	17.87319	0.61255			Sigma	11.61925	0.02846
	Peak3	Barycenter	19.08012	0.54839		Peak2	Barycenter	41.79042	0.02129
		rel. Area	0.061939986	0.003302984			rel. Area	0.268658441	0.000733966
		Sigma	10.06245	0.56712			Sigma	8.15658	0.02323
						Peak3	Barycenter	11.06187	0.01099
30 K / 0 T	Peak1	Barycenter	87.36123	0.01568			rel. Area	0.35170789	0.000514851
Figure: 4.9		rel. Area	0.524389461	0.001367658			Sigma	7.40103	0.01211
		Sigma	8.69172	0.01382					
	Peak2	Barycenter	57.38393	0.06387	80 K / 0 T	Peak1	Barycenter	65.33456	0.03758
		rel. Area	0.386290838	0.001571548	Figure: 4.17		rel. Area	0.140731292	0.000909703
		Sigma	15.26677	0.06498			Sigma	6.07871	0.03636
	Peak3	Barycenter	10.24897	0.04663		Peak2	Barycenter	40.13081	0.07911
		rel. Area	0.0893197	0.000531963			rel. Area	0.136968467	0.001191529
		Sigma	7.82633	0.05045			Sigma	10.00634	0.10761
						Peak3	Barycenter	10.87522	0.00585
40 K / 0 T	Peak1	Barycenter	87.88826	0.01733			rel. Area	0.722300241	0.000695407
Figure: 4.11		rel. Area	0.292877794	0.002037863			Sigma	5.90729	0.00604
		Sigma	7.36326	0.02826					
	Peak2	Barycenter	62.45954	0.11531					
		rel. Area	0.517982354	0.003069897					
		Sigma	20.8838	0.10882					
	Peak3	Barycenter	13.36325	0.03659					
		rel. Area	0.189139852	0.000855358					
		Sigma	8.82704	0.03783					

Table 4.5: Compilation of the analysis of the hyperfine field distribution of the data collected at various temperatures and with and without external applied magnetic field in setup B using model 2 and the Gauss fuctions described in chapter 4.3.

Setup B

Measurement		Parameter	Value	Standard deviation
4.3 K / 0 T	Peak1	Barycenter	98.59633	0.01467
Figure: 4.25		rel. Area	0.880080247	0.001164897
		Sigma	12.8322	0.01123
	Peak2	Barycenter	59.608	0.20711
		rel. Area	0.119919753	0.001278495
		Sigma	18.09687	0.17818
4.3 K / 9 T	Peak1	Barycenter	131.86923	0.08495
Figure: 4.27		rel. Area	0.789647278	0.003716175
		Sigma	21.01255	0.09649
	Peak2	Barycenter	66.34631	0.25676
		rel. Area	0.210352722	0.003263241
		Sigma	17.96301	0.27153
4.3 K / 12 T	Peak1	Barycenter	151.5842	0.04115
Figure: 4.29		rel. Area	0.803580356	0.002162747
		Sigma	23.70504	0.04951
	Peak2	Barycenter	65.11915	0.18326
		rel. Area	0.196419644	0.002293461
		Sigma	25.26268	0.22589
20 K / 12 T	Peak1	Barycenter	150.07941	0.09293
Figure: 4.31		rel. Area	0.719418624	0.004069576
		Sigma	24.27565	0.10115
	Peak2	Barycenter	84.08883	0.26551
		rel. Area	0.199106015	0.003203822
		Sigma	22.76449	0.38941
	Peak3	Barycenter	30.07828	0.20529
		rel. Area	0.081475362	0.002068335
		Sigma	13.26754	0.22782
40 K / 12 T	Peak1	Barycenter	140.30559	0.06089
Figure: 4.33		rel. Area	0.839025817	0.004456826
		Sigma	29.49816	0.10233
	Peak3	Barycenter	33.95065	0.29613
		rel. Area	0.160974183	0.003463918
		Sigma	27.46003	0.39404
100 K / 12 T	Peak1	Barycenter	115.82743	0.07571
Figure: 4.35		rel. Area	1	0
		Sigma	17.31659	0.08376
150 K / 12 T	Peak1	Barycenter	117.39415	0.02441
Figure: 4.37		rel. Area	1	0
		Sigma	8.18982	0.02534

4.4 Discussion of the analysis of model 2

Figure 4.1 to 4.3 show all the measured and analysed Mössbauer spectra.

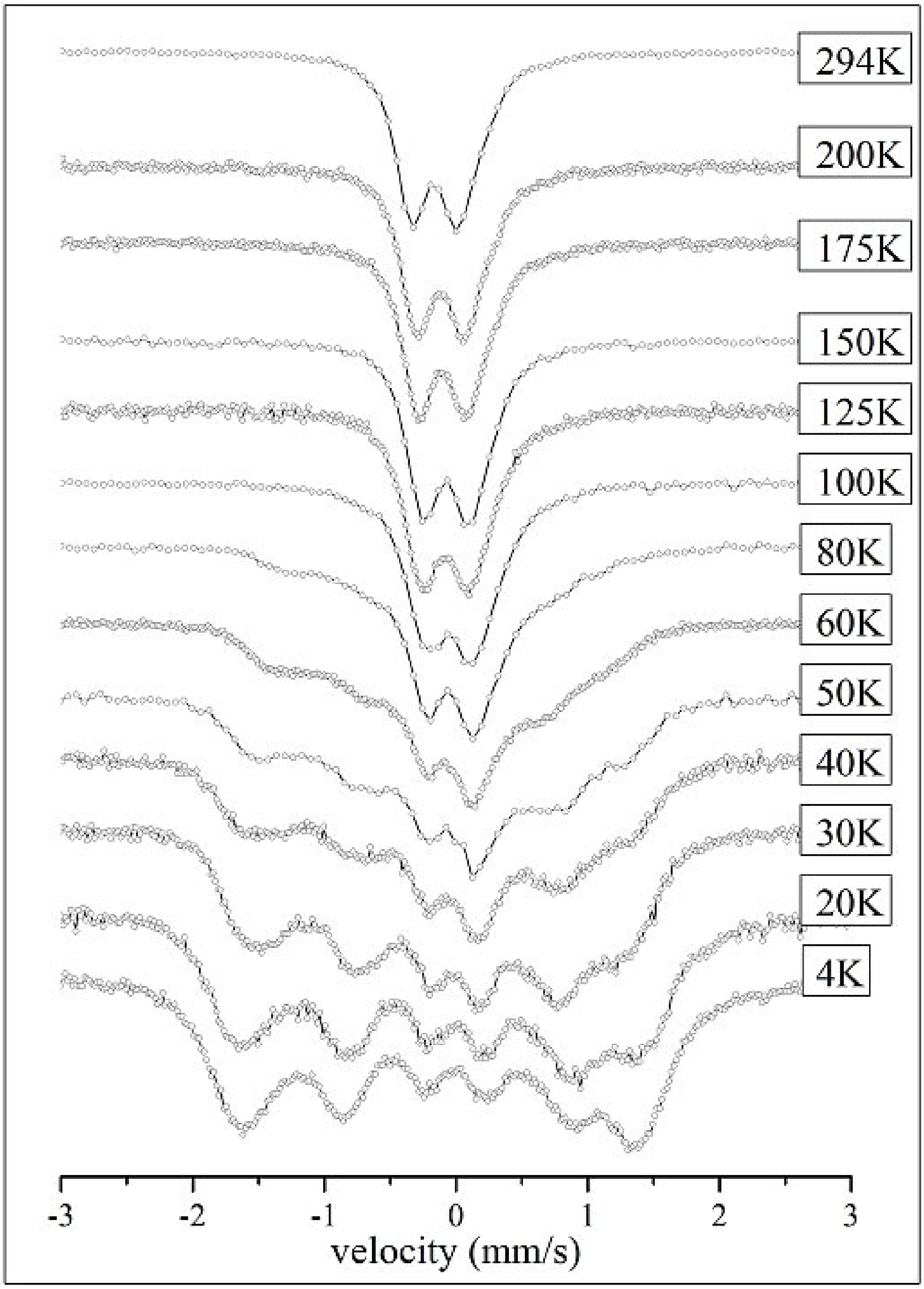

Figure 4.1: Mössbauer spectra at various temperatures without external magnetic field. These measurements have been done using setup A.

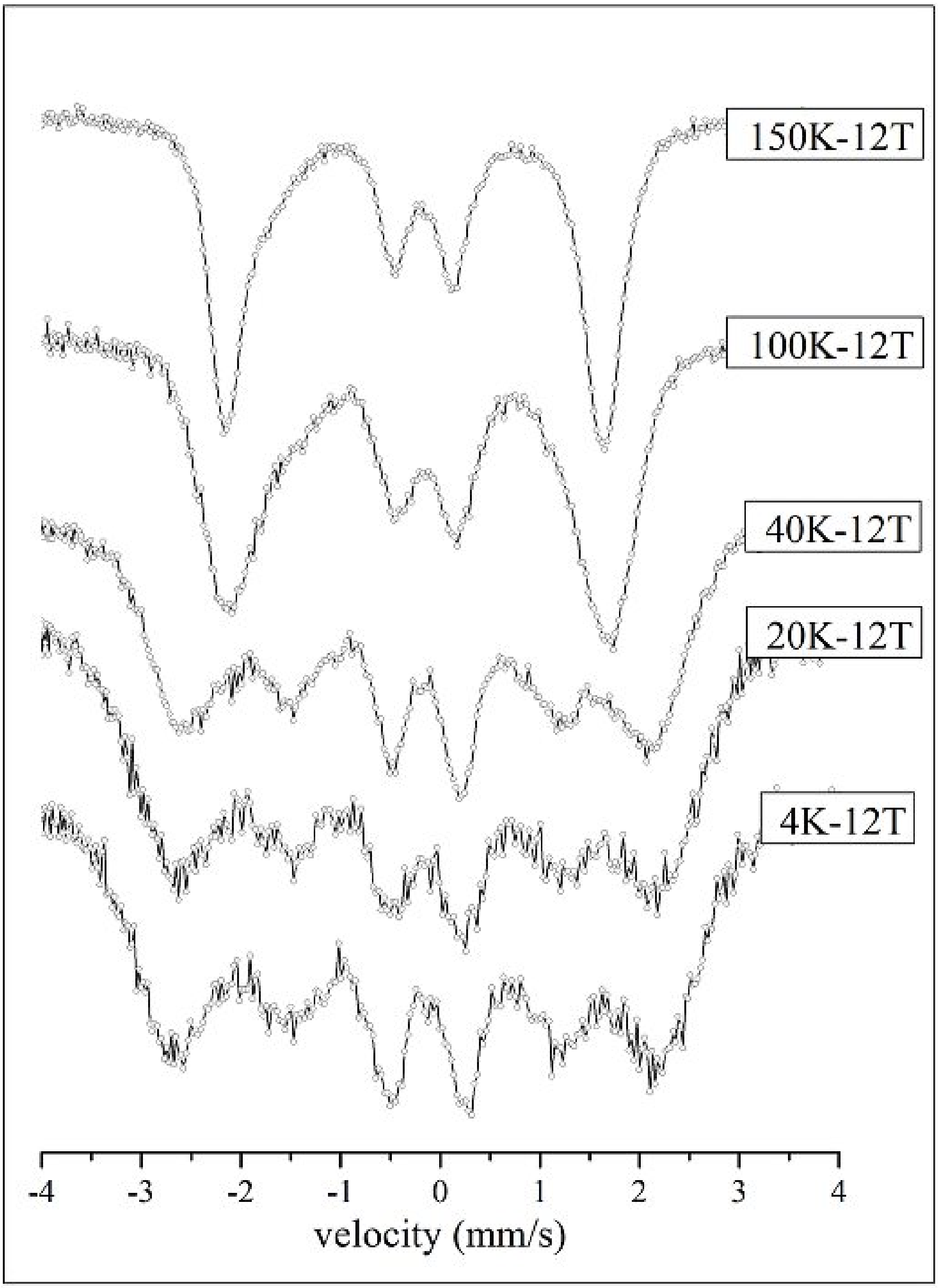

Figure 4.2: Mössbauer spectra at various temperatures with external magnetic field of 12 T. These measurements were done using setup B.

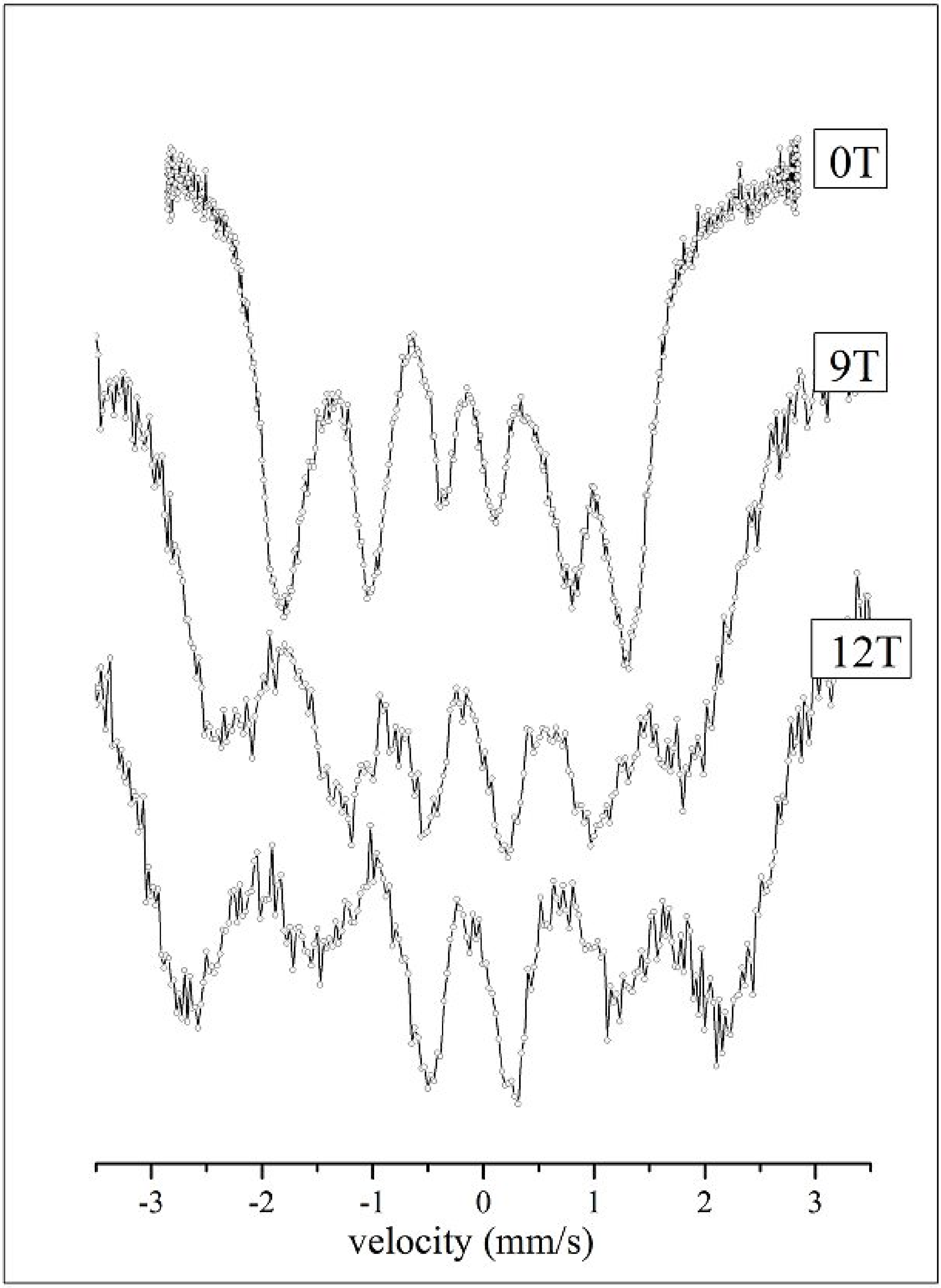

Figure 4.3: Mössbauer spectra at 4.3 K with various external magnetic fields. These measurements have been done using setup B.

The collected data of the Mössbauer measurements in setup A display (figure 4.1) an asymmetric six line spectrum at low temperatures from 4.2 K to 30 K, which slowly merges from 40 K to 80 K into one double peak with small side peaks on a broader background. From 100 K to 294 K a clean two line spectrum is unveiled. The position of the two inner peaks shifts to negative velocities with rising temperature. Figures 4.3 and 4.2 display the collected data obtained during measurements using setup B. Figure 4.2 reveals a similar asymmetric six line spectrum for temperatures below 40 K for measurements that are conducted using an applied magnetic field of 12 T as found for measurements carried out using setup A. The first differences occur at a temperature of 40 K. The spectrum obtained with an applied magnetic field shows greater similarities to the spectra of lower temperatures obtained with the same external applied field, than to the data collected without an external applied magnetic field. The infield measurements conducted at 100 K and 150 K revealed four line spectra, where the inner two line mirror the two lines found at measurements done using setup A and no external magnetic field. The position of the four outer peaks of the spectra obtained at temperatures below 100 K and in an applied magnetic field, reveal the possibility that these peaks collapse with higher temperature into the outer two peaks observed at 100 K and 150 K. The broadening of the outer two peaks of the spectrum obtained at 100 K assists this observation. Figure 4.3 displays the collected data of Mössbauer measurements conducted at 4.3 K and various applied magnetic fields, ranging from 0 T to 12 T. The overall appearance of these spectra is quite similar, with the exception of the fact, that the distance between the peaks rises with rising applied field. This increase in measured hyperfine fields with applied field points to parallel orientation of the internal field and the applied field. As it is known that the magnetic moments for Fe are antiparallel to the internal fields, the magnetic moments should be antiparallel to the external fields. This may point to antiferromagnetic coupling inside the sample.

The vanishing of the second and fifth peak in measurements conducted in external applied magnetic fields for temperatures from 100 K upward (figures 4.34 and 4.36), as well as the fact that measurements without external applied field in the same temperature range reveal spectra displaying only a double (figure 4.18 to 4.23), strongly suggests a paramagnetic behaviour of the sample in that temperature range. This correlates with the finding of the magnetisation measurements done by Rogl et al [1]. They found a magnetic phase transition at around 110 K with paramagnetic behaviour at higher temperatures.

The difference in the value of the center shift for measurements obtained in setup A and B at identical temperatures and without external magnetic field occurs mainly from the different temperature of the source inside the setups (table 4.3). The temperature of source in setup A is constantly kept at room temperature (294 K), whereas the temperature of the source in setup B is kept at approximately 4.3 K for measurements below 30 K, and rose with rising temperature of the absorber to about 15 K at 150 K.

A summary of the obtained hyperfine parameters are given in tables 4.3 to 4.5. The obtained spectra, together with the hyperfine field distributions, are displayed on the following pages.

Detailed reports of the fitted data can be found in the appendix B sorted by rising temperature and applied magnetic field as well as experimental setup.

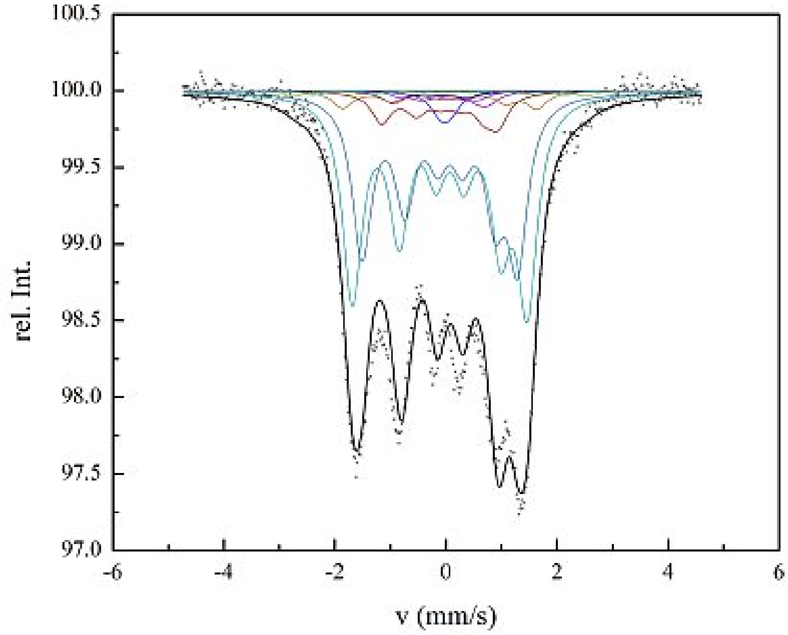

Figure 4.4: Mössbauer spectrum of $(V_{0.92}Fe_{0.08})_2FeB_2$ measured at 4.2 K in 0 T. (setup A)

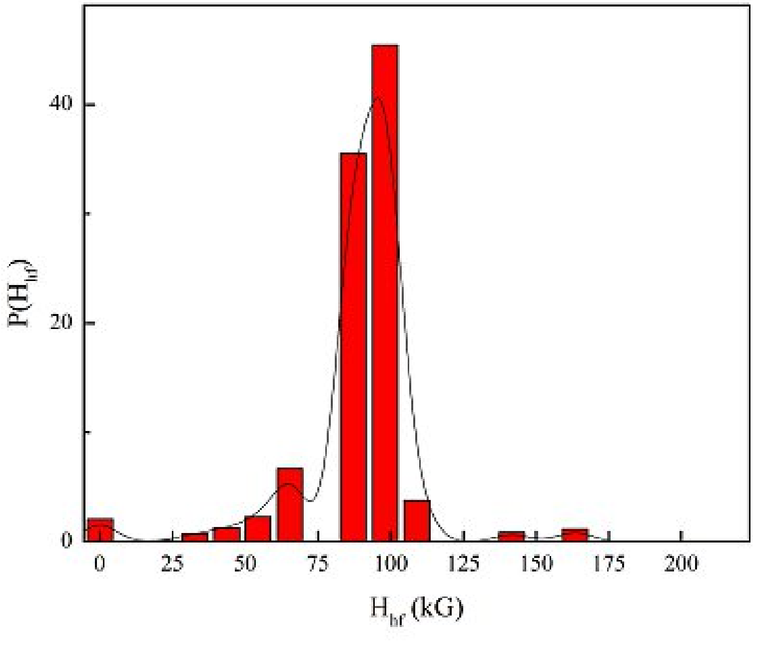

Figure 4.5: Obtained hyperfine field distribution at 4.2 K and 0 T using model 2 (setup A), as well as the calculated function $f(x)$ according to chapter 4.3.

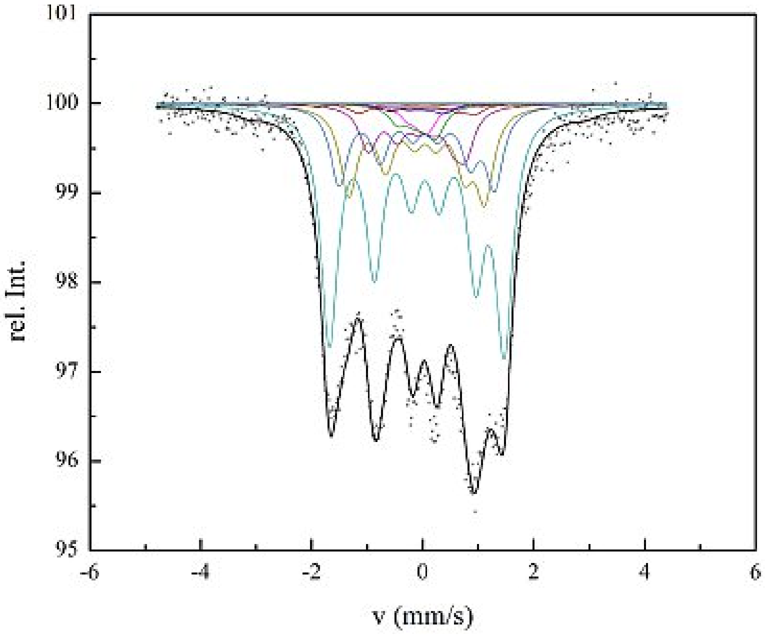

Figure 4.6: Mössbauer spectrum of $(V_{0.92}Fe_{0.08})_2FeB_2$ measured at 20 K in 0 T. (setup A)

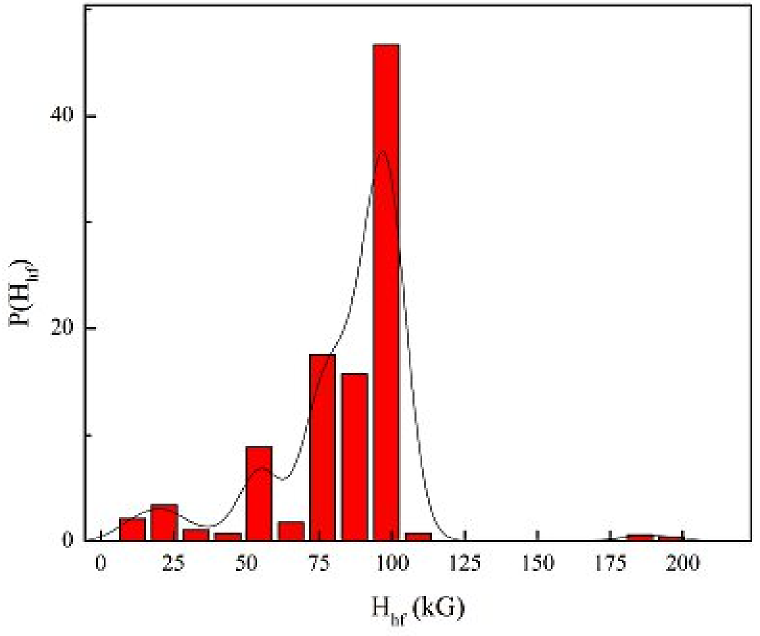

Figure 4.7: Obtained hyperfine field distribution at 20 K and 0 T using model 2 (setup A), as well as the calculated function $f(x)$ according to chapter 4.3.

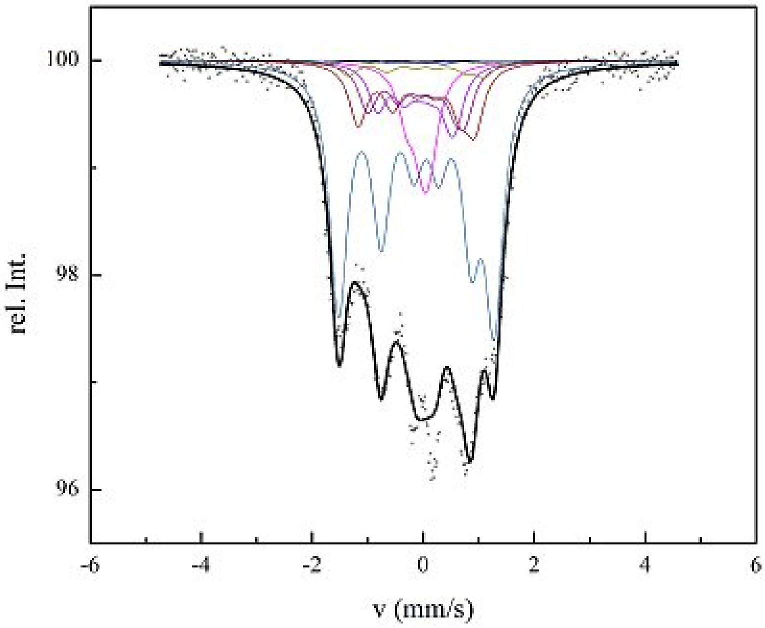

Figure 4.8: Mössbauer spectrum of $(V_{0.92}Fe_{0.08})_2FeB_2$ measured at 30 K in 0 T. (setup A)

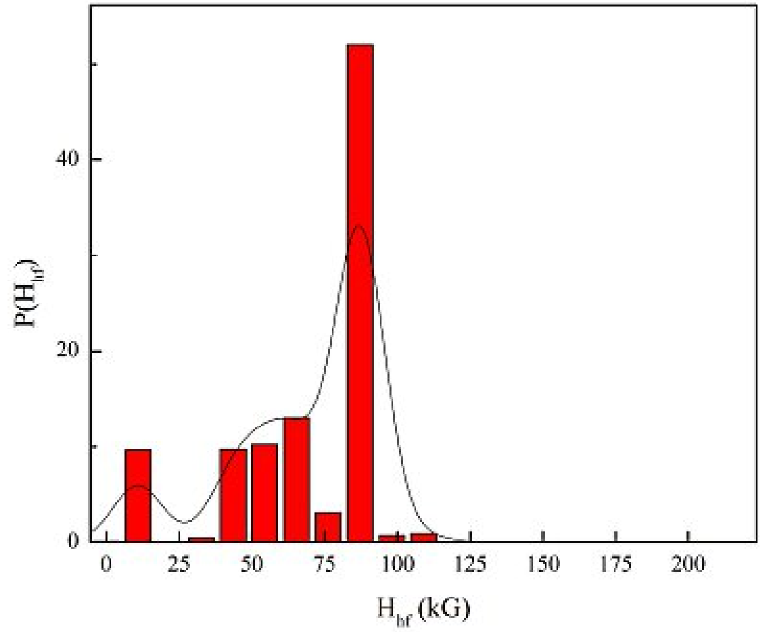

Figure 4.9: Obtained hyperfine field distribution at 30 K and 0 T using model 2 (setup A), as well as the calculated function $f(x)$ according to chapter 4.3.

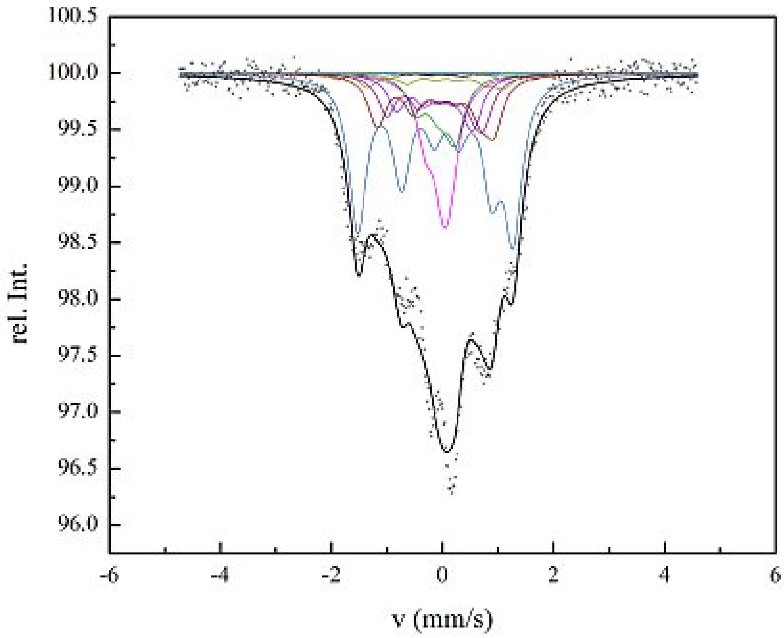

Figure 4.10: Mössbauer spectrum of $(V_{0.92}Fe_{0.08})_2FeB_2$ measured at 40 K in 0 T. (setup A)

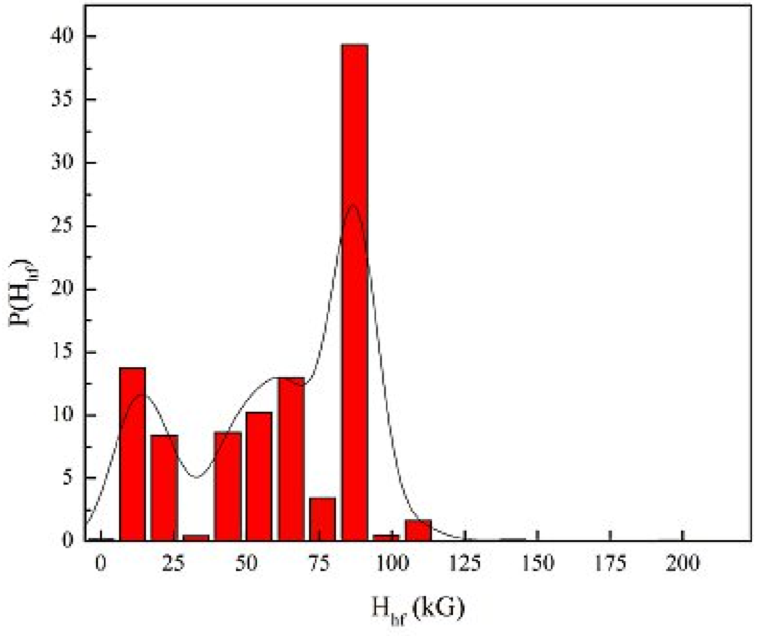

Figure 4.11: Obtained hyperfine field distribution at 40 K and 0 T using model 2 (setup A), as well as the calculated function $f(x)$ according to chapter 4.3.

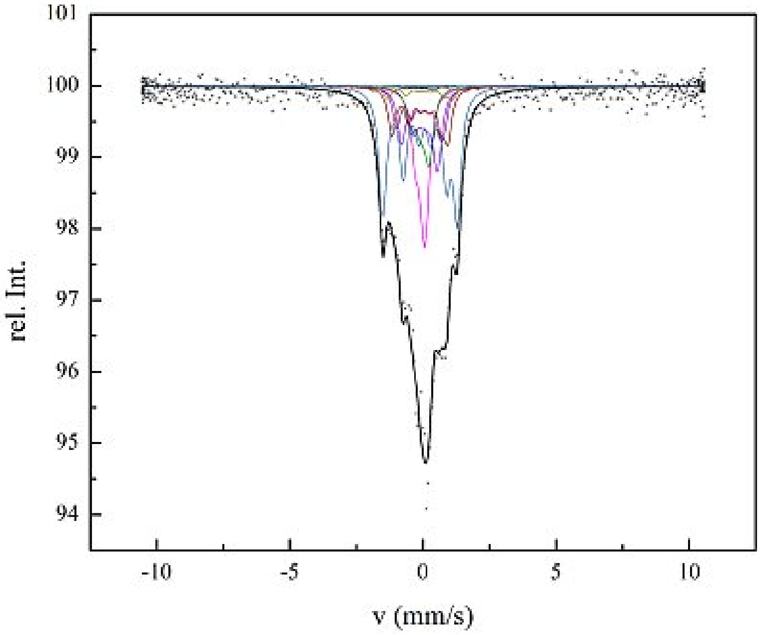

Figure 4.12: Mössbauer spectrum of $(V_{0.92}Fe_{0.08})_2FeB_2$ measured at 50 K in 0 T. (setup A)

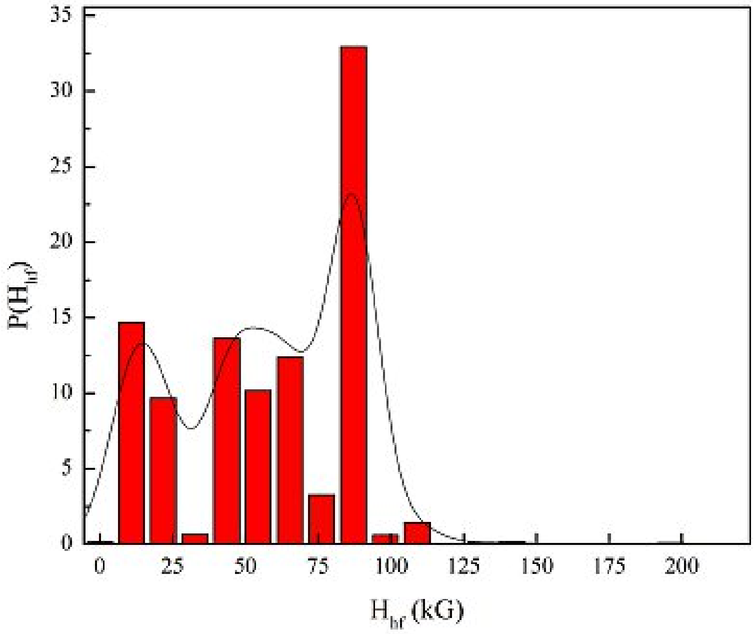

Figure 4.13: Obtained hyperfine field distribution at 50 K and 0 T using model 2 (setup A), as well as the calculated function $f(x)$ according to chapter 4.3.

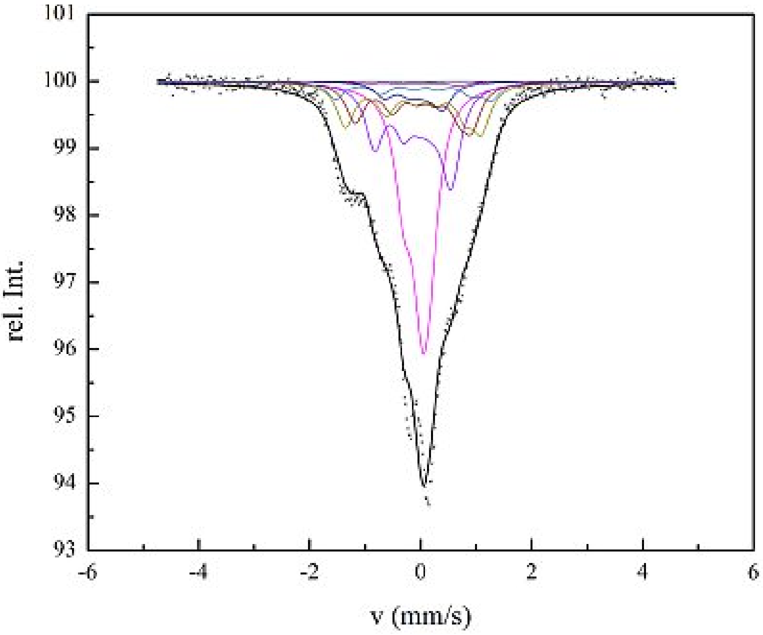

Figure 4.14: Mössbauer spectrum of $(V_{0.92}Fe_{0.08})_2FeB_2$ measured at 60 K in 0 T. (setup A)

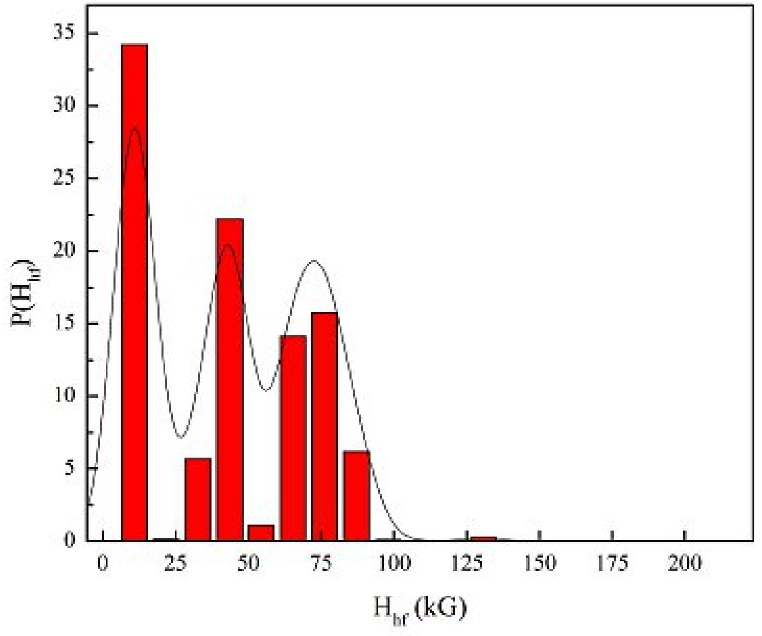

Figure 4.15: Obtained hyperfine field distribution at 60 K and 0 T using model 2 (setup A), as well as the calculated function $f(x)$ according to chapter 4.3.

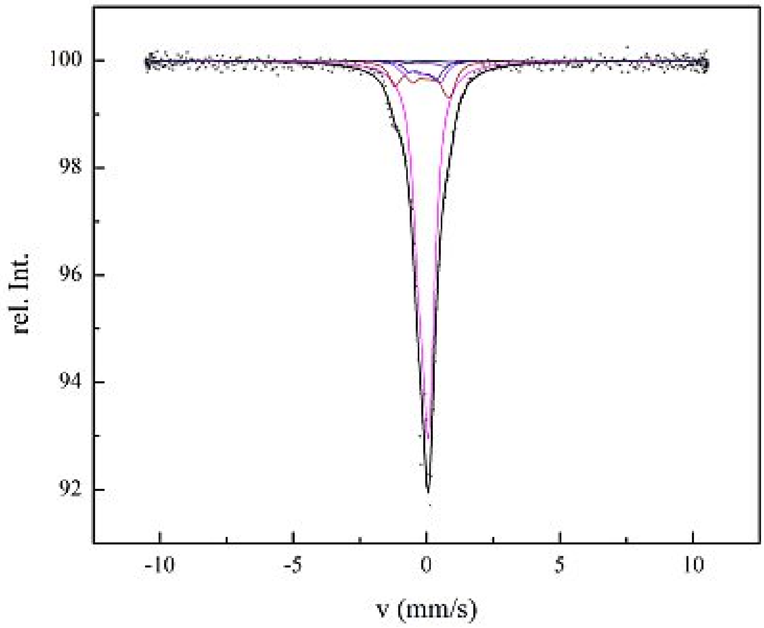

Figure 4.16: Mössbauer spectrum of $(V_{0.92}Fe_{0.08})_2FeB_2$ measured at 80 K in 0 T. (setup A)

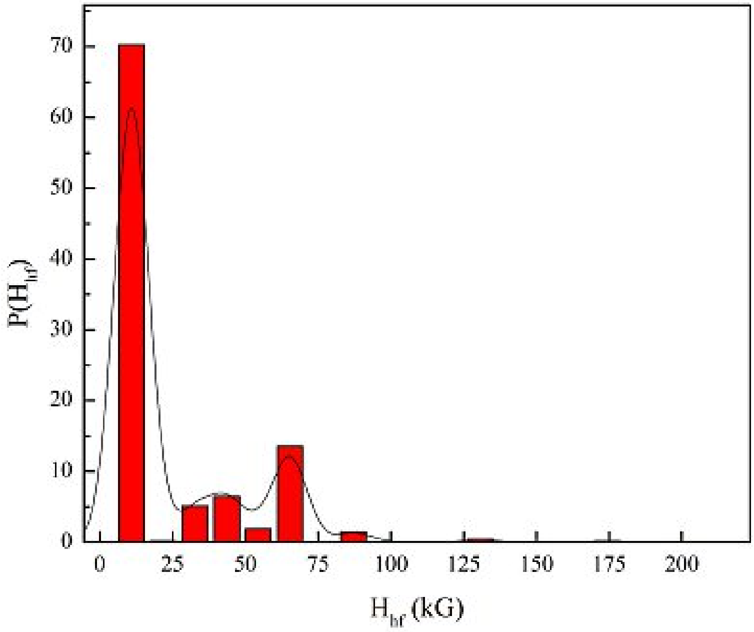

Figure 4.17: Obtained hyperfine field distribution at 80 K and 0 T using model 2 (setup A), as well as the calculated function $f(x)$ according to chapter 4.3.

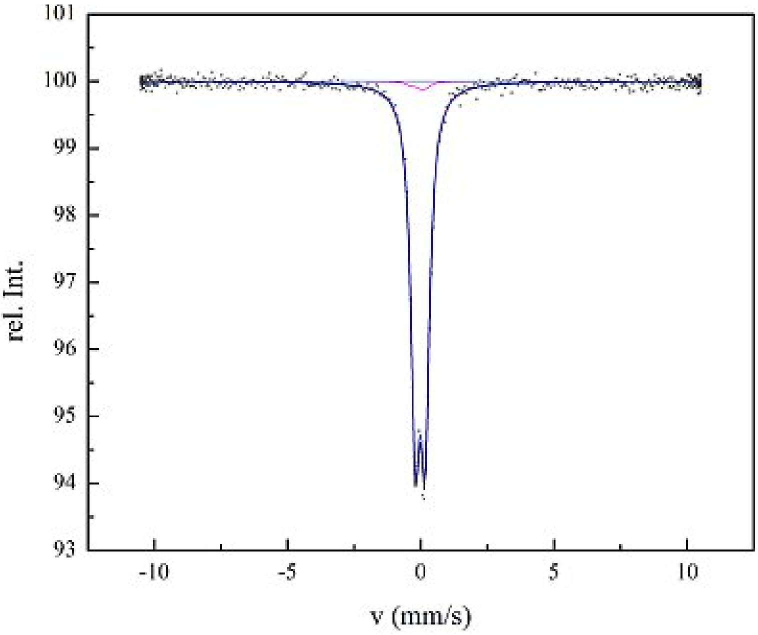

Figure 4.18: Mössbauer spectrum of $(V_{0.92}Fe_{0.08})_2FeB_2$ measured at 100 K in 0 T. (setup A)

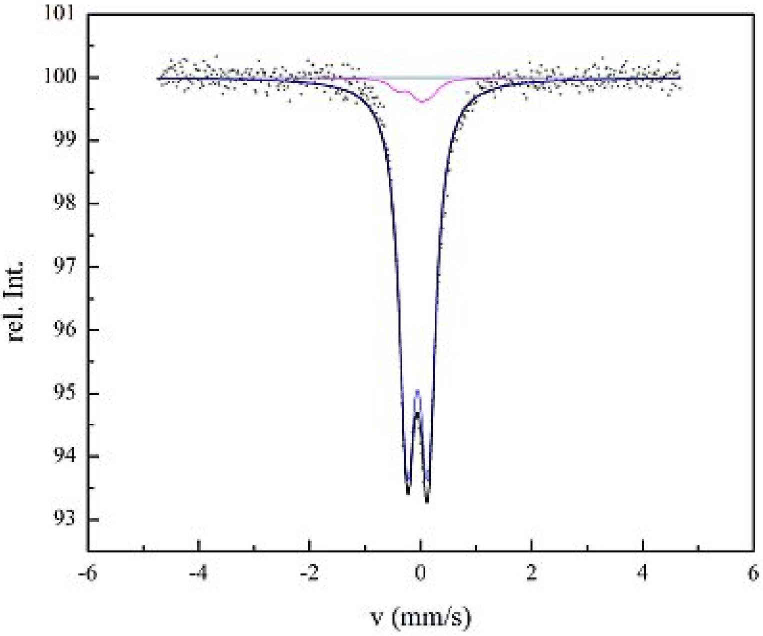

Figure 4.19: Mössbauer spectrum of $(V_{0.92}Fe_{0.08})_2FeB_2$ measured at 125 K in 0 T. (setup A)

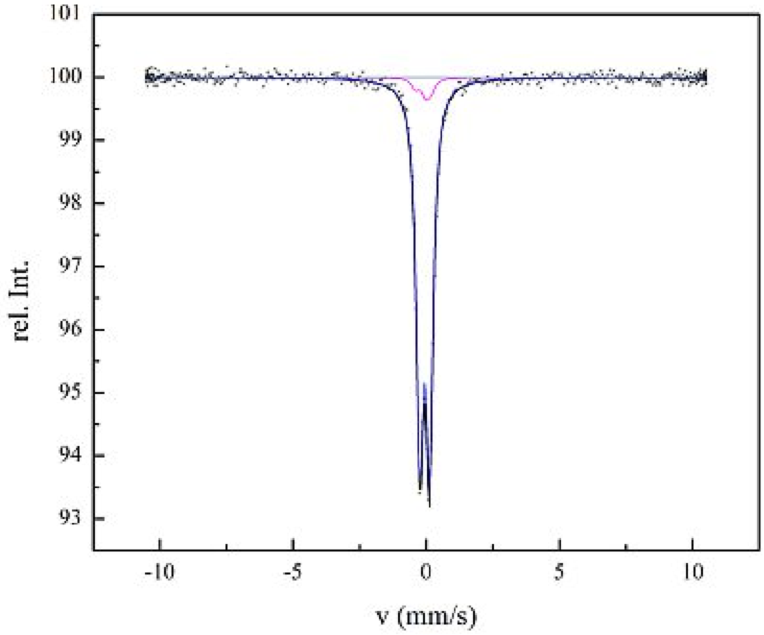

Figure 4.20: Mössbauer spectrum of $(V_{0.92}Fe_{0.08})_2FeB_2$ measured at 150 K in 0 T. (setup A)

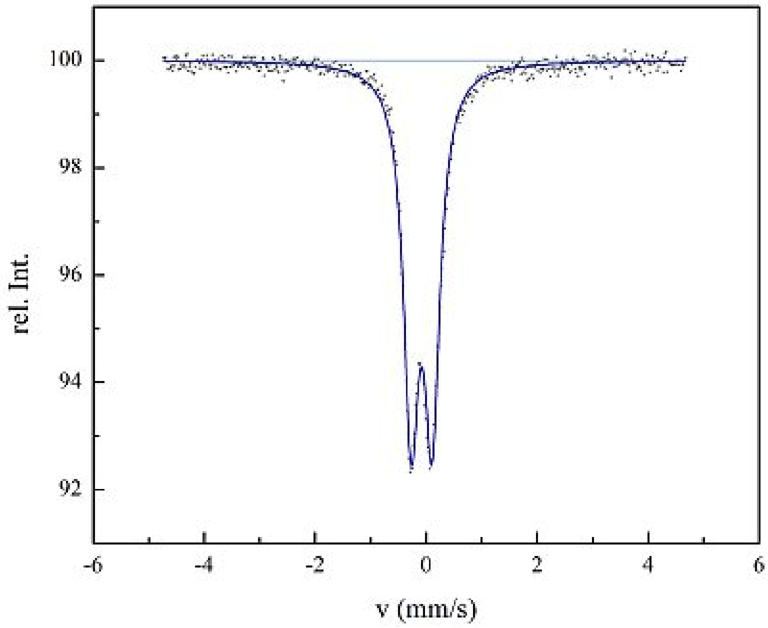

Figure 4.21: Mössbauer spectrum of $(V_{0.92}Fe_{0.08})_2FeB_2$ measured at 175 K in 0 T. (setup A)

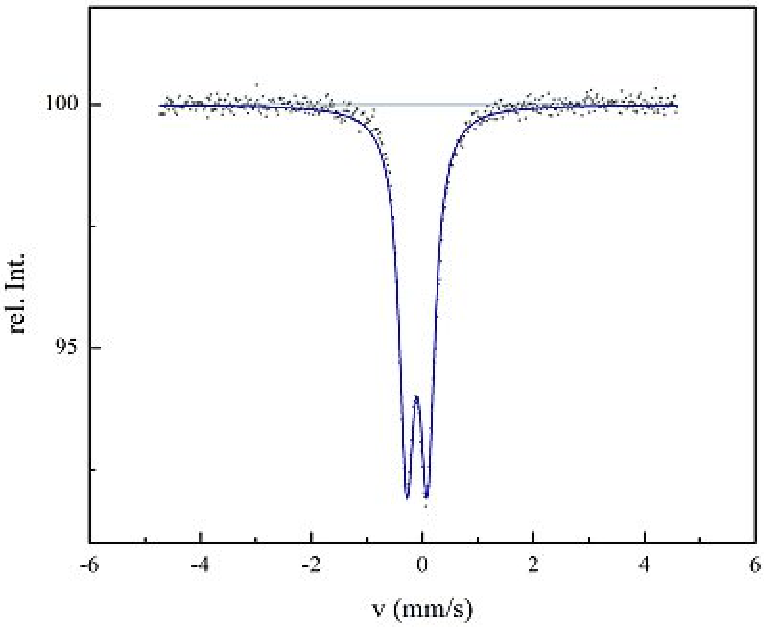

Figure 4.22: Mössbauer spectrum of $(V_{0.92}Fe_{0.08})_2FeB_2$ measured at 200 K in 0 T. (setup A)Plot of the 200 K measurement in setup A .

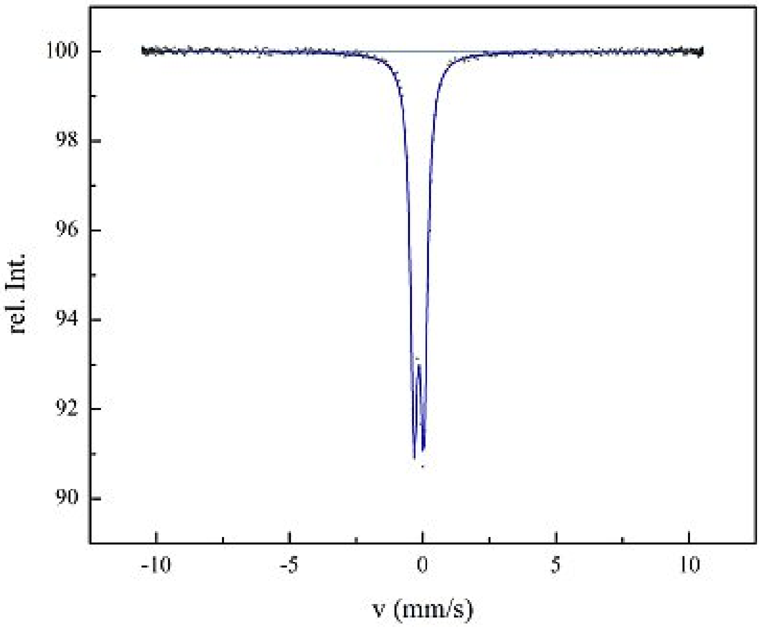

Figure 4.23: Mössbauer spectrum of $(V_{0.92}Fe_{0.08})_2FeB_2$ measured at 294 K in 0 T. (setup A)

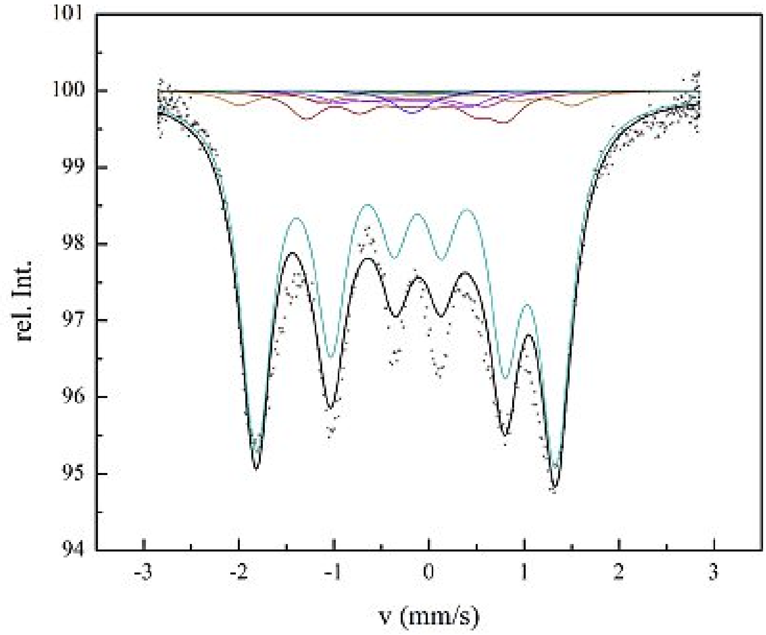

Figure 4.24: Mössbauer spectrum of $(V_{0.92}Fe_{0.08})_2FeB_2$ measured at 4.3 K in 0 T. (setup B)

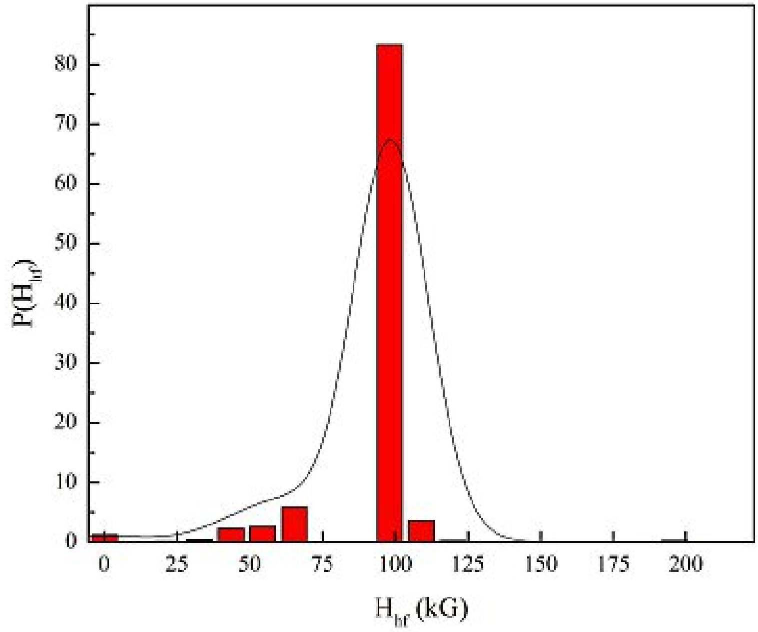

Figure 4.25: Obtained hyperfine field distribution at 4.2 K and 0 T using model 2 (setup B), as well as the calculated function $f(x)$ according to chapter 4.3.

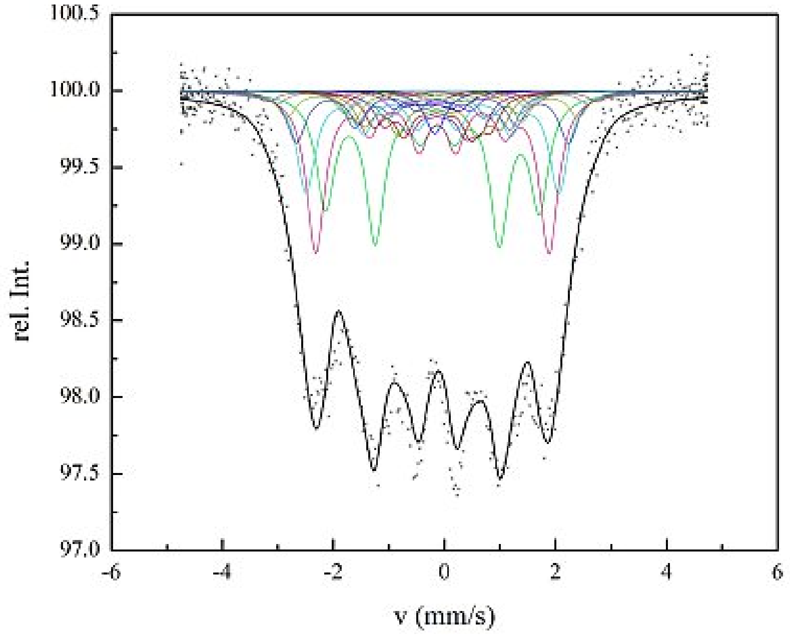

Figure 4.26: Mössbauer spectrum of $(V_{0.92}Fe_{0.08})_2FeB_2$ measured at 4.3 K in 9 T. (setup B)

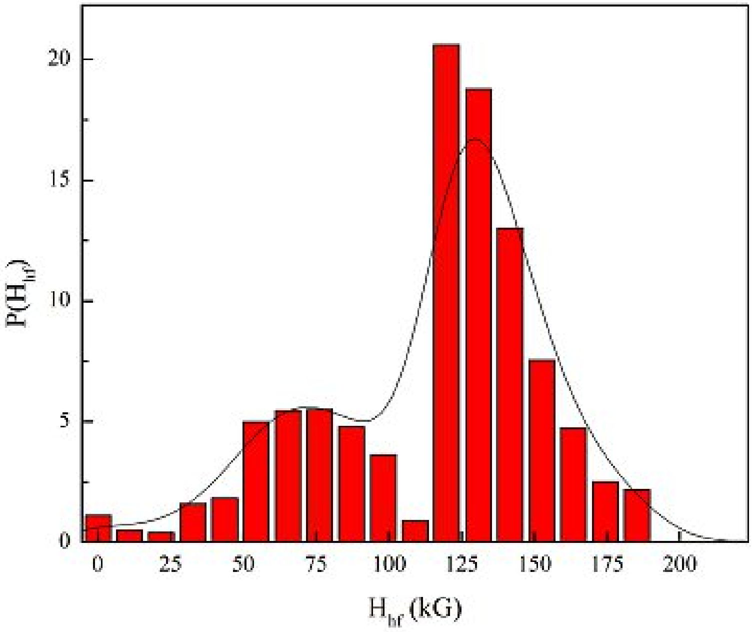

Figure 4.27: Obtained hyperfine field distribution at 4.2 K and 9 T using model 2 (setup B), as well as the calculated function $f(x)$ according to chapter 4.3.

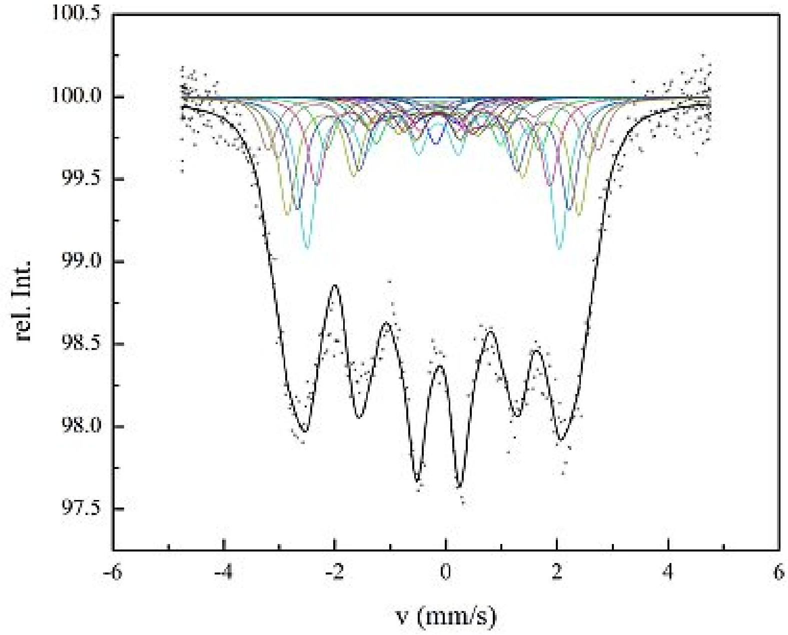

Figure 4.28: Mössbauer spectrum of $(V_{0.92}Fe_{0.08})_2FeB_2$ measured at 4.3 K in 12 T. (setup B)

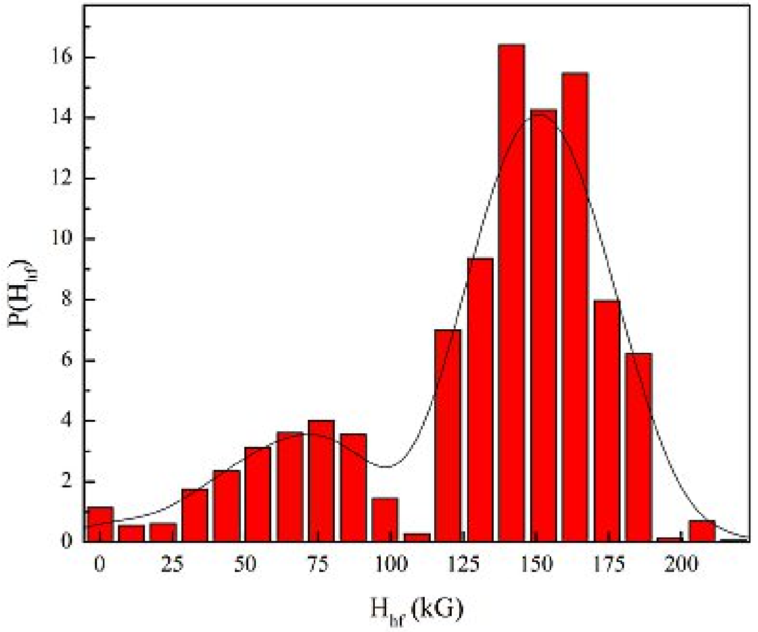

Figure 4.29: Obtained hyperfine field distribution at 4.2 K and 12 T using model 2 (setup B), as well as the calculated function $f(x)$ according to chapter 4.3.

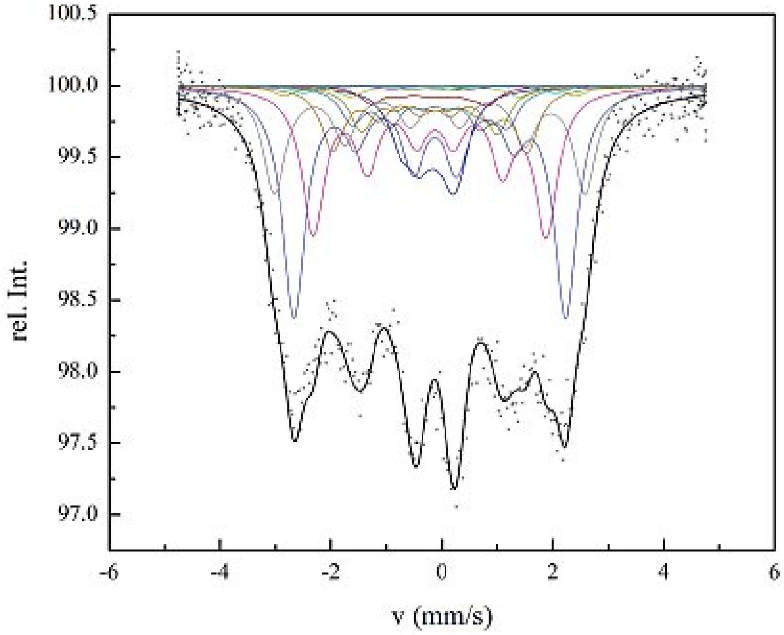

Figure 4.30: Mössbauer spectrum of $(V_{0.92}Fe_{0.08})_2FeB_2$ measured at 20 K in 12 T. (setup B)

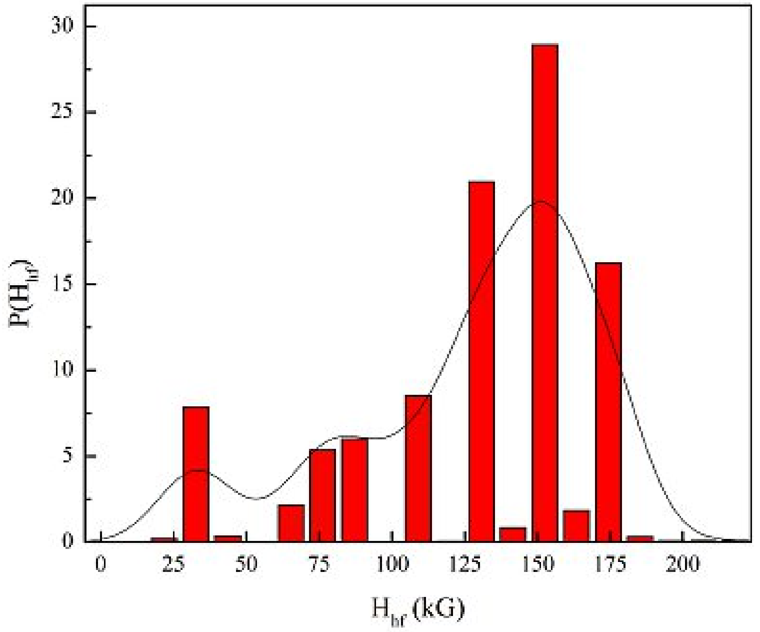

Figure 4.31: Obtained hyperfine field distribution at 20 K and 12 T using model 2 (setup B), as well as the calculated function $f(x)$ according to chapter 4.3.

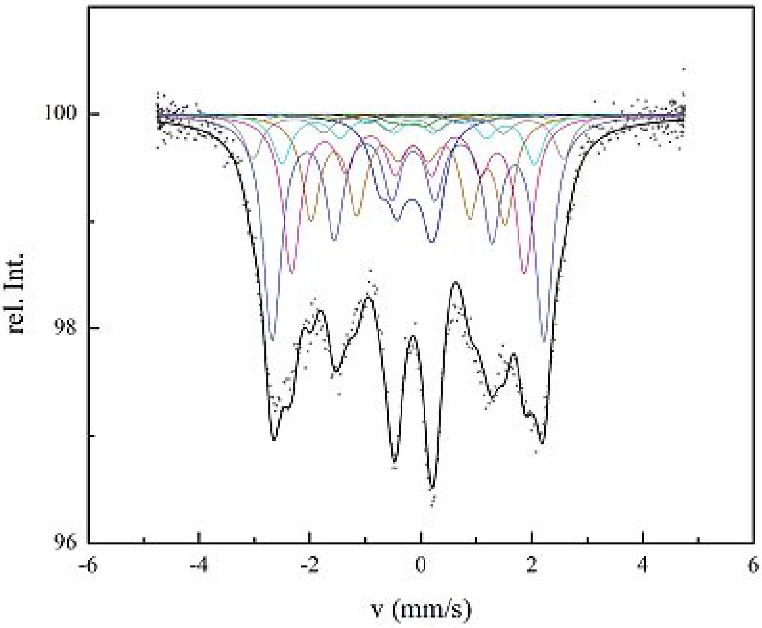

Figure 4.32: Mössbauer spectrum of $(V_{0.92}Fe_{0.08})_2FeB_2$ measured at 40 K in 12 T. (setup B)

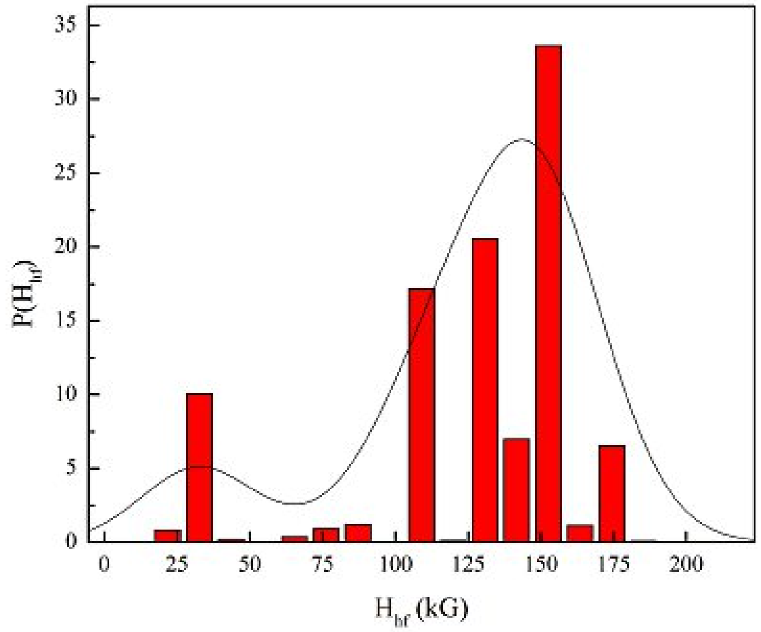

Figure 4.33: Obtained hyperfine field distribution at 40 K and 12 T using model 2 (setup B), as well as the calculated function $f(x)$ according to chapter 4.3.

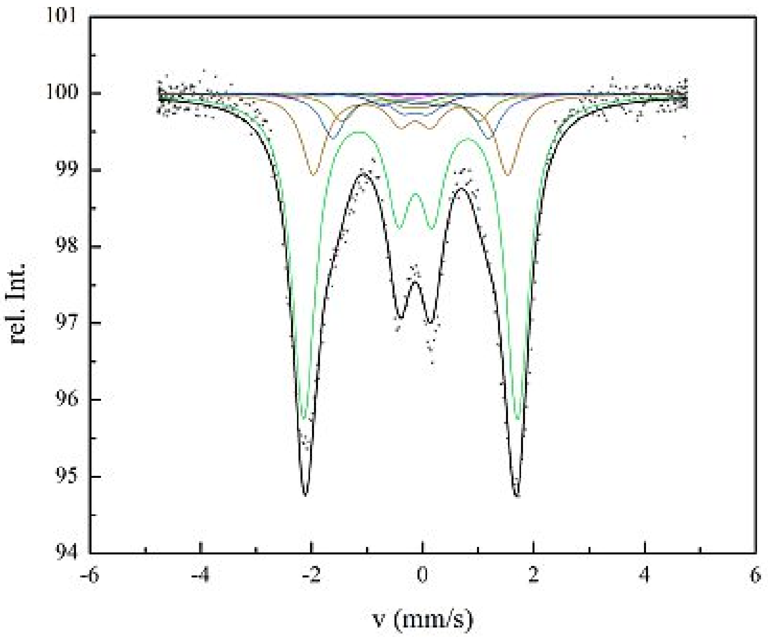

Figure 4.34: Mössbauer spectrum of $(V_{0.92}Fe_{0.08})_2FeB_2$ measured at 100 K in 12 T. (setup B)

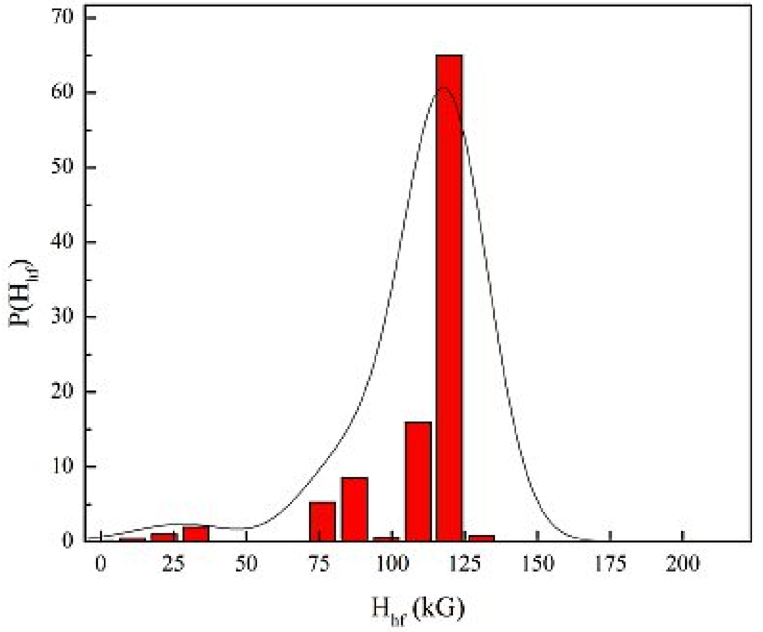

Figure 4.35: Obtained hyperfine field distribution at 100 K and 12 T using model 2 (setup B), as well as the calculated function $f(x)$ according to chapter 4.3.

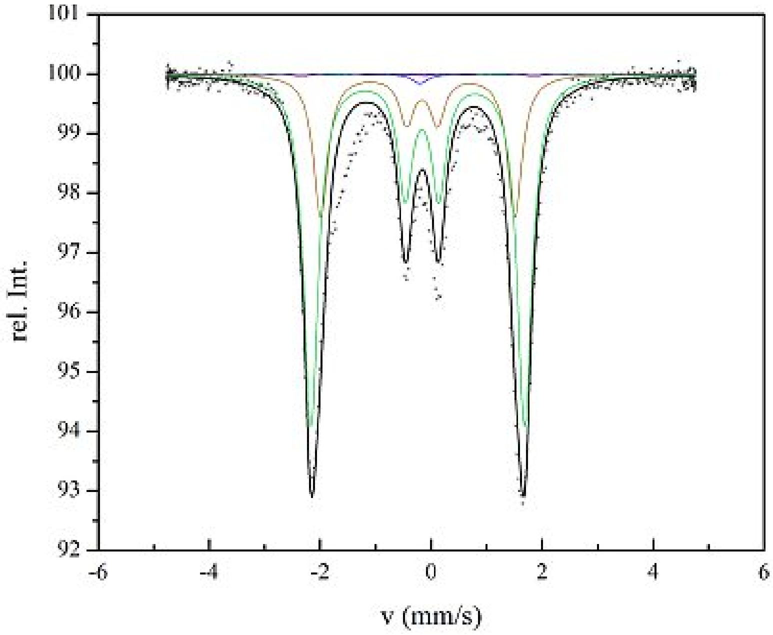

Figure 4.36: Mössbauer spectrum of $(V_{0.92}Fe_{0.08})_2FeB_2$ measured at 150 K in 12 T. (setup B)

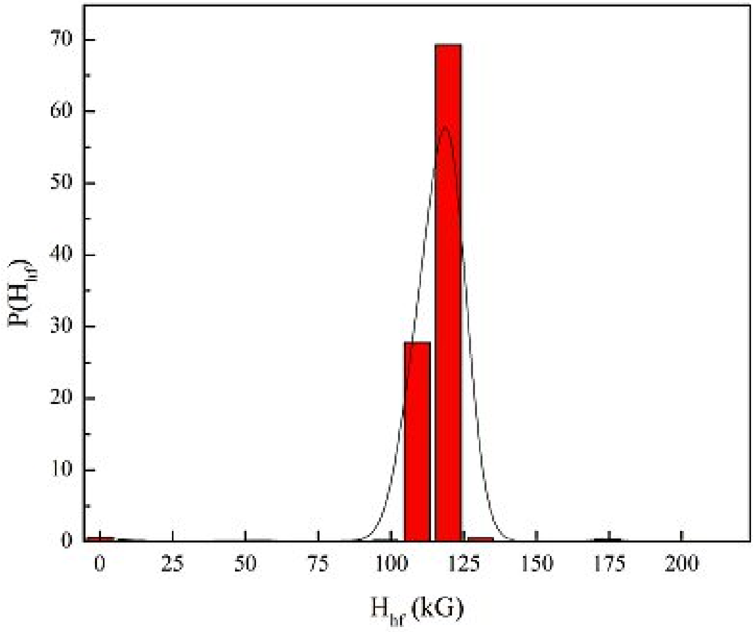

Figure 4.37: Obtained hyperfine field distribution at 150 K and 12 T using model 2 (setup B), as well as the calculated function $f(x)$ according to chapter 4.3.

4.4.1 Quadrupole splitting

The data obtained in setup A reveals an unusual behaviour of the quadrupole splitting at different temperatures. (See figure 4.38) $eQV_{zz}/4$ groups around -0.09 mm/s from 4.2 K to 40 K and around -0.19 mm/s for measurements from 100 K to 294 K. Analysis of the measurements at 50 K and 80 K reveal values around -0.12 mm/s. It was not possible to reproduce this behaviour during measurements within an applied magnetic field of 12 T. See table 4.3.

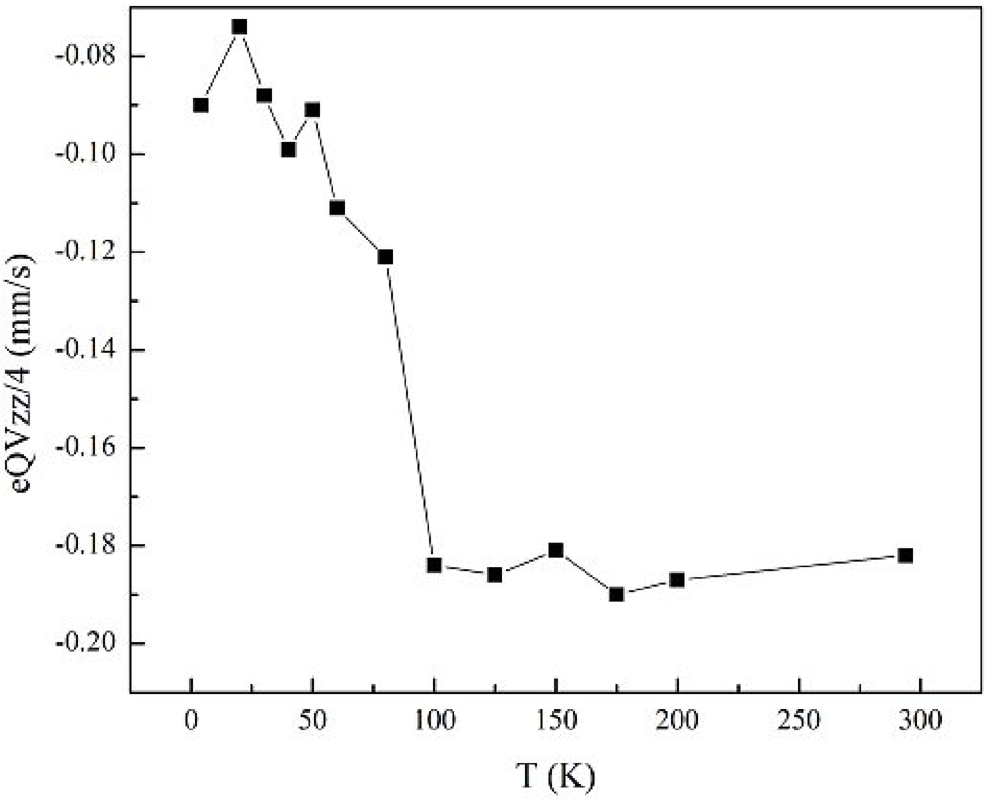

Figure 4.38: Temperature dependence of the quadrupole splitting $eQV_{zz}/4$ obtained from analysis within model 2. (setup A)

4.4.2 Debye temperature

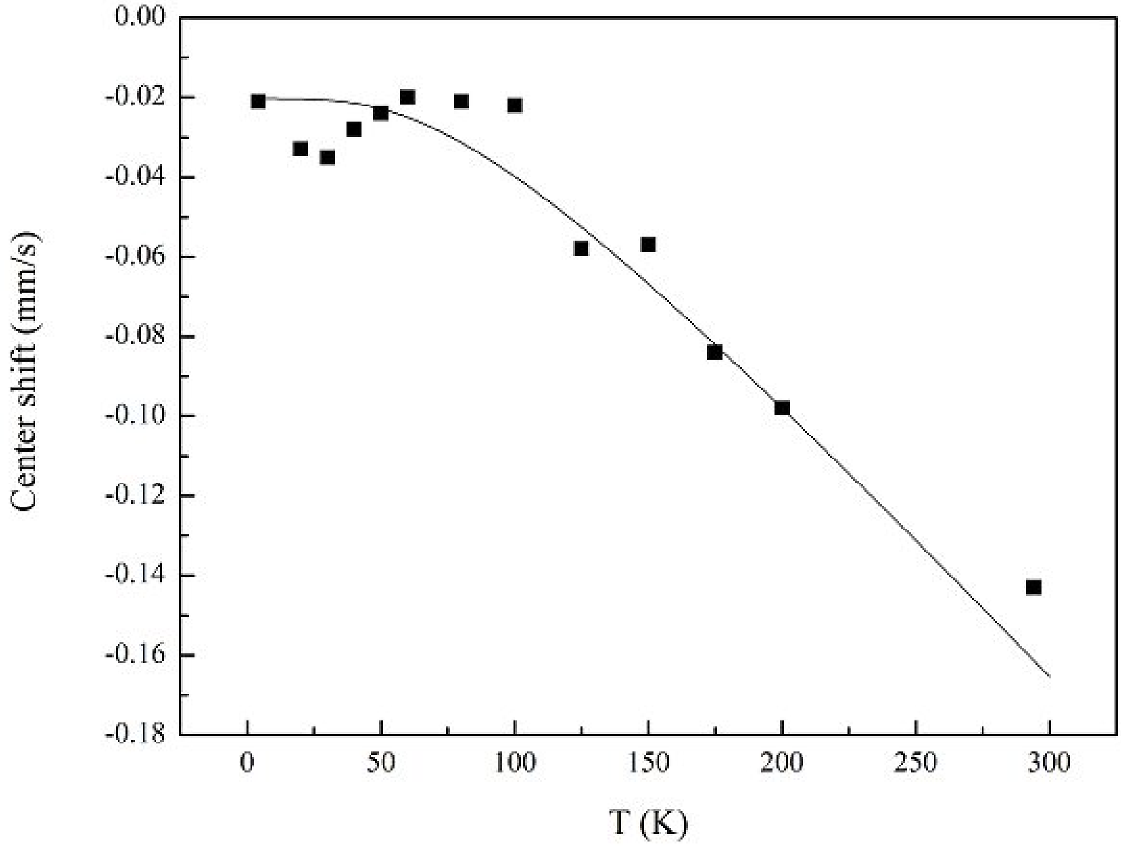

Figure 4.39: Temperature dependence of the center shift of all measurements obtained in setup A. The line is a fit according to the Debye model.

The Debye temperature of $(V_{0.92}Fe_{0.08})_2FeB_2$ was calculated to be 313 K using the Debye model. Figure 4.39 displays the temperature dependency of the measured and calculated values of the center shift in mm/s obtained in zero field.

4.4.3 Distribution of the magnetic hyperfine fields

The following chapter summarizes the analysis of the distribution of the magnetic hyperfine fields. The description of the method used is given in chapter 4.3. The gathered data are also summarized in tabular form in tables 4.4 and 4.5.

Figures 4.40 to 4.42 describe the results of the analysis of the measurements conducted without external magnetic field in setup A. The hyperfine field distribution shows three peaks at all temperatures except for the data collected at 4.2 K, where only two peaks can be found. The barycenters of those peaks, marked with H_0 in figure 4.40, decrease with rising temperature. The relative area of peak 1 (figure 4.41) decreases continuously with rising temperature, whereas the relative area of peak 3 rises with increasing temperature. The relative area of Peak 2 rises in the temperature range from 4.2 K to 40 K but decreases from that temperature onward. This companioned with the unusual high and erratic standard deviation of that peak (figure 4.42). The standard deviations of Peak 1 and 3 are relative constant in comparison to Peak 2. The discussed graphs only display the temperature range from 4.2 K to 80 K, due to the fact that no hyperfine field was found in the analysis of the data collected without external field at higher temperatures.

The analysis of the distribution of the hyperfine field for measurements conducted in an external field of 12 T, figures 4.43 to 4.45, reveal the following results. The barycenter of Peak 1 decreases with rising temperature from 4.3 K to 100 K and remains around the 120 kG from this temperature upward. This hints to a minimal internal magnetic field of the sample during those measurements, as the barycenter is of similar size as the external magnetic field. The peaks 2 and 3 occur only in the temperature ranges of 4.3 K to 20 K and 20 K to 40 K respectively. Their relative areas remain below 20 percent, which makes peak 1 the dominant peak. The standard deviation of peak 1 is relative high for measurements below 40 K and decreases for higher temperature. The standard deviation of peak 2 is relative constant, whereas that of peak 3 is quite erratic.

In figures 4.46 to 4.48 the results of the analysis of the distribution of the hyperfine field of measurements obtained at 4.3 K in various external applied magnetic fields are shown. Peak 1 rises with rising external field as displayed in figure 4.46, whereas peak 2 stays constant. The relative area of both peaks stays within a range of 10 percent over all measurements (figure 4.47). The standard deviation rises with rising temperatures for both peaks (figure 4.48). The increase of the hyperfine splitting with rising external field could indicate antiferromagnetic correlations [22]. This correlates with the negative Weiß temperature obtained by Rogl et al [1], which also indicates possible antiferromagnetic correlations [23].

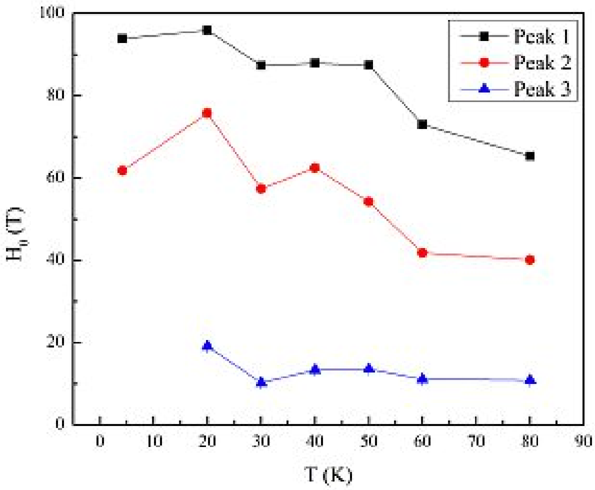

Figure 4.40: Temperature dependence of the barycenter of the peaks of the Gaussian curves obtained during hyperfine field distribution analysis of the data obtained in setup A, using model 2 and the method described in chapter 4.3.

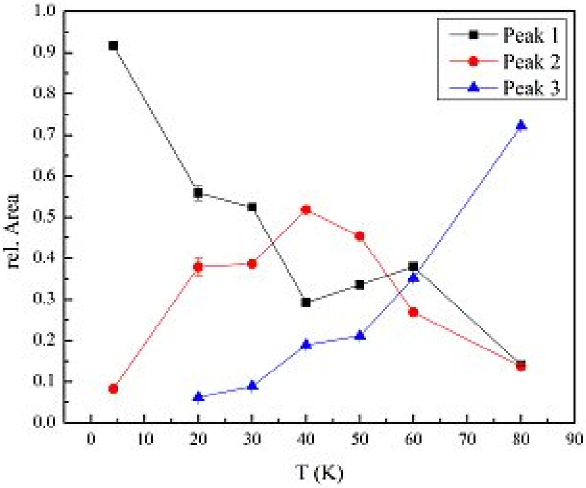

Figure 4.41: Temperature dependence of the relative area of the peaks of the Gaussian curves obtained during hyperfine field distribution analysis of the data obtained in setup A, using model 2 and the method described in chapter 4.3.

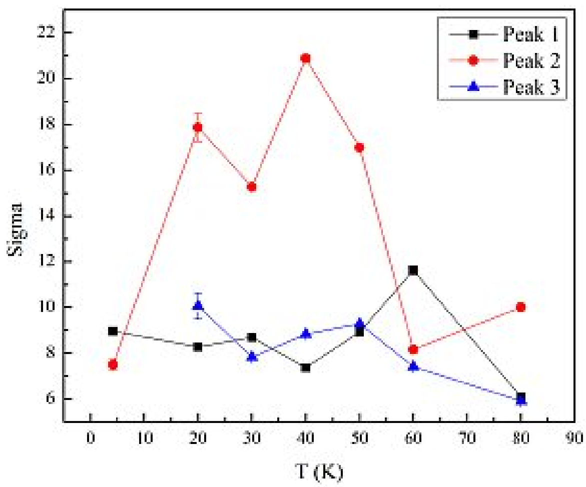

Figure 4.42: Temperature dependence of the standard deviation sigma of the peaks of the Gaussian curves obtained during hyperfine field distribution analysis of the data obtained in setup A, using model 2 and the method described in chapter 4.3.

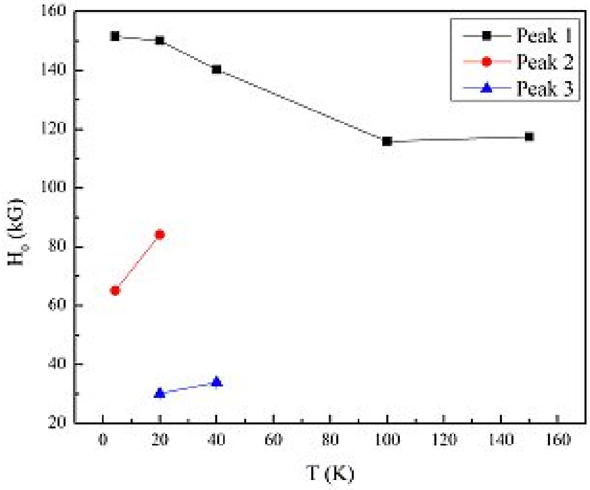

Figure 4.43: Temperature dependence of the barycenter of the peaks of the Gaussian curves obtained during hyperfine field distribution analysis of the data obtained in setup B, using model 2 and the method described in chapter 4.3.

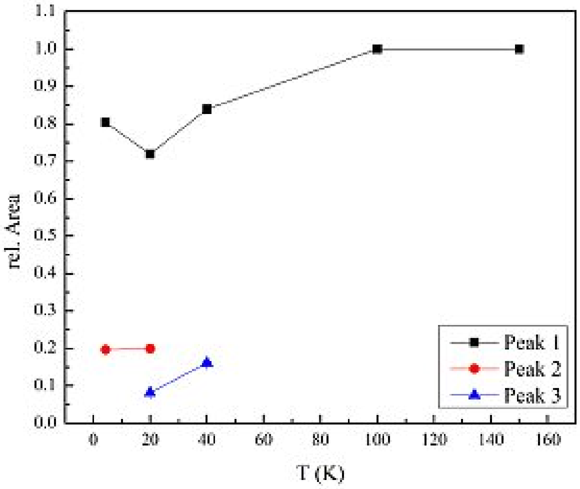

Figure 4.44: Temperature dependence of the relative area of the peaks of the Gaussian curves obtained during hyperfine field distribution analysis of the data obtained in setup B, using model 2 and the method described in chapter 4.3.

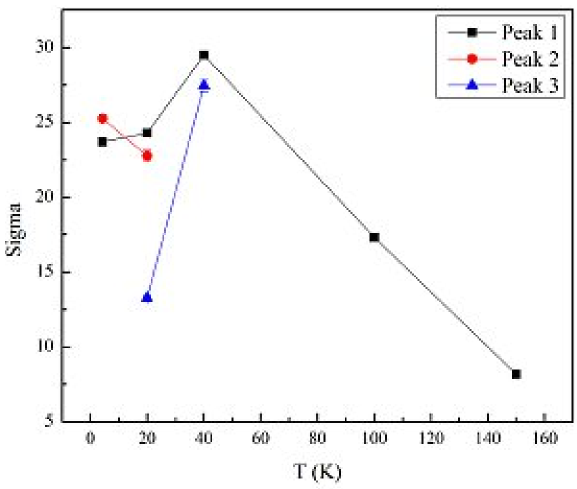

Figure 4.45: Temperature dependence of the standard deviation sigma of the peaks of the Gaussian curves obtained during hyperfine field distribution analysis of the data obtained in setup B, using model 2 and the method described in chapter 4.3.

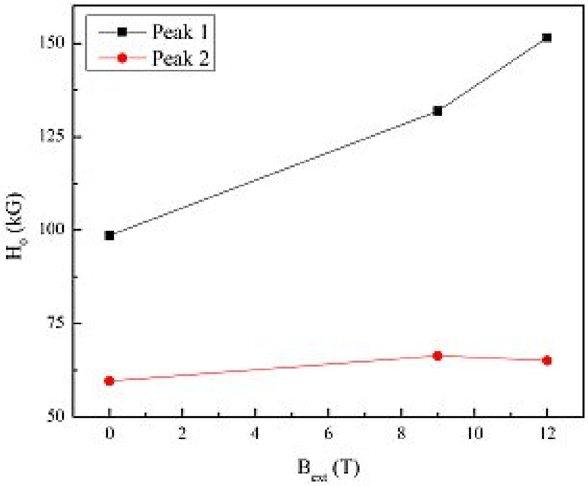

Figure 4.46: Field dependence of the barycenter of the peaks of the Gaussian curves obtained during hyperfine field distribution analysis of the data obtained in setup B at a temperature of 4.3 K, using model 2 and the method described in chapter 4.3.

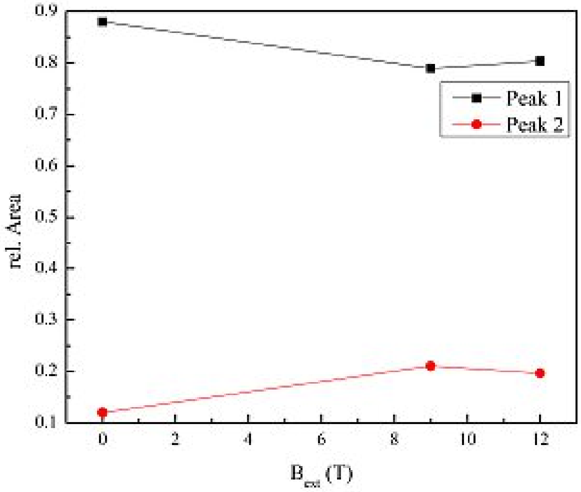

Figure 4.47: Field dependence of the relative area of the peaks of the Gaussian curves obtained during hyperfine field distribution analysis of the data obtained in setup B at a temperature of 4.3 K, using model 2 and the method described in chapter 4.3.

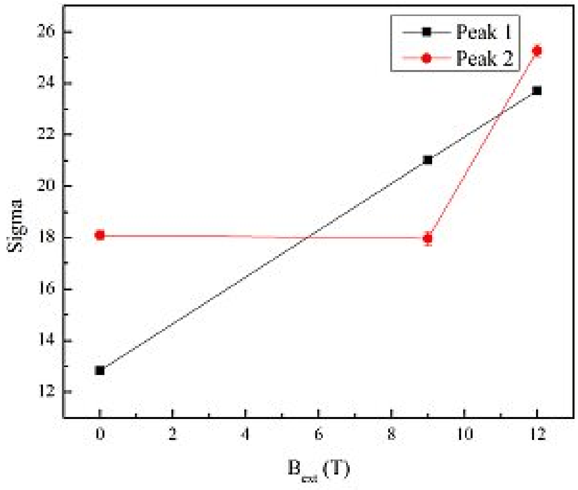

Figure 4.48: Field dependence of the standard deviation sigma of the peaks of the Gaussian curves obtained during hyperfine field distribution analysis of the data obtained in setup B at a temperature of 4.3 K, using model 2 and the method described in chapter 4.3.

A Setup and instructions for the MercuryIPS unit

The following chapters provide detailed information on the setup of the power suppl MercuryIPS, divided into three sections, Hardware, Software inside the unit and Software installed on a accompanying computer.

A.1 Setup

A.1.1 Hardware

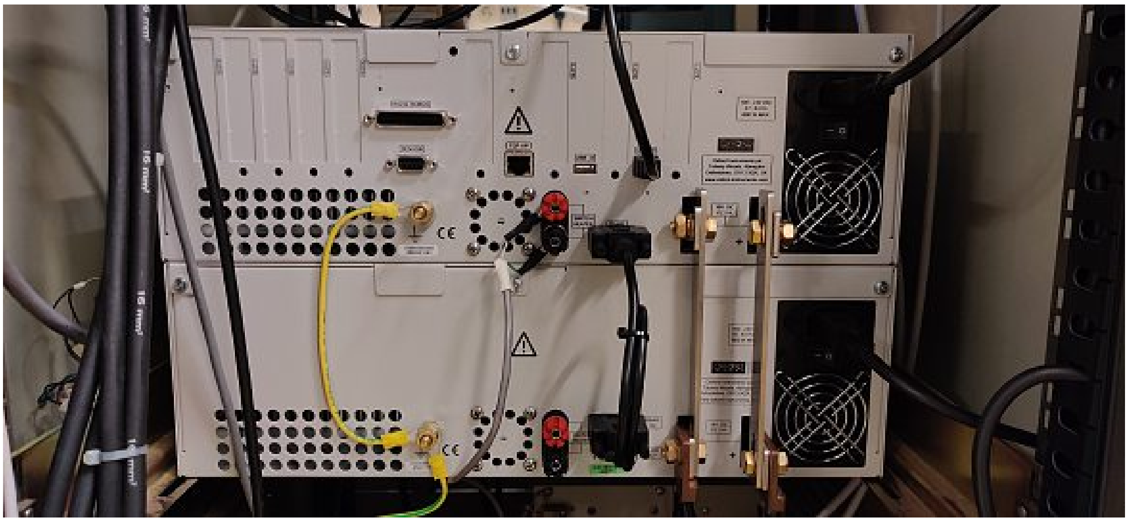

Figure A.1: Backside of MercuryIPS.

Figure A.1 displays the backpanel of the MercuryiPS power supply unit. The following connections have to be controlled, before the unit gets powered on. The functional ground ports of the master and the slave unit have to be connected with each other and the server rack, the switch heater of the magnet has to be connected via the heater ports of the master unit, the two units have to be connected with each other via a RS485 cable using the output connection on the master and the input port of the slave, the computer has to be connected via a USB cable, terminating in a USB-B Port and the two main power terminals have to be connected with each other via the metal-plate on one side of the terminals and the cable running to the magnet has to be mounted on the other side of the terminal. The power cable that is mounted on the negative port is marked with a white tape (not shown in figure A.1).

A.1.2 Software

A.1.2.1 OS of the MercuryIPS unit

The screen of the MercuryiPS Unit will look like figure A.2 after powering up.

Current (A) -0.0006
Magnet (A) -0.0005
Voltage (V) -0.0003

Figure A.2: Homepanel of MercuryIPS.

Tab "Settings" at the bottom of the screen to open the settings menu. (Figure: A.3)

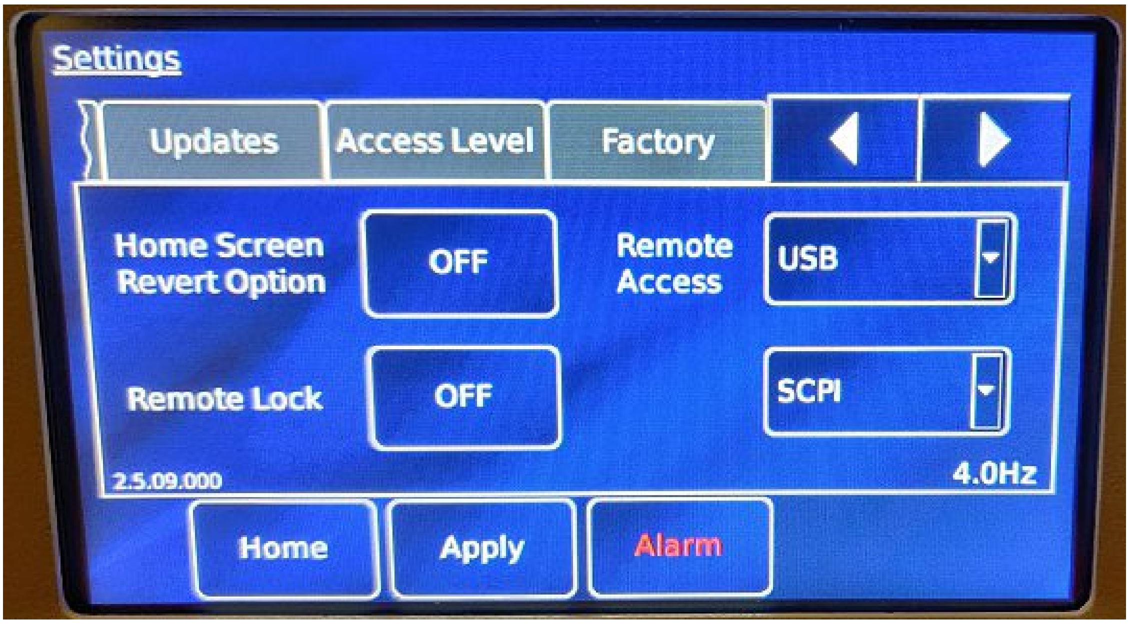

Home Screen Revert Option: OFF
Remote Access: USB
Remote Lock: OFF
SCPI
2.5.09.000
4.0Hz

Figure A.3: Settings menu of MercuryiPS.

Tab the panel on the right side of "Remote Access" to open the menu displayed in figure A.4.

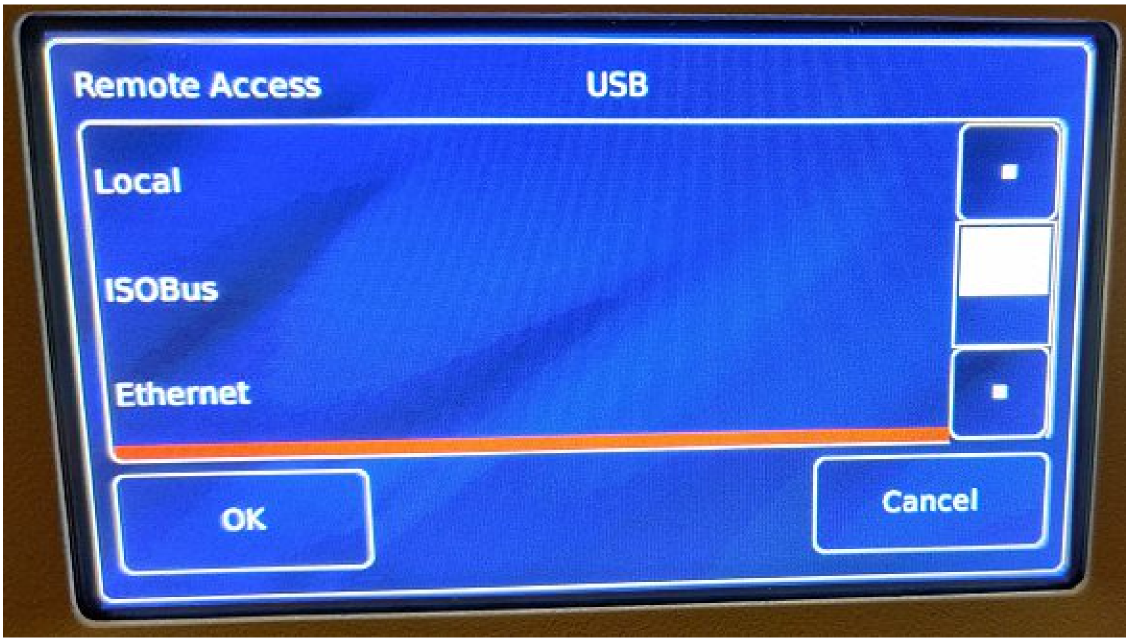

Figure A.4: Submenu of MercuryiPS Settings. Selection of Remote connection.

Select "Local" and press "OK". the screen will display figure A.3 again. Press "Apply" to confirm the choice. Afterwards use the "right arrow" in the top right corner to scroll until the button "Access level" appears and press it. The screen will now display figure A.5.

Figure A.5: Submenu of MercuryiPS settings. Activation of the engineering mode.

Tab the grey box to open the number pad and enter the engineering password. (Figure: A.6) The engineering password is set as "abc123".

abc123

Figure A.6: Number pad with engineering password entered

Tab "OK" to enter the password. The screen will change acording to figure A.7. Press "Apply" to enter the engineering mode.

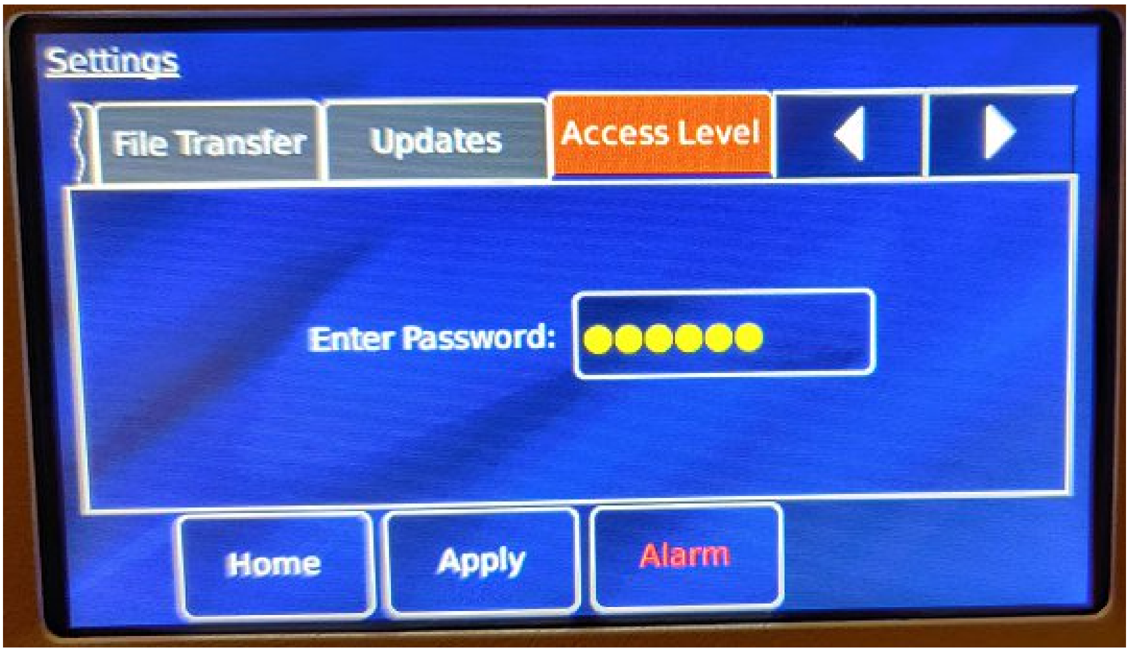

Enter Password: ●●●●●●

Figure A.7: Submenu of MercuryiPS settings. Activation of the engineering mode.

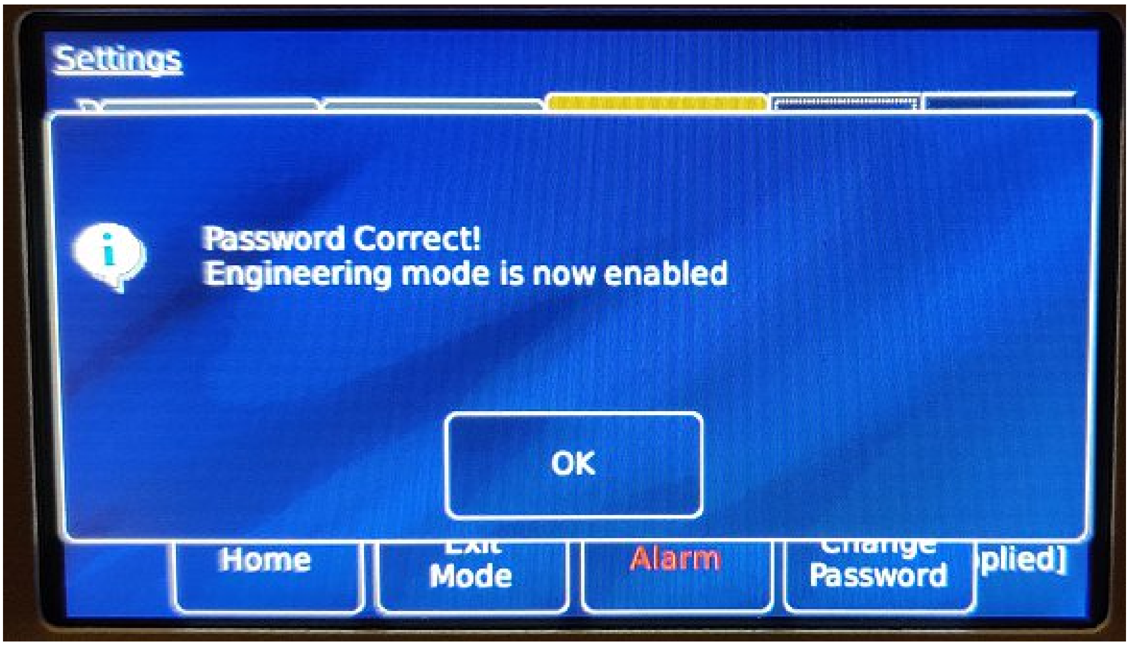

Password Correct!
Engineering mode is now enabled

Figure A.8: Submenu of MercuryiPS settings. Activation of the engineering mode.

The display will change into figure A.8 if the correct password was entered. Tab "OK" to accept the change.

Engineering mode is enabled.

Figure A.9: Submenu of MercuryiPS settings. Activation of the engineering mode.

Tab "Home" on figure A.9 to switch to the home panel again.

Be cautious while using engineering mode, wrong settings could lead to damages of the PSU and the magnet!

After pressing "Config" on the bottom row of figure A.2, figure A.10 will appear.

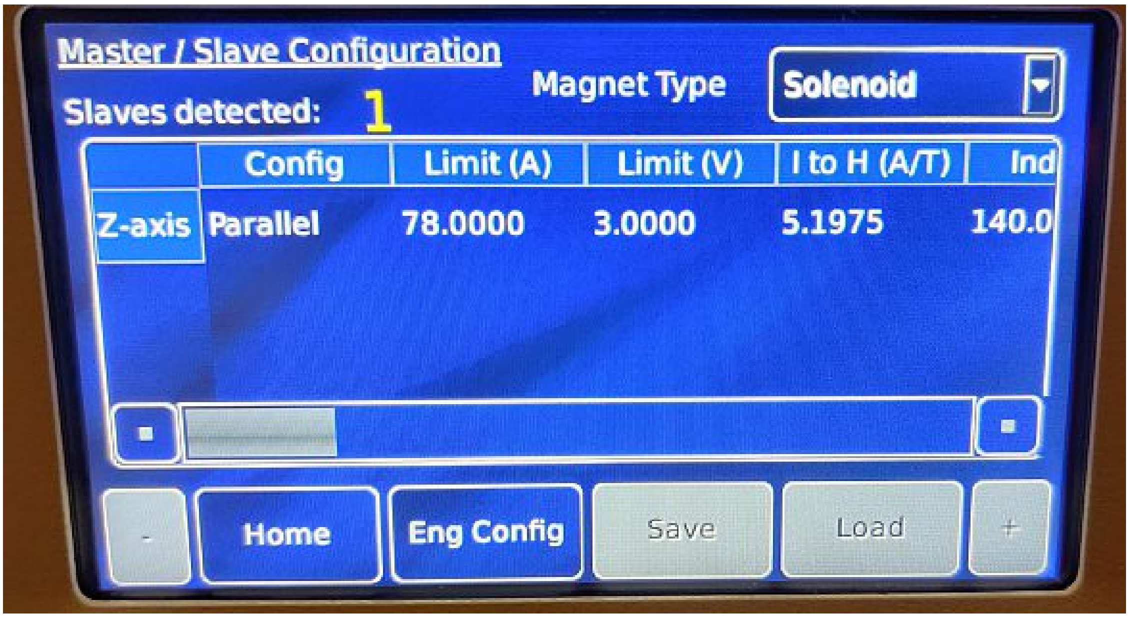

Master / Slave Configuration

Slaves detected: 1

Magnet Type: Solenoid

	Config	Limit (A)	Limit (V)	I to H (A/T)	Ind
Z-axis	Parallel	78.0000	3.0000	5.1975	140.0

Figure A.10: Configuration menu of MercuryiPS.

Insert all values according to table A.1 by tapping on each variable to change its value.

Table A.1: Values for the base configuration of the MercuryiPS unit.

Variable	Value	Variable	Value
Limit (A)	78	Limt (L)	0
Limit (V)	3	Sw Intel	OFF
i to H (A/T)	5.1975	Htr Res (Ω)	0
Ind (H)	140	Sw Res (Ω)	0
Trans (ms)	3000	Lead (Ω)	0.0093
Switch	PSU.M1	Sw on (ms)	10000
Sw Cur (mA)	60	Sw off (ms)	10000
Mode	Unipolar	Catch	OFF
Safety	None	Current Epsilon (A)	0.1000
Limit (K)	999	Current Epsilon (V)	0.005

Afterwards press "Home" and on that Screen tap "Current (A)" to open the "Set Point/ Set Rate" menu. (Figure: A.11)

Set Point / Set Rate (Z axis)

Set Point (A): 1.0003

Set Rate (A/min): 4.0000

Figure A.11: Subpanel of MercuryiPS that displays the current set point and the ramp rate.

Tap on "Rate Limits" to display the menu shown in figure A.12. Enter all values according to table A.2. If there is a line is missing, press the "+" button in the bottom right corner of figure A.12.

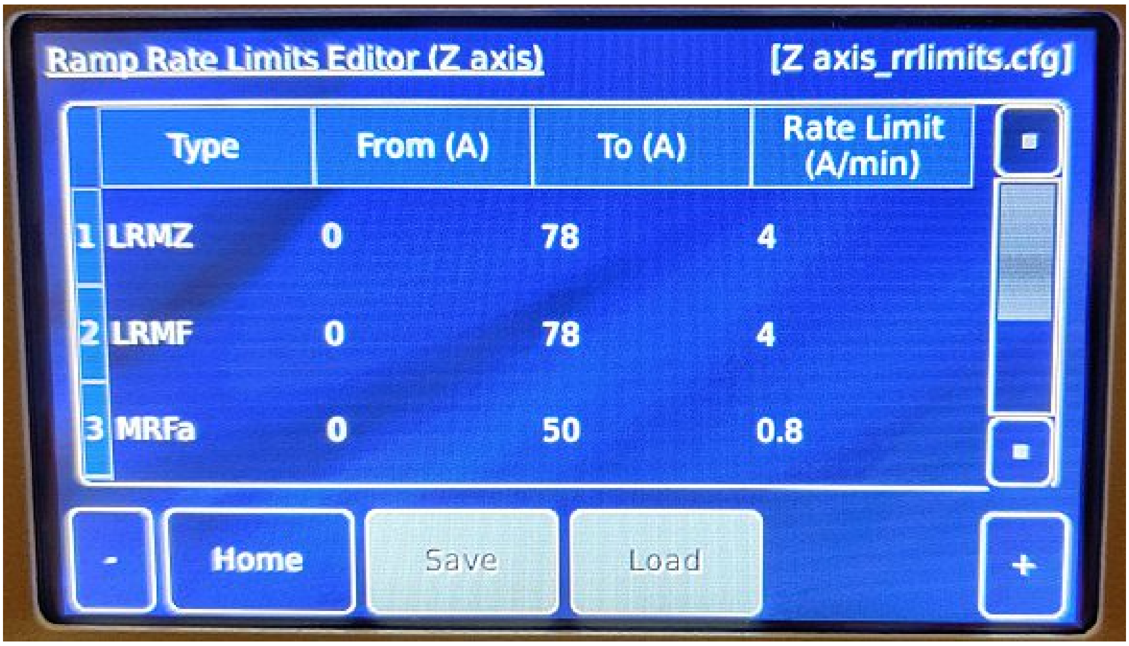

Ramp Rate Limits Editor (Z axis) [Z axis_rrlimits.cfg]

	Type	From (A)	To (A)	Rate Limit (A/min)
1	LRMZ	0	78	4
2	LRMF	0	78	4
3	MRFa	0	50	0.8

Figure A.12: Ramp Rate Limits editor of MercuryiPS

Table A.2: All values for the rate limits of the MercuryiPS.

Type	From (A)	To (A)	Rate Limit (A/min)
LRMZ	0	78	4
LRMF	0	78	4
MRFa	0	50	0.8
MRFa	50.0001	65	0.4
MRFa	65.0001	78	0.16

After completing all mentioned steps, press ”Home” followed by ”Settings” and use the arrow keys in the top right corner to navigate to the sub menu ”Access Level”. The display should look like figure A.9. Tab ”Exit Mode” followed by ”Home”.

To finish the setup redo the first steps, but choose ”USB” instate of ”Local” in figure A.4. The power supply is now ready for use.

Please check [25] if any uncertainty appears.

A.1.2.2 Configuration of the Com-ports for MercuryiPS on a computer

This short section shall provide all necessary steps to configure the Com Ports on a computer running Windows XP, so that the LabView program "MercuryiPS_Controls" can establish a connection with the power supply MercuryiPS.

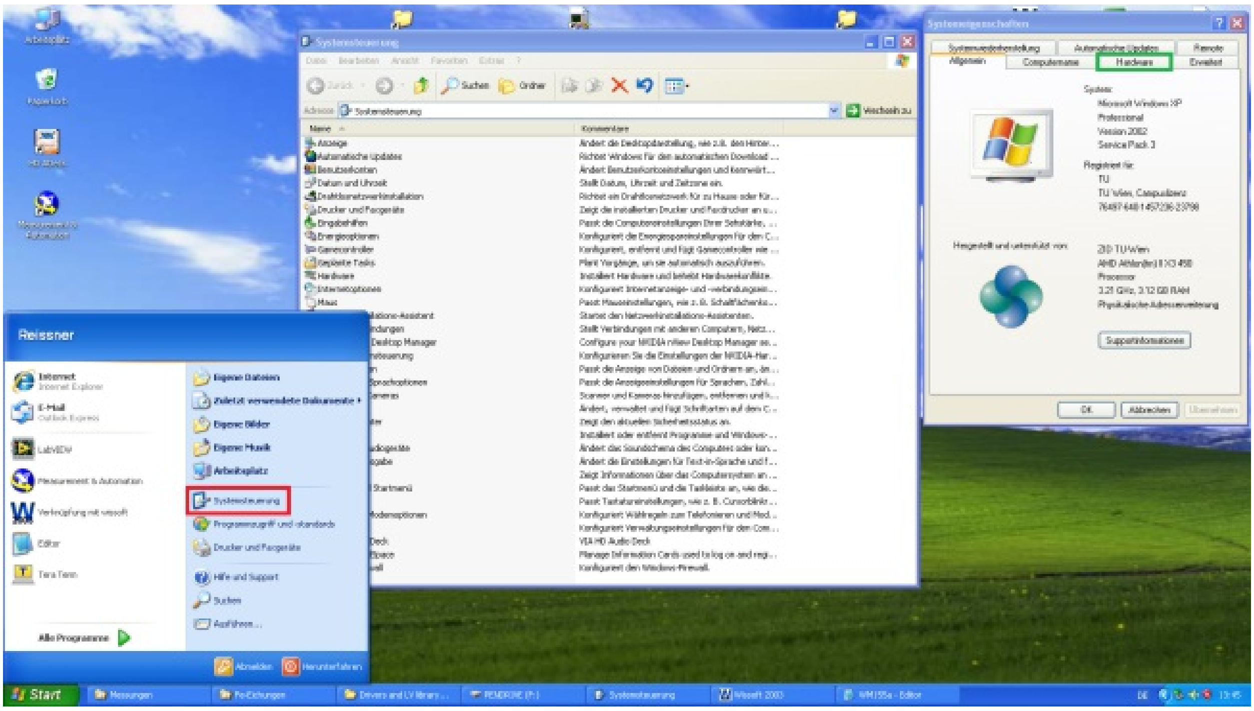

Figure A.13: Illustration for the setup process of the MercuryiPS unit in Windows XP. (Part 1)

Open "Systemsteuerung" by opening the Start menu and pressing the panel marked with a red rectangle in figure A.13. This will open the window displayed in the middle of figure A.13. Search for the button "System" and press it. The panel on the right in figure A.13 will open. Press on the tab "Hardware" which is marked with a green rectangle.

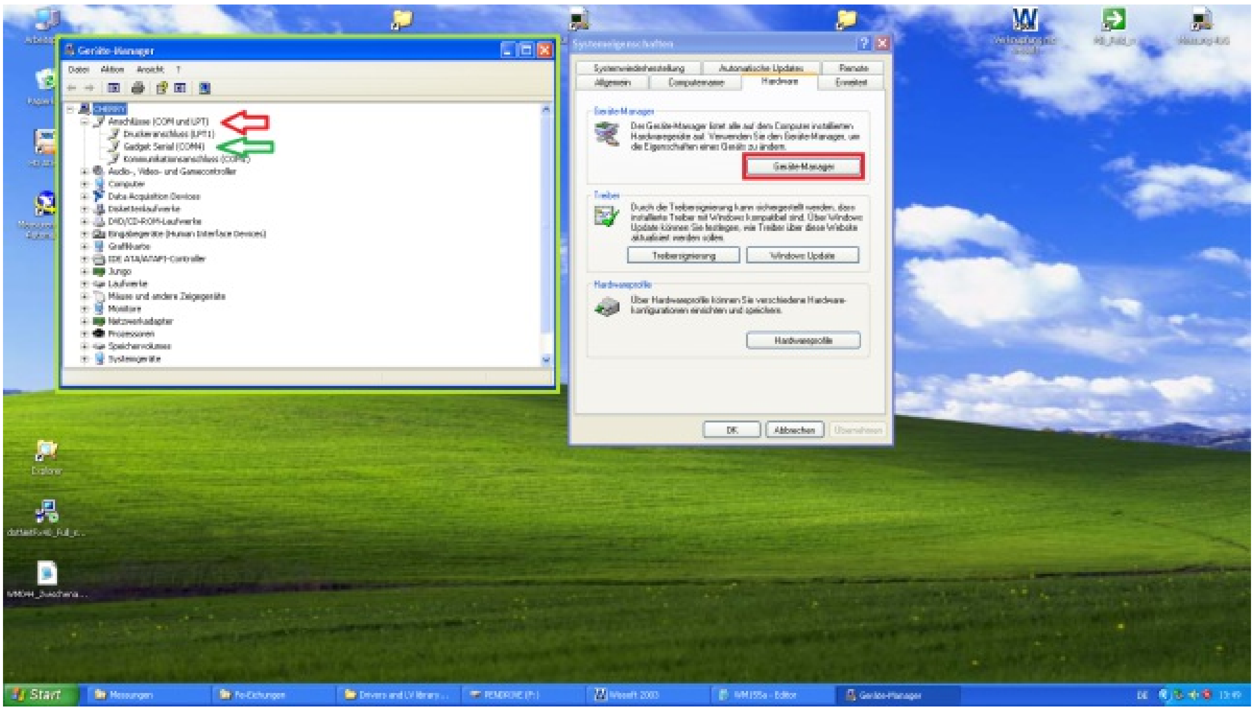

Der Geräte-Manager listet alle auf dem Computer installierten Hardwaregeräte auf. Verwenden Sie den Geräte-Manager, um die Eigenschaften eines Geräts zu ändern.

Durch die Treibersignierung kann sichergestellt werden, dass installierte Treiber mit Windows kompatibel sind. Über Windows Update können Sie festlegen, wie Treiber über diese Website aktualisiert werden sollen.

Über Hardwareprofile können Sie verschiedene Hardwarekonfigurationen einrichten und speichern.

Figure A.14: Illustration for the setup process of the MercuryiPS unit in Windows XP. (Part 2)

The left window in figure A.14 opens after the button "Geräte Manager" is pressed, which is marked with a red rectangle. Press the little plus next to "Anschlüsse (COM und LPT)", marked with a red arrow, followed by "Gadget serial", which is marked with a green arrow.

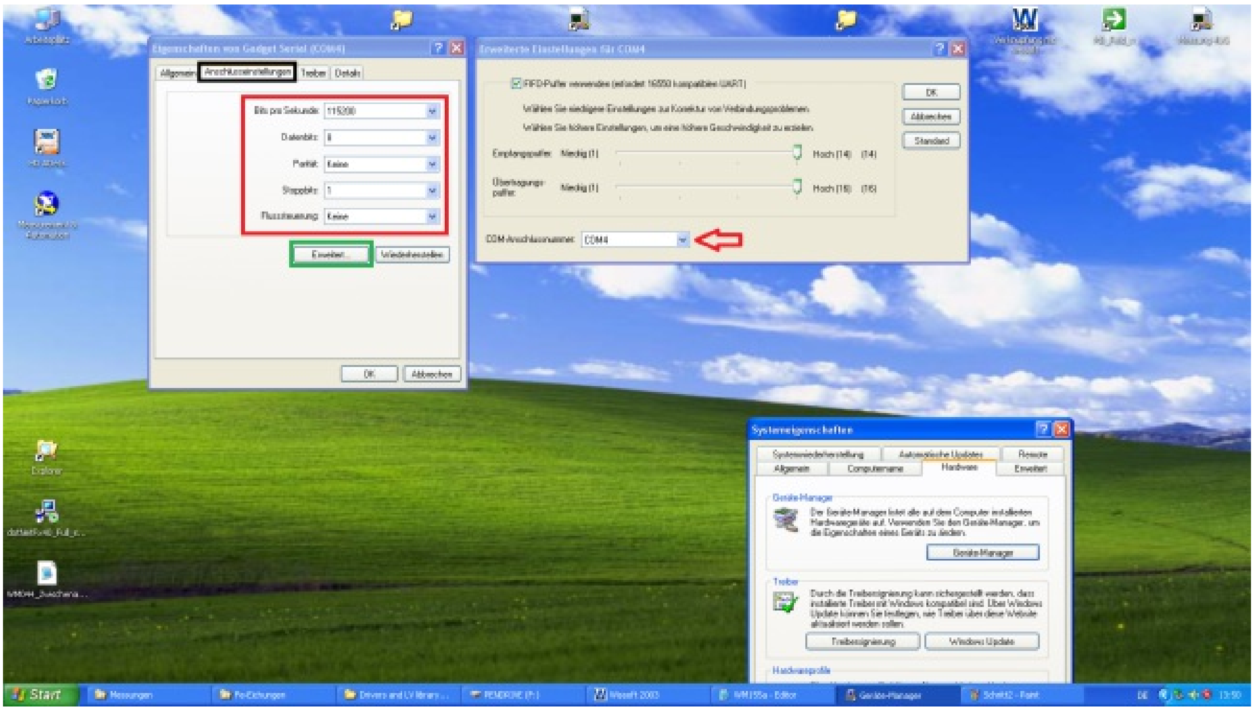

Eigenschaften von Gadget Serial (COM4)

Anschlusseinstellungen

Bits pro Sekunde: 115200
Datenbits: 8
Parität: Keine
Stoppbits: 1
Flusssteuerung: Keine

Erweiterte Einstellungen für COM4

☑ FIFO-Puffer verwenden (erfordert 16550 kompatiblen UART)

Wählen Sie niedrigere Einstellungen zur Korrektur von Verbindungsproblemen.

Wählen Sie höhere Einstellungen, um eine höhere Geschwindigkeit zu erzielen.

Empfangspuffer: Niedrig (1) Hoch (14) (14)
Übertragungspuffer: Niedrig (1) Hoch (16) (16)

COM-Anschlussnummer: COM4

Figure A.15: Illustration for the setup process of the MercuryiPS unit in Windows XP. (Part 3)

A new window will pop up. Press on "Anschlusseigenschaften", marked with a black rectangle, and enter all values displayed in the red rectangle of figure A.15. Afterwards press "Erweitert", marked with a green rectangle, which will open the window displayed on the right. Check if the Drop out Box marked with a red arrow is set to "COM4". Change it to this value, if it is not already.

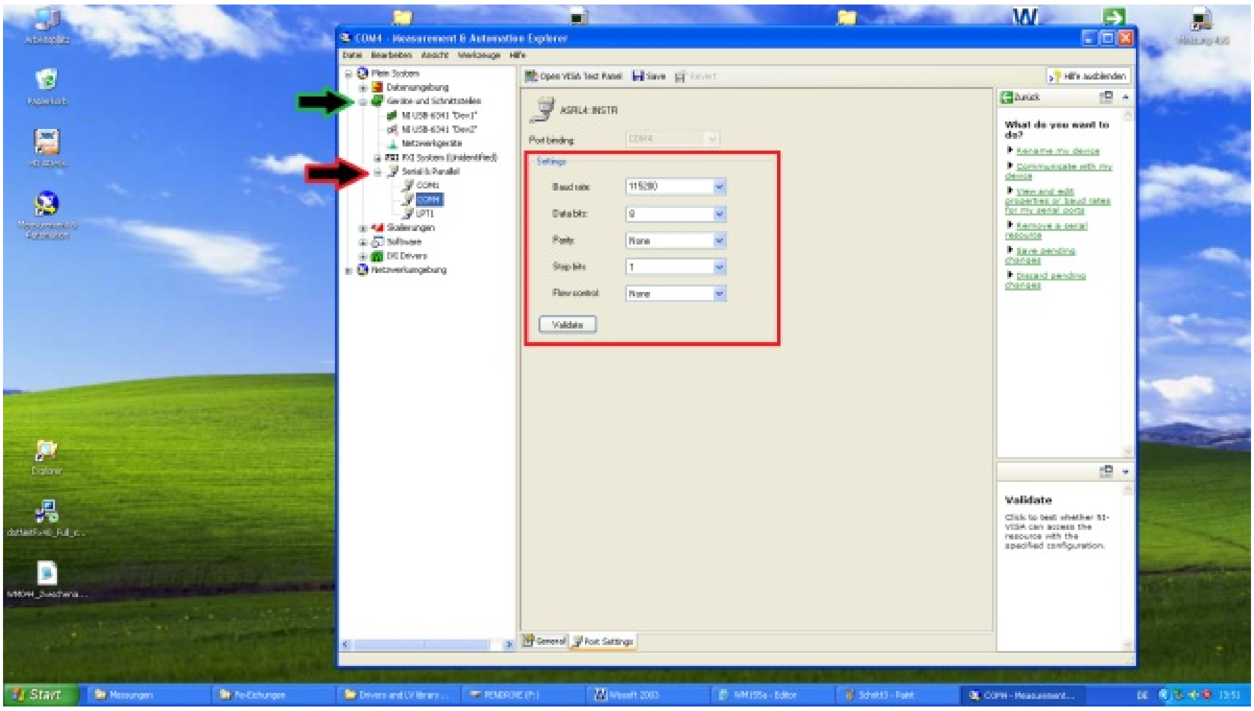

Port binding: COM4
Baud rate: 115200
Data bits: 8
Parity: None
Stop bits: 1
Flow control: None

Figure A.16: Illustration for the setup process of the MercuryiPS unit in NI MAX.

Open the program ”NI MAX”. A window similar to the window in figure A.16 will open. Press on ”Geräte und Schnittstellen” marked with a green arrow, followed by ”Seriell ß Parallel”, marked with a red arrow. Check if the values inside the red rectangle in figure A.16 correlate with the ones on the screen.

A.2 Manual use of the power supply MercuryIPS

Make sure that all steps described in chapter A.1.2.1 have been executed before keeping on with this chapter!

The screen of the MercuryiPS Unit will look like figure A.17 after powering up. In this state it is not possible to change either the main terminal output nor the persistent current of the magnet.


Current (A) -0.0006
Magnet (A) -0.0005
Voltage (V) -0.0003
Clamped
Rate Limit
Quench

Figure A.17: Homepanel of the MercuryiPS in operating state clamped

If the Labview Program "Mercury_Controls" shall be used to control the power supply, no further steps need to be taken.
For manual control hold the "Hold" button for a few seconds until the screen looks like figure A.18.


Current (A) -0.0006
Magnet (A) -0.0005
Voltage (V) 0.0000
Clamped
Rate Limit
Quench

Figure A.18: Homepanel of the MercuryiPS in the operating state hold

Tap the Button "Current (A)" to open the Submenu to set the new set point and ramp rate. (Figure: A.19). A press on "Home" lead back to the Home screen. (Figure: A.18) To ramp only the main output terminal press the button "To Set" and wait until the button "Hold" lights up again. If the persistent current shall also be changed, tap "Heater OFF" once and wait until it lights up and displays "Heater ON", and than press "To Set".


Set Point / Set Rate (Z axis)

Set Point (A) 1.0003

Set Rate (A/min) 4.0000

Figure A.19: Subpanel of MercuryiPS that displays the current set point and the ramp rate.

B Reports of Setup A and B

The following pages summarize the parameters used to fit the data of the measurements using setup A and B.

```
Modell: 1. Modell
```

```
Messung: MW329a           Probe: V1.84Fe1.16B2        vom 12.11.2019 (79.0h)
Ta: 4.2K    Tq: 294K    v: 1.0t    Bext: 0T
```

```
Anzahl der Schritte in der k-H Ebene   (Theta) :   0
                    in der x-y Ebene   ( Phi ) :   0
in k-V Ebene f.H=0, in der H-V Ebene   (Beta ) :   0
                    in der x'-y' Ebene (Alpha) :   0
Kanäle abgeschnitten: Vorne:   0           Bereich Anfang:   1
                     Hinten:   0                     Ende:  20
Glättung: Nein               Anzahl der Überläufe: 0            Spiegeln: Nein
Geraderichten: 0
Geschwindigkeitsparameter:  -4.744374    0.018233    0.059494   -0.026052
Fe Menge (Absorberdicke):  20.0 [mg/cm**2]  (-----)
Maximales t:   0.000
Basislinie: 3832060    Peakhoehe: 100756
```

```
21 Subspektren

Mittleres Feld (ohne antif. Anteil) =  89.294 kG
Mittleres eQVzz/4                   =  -0.090 mm/s
Mittlere Isomerie                   =  -0.021 mm/s

 Spektrum    Feld (kG)   Feld (mm/s)  eQVzz/4      Is       Gamma/2     Al(i)

  1                0.00      0.000     -0.090     -0.021      0.218      0.022
  2               10.90      0.350     -0.090     -0.021      0.218      0.000
  3               21.79      0.700     -0.090     -0.021      0.218      0.001
  4               32.69      1.050     -0.090     -0.021      0.218      0.008
  5               43.59      1.400     -0.090     -0.021      0.218      0.013
  6               54.48      1.750     -0.090     -0.021      0.218      0.023
  7               65.38      2.100     -0.090     -0.021      0.218      0.067
  8               76.28      2.450     -0.090     -0.021      0.218      0.001
  9               87.17      2.800     -0.090     -0.021      0.218      0.355
 10               98.07      3.150     -0.090     -0.021      0.218      0.453
 11              108.97      3.500     -0.090     -0.021      0.218      0.038
 12              119.86      3.850     -0.090     -0.021      0.218      0.000
 13              130.76      4.200     -0.090     -0.021      0.218      0.000
 14              141.66      4.550     -0.090     -0.021      0.218      0.009
 15              152.55      4.900     -0.090     -0.021      0.218      0.000
 16              163.45      5.250     -0.090     -0.021      0.218      0.011
 17              174.35      5.600     -0.090     -0.021      0.218      0.000
 18              185.24      5.950     -0.090     -0.021      0.218      0.000
 19              196.14      6.300     -0.090     -0.021      0.218      0.000
 20              207.04      6.650     -0.090     -0.021      0.218      0.000
 21              217.93      7.000     -0.090     -0.021      0.218      0.000
```

```
                  Theta      Beta      Alpha    Eta    rel.Tiefe  abs.Tiefe    area
                (450-x)*2                                1.Linie    1.Linie
                  für AF
     1              0.000    54.735     0.000  0.000    1.698        21         2.06
     2             54.735     0.000     0.000  0.000    0.017         0         0.02
     3             54.735     0.000     0.000  0.000    0.075         1         0.09
     4             54.735     0.000     0.000  0.000    0.650         8         0.77
     5             54.735     0.000     0.000  0.000    1.083        13         1.26
     6             54.735     0.000     0.000  0.000    2.007        24         2.28
     7             54.735     0.000     0.000  0.000    6.043        73         6.68
     8             54.735     0.000     0.000  0.000    0.047         1         0.05
     9             54.735     0.000     0.000  0.000   34.669       421        35.52
    10             54.735     0.000     0.000  0.000   46.503       565        45.44
    11             54.735     0.000     0.000  0.000    4.075        50         3.77
    12             54.735     0.000     0.000  0.000    0.000         0         0.00
    13             54.735     0.000     0.000  0.000    0.000         0         0.00
    14             54.735     0.000     0.000  0.000    1.170        14         0.87
    15             54.735     0.000     0.000  0.000    0.044         1         0.03
    16             54.735     0.000     0.000  0.000    1.869        23         1.14
    17             54.735     0.000     0.000  0.000    0.000         0         0.00
    18             54.735     0.000     0.000  0.000    0.021         0         0.01
    19             54.735     0.000     0.000  0.000    0.000         0         0.00
    20             54.735     0.000     0.000  0.000    0.030         0         0.01
    21             54.735     0.000     0.000  0.000    0.000         0         0.00
________________________________________________________________________________

 Relevanter Teil: 418 (420) Kanäle (Abweichung von Basis größer als 2 %)


 Weighted mean square deviation (gesamt)  :        2426.05    (       1932.16)
 Weighted mean square deviation (relevant):        2317.43    (       1822.87)
 Standardabweichung des Mittelwertes (Gesamtes Spektrum):             187.074
                                                              (       167.045)
                         (Relevanter Teil des Spektrums):             223.921
                                                              (       197.749)
 Korrelationskoeffizient             (Gesamtes Spektrum):            0.993599
                                                              (      0.994799)
                         (Relevanter Teil des Spektrums):            0.992483
                                                              (      0.993973)
 Statistischer Fehler =    0.000510839     Effekt (Fitkurve) =   1.0 %
                          (    0.0000    )                     (  0.0)
 Mittelwert d. Untergrunds (zw.   1. und  20. Kanal): YM=  3832444.
 Std. Abw.  d. Untergrunds (zw.   1. und  20. Kanal): YV=   2013.48

 Effekt aus Messspektrum (341 relevante Kanäle)     : 1.2
________________________________________________________________________________

Anm.:
________________________________________________________________________________

erstellt am 25.01.2021 um 15:18:49
```

```
Modell: 1. Modell

Messung: MW362a           Probe: V1.84Fe1.16B2        vom 03.02.2021 (190.0h)
Ta: 20K    Tq: 294K    v: 1.0t    Bext: 0T

Anzahl der Schritte in der k-H Ebene   (Theta) :   0
                    in der x-y Ebene   ( Phi ) :   0
in k-V Ebene f.H=0, in der H-V Ebene   (Beta ) :   0
                    in der x'-y' Ebene (Alpha) :   0
Kanäle abgeschnitten: Vorne:   0           Bereich Anfang:   1
                     Hinten:  20                     Ende:  20
Glättung: Nein               Anzahl der Überläufe: 0            Spiegeln: Nein
Geraderichten: 0
Geschwindigkeitsparameter:  -4.811299    0.018728    0.001201   -0.006505
Fe Menge (Absorberdicke):  20.0 [mg/cm**2]  (   0.0)
Maximales t:   1.885
Moerup-Both wird verwendet
Basislinie: 699110     Peakhoehe: 30487

21 Subspektren

Mittleres Feld (ohne antif. Anteil) =  83.660 kG
Mittleres eQVzz/4                   =  -0.074 mm/s
Mittlere Isomerie                   =  -0.033 mm/s

 Spektrum    Feld (kG)   Feld (mm/s)  eQVzz/4      Is       Gamma/2     Al(i)

  1                0.00      0.000     -0.074     -0.033      0.190      0.000
  2               10.90      0.350     -0.074     -0.033      0.190      0.021
  3               21.79      0.700     -0.074     -0.033      0.190      0.033
  4               32.69      1.050     -0.074     -0.033      0.190      0.011
  5               43.59      1.400     -0.074     -0.033      0.190      0.007
  6               54.48      1.750     -0.074     -0.033      0.190      0.088
  7               65.38      2.100     -0.074     -0.033      0.190      0.018
  8               76.28      2.450     -0.074     -0.033      0.190      0.176
  9               87.17      2.800     -0.074     -0.033      0.190      0.157
 10               98.07      3.150     -0.074     -0.033      0.190      0.468
 11              108.97      3.500     -0.074     -0.033      0.190      0.008
 12              119.86      3.850     -0.074     -0.033      0.190      0.000
 13              130.76      4.200     -0.074     -0.033      0.190      0.000
 14              141.66      4.550     -0.074     -0.033      0.190      0.000
 15              152.55      4.900     -0.074     -0.033      0.190      0.000
 16              163.45      5.250     -0.074     -0.033      0.190      0.000
 17              174.35      5.600     -0.074     -0.033      0.190      0.001
 18              185.24      5.950     -0.074     -0.033      0.190      0.007
 19              196.14      6.300     -0.074     -0.033      0.190      0.004
 20              207.04      6.650     -0.074     -0.033      0.190      0.000
 21              217.93      7.000     -0.074     -0.033      0.190      0.000
```

```
                  Theta       Beta      Alpha     Eta    rel.Tiefe  abs.Tiefe     area
                (450-x)*2                                  1.Linie    1.Linie
                  für AF
   1              0.000     54.735     0.000   0.000    0.012          0         0.02
   2             54.735      0.000     0.000   0.000    1.760          6         2.14
   3             54.735      0.000     0.000   0.000    2.901         11         3.43
   4             54.735      0.000     0.000   0.000    0.909          3         1.08
   5             54.735      0.000     0.000   0.000    0.640          2         0.75
   6             54.735      0.000     0.000   0.000    7.751         29         8.83
   7             54.735      0.000     0.000   0.000    1.620          6         1.79
   8             54.735      0.000     0.000   0.000   16.525         61        17.55
   9             54.735      0.000     0.000   0.000   15.483         57        15.71
  10             54.735      0.000     0.000   0.000   48.480        179        46.69
  11             54.735      0.000     0.000   0.000    0.876          3         0.79
  12             54.735      0.000     0.000   0.000    0.049          0         0.04
  13             54.735      0.000     0.000   0.000    0.001          0         0.00
  14             54.735      0.000     0.000   0.000    0.003          0         0.00
  15             54.735      0.000     0.000   0.000    0.000          0         0.00
  16             54.735      0.000     0.000   0.000    0.009          0         0.01
  17             54.735      0.000     0.000   0.000    0.175          1         0.09
  18             54.735      0.000     0.000   0.000    1.538          6         0.65
  19             54.735      0.000     0.000   0.000    1.236          5         0.43
  20             54.735      0.000     0.000   0.000    0.030          0         0.01
  21             54.735      0.000     0.000   0.000    0.000          0         0.00
________________________________________________________________________________

 Relevanter Teil: 396 (397) Kanäle (Abweichung von Basis größer als 2 %)


 Weighted mean square deviation (gesamt)  :         757.27    (       734.703)
 Weighted mean square deviation (relevant):        668.549    (       645.882)
 Standardabweichung des Mittelwertes (Gesamtes Spektrum):             46.3893
                                                              (       45.7101)
                         (Relevanter Teil des Spektrums):             54.1057
                                                              (       53.0671)
 Korrelationskoeffizient             (Gesamtes Spektrum):            0.995185
                                                              (      0.995324)
                         (Relevanter Teil des Spektrums):            0.994712
                                                              (      0.994902)
 Statistischer Fehler =      0.00119599     Effekt (Fitkurve) =   1.7 %
                        (     0.0000    )                      (  0.0)
 Mittelwert d. Untergrunds (zw.   1. und  20. Kanal): YM=   698761.
 Std. Abw.  d. Untergrunds (zw.   1. und  20. Kanal): YV=   764.221

 Effekt aus Messspektrum (317 relevante Kanäle)     : 2.1
________________________________________________________________________________

Anm.:
________________________________________________________________________________

erstellt am 04.02.2021 um 10:02:13
```

```
Modell: 1. Modell
```

```
Messung: MW180a           Probe: V1.81Fe0.16B2        vom 22.02.2017 (43.0h)
Ta: 30K    Tq: 294K    v: 1.0    Bext: 0T
```

```
Anzahl der Schritte in der k-H Ebene   (Theta) :   0
                    in der x-y Ebene   ( Phi ) :   0
in k-V Ebene f.H=0, in der H-V Ebene   (Beta ) :   0
                    in der x'-y' Ebene (Alpha) :   0
Kanäle abgeschnitten: Vorne:   0           Bereich Anfang:   1
                     Hinten:   0                     Ende:  20
Glättung: Nein               Anzahl der Überläufe: 0            Spiegeln: Nein
Geraderichten: 0
Geschwindigkeitsparameter:  -4.750569    0.018224    0.050958    0.003936
Fe Menge (Absorberdicke):  20.0 [mg/cm**2]  (  0.0)
Maximales t:   1.885
Moerup-Both wird verwendet
Basislinie: 1774729    Peakhoehe: 66250
```

```
21 Subspektren

Mittleres Feld (ohne antif. Anteil) =  69.015 kG
Mittleres eQVzz/4                   =  -0.088 mm/s
Mittlere Isomerie                   =  -0.035 mm/s

 Spektrum    Feld (kG)   Feld (mm/s)  eQVzz/4      Is       Gamma/2     Al(i)

  1                0.00      0.000     -0.088     -0.035      0.197      0.001
  2               10.90      0.350     -0.088     -0.035      0.197      0.096
  3               21.79      0.700     -0.088     -0.035      0.197      0.000
  4               32.69      1.050     -0.088     -0.035      0.197      0.004
  5               43.59      1.400     -0.088     -0.035      0.197      0.097
  6               54.48      1.750     -0.088     -0.035      0.197      0.102
  7               65.38      2.100     -0.088     -0.035      0.197      0.130
  8               76.28      2.450     -0.088     -0.035      0.197      0.031
  9               87.17      2.800     -0.088     -0.035      0.197      0.521
 10               98.07      3.150     -0.088     -0.035      0.197      0.007
 11              108.97      3.500     -0.088     -0.035      0.197      0.009
 12              119.86      3.850     -0.088     -0.035      0.197      0.000
 13              130.76      4.200     -0.088     -0.035      0.197      0.000
 14              141.66      4.550     -0.088     -0.035      0.197      0.000
 15              152.55      4.900     -0.088     -0.035      0.197      0.000
 16              163.45      5.250     -0.088     -0.035      0.197      0.000
 17              174.35      5.600     -0.088     -0.035      0.197      0.000
 18              185.24      5.950     -0.088     -0.035      0.197      0.000
 19              196.14      6.300     -0.088     -0.035      0.197      0.000
 20              207.04      6.650     -0.088     -0.035      0.197      0.000
 21              217.93      7.000     -0.088     -0.035      0.197      0.000
```

```
                Theta     Beta     Alpha    Eta   rel.Tiefe  abs.Tiefe    area
              (450-x)*2                            1.Linie    1.Linie
                für AF
   1              0.000   54.735    0.000  0.000   0.075         1         0.09
   2             54.735    0.000    0.000  0.000   8.578        57         9.67
   3             54.735    0.000    0.000  0.000   0.001         0         0.00
   4             54.735    0.000    0.000  0.000   0.392         3         0.43
   5             54.735    0.000    0.000  0.000   8.993        60         9.75
   6             54.735    0.000    0.000  0.000   9.664        65        10.24
   7             54.735    0.000    0.000  0.000   12.633        84        13.00
   8             54.735    0.000    0.000  0.000   3.133        21         3.11
   9             54.735    0.000    0.000  0.000   54.631       365        52.05
  10             54.735    0.000    0.000  0.000   0.793         5         0.72
  11             54.735    0.000    0.000  0.000   1.044         7         0.90
  12             54.735    0.000    0.000  0.000   0.009         0         0.01
  13             54.735    0.000    0.000  0.000   0.006         0         0.00
  14             54.735    0.000    0.000  0.000   0.002         0         0.00
  15             54.735    0.000    0.000  0.000   0.003         0         0.00
  16             54.735    0.000    0.000  0.000   0.032         0         0.02
  17             54.735    0.000    0.000  0.000   0.005         0         0.00
  18             54.735    0.000    0.000  0.000   0.004         0         0.00
  19             54.735    0.000    0.000  0.000   0.000         0         0.00
  20             54.735    0.000    0.000  0.000   0.000         0         0.00
  21             54.735    0.000    0.000  0.000   0.000         0         0.00
________________________________________________________________________________

 Relevanter Teil: 382 (382) Kanäle (Abweichung von Basis größer als 2 %)


 Weighted mean square deviation (gesamt)  :        1735.83    (       1735.83)
 Weighted mean square deviation (relevant):         1585.9    (        1585.9)
 Standardabweichung des Mittelwertes (Gesamtes Spektrum):               107.44
                                                              (        107.44)
                         (Relevanter Teil des Spektrums):              137.559
                                                              (       137.559)
 Korrelationskoeffizient             (Gesamtes Spektrum):             0.995174
                                                              (      0.995174)
                         (Relevanter Teil des Spektrums):             0.994367
                                                              (      0.994367)
 Statistischer Fehler =    0.000750644     Effekt (Fitkurve) =   1.5 %
                        (    0.0000    )                       (  0.0)
 Mittelwert d. Untergrunds (zw.   1. und  20. Kanal): YM=  1774842.
 Std. Abw.  d. Untergrunds (zw.   1. und  20. Kanal): YV=   1099.55

 Effekt aus Messspektrum (334 relevante Kanäle)     : 1.7
________________________________________________________________________________

Anm.:
________________________________________________________________________________

erstellt am 25.01.2021 um 09:49:16
```

```
Modell: 1. Modell

Messung: MW331a           Probe: V1.84Fe1.16B2        vom 18.11.2019 (139.0h)
Ta: 40K    Tq: 294K    v: 1.0t    Bext: 0T

Anzahl der Schritte in der k-H Ebene   (Theta) :   0
                    in der x-y Ebene   ( Phi ) :   0
in k-V Ebene f.H=0, in der H-V Ebene   (Beta ) :   0
                    in der x'-y' Ebene (Alpha) :   0
Kanäle abgeschnitten: Vorne:   0           Bereich Anfang:   1
                     Hinten:   0                     Ende:  20
Glättung: Nein               Anzahl der Überläufe: 0            Spiegeln: Nein
Geraderichten: 0
Geschwindigkeitsparameter:  -4.744374    0.018233    0.059494   -0.026052
Fe Menge (Absorberdicke):  20.0 [mg/cm**2]  (  0.0)
Maximales t:   1.885
Moerup-Both wird verwendet
Basislinie: 1583796    Peakhoehe: 53081

21 Subspektren

Mittleres Feld (ohne antif. Anteil) =  61.149 kG
Mittleres eQVzz/4                   =  -0.099 mm/s
Mittlere Isomerie                   =  -0.028 mm/s

 Spektrum    Feld (kG)   Feld (mm/s)  eQVzz/4      Is       Gamma/2     Al(i)

  1                0.00      0.000     -0.099     -0.028      0.192      0.002
  2               10.90      0.350     -0.099     -0.028      0.192      0.138
  3               21.79      0.700     -0.099     -0.028      0.192      0.084
  4               32.69      1.050     -0.099     -0.028      0.192      0.005
  5               43.59      1.400     -0.099     -0.028      0.192      0.086
  6               54.48      1.750     -0.099     -0.028      0.192      0.102
  7               65.38      2.100     -0.099     -0.028      0.192      0.130
  8               76.28      2.450     -0.099     -0.028      0.192      0.034
  9               87.17      2.800     -0.099     -0.028      0.192      0.393
 10               98.07      3.150     -0.099     -0.028      0.192      0.005
 11              108.97      3.500     -0.099     -0.028      0.192      0.016
 12              119.86      3.850     -0.099     -0.028      0.192      0.000
 13              130.76      4.200     -0.099     -0.028      0.192      0.001
 14              141.66      4.550     -0.099     -0.028      0.192      0.001
 15              152.55      4.900     -0.099     -0.028      0.192      0.000
 16              163.45      5.250     -0.099     -0.028      0.192      0.000
 17              174.35      5.600     -0.099     -0.028      0.192      0.000
 18              185.24      5.950     -0.099     -0.028      0.192      0.000
 19              196.14      6.300     -0.099     -0.028      0.192      0.001
 20              207.04      6.650     -0.099     -0.028      0.192      0.000
 21              217.93      7.000     -0.099     -0.028      0.192      0.000
```

```
                Theta     Beta     Alpha   Eta   rel.Tiefe  abs.Tiefe    area
              (450-x)*2                           1.Linie    1.Linie
                für AF
   1              0.000   54.735    0.000  0.000   0.123         1        0.14
   2             54.735    0.000    0.000  0.000   12.452         54       13.77
   3             54.735    0.000    0.000  0.000   7.665        33        8.42
   4             54.735    0.000    0.000  0.000   0.419         2        0.45
   5             54.735    0.000    0.000  0.000   8.108        35        8.64
   6             54.735    0.000    0.000  0.000   9.803        42       10.21
   7             54.735    0.000    0.000  0.000   12.860        55       13.02
   8             54.735    0.000    0.000  0.000   3.520        15        3.45
   9             54.735    0.000    0.000  0.000   41.886       180       39.38
  10             54.735    0.000    0.000  0.000   0.558         2        0.50
  11             54.735    0.000    0.000  0.000   1.938         8        1.65
  12             54.735    0.000    0.000  0.000   0.029         0        0.02
  13             54.735    0.000    0.000  0.000   0.085         0        0.06
  14             54.735    0.000    0.000  0.000   0.167         1        0.12
  15             54.735    0.000    0.000  0.000   0.011         0        0.01
  16             54.735    0.000    0.000  0.000   0.042         0        0.02
  17             54.735    0.000    0.000  0.000   0.055         0        0.03
  18             54.735    0.000    0.000  0.000   0.027         0        0.01
  19             54.735    0.000    0.000  0.000   0.245         1        0.09
  20             54.735    0.000    0.000  0.000   0.008         0        0.00
  21             54.735    0.000    0.000  0.000   0.000         0        0.00
```

```
 Relevanter Teil: 351 (351) Kanäle (Abweichung von Basis größer als 2 %)


 Weighted mean square deviation (gesamt)  :        1468.19    (       1468.19)
 Weighted mean square deviation (relevant):        1304.04    (       1304.04)
 Standardabweichung des Mittelwertes (Gesamtes Spektrum):              93.463
                                                              (        93.463)
                        (Relevanter Teil des Spektrums):              128.403
                                                              (       128.403)
 Korrelationskoeffizient            (Gesamtes Spektrum):             0.992364
                                                              (      0.992364)
                        (Relevanter Teil des Spektrums):             0.990749
                                                              (      0.990749)
 Statistischer Fehler =    0.000794603     Effekt (Fitkurve) =   1.2 %
                       (    0.0000    )                        (  0.0)
 Mittelwert d. Untergrunds (zw.   1. und  20. Kanal): YM=  1583405.
 Std. Abw.  d. Untergrunds (zw.   1. und  20. Kanal): YV=   1120.42

 Effekt aus Messspektrum (280 relevante Kanäle)     : 1.5
```

Anm.:

---

erstellt am 25.01.2021 um 10:12:33

```
Modell: 1. Modell

Messung: MW207            Probe: V1.84Fe1.16B2        vom 02.06.2017 (34.0h)
Ta: 50K    Tq: 294K    v: 2.2s    Bext: 0T

Anzahl der Schritte in der k-H Ebene   (Theta) :   0
                    in der x-y Ebene   ( Phi ) :   0
in k-V Ebene f.H=0, in der H-V Ebene   (Beta ) :   0
                    in der x'-y' Ebene (Alpha) :   0
Kanäle abgeschnitten: Vorne:   0           Bereich Anfang:   1
                     Hinten:   0                     Ende:  20
Glättung: Nein               Anzahl der Überläufe: 0            Spiegeln: Nein
Geraderichten: 0
Geschwindigkeitsparameter:  10.547052    0.255214    0.000502   -0.006942
Fe Menge (Absorberdicke):  20.0 [mg/cm**2]  (  0.0)
Maximales t:   1.885
Moerup-Both wird verwendet
Basislinie: 769499     Peakhoehe: 40611

21 Subspektren

Mittleres Feld (ohne antif. Anteil) =  57.553 kG
Mittleres eQVzz/4                   =  -0.091 mm/s
Mittlere Isomerie                   =  -0.024 mm/s

 Spektrum    Feld (kG)   Feld (mm/s)  eQVzz/4      Is       Gamma/2     Al(i)

  1                0.00      0.000     -0.091     -0.024      0.173      0.002
  2               10.90      0.350     -0.091     -0.024      0.173      0.147
  3               21.79      0.700     -0.091     -0.024      0.173      0.097
  4               32.69      1.050     -0.091     -0.024      0.173      0.006
  5               43.59      1.400     -0.091     -0.024      0.173      0.137
  6               54.48      1.750     -0.091     -0.024      0.173      0.102
  7               65.38      2.100     -0.091     -0.024      0.173      0.124
  8               76.28      2.450     -0.091     -0.024      0.173      0.033
  9               87.17      2.800     -0.091     -0.024      0.173      0.328
 10               98.07      3.150     -0.091     -0.024      0.173      0.006
 11              108.97      3.500     -0.091     -0.024      0.173      0.014
 12              119.86      3.850     -0.091     -0.024      0.173      0.000
 13              130.76      4.200     -0.091     -0.024      0.173      0.001
 14              141.66      4.550     -0.091     -0.024      0.173      0.001
 15              152.55      4.900     -0.091     -0.024      0.173      0.000
 16              163.45      5.250     -0.091     -0.024      0.173      0.000
 17              174.35      5.600     -0.091     -0.024      0.173      0.000
 18              185.24      5.950     -0.091     -0.024      0.173      0.000
 19              196.14      6.300     -0.091     -0.024      0.173      0.001
 20              207.04      6.650     -0.091     -0.024      0.173      0.000
 21              217.93      7.000     -0.091     -0.024      0.173      0.000
```

```
                Theta      Beta      Alpha    Eta    rel.Tiefe  abs.Tiefe     area
              (450-x)*2                             1.Linie    1.Linie
                für AF
   1             0.000    54.735     0.000  0.000    0.353        192        0.15
   2            54.735     0.000     0.000  0.000   28.772      15634       14.67
   3            54.735     0.000     0.000  0.000   15.245       8284        9.67
   4            54.735     0.000     0.000  0.000    0.522        284        0.63
   5            54.735     0.000     0.000  0.000   10.794       5865       13.64
   6            54.735     0.000     0.000  0.000    7.856       4269      10.17
   7            54.735     0.000     0.000  0.000    8.634       4692      12.37
   8            54.735     0.000     0.000  0.000    2.325       1263       3.26
   9            54.735     0.000     0.000  0.000   23.788      12926       32.94
  10            54.735     0.000     0.000  0.000    0.442        240       0.61
  11            54.735     0.000     0.000  0.000    0.968        526       1.45
  12            54.735     0.000     0.000  0.000    0.018         10       0.03
  13            54.735     0.000     0.000  0.000    0.059         32       0.08
  14            54.735     0.000     0.000  0.000    0.100         54       0.14
  15            54.735     0.000     0.000  0.000    0.008          4       0.01
  16            54.735     0.000     0.000  0.000    0.015          8       0.02
  17            54.735     0.000     0.000  0.000    0.023         12       0.03
  18            54.735     0.000     0.000  0.000    0.007          4       0.01
  19            54.735     0.000     0.000  0.000    0.063         34       0.09
  20            54.735     0.000     0.000  0.000    0.008          4       0.01
  21            54.735     0.000     0.000  0.000    0.000          0       0.00
________________________________________________________________________________

 Relevanter Teil:  92 ( 92) Kanäle (Abweichung von Basis größer als 2 %)


 Weighted mean square deviation (gesamt)  :        738.386    (        738.386)
 Weighted mean square deviation (relevant):        241.893    (        241.893)
 Standardabweichung des Mittelwertes (Gesamtes Spektrum):              46.2843
                                                              (        46.2843)
                        (Relevanter Teil des Spektrums):              146.259
                                                              (        146.259)
 Korrelationskoeffizient            (Gesamtes Spektrum):              0.991707
                                                              (       0.991707)
                        (Relevanter Teil des Spektrums):              0.993929
                                                              (       0.993929)
 Statistischer Fehler =     0.00113998     Effekt (Fitkurve) =   1.9 %
                         (    0.0000    )                      (  0.0)
 Mittelwert d. Untergrunds (zw.   1. und  20. Kanal): YM=   769114.
 Std. Abw.  d. Untergrunds (zw.   1. und  20. Kanal): YV=   747.749

 Effekt aus Messspektrum (133 relevante Kanäle)     : 1.4
________________________________________________________________________________

Anm.:
________________________________________________________________________________

erstellt am 25.01.2021 um 10:19:03
```

```
Modell: 1. Modell

Messung: MW182a           Probe: V1.81Fe0.16B2        vom 27.02.2017 (22.0h)
Ta: 60K    Tq: 294K    v: 1.0    Bext: 0T

Anzahl der Schritte in der k-H Ebene   (Theta) :   0
                    in der x-y Ebene   ( Phi ) :   0
in k-V Ebene f.H=0, in der H-V Ebene   (Beta ) :   0
                    in der x'-y' Ebene (Alpha) :   0
Kanäle abgeschnitten: Vorne:   0           Bereich Anfang:   1
                     Hinten:   0                     Ende:  20
Glättung: Nein               Anzahl der Überläufe: 0            Spiegeln: Nein
Geraderichten: 0
Geschwindigkeitsparameter:  -4.750569    0.018224    0.050958    0.003936
Fe Menge (Absorberdicke):  20.0 [mg/cm**2]  (-----)
Maximales t:   0.000
Moerup-Both wird verwendet
Basislinie: 2426275    Peakhoehe: 146381

21 Subspektren

Mittleres Feld (ohne antif. Anteil) =  43.235 kG
Mittleres eQVzz/4                   =  -0.111 mm/s
Mittlere Isomerie                   =  -0.020 mm/s

 Spektrum    Feld (kG)   Feld (mm/s)  eQVzz/4      Is       Gamma/2     Al(i)

  1                0.00      0.000     -0.111     -0.020      0.197      0.000
  2               10.90      0.350     -0.111     -0.020      0.197      0.343
  3               21.79      0.700     -0.111     -0.020      0.197      0.001
  4               32.69      1.050     -0.111     -0.020      0.197      0.054
  5               43.59      1.400     -0.111     -0.020      0.197      0.223
  6               54.48      1.750     -0.111     -0.020      0.197      0.011
  7               65.38      2.100     -0.111     -0.020      0.197      0.142
  8               76.28      2.450     -0.111     -0.020      0.197      0.159
  9               87.17      2.800     -0.111     -0.020      0.197      0.062
 10               98.07      3.150     -0.111     -0.020      0.197      0.001
 11              108.97      3.500     -0.111     -0.020      0.197      0.000
 12              119.86      3.850     -0.111     -0.020      0.197      0.000
 13              130.76      4.200     -0.111     -0.020      0.197      0.003
 14              141.66      4.550     -0.111     -0.020      0.197      0.000
 15              152.55      4.900     -0.111     -0.020      0.197      0.000
 16              163.45      5.250     -0.111     -0.020      0.197      0.000
 17              174.35      5.600     -0.111     -0.020      0.197      0.000
 18              185.24      5.950     -0.111     -0.020      0.197      0.000
 19              196.14      6.300     -0.111     -0.020      0.197      0.000
 20              207.04      6.650     -0.111     -0.020      0.197      0.000
 21              217.93      7.000     -0.111     -0.020      0.197      0.000
```

```
                  Theta       Beta      Alpha    Eta    rel.Tiefe  abs.Tiefe    area
                (450-x)*2                                 1.Linie    1.Linie
                  für AF
     1             0.000    54.735     0.000  0.000     0.025         0         0.03
     2            54.735     0.000     0.000  0.000    32.256       252        34.23
     3            54.735     0.000     0.000  0.000     0.123         1         0.13
     4            54.735     0.000     0.000  0.000     5.588        44         5.68
     5            54.735     0.000     0.000  0.000    21.765       170        22.22
     6            54.735     0.000     0.000  0.000     1.074         8         1.07
     7            54.735     0.000     0.000  0.000    14.609       114        14.15
     8            54.735     0.000     0.000  0.000    16.892       132        15.79
     9            54.735     0.000     0.000  0.000     6.898        54         6.19
    10            54.735     0.000     0.000  0.000     0.112         1         0.10
    11            54.735     0.000     0.000  0.000     0.053         0         0.04
    12            54.735     0.000     0.000  0.000     0.015         0         0.01
    13            54.735     0.000     0.000  0.000     0.392         3         0.28
    14            54.735     0.000     0.000  0.000     0.006         0         0.00
    15            54.735     0.000     0.000  0.000     0.000         0         0.00
    16            54.735     0.000     0.000  0.000     0.028         0         0.02
    17            54.735     0.000     0.000  0.000     0.008         0         0.00
    18            54.735     0.000     0.000  0.000     0.008         0         0.00
    19            54.735     0.000     0.000  0.000     0.128         1         0.04
    20            54.735     0.000     0.000  0.000     0.019         0         0.01
    21            54.735     0.000     0.000  0.000     0.000         0         0.00
________________________________________________________________________________

 Relevanter Teil: 287 (287) Kanäle (Abweichung von Basis größer als 2 %)


 Weighted mean square deviation (gesamt)  :        3053.89    (       3053.89)
 Weighted mean square deviation (relevant):        2811.93    (       2811.93)
 Standardabweichung des Mittelwertes (Gesamtes Spektrum):             165.128
                                                              (       165.128)
                         (Relevanter Teil des Spektrums):             282.421
                                                              (       282.421)
 Korrelationskoeffizient             (Gesamtes Spektrum):            0.995541
                                                              (      0.995541)
                         (Relevanter Teil des Spektrums):             0.99405
                                                              (       0.99405)
 Statistischer Fehler =     0.000641993     Effekt (Fitkurve) =   1.9 %
                        (     0.0000     )                     (  0.0)
 Mittelwert d. Untergrunds (zw.   1. und  20. Kanal): YM=  2426062.
 Std. Abw.  d. Untergrunds (zw.   1. und  20. Kanal): YV=   1580.06

 Effekt aus Messspektrum (280 relevante Kanäle)     : 1.9
________________________________________________________________________________

Anm.:
________________________________________________________________________________

erstellt am 25.01.2021 um 13:41:55
```

```
Modell: 1. Modell

Messung: MW208            Probe: V1.84Fe1.16B2        vom 09.06.2017 (198.0h)
Ta: 80K    Tq: 294K    v: 2.2s    Bext: 0T

Anzahl der Schritte in der k-H Ebene   (Theta) :   0
                    in der x-y Ebene   ( Phi ) :   0
in k-V Ebene f.H=0, in der H-V Ebene   (Beta ) :   0
                    in der x'-y' Ebene (Alpha) :   0
Kanäle abgeschnitten: Vorne:    0           Bereich Anfang:   1
                     Hinten:    0                     Ende:  20
Glättung: Nein               Anzahl der Überläufe: 0           Spiegeln: Nein
Geraderichten: 0
Geschwindigkeitsparameter:  10.536363    0.255132    0.000837   -0.008770
Fe Menge (Absorberdicke):  20.0 [mg/cm**2]  (   0.0)
Maximales t:   1.885
Moerup-Both wird verwendet
Basislinie: 1655434    Peakhoehe: 133261

21 Subspektren

Mittleres Feld (ohne antif. Anteil) =  24.826 kG
Mittleres eQVzz/4                   =  -0.121 mm/s
Mittlere Isomerie                   =  -0.021 mm/s

 Spektrum    Feld (kG)   Feld (mm/s)   eQVzz/4       Is        Gamma/2      Al(i)

  1                0.00      0.000     -0.121     -0.021      0.256      0.001
  2               10.90      0.350     -0.121     -0.021      0.256      0.703
  3               21.79      0.700     -0.121     -0.021      0.256      0.002
  4               32.69      1.050     -0.121     -0.021      0.256      0.051
  5               43.59      1.400     -0.121     -0.021      0.256      0.065
  6               54.48      1.750     -0.121     -0.021      0.256      0.019
  7               65.38      2.100     -0.121     -0.021      0.256      0.135
  8               76.28      2.450     -0.121     -0.021      0.256      0.000
  9               87.17      2.800     -0.121     -0.021      0.256      0.015
 10               98.07      3.150     -0.121     -0.021      0.256      0.001
 11              108.97      3.500     -0.121     -0.021      0.256      0.001
 12              119.86      3.850     -0.121     -0.021      0.256      0.000
 13              130.76      4.200     -0.121     -0.021      0.256      0.005
 14              141.66      4.550     -0.121     -0.021      0.256      0.000
 15              152.55      4.900     -0.121     -0.021      0.256      0.000
 16              163.45      5.250     -0.121     -0.021      0.256      0.000
 17              174.35      5.600     -0.121     -0.021      0.256      0.002
 18              185.24      5.950     -0.121     -0.021      0.256      0.000
 19              196.14      6.300     -0.121     -0.021      0.256      0.001
 20              207.04      6.650     -0.121     -0.021      0.256      0.000
 21              217.93      7.000     -0.121     -0.021      0.256      0.000
```

```
                Theta     Beta     Alpha   Eta   rel.Tiefe  abs.Tiefe    area
              (450-x)*2                           1.Linie    1.Linie
                für AF
   1              0.000   54.735    0.000  0.000   0.073        97        0.06
   2             54.735    0.000    0.000  0.000   83.197    110353       70.26
   3             54.735    0.000    0.000  0.000   0.171      227         0.17
   4             54.735    0.000    0.000  0.000   3.997      5301        5.09
   5             54.735    0.000    0.000  0.000   4.776      6336        6.49
   6             54.735    0.000    0.000  0.000   1.176      1560        1.87
   7             54.735    0.000    0.000  0.000   5.615      7448       13.55
   8             54.735    0.000    0.000  0.000   0.008        10        0.02
   9             54.735    0.000    0.000  0.000   0.604       801        1.47
  10             54.735    0.000    0.000  0.000   0.035        46        0.09
  11             54.735    0.000    0.000  0.000   0.019        26        0.05
  12             54.735    0.000    0.000  0.000   0.009        12        0.02
  13             54.735    0.000    0.000  0.000   0.180       238        0.46
  14             54.735    0.000    0.000  0.000   0.002         3        0.01
  15             54.735    0.000    0.000  0.000   0.000         0        0.00
  16             54.735    0.000    0.000  0.000   0.015        20        0.04
  17             54.735    0.000    0.000  0.000   0.075        99        0.20
  18             54.735    0.000    0.000  0.000   0.000         0        0.00
  19             54.735    0.000    0.000  0.000   0.040        53        0.11
  20             54.735    0.000    0.000  0.000   0.007        10        0.02
  21             54.735    0.000    0.000  0.000   0.000         0        0.00
________________________________________________________________________________

 Relevanter Teil:  80 ( 80) Kanäle (Abweichung von Basis größer als 2 %)


 Weighted mean square deviation (gesamt)  :        2204.23    (       2204.23)
 Weighted mean square deviation (relevant):        1700.11    (       1700.11)
 Standardabweichung des Mittelwertes (Gesamtes Spektrum):              115.34
                                                              (        115.34)
                         (Relevanter Teil des Spektrums):             647.145
                                                              (       647.145)
 Korrelationskoeffizient             (Gesamtes Spektrum):            0.990178
                                                              (      0.990178)
                         (Relevanter Teil des Spektrums):            0.988507
                                                              (      0.988507)
 Statistischer Fehler =     0.00077722     Effekt (Fitkurve) =   1.9 %
                        (    0.0000    )                       (  0.0)
 Mittelwert d. Untergrunds (zw.   1. und  20. Kanal): YM=  1654607.
 Std. Abw.  d. Untergrunds (zw.   1. und  20. Kanal): YV=   980.431

 Effekt aus Messspektrum (131 relevante Kanäle)    : 1.2
________________________________________________________________________________

Anm.:
________________________________________________________________________________

erstellt am 25.01.2021 um 13:57:38
```

```
Modell: 1. Modell
```

```
Messung: MW173            Probe: V1.89Fe1.16B2       vom 16.01.2017 (159.0h)
Ta: 100K    Tq: 294K    v: 2.2s    Bext: 0T
```

```
Anzahl der Schritte in der k-H Ebene   (Theta) :   0
                    in der x-y Ebene   ( Phi ) :   0
in k-V Ebene f.H=0, in der H-V Ebene   (Beta ) :   0
                    in der x'-y' Ebene (Alpha) :   0
Kanäle abgeschnitten: Vorne:   0          Bereich Anfang:   1
                     Hinten:   0                    Ende:  20
Glättung: Nein             Anzahl der Überläufe: 0            Spiegeln: Nein
Geraderichten: 0
Geschwindigkeitsparameter:  10.504958    0.255076    0.000357   -0.003983
Fe Menge (Absorberdicke):  40.0 [mg/cm**2]  (-----)
Maximales t:   3.770
Moerup-Both wird verwendet
Basislinie: 2729864    Peakhoehe: 166177
```

```
21 Subspektren

Mittleres Feld (ohne antif. Anteil) =   0.322 kG
Mittleres eQVzz/4                   =  -0.184 mm/s
Mittlere Isomerie                   =  -0.022 mm/s

 Spektrum    Feld (kG)   Feld (mm/s)  eQVzz/4      Is       Gamma/2     Al(i)

  1             0.00       0.000     -0.184     -0.022      0.201      0.981
  2            10.90       0.350     -0.184     -0.022      0.201      0.019
  3            21.79       0.700     -0.184     -0.022      0.201      0.000
  4            32.69       1.050     -0.184     -0.022      0.201      0.000
  5            43.59       1.400     -0.184     -0.022      0.201      0.000
  6            54.48       1.750     -0.184     -0.022      0.201      0.000
  7            65.38       2.100     -0.184     -0.022      0.201      0.000
  8            76.28       2.450     -0.184     -0.022      0.201      0.000
  9            87.17       2.800     -0.184     -0.022      0.201      0.000
 10            98.07       3.150     -0.184     -0.022      0.201      0.000
 11           108.97       3.500     -0.184     -0.022      0.201      0.000
 12           119.86       3.850     -0.184     -0.022      0.201      0.000
 13           130.76       4.200     -0.184     -0.022      0.201      0.000
 14           141.66       4.550     -0.184     -0.022      0.201      0.000
 15           152.55       4.900     -0.184     -0.022      0.201      0.000
 16           163.45       5.250     -0.184     -0.022      0.201      0.000
 17           174.35       5.600     -0.184     -0.022      0.201      0.000
 18           185.24       5.950     -0.184     -0.022      0.201      0.000
 19           196.14       6.300     -0.184     -0.022      0.201      0.000
 20           207.04       6.650     -0.184     -0.022      0.201      0.000
 21           217.93       7.000     -0.184     -0.022      0.201      0.000
```

```
                Theta     Beta     Alpha   Eta   rel.Tiefe  abs.Tiefe    area
              (450-x)*2                           1.Linie    1.Linie
                für AF
   1              0.000   54.735    0.000  0.000   97.167    153579       97.05
   2             54.735    0.000    0.000  0.000   2.833      4477        2.95
   3             54.735    0.000    0.000  0.000   0.000         0        0.00
   4             54.735    0.000    0.000  0.000   0.000         0        0.00
   5             54.735    0.000    0.000  0.000   0.000         0        0.00
   6             54.735    0.000    0.000  0.000   0.000         0        0.00
   7             54.735    0.000    0.000  0.000   0.000         0        0.00
   8             54.735    0.000    0.000  0.000   0.000         0        0.00
   9             54.735    0.000    0.000  0.000   0.000         0        0.00
  10             54.735    0.000    0.000  0.000   0.000         0        0.00
  11             54.735    0.000    0.000  0.000   0.000         0        0.00
  12             54.735    0.000    0.000  0.000   0.000         0        0.00
  13             54.735    0.000    0.000  0.000   0.000         0        0.00
  14             54.735    0.000    0.000  0.000   0.000         0        0.00
  15             54.735    0.000    0.000  0.000   0.000         0        0.00
  16             54.735    0.000    0.000  0.000   0.000         0        0.00
  17             54.735    0.000    0.000  0.000   0.000         0        0.00
  18             54.735    0.000    0.000  0.000   0.000         0        0.00
  19             54.735    0.000    0.000  0.000   0.000         0        0.00
  20             54.735    0.000    0.000  0.000   0.000         0        0.00
  21             54.735    0.000    0.000  0.000   0.000         0        0.00
________________________________________________________________________________

 Relevanter Teil:  57 ( 57) Kanäle (Abweichung von Basis größer als 2 %)


 Weighted mean square deviation (gesamt)   :        701.32    (       702.985)
 Weighted mean square deviation (relevant):        231.596    (       233.204)
 Standardabweichung des Mittelwertes (Gesamtes Spektrum):             84.9984
                                                              (       85.0971)
                         (Relevanter Teil des Spektrums):             436.653
                                                              (       438.171)
 Korrelationskoeffizient             (Gesamtes Spektrum):            0.996387
                                                              (      0.996381)
                         (Relevanter Teil des Spektrums):            0.998236
                                                              (      0.998218)
 Statistischer Fehler =    0.000605243     Effekt (Fitkurve) =   1.6 %
                        (    0.0000    )                       (  0.0)
 Mittelwert d. Untergrunds (zw.   1. und  20. Kanal): YM=  2729499.
 Std. Abw.  d. Untergrunds (zw.   1. und  20. Kanal): YV=   1628.22

 Effekt aus Messspektrum (109 relevante Kanäle)     : 0.9
________________________________________________________________________________

Anm.:
________________________________________________________________________________

erstellt am 21.01.2021 um 12:16:43
```

```
Modell: 1. Modell

Messung: MW332a           Probe: V1.84Fe1.16B2        vom 22.11.2019 (72.0h)
Ta: 125K    Tq: 294K    v: 1.0t    Bext: 0T

Anzahl der Schritte in der k-H Ebene   (Theta) :   0
                    in der x-y Ebene   ( Phi ) :   0
in k-V Ebene f.H=0, in der H-V Ebene   (Beta ) :   0
                    in der x'-y' Ebene (Alpha) :   0
Kanäle abgeschnitten: Vorne:   0          Bereich Anfang:   1
                     Hinten:   0                    Ende:  20
Glättung: Nein               Anzahl der Überläufe: 0           Spiegeln: Nein
Geraderichten: 0
Geschwindigkeitsparameter:  -4.748140    0.018396    0.009442   -0.008691
Fe Menge (Absorberdicke):  20.0 [mg/cm**2]  (  0.0)
Maximales t:   1.885
Moerup-Both wird verwendet
Basislinie: 698348     Peakhoehe: 47002

21 Subspektren

Mittleres Feld (ohne antif. Anteil) =   0.644 kG
Mittleres eQVzz/4                   =  -0.186 mm/s
Mittlere Isomerie                   =  -0.058 mm/s

 Spektrum    Feld (kG)   Feld (mm/s)  eQVzz/4      Is       Gamma/2     Al(i)

  1                0.00      0.000     -0.186     -0.058      0.170      0.948
  2               10.90      0.350     -0.186     -0.058      0.170      0.052
  3               21.79      0.700     -0.186     -0.058      0.170      0.000
  4               32.69      1.050     -0.186     -0.058      0.170      0.000
  5               43.59      1.400     -0.186     -0.058      0.170      0.000
  6               54.48      1.750     -0.186     -0.058      0.170      0.000
  7               65.38      2.100     -0.186     -0.058      0.170      0.000
  8               76.28      2.450     -0.186     -0.058      0.170      0.000
  9               87.17      2.800     -0.186     -0.058      0.170      0.000
 10               98.07      3.150     -0.186     -0.058      0.170      0.000
 11              108.97      3.500     -0.186     -0.058      0.170      0.000
 12              119.86      3.850     -0.186     -0.058      0.170      0.000
 13              130.76      4.200     -0.186     -0.058      0.170      0.000
 14              141.66      4.550     -0.186     -0.058      0.170      0.000
 15              152.55      4.900     -0.186     -0.058      0.170      0.000
 16              163.45      5.250     -0.186     -0.058      0.170      0.000
 17              174.35      5.600     -0.186     -0.058      0.170      0.000
 18              185.24      5.950     -0.186     -0.058      0.170      0.000
 19              196.14      6.300     -0.186     -0.058      0.170      0.000
 20              207.04      6.650     -0.186     -0.058      0.170      0.000
 21              217.93      7.000     -0.186     -0.058      0.170      0.000
```

```
                Theta     Beta     Alpha   Eta   rel.Tiefe  abs.Tiefe    area
              (450-x)*2                           1.Linie    1.Linie
                für AF
   1              0.000   54.735    0.000  0.000   93.784        98       94.09
   2             54.735    0.000    0.000  0.000   6.216         6        5.91
   3             54.735    0.000    0.000  0.000   0.000         0        0.00
   4             54.735    0.000    0.000  0.000   0.000         0        0.00
   5             54.735    0.000    0.000  0.000   0.000         0        0.00
   6             54.735    0.000    0.000  0.000   0.000         0        0.00
   7             54.735    0.000    0.000  0.000   0.000         0        0.00
   8             54.735    0.000    0.000  0.000   0.000         0        0.00
   9             54.735    0.000    0.000  0.000   0.000         0        0.00
  10             54.735    0.000    0.000  0.000   0.000         0        0.00
  11             54.735    0.000    0.000  0.000   0.000         0        0.00
  12             54.735    0.000    0.000  0.000   0.000         0        0.00
  13             54.735    0.000    0.000  0.000   0.000         0        0.00
  14             54.735    0.000    0.000  0.000   0.000         0        0.00
  15             54.735    0.000    0.000  0.000   0.000         0        0.00
  16             54.735    0.000    0.000  0.000   0.000         0        0.00
  17             54.735    0.000    0.000  0.000   0.000         0        0.00
  18             54.735    0.000    0.000  0.000   0.000         0        0.00
  19             54.735    0.000    0.000  0.000   0.000         0        0.00
  20             54.735    0.000    0.000  0.000   0.000         0        0.00
  21             54.735    0.000    0.000  0.000   0.000         0        0.00
________________________________________________________________________________

 Relevanter Teil: 172 (172) Kanäle (Abweichung von Basis größer als 2 %)


 Weighted mean square deviation (gesamt)  :        906.665    (       906.666)
 Weighted mean square deviation (relevant):        516.957    (       516.957)
 Standardabweichung des Mittelwertes (Gesamtes Spektrum):             48.9298
                                                              (       48.9298)
                         (Relevanter Teil des Spektrums):             109.716
                                                              (       109.716)
 Korrelationskoeffizient             (Gesamtes Spektrum):            0.995032
                                                              (      0.995032)
                         (Relevanter Teil des Spektrums):            0.996073
                                                              (      0.996073)
 Statistischer Fehler =     0.00119664     Effekt (Fitkurve) =   1.8 %
                        (    0.0000    )                        (  0.0)
 Mittelwert d. Untergrunds (zw.   1. und  20. Kanal): YM=   698598.
 Std. Abw.  d. Untergrunds (zw.   1. und  20. Kanal): YV=   783.337

 Effekt aus Messspektrum (197 relevante Kanäle)     : 1.6
________________________________________________________________________________

Anm.:
________________________________________________________________________________

erstellt am 21.01.2021 um 11:46:47
```

```
Modell: 1. Modell
________________________________________________________________________________

Messung: MW174            Probe: V1.89Fe1.16B2        vom 19.01.2017 (231.0h)
Ta: 150K    Tq: 294K    v: 2.2s    Bext: 0T
________________________________________________________________________________

Anzahl der Schritte in der k-H Ebene   (Theta) :   0
                    in der x-y Ebene   ( Phi ) :   0
in k-V Ebene f.H=0, in der H-V Ebene   (Beta ) :   0
                    in der x'-y' Ebene (Alpha) :   0
Kanäle abgeschnitten: Vorne:   0           Bereich Anfang:   1
                     Hinten:   0                     Ende:  20
Glättung: Nein              Anzahl der Überläufe: 0            Spiegeln: Nein
Geraderichten: 0
Geschwindigkeitsparameter:  10.504958    0.255076    0.000357   -0.003983
Fe Menge (Absorberdicke):  20.0 [mg/cm**2]  (  0.0)
Maximales t:   1.885
Moerup-Both wird verwendet
Basislinie: 3079356    Peakhoehe: 209652
________________________________________________________________________________

21 Subspektren

Mittleres Feld (ohne antif. Anteil) =   0.630 kG
Mittleres eQVzz/4                   =  -0.181 mm/s
Mittlere Isomerie                   =  -0.057 mm/s

 Spektrum    Feld (kG)   Feld (mm/s)  eQVzz/4      Is       Gamma/2     Al(i)

  1                0.00      0.000     -0.181     -0.057      0.158      0.950
  2               10.90      0.350     -0.181     -0.057      0.158      0.050
  3               21.79      0.700     -0.181     -0.057      0.158      0.000
  4               32.69      1.050     -0.181     -0.057      0.158      0.000
  5               43.59      1.400     -0.181     -0.057      0.158      0.000
  6               54.48      1.750     -0.181     -0.057      0.158      0.000
  7               65.38      2.100     -0.181     -0.057      0.158      0.000
  8               76.28      2.450     -0.181     -0.057      0.158      0.000
  9               87.17      2.800     -0.181     -0.057      0.158      0.000
 10               98.07      3.150     -0.181     -0.057      0.158      0.000
 11              108.97      3.500     -0.181     -0.057      0.158      0.000
 12              119.86      3.850     -0.181     -0.057      0.158      0.000
 13              130.76      4.200     -0.181     -0.057      0.158      0.000
 14              141.66      4.550     -0.181     -0.057      0.158      0.000
 15              152.55      4.900     -0.181     -0.057      0.158      0.000
 16              163.45      5.250     -0.181     -0.057      0.158      0.000
 17              174.35      5.600     -0.181     -0.057      0.158      0.000
 18              185.24      5.950     -0.181     -0.057      0.158      0.000
 19              196.14      6.300     -0.181     -0.057      0.158      0.000
 20              207.04      6.650     -0.181     -0.057      0.158      0.000
 21              217.93      7.000     -0.181     -0.057      0.158      0.000
```

```
                Theta      Beta      Alpha    Eta    rel.Tiefe  abs.Tiefe    area
              (450-x)*2                               1.Linie    1.Linie
                für AF
  1              0.000    54.735     0.000  0.000    94.612     193322       94.22
  2             54.735     0.000     0.000  0.000    5.388      11009        5.78
  3             54.735     0.000     0.000  0.000    0.000          0        0.00
  4             54.735     0.000     0.000  0.000    0.000          0        0.00
  5             54.735     0.000     0.000  0.000    0.000          0        0.00
  6             54.735     0.000     0.000  0.000    0.000          0        0.00
  7             54.735     0.000     0.000  0.000    0.000          0        0.00
  8             54.735     0.000     0.000  0.000    0.000          0        0.00
  9             54.735     0.000     0.000  0.000    0.000          0        0.00
 10             54.735     0.000     0.000  0.000    0.000          0        0.00
 11             54.735     0.000     0.000  0.000    0.000          0        0.00
 12             54.735     0.000     0.000  0.000    0.000          0        0.00
 13             54.735     0.000     0.000  0.000    0.000          0        0.00
 14             54.735     0.000     0.000  0.000    0.000          0        0.00
 15             54.735     0.000     0.000  0.000    0.000          0        0.00
 16             54.735     0.000     0.000  0.000    0.000          0        0.00
 17             54.735     0.000     0.000  0.000    0.000          0        0.00
 18             54.735     0.000     0.000  0.000    0.000          0        0.00
 19             54.735     0.000     0.000  0.000    0.000          0        0.00
 20             54.735     0.000     0.000  0.000    0.000          0        0.00
 21             54.735     0.000     0.000  0.000    0.000          0        0.00
________________________________________________________________________________

 Relevanter Teil:  47 ( 47) Kanäle (Abweichung von Basis größer als 2 %)


 Weighted mean square deviation (gesamt)  :        839.583    (       839.584)
 Weighted mean square deviation (relevant):         359.04    (       359.041)
 Standardabweichung des Mittelwertes (Gesamtes Spektrum):             98.7897
                                                              (       98.7897)
                         (Relevanter Teil des Spektrums):             704.729
                                                              (       704.729)
 Korrelationskoeffizient             (Gesamtes Spektrum):            0.996356
                                                              (      0.996356)
                         (Relevanter Teil des Spektrums):            0.997694
                                                              (      0.997694)
 Statistischer Fehler =    0.000569862     Effekt (Fitkurve) =   1.8 %
                          (    0.0000    )                     (  0.0)
 Mittelwert d. Untergrunds (zw.   1. und  20. Kanal): YM=  3079816.
 Std. Abw.  d. Untergrunds (zw.   1. und  20. Kanal): YV=   2002.49

 Effekt aus Messspektrum (100 relevante Kanäle)     : 0.9
________________________________________________________________________________

Anm.:
________________________________________________________________________________

erstellt am 21.01.2021 um 11:31:39
```

```
Modell: 1. Modell
```

```
Messung: MW332a          Probe: V1.84Fe1.16B2       vom 22.11.2019 (72.0h)
Ta: 175K    Tq: 294K    v: 1.0t    Bext: 0T
```

```
Anzahl der Schritte in der k-H Ebene   (Theta) :   0
                    in der x-y Ebene   ( Phi ) :   0
in k-V Ebene f.H=0, in der H-V Ebene   (Beta ) :   0
                    in der x'-y' Ebene (Alpha) :   0
Kanäle abgeschnitten: Vorne:   0          Bereich Anfang:   1
                     Hinten:   0                    Ende:  20
Glättung: Nein             Anzahl der Überläufe: 0           Spiegeln: Nein
Geraderichten: 0
Geschwindigkeitsparameter:  -4.748140    0.018396    0.009442   -0.008691
Fe Menge (Absorberdicke):  20.0 [mg/cm**2]  (  0.0)
Maximales t:   1.885
Moerup-Both wird verwendet
Basislinie: 1143604    Peakhoehe: 86339
```

```
21 Subspektren

Mittleres Feld (ohne antif. Anteil) =   0.000 kG
Mittleres eQVzz/4                   =  -0.190 mm/s
Mittlere Isomerie                   =  -0.084 mm/s

 Spektrum     Feld (kG)   Feld (mm/s)  eQVzz/4      Is       Gamma/2     Al(i)

   1              0.00       0.000      -0.190    -0.084      0.169      1.000
   2             10.90       0.350      -0.190    -0.084      0.169      0.000
   3             21.79       0.700      -0.190    -0.084      0.169      0.000
   4             32.69       1.050      -0.190    -0.084      0.169      0.000
   5             43.59       1.400      -0.190    -0.084      0.169      0.000
   6             54.48       1.750      -0.190    -0.084      0.169      0.000
   7             65.38       2.100      -0.190    -0.084      0.169      0.000
   8             76.28       2.450      -0.190    -0.084      0.169      0.000
   9             87.17       2.800      -0.190    -0.084      0.169      0.000
  10             98.07       3.150      -0.190    -0.084      0.169      0.000
  11            108.97       3.500      -0.190    -0.084      0.169      0.000
  12            119.86       3.850      -0.190    -0.084      0.169      0.000
  13            130.76       4.200      -0.190    -0.084      0.169      0.000
  14            141.66       4.550      -0.190    -0.084      0.169      0.000
  15            152.55       4.900      -0.190    -0.084      0.169      0.000
  16            163.45       5.250      -0.190    -0.084      0.169      0.000
  17            174.35       5.600      -0.190    -0.084      0.169      0.000
  18            185.24       5.950      -0.190    -0.084      0.169      0.000
  19            196.14       6.300      -0.190    -0.084      0.169      0.000
  20            207.04       6.650      -0.190    -0.084      0.169      0.000
  21            217.93       7.000      -0.190    -0.084      0.169      0.000
```

```
                Theta     Beta     Alpha   Eta   rel.Tiefe  abs.Tiefe    area
              (450-x)*2                           1.Linie    1.Linie
                für AF
   1              0.000   54.735    0.000  0.000   100.000       188      100.00
   2             54.735    0.000    0.000  0.000   0.000         0        0.00
   3             54.735    0.000    0.000  0.000   0.000         0        0.00
   4             54.735    0.000    0.000  0.000   0.000         0        0.00
   5             54.735    0.000    0.000  0.000   0.000         0        0.00
   6             54.735    0.000    0.000  0.000   0.000         0        0.00
   7             54.735    0.000    0.000  0.000   0.000         0        0.00
   8             54.735    0.000    0.000  0.000   0.000         0        0.00
   9             54.735    0.000    0.000  0.000   0.000         0        0.00
  10             54.735    0.000    0.000  0.000   0.000         0        0.00
  11             54.735    0.000    0.000  0.000   0.000         0        0.00
  12             54.735    0.000    0.000  0.000   0.000         0        0.00
  13             54.735    0.000    0.000  0.000   0.000         0        0.00
  14             54.735    0.000    0.000  0.000   0.000         0        0.00
  15             54.735    0.000    0.000  0.000   0.000         0        0.00
  16             54.735    0.000    0.000  0.000   0.000         0        0.00
  17             54.735    0.000    0.000  0.000   0.000         0        0.00
  18             54.735    0.000    0.000  0.000   0.000         0        0.00
  19             54.735    0.000    0.000  0.000   0.000         0        0.00
  20             54.735    0.000    0.000  0.000   0.000         0        0.00
  21             54.735    0.000    0.000  0.000   0.000         0        0.00
________________________________________________________________________________

 Relevanter Teil: 172 (172) Kanäle (Abweichung von Basis größer als 2 %)


 Weighted mean square deviation (gesamt)  :        1195.56    (       1195.56)
 Weighted mean square deviation (relevant):        808.132    (       808.132)
 Standardabweichung des Mittelwertes (Gesamtes Spektrum):              71.439
                                                              (        71.439)
                         (Relevanter Teil des Spektrums):             174.232
                                                              (       174.232)
 Korrelationskoeffizient             (Gesamtes Spektrum):            0.996572
                                                              (      0.996572)
                         (Relevanter Teil des Spektrums):            0.996733
                                                              (      0.996733)
 Statistischer Fehler =     0.000935109     Effekt (Fitkurve) =   2.0 %
                        (    0.0000    )                       (  0.0)
 Mittelwert d. Untergrunds (zw.   1. und  20. Kanal): YM=  1143033.
 Std. Abw.  d. Untergrunds (zw.   1. und  20. Kanal): YV=   1057.64

 Effekt aus Messspektrum (199 relevante Kanäle)     : 1.7
________________________________________________________________________________

Anm.:
________________________________________________________________________________

erstellt am 21.01.2021 um 11:24:31
```

```
Modell: 1. Modell
________________________________________________________________________________

Messung: MW330a          Probe: V1.84Fe1.16B2        vom 14.11.2019 (42.0h)
Ta: 200K    Tq: 294K    v: 1.0t    Bext: 0T
________________________________________________________________________________

Anzahl der Schritte in der k-H Ebene   (Theta) :   0
                    in der x-y Ebene   ( Phi ) :   0
in k-V Ebene f.H=0, in der H-V Ebene   (Beta ) :   0
                    in der x'-y' Ebene (Alpha) :   0
Kanäle abgeschnitten: Vorne:   0          Bereich Anfang:   1
                     Hinten:   0                    Ende:  20
Glättung: Nein             Anzahl der Überläufe: 0            Spiegeln: Nein
Geraderichten: 0
Geschwindigkeitsparameter:  -4.744374    0.018233    0.059494   -0.026052
Fe Menge (Absorberdicke):  20.0 [mg/cm**2]  (  0.0)
Maximales t:   1.885
Moerup-Both wird verwendet
Basislinie: 741933     Peakhoehe: 59990
________________________________________________________________________________

21 Subspektren

Mittleres Feld (ohne antif. Anteil) =   0.000 kG
Mittleres eQVzz/4                   =  -0.187 mm/s
Mittlere Isomerie                   =  -0.098 mm/s

 Spektrum    Feld (kG)   Feld (mm/s)  eQVzz/4      Is       Gamma/2     Al(i)

  1             0.00       0.000      -0.187     -0.098      0.163      1.000
  2            10.90       0.350      -0.187     -0.098      0.163      0.000
  3            21.79       0.700      -0.187     -0.098      0.163      0.000
  4            32.69       1.050      -0.187     -0.098      0.163      0.000
  5            43.59       1.400      -0.187     -0.098      0.163      0.000
  6            54.48       1.750      -0.187     -0.098      0.163      0.000
  7            65.38       2.100      -0.187     -0.098      0.163      0.000
  8            76.28       2.450      -0.187     -0.098      0.163      0.000
  9            87.17       2.800      -0.187     -0.098      0.163      0.000
 10            98.07       3.150      -0.187     -0.098      0.163      0.000
 11           108.97       3.500      -0.187     -0.098      0.163      0.000
 12           119.86       3.850      -0.187     -0.098      0.163      0.000
 13           130.76       4.200      -0.187     -0.098      0.163      0.000
 14           141.66       4.550      -0.187     -0.098      0.163      0.000
 15           152.55       4.900      -0.187     -0.098      0.163      0.000
 16           163.45       5.250      -0.187     -0.098      0.163      0.000
 17           174.35       5.600      -0.187     -0.098      0.163      0.000
 18           185.24       5.950      -0.187     -0.098      0.163      0.000
 19           196.14       6.300      -0.187     -0.098      0.163      0.000
 20           207.04       6.650      -0.187     -0.098      0.163      0.000
 21           217.93       7.000      -0.187     -0.098      0.163      0.000
```

```
                Theta     Beta     Alpha   Eta   rel.Tiefe  abs.Tiefe    area
              (450-x)*2                           1.Linie    1.Linie
                für AF
   1              0.000   54.735    0.000  0.000   100.000     35356      100.00
   2             54.735    0.000    0.000  0.000   0.000         0        0.00
   3             54.735    0.000    0.000  0.000   0.000         0        0.00
   4             54.735    0.000    0.000  0.000   0.000         0        0.00
   5             54.735    0.000    0.000  0.000   0.000         0        0.00
   6             54.735    0.000    0.000  0.000   0.000         0        0.00
   7             54.735    0.000    0.000  0.000   0.000         0        0.00
   8             54.735    0.000    0.000  0.000   0.000         0        0.00
   9             54.735    0.000    0.000  0.000   0.000         0        0.00
  10             54.735    0.000    0.000  0.000   0.000         0        0.00
  11             54.735    0.000    0.000  0.000   0.000         0        0.00
  12             54.735    0.000    0.000  0.000   0.000         0        0.00
  13             54.735    0.000    0.000  0.000   0.000         0        0.00
  14             54.735    0.000    0.000  0.000   0.000         0        0.00
  15             54.735    0.000    0.000  0.000   0.000         0        0.00
  16             54.735    0.000    0.000  0.000   0.000         0        0.00
  17             54.735    0.000    0.000  0.000   0.000         0        0.00
  18             54.735    0.000    0.000  0.000   0.000         0        0.00
  19             54.735    0.000    0.000  0.000   0.000         0        0.00
  20             54.735    0.000    0.000  0.000   0.000         0        0.00
  21             54.735    0.000    0.000  0.000   0.000         0        0.00
________________________________________________________________________________

 Relevanter Teil: 165 (165) Kanäle (Abweichung von Basis größer als 2 %)


 Weighted mean square deviation (gesamt)  :       1068.94     (      1068.94)
 Weighted mean square deviation (relevant):       684.919     (      684.919)
 Standardabweichung des Mittelwertes (Gesamtes Spektrum):            54.5114
                                                               (      54.5114)
                         (Relevanter Teil des Spektrums):            134.884
                                                               (      134.884)
 Korrelationskoeffizient             (Gesamtes Spektrum):           0.996047
                                                               (     0.996047)
                         (Relevanter Teil des Spektrums):           0.996348
                                                               (     0.996348)
 Statistischer Fehler =     0.00116096     Effekt (Fitkurve) =   2.2 %
                        (    0.0000    )                       (  0.0)
 Mittelwert d. Untergrunds (zw.   1. und  20. Kanal): YM=   741563.
 Std. Abw.  d. Untergrunds (zw.   1. und  20. Kanal): YV=   994.959

 Effekt aus Messspektrum (128 relevante Kanäle)     : 2.7
________________________________________________________________________________

Anm.:
________________________________________________________________________________

erstellt am 21.01.2021 um 11:11:32
```

```
Modell: 1. Modell
```

```
Messung: MW171            Probe: V1.89Fe1.16B2        vom 09.01.2017 (87.0h)
Ta: 294K    Tq: 294K    v: 2.2s    Bext: 0T
```

```
Anzahl der Schritte in der k-H Ebene   (Theta) :   0
                    in der x-y Ebene   ( Phi ) :   0
in k-V Ebene f.H=0, in der H-V Ebene   (Beta ) :   0
                    in der x'-y' Ebene (Alpha) :   0
Kanäle abgeschnitten: Vorne:   0           Bereich Anfang:   1
                     Hinten:   0                     Ende:  20
Glättung: Nein               Anzahl der Überläufe: 0            Spiegeln: Nein
Geraderichten: 0
Geschwindigkeitsparameter:  10.504958    0.255076    0.000357   -0.003983
Fe Menge (Absorberdicke):  20.0 [mg/cm**2]  ( 20.0)
Maximales t:   1.885
Basislinie: 5318209    Peakhoehe: 483719
```

```
21 Subspektren

Mittleres Feld (ohne antif. Anteil) =   0.000 kG
Mittleres eQVzz/4                   =  -0.182 mm/s
Mittlere Isomerie                   =  -0.143 mm/s

 Spektrum    Feld (kG)   Feld (mm/s)  eQVzz/4      Is       Gamma/2     Al(i)

  1                0.00      0.000     -0.182     -0.143      0.165      1.000
  2               10.90      0.350     -0.182     -0.143      0.165      0.000
  3               21.79      0.700     -0.182     -0.143      0.165      0.000
  4               32.69      1.050     -0.182     -0.143      0.165      0.000
  5               43.59      1.400     -0.182     -0.143      0.165      0.000
  6               54.48      1.750     -0.182     -0.143      0.165      0.000
  7               65.38      2.100     -0.182     -0.143      0.165      0.000
  8               76.28      2.450     -0.182     -0.143      0.165      0.000
  9               87.17      2.800     -0.182     -0.143      0.165      0.000
 10               98.07      3.150     -0.182     -0.143      0.165      0.000
 11              108.97      3.500     -0.182     -0.143      0.165      0.000
 12              119.86      3.850     -0.182     -0.143      0.165      0.000
 13              130.76      4.200     -0.182     -0.143      0.165      0.000
 14              141.66      4.550     -0.182     -0.143      0.165      0.000
 15              152.55      4.900     -0.182     -0.143      0.165      0.000
 16              163.45      5.250     -0.182     -0.143      0.165      0.000
 17              174.35      5.600     -0.182     -0.143      0.165      0.000
 18              185.24      5.950     -0.182     -0.143      0.165      0.000
 19              196.14      6.300     -0.182     -0.143      0.165      0.000
 20              207.04      6.650     -0.182     -0.143      0.165      0.000
 21              217.93      7.000     -0.182     -0.143      0.165      0.000
```

```
                  Theta      Beta      Alpha    Eta    rel.Tiefe  abs.Tiefe    area
                (450-x)*2                                1.Linie    1.Linie
                  für AF
  1                0.000    54.735     0.000   0.000   100.000     451515      100.00
  2               54.735     0.000     0.000   0.000   0.000          0        0.00
  3               54.735     0.000     0.000   0.000   0.000          0        0.00
  4               54.735     0.000     0.000   0.000   0.000          0        0.00
  5               54.735     0.000     0.000   0.000   0.000          0        0.00
  6               54.735     0.000     0.000   0.000   0.000          0        0.00
  7               54.735     0.000     0.000   0.000   0.000          0        0.00
  8               54.735     0.000     0.000   0.000   0.000          0        0.00
  9               54.735     0.000     0.000   0.000   0.000          0        0.00
 10               54.735     0.000     0.000   0.000   0.000          0        0.00
 11               54.735     0.000     0.000   0.000   0.000          0        0.00
 12               54.735     0.000     0.000   0.000   0.000          0        0.00
 13               54.735     0.000     0.000   0.000   0.000          0        0.00
 14               54.735     0.000     0.000   0.000   0.000          0        0.00
 15               54.735     0.000     0.000   0.000   0.000          0        0.00
 16               54.735     0.000     0.000   0.000   0.000          0        0.00
 17               54.735     0.000     0.000   0.000   0.000          0        0.00
 18               54.735     0.000     0.000   0.000   0.000          0        0.00
 19               54.735     0.000     0.000   0.000   0.000          0        0.00
 20               54.735     0.000     0.000   0.000   0.000          0        0.00
 21               54.735     0.000     0.000   0.000   0.000          0        0.00
________________________________________________________________________________

 Relevanter Teil:  48 ( 48) Kanäle (Abweichung von Basis größer als 2 %)


 Weighted mean square deviation (gesamt)  :        1802.72    (       1802.72)
 Weighted mean square deviation (relevant):        1351.32    (       1351.32)
 Standardabweichung des Mittelwertes (Gesamtes Spektrum):             187.718
                                                             (        187.718)
                        (Relevanter Teil des Spektrums):              1738.55
                                                             (        1738.55)
 Korrelationskoeffizient             (Gesamtes Spektrum):            0.997605
                                                             (       0.997605)
                        (Relevanter Teil des Spektrums):             0.997222
                                                             (       0.997222)
 Statistischer Fehler =     0.000433628     Effekt (Fitkurve) =   2.4 %
                           (    0.0000    )                     (  0.0)
 Mittelwert d. Untergrunds (zw.   1. und  20. Kanal): YM=  5318550.
 Std. Abw.  d. Untergrunds (zw.   1. und  20. Kanal): YV=   2360.81

 Effekt aus Messspektrum (118 relevante Kanäle)     : 1.0
________________________________________________________________________________

Anm.:
________________________________________________________________________________

erstellt am 21.01.2021 um 10:24:33
```

```
Modell: 1. Modell
```

```
Messung: WM174            Probe: V1.84Fe1.16B2        vom 18.12.2020 (67.0h)
Ta: 5K    Tq: 4.8K    v: 1.5s     Bext: 0T
```

```
Anzahl der Schritte in der k-H Ebene   (Theta) :  20
                    in der x-y Ebene   ( Phi ) :  20
in k-V Ebene f.H=0, in der H-V Ebene   (Beta ) :   0
                    in der x'-y' Ebene (Alpha) :   0
Kanäle abgeschnitten: Vorne:   0           Bereich Anfang:   1
                     Hinten:   0                     Ende:  20
Glättung: Nein               Anzahl der Überläufe: 0            Spiegeln: Nein
Geraderichten: 0
Geschwindigkeitsparameter:   2.846234    0.256609    0.001286   -0.003417
Fe Menge (Absorberdicke):  20.0 [mg/cm**2]  (  0.0)
Maximales t:   1.885
Moerup-Both wird verwendet
Basislinie: 708271     Peakhoehe: 36617
```

```
21 Subspektren

Mittleres Feld (ohne antif. Anteil) =  92.931 kG
Mittleres eQVzz/4                   =  -0.062 mm/s
Mittlere Isomerie                   =  -0.180 mm/s

 Spektrum    Feld (kG)   Feld (mm/s)  eQVzz/4      Is       Gamma/2     Al(i)

  1                0.00      0.000     -0.062     -0.180      0.203      0.016
  2               10.90      0.350     -0.062     -0.180      0.203      0.000
  3               21.79      0.700     -0.062     -0.180      0.203      0.002
  4               32.69      1.050     -0.062     -0.180      0.203      0.004
  5               43.59      1.400     -0.062     -0.180      0.203      0.025
  6               54.48      1.750     -0.062     -0.180      0.203      0.027
  7               65.38      2.100     -0.062     -0.180      0.203      0.062
  8               76.28      2.450     -0.062     -0.180      0.203      0.000
  9               87.17      2.800     -0.062     -0.180      0.203      0.000
 10               98.07      3.150     -0.062     -0.180      0.203      0.824
 11              108.97      3.500     -0.062     -0.180      0.203      0.034
 12              119.86      3.850     -0.062     -0.180      0.203      0.002
 13              130.76      4.200     -0.062     -0.180      0.203      0.000
 14              141.66      4.550     -0.062     -0.180      0.203      0.000
 15              152.55      4.900     -0.062     -0.180      0.203      0.000
 16              163.45      5.250     -0.062     -0.180      0.203      0.000
 17              174.35      5.600     -0.062     -0.180      0.203      0.000
 18              185.24      5.950     -0.062     -0.180      0.203      0.000
 19              196.14      6.300     -0.062     -0.180      0.203      0.003
 20              207.04      6.650     -0.062     -0.180      0.203      0.000
 21              217.93      7.000     -0.062     -0.180      0.203      0.000
```

```
                 Theta      Beta      Alpha    Eta    rel.Tiefe  abs.Tiefe    area
               (450-x)*2                               1.Linie    1.Linie
                 für AF
   1               0.000   54.735     0.000  0.000    0.738        10        1.24
   2              54.735    0.000     0.000  0.000    0.026         0        0.04
   3              54.735    0.000     0.000  0.000    0.092         1        0.15
   4              54.735    0.000     0.000  0.000    0.242         3        0.37
   5              54.735    0.000     0.000  0.000    1.545        21        2.31
   6              54.735    0.000     0.000  0.000    1.780        24        2.55
   7              54.735    0.000     0.000  0.000    4.327        58        5.85
   8              54.735    0.000     0.000  0.000    0.003         0        0.00
   9              54.735    0.000     0.000  0.000    0.011         0        0.01
  10              54.735    0.000     0.000  0.000   79.570      1075       83.30
  11              54.735    0.000     0.000  0.000    3.807        51        3.53
  12              54.735    0.000     0.000  0.000    0.337         5        0.27
  13              54.735    0.000     0.000  0.000    0.073         1        0.05
  14              54.735    0.000     0.000  0.000    0.106         1        0.06
  15              54.735    0.000     0.000  0.000    0.000         0        0.00
  16              54.735    0.000     0.000  0.000    0.021         0        0.00
  17              54.735    0.000     0.000  0.000    0.123         2        0.01
  18              54.735    0.000     0.000  0.000    0.010         0        0.00
  19              54.735    0.000     0.000  0.000    7.159        97        0.26
  20              54.735    0.000     0.000  0.000    0.030         0        0.00
  21              54.735    0.000     0.000  0.000    0.000         0        0.00
________________________________________________________________________________

 Relevanter Teil: 512 (512) Kanäle (Abweichung von Basis größer als 2 %)


 Weighted mean square deviation (gesamt)  :        1940.62    (       1940.62)
 Weighted mean square deviation (relevant):        1940.62    (       1940.62)
 Standardabweichung des Mittelwertes (Gesamtes Spektrum):             71.6788
                                                              (       71.6788)
                         (Relevanter Teil des Spektrums):             71.6788
                                                              (       71.6788)
 Korrelationskoeffizient             (Gesamtes Spektrum):            0.990037
                                                              (      0.990037)
                         (Relevanter Teil des Spektrums):            0.990037
                                                              (      0.990037)
 Statistischer Fehler =     0.00118823     Effekt (Fitkurve) =   1.8 %
                          (    0.0000    )                     (  0.0)
 Mittelwert d. Untergrunds (zw.   1. und  20. Kanal): YM=   706618.
 Std. Abw.  d. Untergrunds (zw.   1. und  20. Kanal): YV=   1256.22

 Effekt aus Messspektrum (322 relevante Kanäle)     : 2.5
________________________________________________________________________________

Anm.:
________________________________________________________________________________

erstellt am 27.01.2021 um 12:16:29
```

```
Modell: 1. Modell

Messung: WM181a           Probe: V1.84Fe1.16B2        vom 01.02.2021 (260.0h)
Ta: 4.3K    Tq: 5K    v: 2.5s    Bext: 9T

Anzahl der Schritte in der k-H Ebene   (Theta) :  20
                    in der x-y Ebene   ( Phi ) :  20
in k-V Ebene f.H=0, in der H-V Ebene   (Beta ) :   0
                    in der x'-y' Ebene (Alpha) :   0
Kanäle abgeschnitten: Vorne:   0           Bereich Anfang:   1
                     Hinten:   0                     Ende:  20
Glättung: Nein               Anzahl der Überläufe: 0            Spiegeln: Nein
Geraderichten: 0
Geschwindigkeitsparameter:   4.736749    0.257365   -0.000119   -0.000165
Fe Menge (Absorberdicke):  20.0 [mg/cm**2]  (  0.0)
Maximales t:   1.884
Moerup-Both wird verwendet
Basislinie: 1074030    Peakhoehe: 27223

21 Subspektren

Mittleres Feld (ohne antif. Anteil) = 116.023 kG
Mittleres eQVzz/4                   =  -0.044 mm/s
Mittlere Isomerie                   =  -0.174 mm/s

 Spektrum    Feld (kG)   Feld (mm/s)  eQVzz/4      Is       Gamma/2     Al(i)

  1                0.00      0.000     -0.044     -0.174      0.203      0.018
  2               10.90      0.350     -0.044     -0.174      0.203      0.007
  3               21.79      0.700     -0.044     -0.174      0.203      0.006
  4               32.69      1.050     -0.044     -0.174      0.203      0.018
  5               43.59      1.400     -0.044     -0.174      0.203      0.024
  6               54.48      1.750     -0.044     -0.174      0.203      0.044
  7               65.38      2.100     -0.044     -0.174      0.203      0.045
  8               76.28      2.450     -0.044     -0.174      0.203      0.047
  9               87.17      2.800     -0.044     -0.174      0.203      0.053
 10               98.07      3.150     -0.044     -0.174      0.203      0.030
 11              108.97      3.500     -0.044     -0.174      0.203      0.007
 12              119.86      3.850     -0.044     -0.174      0.203      0.167
 13              130.76      4.200     -0.044     -0.174      0.203      0.237
 14              141.66      4.550     -0.044     -0.174      0.203      0.149
 15              152.55      4.900     -0.044     -0.174      0.203      0.076
 16              163.45      5.250     -0.044     -0.174      0.203      0.038
 17              174.35      5.600     -0.044     -0.174      0.203      0.019
 18              185.24      5.950     -0.044     -0.174      0.203      0.016
 19              196.14      6.300     -0.044     -0.174      0.203      0.000
 20              207.04      6.650     -0.044     -0.174      0.203      0.000
 21              217.93      7.000     -0.044     -0.174      0.203      0.000
```

```
                  Theta      Beta      Alpha    Eta    rel.Tiefe  abs.Tiefe    area
                (450-x)*2                                1.Linie    1.Linie
                  für AF
  1               0.000    54.735     0.000   0.000    4.729       1827        1.11
  2              30.758     0.000     0.000   0.000    1.375        531        0.48
  3               5.010     0.000     0.000   0.000    0.729        282        0.39
  4              48.956     0.000     0.000   0.000    2.761       1067        1.59
  5              37.509     0.000     0.000   0.000    2.635       1018        1.82
  6              74.813     0.000     0.000   0.000    5.715       2209        4.99
  7              96.372     0.000     0.000   0.000    5.686       2197        5.45
  8             101.142     0.000     0.000   0.000    5.521       2134        5.49
  9             129.781     0.000     0.000   0.000    5.079       1963        4.78
 10              97.631     0.000     0.000   0.000    3.130       1209        3.62
 11             103.333     0.000     0.000   0.000    0.768        297        0.87
 12              82.361     0.000     0.000   0.000   19.052        7363       20.61
 13              32.743     0.000     0.000   0.000   19.105        7383       18.78
 14              41.842     0.000     0.000   0.000   11.046        4269       13.02
 15              52.850     0.000     0.000   0.000    4.624       1787        7.54
 16              73.632     0.000     0.000   0.000    3.973       1535        4.74
 17              91.630     0.000     0.000   0.000    2.271        877        2.51
 18              85.546     0.000     0.000   0.000    1.767        683        2.17
 19              82.532     0.000     0.000   0.000    0.001          0        0.00
 20              57.075     0.000     0.000   0.000    0.003          1        0.00
 21              88.992     0.000     0.000   0.000    0.033         13        0.04
________________________________________________________________________________

 Relevanter Teil: 473 (473) Kanäle (Abweichung von Basis größer als 2 %)


 Weighted mean square deviation (gesamt)  :        794.826    (        794.826)
 Weighted mean square deviation (relevant):        737.917    (        737.917)
 Standardabweichung des Mittelwertes (Gesamtes Spektrum):               56.8461
                                                              (         56.8461)
                        (Relevanter Teil des Spektrums):               59.2713
                                                              (         59.2713)
 Korrelationskoeffizient             (Gesamtes Spektrum):              0.992423
                                                              (        0.992423)
                        (Relevanter Teil des Spektrums):              0.992486
                                                              (        0.992486)
 Statistischer Fehler =     0.000964921     Effekt (Fitkurve) =   0.9 %
                          (    0.0000    )                       (  0.0)
 Mittelwert d. Untergrunds (zw.   1. und  20. Kanal): YM=  1073493.
 Std. Abw.  d. Untergrunds (zw.   1. und  20. Kanal): YV=   1631.08

 Effekt aus Messspektrum (231 relevante Kanäle)     : 1.7
________________________________________________________________________________

Anm.:
________________________________________________________________________________

erstellt am 01.02.2021 um 11:39:20
```

```
Modell: 1. Modell
```

```
Messung: WM176a           Probe: V1.84Fe1.16B2        vom 30.12.2020 (217.0h)
Ta: 4.8K    Tq: 4.8K    v: 2.5s    Bext: 12T
```

```
Anzahl der Schritte in der k-H Ebene   (Theta) :  20
                    in der x-y Ebene   ( Phi ) :  20
in k-V Ebene f.H=0, in der H-V Ebene   (Beta ) :   0
                    in der x'-y' Ebene (Alpha) :   0
Kanäle abgeschnitten: Vorne:   0           Bereich Anfang:   1
                     Hinten:   0                     Ende:  20
Glättung: Nein               Anzahl der Überläufe: 0            Spiegeln: Nein
Geraderichten: 0
Geschwindigkeitsparameter:   4.755919    0.257292    0.000077   -0.002320
Fe Menge (Absorberdicke):  20.0 [mg/cm**2]  (-----)
Maximales t:   0.000
Basislinie: 909243     Peakhoehe: 21501
```

```
21 Subspektren

Mittleres Feld (ohne antif. Anteil) = 131.873 kG
Mittleres eQVzz/4                   =  -0.045 mm/s
Mittlere Isomerie                   =  -0.185 mm/s

 Spektrum    Feld (kG)   Feld (mm/s)  eQVzz/4      Is       Gamma/2     Al(i)

  1                0.00      0.000     -0.045     -0.185      0.192      0.017
  2               10.90      0.350     -0.045     -0.185      0.192      0.006
  3               21.79      0.700     -0.045     -0.185      0.192      0.006
  4               32.69      1.050     -0.045     -0.185      0.192      0.014
  5               43.59      1.400     -0.045     -0.185      0.192      0.019
  6               54.48      1.750     -0.045     -0.185      0.192      0.025
  7               65.38      2.100     -0.045     -0.185      0.192      0.028
  8               76.28      2.450     -0.045     -0.185      0.192      0.032
  9               87.17      2.800     -0.045     -0.185      0.192      0.028
 10               98.07      3.150     -0.045     -0.185      0.192      0.014
 11              108.97      3.500     -0.045     -0.185      0.192      0.003
 12              119.86      3.850     -0.045     -0.185      0.192      0.064
 13              130.76      4.200     -0.045     -0.185      0.192      0.111
 14              141.66      4.550     -0.045     -0.185      0.192      0.191
 15              152.55      4.900     -0.045     -0.185      0.192      0.141
 16              163.45      5.250     -0.045     -0.185      0.192      0.148
 17              174.35      5.600     -0.045     -0.185      0.192      0.077
 18              185.24      5.950     -0.045     -0.185      0.192      0.067
 19              196.14      6.300     -0.045     -0.185      0.192      0.001
 20              207.04      6.650     -0.045     -0.185      0.192      0.008
 21              217.93      7.000     -0.045     -0.185      0.192      0.001


               Theta     Beta     Alpha   Eta   rel.Tiefe  abs.Tiefe    area
```

```
              (450-x)*2                           1.Linie    1.Linie
                für AF
   1              0.000   54.735    0.000  0.000   4.372      1687        1.14
   2             54.040    0.000    0.000  0.000   1.466       566        0.55
   3             70.168    0.000    0.000  0.000   1.321       510        0.62
   4             88.072    0.000    0.000  0.000   2.897      1118        1.75
   5             83.180    0.000    0.000  0.000   2.928      1130        2.35
   6             91.800    0.000    0.000  0.000   3.456      1334        3.14
   7             90.317    0.000    0.000  0.000   3.669      1416        3.61
   8             96.070    0.000    0.000  0.000   4.069      1570        4.02
   9             93.877    0.000    0.000  0.000   3.658      1411        3.56
  10             59.301    0.000    0.000  0.000   1.293       499        1.44
  11             55.167    0.000    0.000  0.000   0.269       104        0.28
  12             62.263    0.000    0.000  0.000   5.773      2228        6.99
  13             38.907    0.000    0.000  0.000   9.856      3803        9.36
  14             39.681    0.000    0.000  0.000  17.102       6599       16.41
  15             52.850    0.000    0.000  0.000  12.712       4905       14.26
  16             53.973    0.000    0.000  0.000  13.021       5024       15.46
  17             51.213    0.000    0.000  0.000   6.448      2488        7.97
  18             39.702    0.000    0.000  0.000   5.095      1966        6.22
  19             35.394    0.000    0.000  0.000   0.101        39        0.14
  20             23.539    0.000    0.000  0.000   0.475       183        0.70
  21             41.138    0.000    0.000  0.000   0.019         7        0.06
________________________________________________________________________________

 Relevanter Teil: 487 (487) Kanäle (Abweichung von Basis größer als 2 %)


 Weighted mean square deviation (gesamt)  :        681.876    (       681.876)
 Weighted mean square deviation (relevant):        650.304    (       650.304)
 Standardabweichung des Mittelwertes (Gesamtes Spektrum):             48.4548
                                                              (       48.4548)
                         (Relevanter Teil des Spektrums):             49.7407
                                                              (       49.7407)
 Korrelationskoeffizient             (Gesamtes Spektrum):            0.989175
                                                              (      0.989175)
                         (Relevanter Teil des Spektrums):            0.989206
                                                              (      0.989206)
 Statistischer Fehler =     0.00104872     Effekt (Fitkurve) =   0.9 %
                        (    0.0000    )                       (  0.0)
 Mittelwert d. Untergrunds (zw.   1. und  20. Kanal): YM=   908789.
 Std. Abw.  d. Untergrunds (zw.   1. und  20. Kanal): YV=   1530.37

 Effekt aus Messspektrum (266 relevante Kanäle)     : 1.5
________________________________________________________________________________

Anm.:
________________________________________________________________________________

erstellt am 27.01.2021 um 10:21:14
```

```
Modell: 1. Modell
```

```
Messung: WM180a           Probe: V1.84Fe1.16B2        vom 20.01.2021 (122.0h)
Ta: 20K    Tq: 13.2K    v: 2.5s    Bext: 12T
```

```
Anzahl der Schritte in der k-H Ebene   (Theta) :  20
                    in der x-y Ebene   ( Phi ) :  20
in k-V Ebene f.H=0, in der H-V Ebene   (Beta ) :   0
                    in der x'-y' Ebene (Alpha) :   0
Kanäle abgeschnitten: Vorne:   0           Bereich Anfang:   1
                     Hinten:   0                     Ende:  20
Glättung: Nein               Anzahl der Überläufe: 0            Spiegeln: Nein
Geraderichten: 0
Geschwindigkeitsparameter:   4.758174    0.257364    0.002846   -0.004211
Fe Menge (Absorberdicke):  20.0 [mg/cm**2]  ( 20.0)
Maximales t:   2.013
Moerup-Both wird verwendet
Basislinie: 861487     Peakhoehe: 24323
```

```
21 Subspektren

Mittleres Feld (ohne antif. Anteil) = 128.127 kG
Mittleres eQVzz/4                   =  -0.047 mm/s
Mittlere Isomerie                   =  -0.174 mm/s

 Spektrum    Feld (kG)   Feld (mm/s)  eQVzz/4      Is       Gamma/2     Al(i)

  1                0.00      0.000     -0.047     -0.174      0.248      0.000
  2               10.90      0.350     -0.047     -0.174      0.248      0.000
  3               21.79      0.700     -0.047     -0.174      0.248      0.002
  4               32.69      1.050     -0.047     -0.174      0.248      0.062
  5               43.59      1.400     -0.047     -0.174      0.248      0.004
  6               54.48      1.750     -0.047     -0.174      0.248      0.000
  7               65.38      2.100     -0.047     -0.174      0.248      0.024
  8               76.28      2.450     -0.047     -0.174      0.248      0.060
  9               87.17      2.800     -0.047     -0.174      0.248      0.050
 10               98.07      3.150     -0.047     -0.174      0.248      0.000
 11              108.97      3.500     -0.047     -0.174      0.248      0.089
 12              119.86      3.850     -0.047     -0.174      0.248      0.000
 13              130.76      4.200     -0.047     -0.174      0.248      0.204
 14              141.66      4.550     -0.047     -0.174      0.248      0.011
 15              152.55      4.900     -0.047     -0.174      0.248      0.324
 16              163.45      5.250     -0.047     -0.174      0.248      0.014
 17              174.35      5.600     -0.047     -0.174      0.248      0.149
 18              185.24      5.950     -0.047     -0.174      0.248      0.002
 19              196.14      6.300     -0.047     -0.174      0.248      0.001
 20              207.04      6.650     -0.047     -0.174      0.248      0.001
 21              217.93      7.000     -0.047     -0.174      0.248      0.001
```

```
                 Theta      Beta      Alpha    Eta    rel.Tiefe  abs.Tiefe    area
               (450-x)*2                                1.Linie    1.Linie
                 für AF
   1              0.000    54.735     0.000  0.000    2.140        13         0.01
   2            123.466     0.000     0.000  0.000    0.289         2         0.00
   3             45.956     0.000     0.000  0.000    0.144         1         0.21
   4             75.225     0.000     0.000  0.000    5.439        34         7.84
   5             43.995     0.000     0.000  0.000    0.256         2         0.37
   6             46.800     0.000     0.000  0.000    0.022         0         0.03
   7             41.282     0.000     0.000  0.000    1.569        10         2.15
   8             39.763     0.000     0.000  0.000    4.031        25         5.36
   9             67.519     0.000     0.000  0.000    4.588        29         6.00
  10             70.084     0.000     0.000  0.000    0.015         0         0.02
  11             44.406     0.000     0.000  0.000    7.138        45         8.53
  12             57.121     0.000     0.000  0.000    0.043         0         0.05
  13             48.993     0.000     0.000  0.000   19.284       121        20.98
  14             15.780     0.000     0.000  0.000    0.876         6         0.84
  15             31.807     0.000     0.000  0.000   31.398       197        28.93
  16             71.543     0.000     0.000  0.000    1.995        13         1.86
  17             48.100     0.000     0.000  0.000   19.899       125        16.23
  18             67.145     0.000     0.000  0.000    0.425         3         0.33
  19             25.395     0.000     0.000  0.000    0.113         1         0.07
  20             51.070     0.000     0.000  0.000    0.148         1         0.09
  21             49.388     0.000     0.000  0.000    0.189         1         0.10
________________________________________________________________________________

 Relevanter Teil: 512 (512) Kanäle (Abweichung von Basis größer als 2 %)


 Weighted mean square deviation (gesamt)  :        674.997    (       674.997)
 Weighted mean square deviation (relevant):        674.997    (       674.997)
 Standardabweichung des Mittelwertes (Gesamtes Spektrum):             46.9024
                                                              (       46.9024)
                        (Relevanter Teil des Spektrums):             46.9024
                                                              (       46.9024)
 Korrelationskoeffizient             (Gesamtes Spektrum):            0.992174
                                                              (      0.992174)
                        (Relevanter Teil des Spektrums):            0.992174
                                                              (      0.992174)
 Statistischer Fehler =       0.0010774     Effekt (Fitkurve) =   1.0 %
                        (     0.0000    )                      (  0.0)
 Mittelwert d. Untergrunds (zw.   1. und  20. Kanal): YM=   861057.
 Std. Abw.  d. Untergrunds (zw.   1. und  20. Kanal): YV=   1250.95

 Effekt aus Messspektrum (282 relevante Kanäle)     : 1.7
________________________________________________________________________________

Anm.:
________________________________________________________________________________

erstellt am 02.02.2021 um 13:02:38
```

```
Modell: 1. Modell
________________________________________________________________________________

Messung: WM177a           Probe: V1.84Fe1.16B2        vom 07.01.2021 (68.0h)
Ta: 40K    Tq: 13.1K    v: 2.5s    Bext: 12T
________________________________________________________________________________

Anzahl der Schritte in der k-H Ebene   (Theta) :  20
                    in der x-y Ebene   ( Phi ) :  20
in k-V Ebene f.H=0, in der H-V Ebene   (Beta ) :   0
                    in der x'-y' Ebene (Alpha) :   0
Kanäle abgeschnitten: Vorne:   0          Bereich Anfang:   1
                     Hinten:   0                    Ende:  20
Glättung: Nein              Anzahl der Überläufe: 0            Spiegeln: Nein
Geraderichten: 0
Geschwindigkeitsparameter:   4.749682    0.257392    0.000965    0.002639
Fe Menge (Absorberdicke):  20.0 [mg/cm**2]  (-----)
Maximales t:   1.796
Moerup-Both wird verwendet
Basislinie: 942591     Peakhoehe: 32806
________________________________________________________________________________

21 Subspektren

Mittleres Feld (ohne antif. Anteil) = 126.207 kG
Mittleres eQVzz/4                   =  -0.046 mm/s
Mittlere Isomerie                   =  -0.185 mm/s

 Spektrum    Feld (kG)   Feld (mm/s)  eQVzz/4      Is       Gamma/2     Al(i)

  1                0.00      0.000     -0.046     -0.185      0.196      0.000
  2               10.90      0.350     -0.046     -0.185      0.196      0.000
  3               21.79      0.700     -0.046     -0.185      0.196      0.007
  4               32.69      1.050     -0.046     -0.185      0.196      0.082
  5               43.59      1.400     -0.046     -0.185      0.196      0.002
  6               54.48      1.750     -0.046     -0.185      0.196      0.000
  7               65.38      2.100     -0.046     -0.185      0.196      0.004
  8               76.28      2.450     -0.046     -0.185      0.196      0.008
  9               87.17      2.800     -0.046     -0.185      0.196      0.010
 10               98.07      3.150     -0.046     -0.185      0.196      0.000
 11              108.97      3.500     -0.046     -0.185      0.196      0.154
 12              119.86      3.850     -0.046     -0.185      0.196      0.001
 13              130.76      4.200     -0.046     -0.185      0.196      0.238
 14              141.66      4.550     -0.046     -0.185      0.196      0.075
 15              152.55      4.900     -0.046     -0.185      0.196      0.340
 16              163.45      5.250     -0.046     -0.185      0.196      0.010
 17              174.35      5.600     -0.046     -0.185      0.196      0.067
 18              185.24      5.950     -0.046     -0.185      0.196      0.001
 19              196.14      6.300     -0.046     -0.185      0.196      0.000
 20              207.04      6.650     -0.046     -0.185      0.196      0.000
 21              217.93      7.000     -0.046     -0.185      0.196      0.000
```

```
                Theta     Beta     Alpha   Eta   rel.Tiefe  abs.Tiefe    area
              (450-x)*2                           1.Linie    1.Linie
                für AF
    1            0.000   54.735    0.000  0.000   0.050        21        0.01
    2           84.856    0.000    0.000  0.000   0.055        23        0.02
    3           72.931    0.000    0.000  0.000   1.870       798        0.82
    4           83.707    0.000    0.000  0.000   18.030      7699       10.06
    5           84.500    0.000    0.000  0.000   0.282       120        0.19
    6           75.014    0.000    0.000  0.000   0.011         5        0.01
    7           60.561    0.000    0.000  0.000   0.456       195        0.37
    8           68.435    0.000    0.000  0.000   1.025       438        0.91
    9           79.665    0.000    0.000  0.000   1.126       481        1.20
   10           70.084    0.000    0.000  0.000   0.015         6        0.02
   11           64.589    0.000    0.000  0.000   14.984      6398       17.18
   12           54.816    0.000    0.000  0.000   0.101        43        0.11
   13           38.340    0.000    0.000  0.000   21.757      9290       20.59
   14           44.525    0.000    0.000  0.000   6.281      2682        7.01
   15           48.662    0.000    0.000  0.000   28.338     12100       33.64
   16           58.444    0.000    0.000  0.000   0.865       369        1.14
   17           42.620    0.000    0.000  0.000   4.655      1988        6.53
   18           45.570    0.000    0.000  0.000   0.047        20        0.09
   19           44.376    0.000    0.000  0.000   0.013         6        0.03
   20           50.463    0.000    0.000  0.000   0.012         5        0.02
   21           58.673    0.000    0.000  0.000   0.027        12        0.05
________________________________________________________________________________

 Relevanter Teil: 458 (458) Kanäle (Abweichung von Basis größer als 2 %)


 Weighted mean square deviation (gesamt)  :        823.722    (       823.722)
 Weighted mean square deviation (relevant):         732.44    (        732.44)
 Standardabweichung des Mittelwertes (Gesamtes Spektrum):               54.14
                                                              (         54.14)
                         (Relevanter Teil des Spektrums):             57.0299
                                                              (       57.0299)
 Korrelationskoeffizient             (Gesamtes Spektrum):            0.993748
                                                              (      0.993748)
                         (Relevanter Teil des Spektrums):            0.993771
                                                              (      0.993771)
 Statistischer Fehler =        0.00103     Effekt (Fitkurve) =   1.2 %
                        (    0.0000    )                        (  0.0)
 Mittelwert d. Untergrunds (zw.   1. und  20. Kanal): YM=   942519.
 Std. Abw.  d. Untergrunds (zw.   1. und  20. Kanal): YV=   1081.10

 Effekt aus Messspektrum (295 relevante Kanäle)     : 1.7
________________________________________________________________________________

Anm.:
________________________________________________________________________________

erstellt am 27.01.2021 um 11:10:23
```

```
Modell: 1. Modell
```

```
Messung: WM179a           Probe: V1.84Fe1.16B2        vom 14.01.2021 (72.0h)
Ta: 100K    Tq: 15.2K    v: 2.5s    Bext: 12T
```

```
Anzahl der Schritte in der k-H Ebene   (Theta) :  20
                    in der x-y Ebene   ( Phi ) :  20
in k-V Ebene f.H=0, in der H-V Ebene   (Beta ) :   0
                    in der x'-y' Ebene (Alpha) :   0
Kanäle abgeschnitten: Vorne:   0          Bereich Anfang:   1
                     Hinten:   0                    Ende:  20
Glättung: Nein               Anzahl der Überläufe: 0          Spiegeln: Nein
Geraderichten: 0
Geschwindigkeitsparameter:   4.755431    0.257107    0.000151   -0.002118
Fe Menge (Absorberdicke):  20.0 [mg/cm**2]  (-----)
Maximales t:   2.827
Moerup-Both wird verwendet
Basislinie: 713462     Peakhoehe: 37536
```

```
21 Subspektren

Mittleres Feld (ohne antif. Anteil) = 109.712 kG
Mittleres eQVzz/4                   =  -0.043 mm/s
Mittlere Isomerie                   =  -0.175 mm/s

 Spektrum    Feld (kG)   Feld (mm/s)  eQVzz/4      Is       Gamma/2     Al(i)

  1                0.00      0.000     -0.043     -0.175      0.256      0.001
  2               10.90      0.350     -0.043     -0.175      0.256      0.004
  3               21.79      0.700     -0.043     -0.175      0.256      0.011
  4               32.69      1.050     -0.043     -0.175      0.256      0.021
  5               43.59      1.400     -0.043     -0.175      0.256      0.001
  6               54.48      1.750     -0.043     -0.175      0.256      0.000
  7               65.38      2.100     -0.043     -0.175      0.256      0.000
  8               76.28      2.450     -0.043     -0.175      0.256      0.054
  9               87.17      2.800     -0.043     -0.175      0.256      0.087
 10               98.07      3.150     -0.043     -0.175      0.256      0.005
 11              108.97      3.500     -0.043     -0.175      0.256      0.160
 12              119.86      3.850     -0.043     -0.175      0.256      0.644
 13              130.76      4.200     -0.043     -0.175      0.256      0.008
 14              141.66      4.550     -0.043     -0.175      0.256      0.001
 15              152.55      4.900     -0.043     -0.175      0.256      0.000
 16              163.45      5.250     -0.043     -0.175      0.256      0.000
 17              174.35      5.600     -0.043     -0.175      0.256      0.000
 18              185.24      5.950     -0.043     -0.175      0.256      0.000
 19              196.14      6.300     -0.043     -0.175      0.256      0.000
 20              207.04      6.650     -0.043     -0.175      0.256      0.000
 21              217.93      7.000     -0.043     -0.175      0.256      0.000
```

```
                Theta     Beta     Alpha   Eta   rel.Tiefe  abs.Tiefe    area
              (450-x)*2                           1.Linie    1.Linie
                für AF
   1              0.000   54.735    0.000  0.000   17.089       105        0.12
   2             -0.666    0.000    0.000  0.000   0.261         2        0.41
   3             -0.302    0.000    0.000  0.000   0.672         4        1.04
   4             -0.155    0.000    0.000  0.000   1.300         8        1.98
   5             -0.010    0.000    0.000  0.000   0.056         0        0.08
   6             -0.017    0.000    0.000  0.000   0.000         0        0.00
   7             -0.046    0.000    0.000  0.000   0.014         0        0.02
   8              0.712    0.000    0.000  0.000   3.779        23        5.25
   9              0.965    0.000    0.000  0.000   6.357        39        8.53
  10             -0.171    0.000    0.000  0.000   0.419         3        0.54
  11             -0.720    0.000    0.000  0.000   13.025        80       15.97
  12             -0.152    0.000    0.000  0.000   55.994       344       65.01
  13             -0.768    0.000    0.000  0.000   0.773         5        0.84
  14             -0.171    0.000    0.000  0.000   0.069         0        0.07
  15             -0.127    0.000    0.000  0.000   0.011         0        0.01
  16              0.442    0.000    0.000  0.000   0.035         0        0.03
  17              0.666    0.000    0.000  0.000   0.007         0        0.01
  18              0.782    0.000    0.000  0.000   0.052         0        0.04
  19              0.673    0.000    0.000  0.000   0.018         0        0.01
  20              0.412    0.000    0.000  0.000   0.043         0        0.02
  21              0.100    0.000    0.000  0.000   0.026         0        0.01
________________________________________________________________________________

 Relevanter Teil: 379 (351) Kanäle (Abweichung von Basis größer als 2 %)


 Weighted mean square deviation (gesamt)  :        1680.99    (       1417.47)
 Weighted mean square deviation (relevant):        1541.22    (       1257.56)
 Standardabweichung des Mittelwertes (Gesamtes Spektrum):             67.1226
                                                               (      61.5364)
                         (Relevanter Teil des Spektrums):             86.7894
                                                               (      84.4772)
 Korrelationskoeffizient             (Gesamtes Spektrum):            0.990471
                                                               (     0.989889)
                         (Relevanter Teil des Spektrums):            0.990212
                                                               (     0.988824)
 Statistischer Fehler =      0.0011839     Effekt (Fitkurve) =   1.4 %
                        (    0.0000    )                        (  0.0)
 Mittelwert d. Untergrunds (zw.   1. und  20. Kanal): YM=   713105.
 Std. Abw.  d. Untergrunds (zw.   1. und  20. Kanal): YV=   909.249

 Effekt aus Messspektrum (242 relevante Kanäle)      : 1.9
________________________________________________________________________________

Anm.:
________________________________________________________________________________

erstellt am 02.02.2021 um 14:41:37
```

```
Modell: 1. Modell
```

```
Messung: WM178a           Probe: V1.84Fe1.16B2        vom 11.01.2021 (91.0h)
Ta: 150K    Tq: 15.5K    v: 2.5s    Bext: 12T
```

```
Anzahl der Schritte in der k-H Ebene   (Theta) :   0
                    in der x-y Ebene   ( Phi ) :   0
in k-V Ebene f.H=0, in der H-V Ebene   (Beta ) :   0
                    in der x'-y' Ebene (Alpha) :   0
Kanäle abgeschnitten: Vorne:   0           Bereich Anfang:   1
                     Hinten:   0                     Ende:  20
Glättung: Nein               Anzahl der Überläufe: 0            Spiegeln: Nein
Geraderichten: 0
Geschwindigkeitsparameter:   4.756300    0.257243    0.000156   -0.000762
Fe Menge (Absorberdicke):  20.0 [mg/cm**2]  ( 20.0)
Maximales t:   2.828
Moerup-Both wird verwendet
Basislinie: 1065497    Peakhoehe: 75728
```

```
21 Subspektren

Mittleres Feld (ohne antif. Anteil) = 115.612 kG
Mittleres eQVzz/4                   =  -0.037 mm/s
Mittlere Isomerie                   =  -0.205 mm/s

 Spektrum    Feld (kG)   Feld (mm/s)  eQVzz/4      Is       Gamma/2     Al(i)

  1                0.00      0.000     -0.037     -0.205      0.160      0.005
  2               10.90      0.350     -0.037     -0.205      0.160      0.002
  3               21.79      0.700     -0.037     -0.205      0.160      0.001
  4               32.69      1.050     -0.037     -0.205      0.160      0.001
  5               43.59      1.400     -0.037     -0.205      0.160      0.001
  6               54.48      1.750     -0.037     -0.205      0.160      0.002
  7               65.38      2.100     -0.037     -0.205      0.160      0.001
  8               76.28      2.450     -0.037     -0.205      0.160      0.001
  9               87.17      2.800     -0.037     -0.205      0.160      0.001
 10               98.07      3.150     -0.037     -0.205      0.160      0.002
 11              108.97      3.500     -0.037     -0.205      0.160      0.281
 12              119.86      3.850     -0.037     -0.205      0.160      0.691
 13              130.76      4.200     -0.037     -0.205      0.160      0.005
 14              141.66      4.550     -0.037     -0.205      0.160      0.000
 15              152.55      4.900     -0.037     -0.205      0.160      0.000
 16              163.45      5.250     -0.037     -0.205      0.160      0.000
 17              174.35      5.600     -0.037     -0.205      0.160      0.004
 18              185.24      5.950     -0.037     -0.205      0.160      0.000
 19              196.14      6.300     -0.037     -0.205      0.160      0.000
 20              207.04      6.650     -0.037     -0.205      0.160      0.000
 21              217.93      7.000     -0.037     -0.205      0.160      0.000
```

```
                Theta     Beta     Alpha   Eta   rel.Tiefe  abs.Tiefe    area
              (450-x)*2                           1.Linie    1.Linie
                für AF
   1              0.000   54.735    0.000  0.000   2.145      1642         0.65
   2              0.000    0.000    0.000  0.000   0.353       270         0.17
   3              0.000    0.000    0.000  0.000   0.143       109         0.10
   4              0.000    0.000    0.000  0.000   0.059        45         0.05
   5              0.000    0.000    0.000  0.000   0.155       119         0.13
   6              0.000    0.000    0.000  0.000   0.218       167         0.20
   7              0.000    0.000    0.000  0.000   0.117        90         0.11
   8              0.000    0.000    0.000  0.000   0.116        89         0.11
   9              0.000    0.000    0.000  0.000   0.146       111         0.13
  10              0.000    0.000    0.000  0.000   0.228       174         0.22
  11              0.000    0.000    0.000  0.000   26.738     20473        27.79
  12              0.000    0.000    0.000  0.000   68.638     52553        69.30
  13              0.000    0.000    0.000  0.000   0.515       394         0.51
  14              0.000    0.000    0.000  0.000   0.046        35         0.05
  15              0.000    0.000    0.000  0.000   0.009         7         0.01
  16              0.000    0.000    0.000  0.000   0.014        11         0.02
  17              0.000    0.000    0.000  0.000   0.334       256         0.39
  18              0.000    0.000    0.000  0.000   0.009         7         0.01
  19              0.000    0.000    0.000  0.000   0.017        13         0.02
  20              0.000    0.000    0.000  0.000   0.000         0         0.00
  21              0.000    0.000    0.000  0.000   0.001         1         0.00

 Relevanter Teil: 259 (512) Kanäle (Abweichung von Basis größer als 2 %)


 Weighted mean square deviation (gesamt)  :        2486.63    (       -1.#IND)
 Weighted mean square deviation (relevant):        2227.35    (       -1.#IND)
 Standardabweichung des Mittelwertes (Gesamtes Spektrum):             99.4838
                                                              (       -1.#IND)
                         (Relevanter Teil des Spektrums):             186.064
                                                              (       -1.#IND)
 Korrelationskoeffizient             (Gesamtes Spektrum):            0.990695
                                                              (       -1.#IND)
                         (Relevanter Teil des Spektrums):            0.988144
                                                              (       -1.#IND)
 Statistischer Fehler =     0.000968777     Effekt (Fitkurve) =   1.7 %
                         (    0.0000    )                      (  0.0)
 Mittelwert d. Untergrunds (zw.   1. und  20. Kanal): YM=  1064965.
 Std. Abw.  d. Untergrunds (zw.   1. und  20. Kanal): YV=   1062.57

 Effekt aus Messspektrum (251 relevante Kanäle)     : 1.8

Anm.:

erstellt am 22.01.2021 um 13:37:04
```

C Program code

C.1 MercuryIPS_Controlls

C.1.1 Description

The program "MercuryiPS_Controls" consists of five parts, as it is shown in figure C.2. The start with the establishment of the connection between the program and the power supply unit (figure C.3), the three loops, measurement and stopper, ramping and clamp, within the main loop (figures C.6 to C.17), and the end of the program that closes the connection (figure C.4).

The connection with the MercuryiPS unit is established via the SubVI "Open System". It requires the following inputs. An empty error container, the used COM-Port (COM4), the type of connection (USB) and two Boolean constants set to true, to reset all old connections and activate the ID-Query. The main output of that SubVI is the container variable "Mercury Reference". It contains all informations about the power supply and its sub devices. The second output is the main error line, which runs through the whole program. The status of the error line gets checked immediately afterwards via a error handler. The boolean indicator "connection ready" will be set to true and a LED will light up, if the connection between the computer and the power supply was established without any problems, otherwise a popup window will appear that describes the error and allows the user to stop the program. The SubVI "Open magnet" will be called afterwards, using the constant "Z-Axis", which enables further communication between the subdevices within the MercuryiPS unit and the PC. The boolean value "false" will be written onto the variables "stop all" and "stop intern" parallel to all of that.

The two main wires, "Mercury Reference" and "Error" tunnel inside the main while loop, which keeps the program running until the "Quit program" button on the front panel gets pressed. This loop consist of the three independent loops. Ordering from top to bottom: Measurement and stopper loop, ramp loop and Clamp loop. The main two wires enter all loops in parallel, which leads to parallel execution of the three sub loops.

The Measurement and stopper loop consists of two parts. The Measurement part of the loop consists of the SubVI's "Current", "Current Rate", "Persist Field", "Persis Current" and "Voltage". These SubVI's extract the current values of the terminal current in Ampere, the current rate in Ampere per minute, the magnetic field in tesla and the persistent current in Ampere of the magnet and the voltage at the terminal outputs out of the power supply and writes these values on identical named variables. The value of the voltage will be checked in addition to ensure, that it is between ±3 Volt. If this is not the case the indicator "Quench" will light up at the frontpanel, as the boolean variable "Quench?" will be set to "false". At the end of this part a error handler will check the error line for any problems and display them in a popup window. The stopper part of the loop checks the status of the buttons "Quit program" and "Stop ramp". Its boolean values will be written onto the variables "stop all" and "stop intern" respectively. The loop will stop if "Quit program" or "stop ramp" report a boolean "true". The main loop will stop in addition if "Quit program" is set to true. A red LED will light up on the front panel, if "stop intern" gets triggered. This shall indicate the user to wait with new inputs until the light extinguishes.

The ramp loop consists of two parts that are connected in series, the ramp set point set loop and the ramp case. The ramp set point set loop starts by transmitting the boolean value "false" to the indicators "equalizing terminals and magnet current", "ramping magnet" and "ramping terminals only". This ensures that the corresponding LEDs on the front panel are deactivated. Furthermore will the value of the boolean variable "Lambda" be written onto the indicator "Lambda display" and be provided for the next part via a tunnel. The boolean variables "stop all", "stop intern", "Ramp to zero" and "start ramp" get called in parallel. A boolean "true" in any of these variables will stop the loop. Additionally will the variable "ramps activ?" be set to "true" if "Ramp to zero" or "Start ramp" are set to "true" and the value of "Ramp to zero" decides which case will be executed next.

The value zero will be written onto the variables "Target field in [A]" and "Target field in [T]", if a boolean "true" was reported by "Ramp to zero". The value zero, the variable "Mercury Reference" and the Error line get provided for the second part of the ramp loop via tunnels. (figure C.17)

Two different cases are possible if a boolean "false" was reported by "Ramp to zero". Depending on the boolean state of the control "Ampere or Tesla" will either be the value of "Target field in [T]" (figure C.15) or "Target field in [A]" (figure C.16) be used in the second part of the ramp loop. The not used variable will be calculated and displayed at the front panel by multiplying or dividing the other variable with the Current to field factor, which gets extracted from the power supply using the SubVI "Curr to Fld". The set point in Ampere will be handed to the ramp case via tunnel.

The ramp case is divided into two possible cases, which get selected depending on the boolean value of the logical "OR" function of "stop intern" and "Quit program" called inside the ramp set point set loop. The ramp case will pass the variable "Mercury Reference" and the error line through to the end of the program If "true" gets reported (figure C.14).

The programm will initiate a ramp, if the ramp set point set loop ends, but the variable "stop intern" and stop all" are set to "false". The Ramp case starts by reading the value of the variable "Magnetic Current in [A]" into the VI "check_saved_persis_current", which outputs the last known current inside the magnet. The case structure "Lambda Check" will be executed parallel to that. The state of the button "Lambda", located on the fornt panel, decides which case shall be executed. The value of the new set point in [A] will be directly handed to the VI "Create_Protokol", the SubVI "Target Current" and the following for loop, if the button is in its boolean "true" state (figure C.10). Otherwise will the value be checked if it is below 70,7 Ampere (figure C.11). The value of the set point will be distributed the same way as above, if this is the case. A popup window will appear and the program will stop, if the value of "Target field in [A]" is greater than 70,7 (figure C.9). The VI "Create_Protokol" will be called using the output of the VI "check_saved_persis_current" as a starting value and the output of the Lambda case as a ending value. Furthermore will a boolean "true" be transmitted to the VI, which indicates that this is the start of a ramp. The VI "Set_terminal_current_to_pers_current" will be called afterwards including the VI "check_saved_persis_current" and the two references for "stop intern", which will end the VI if the button "Stop ramp" gets pressed, and for "equalizing terminals and magnet current", which indicates that this VI is running via a LED on the front panel. The new set point will be set in the power supply using the SubVI "Target Current" afterwards. A for loop with only one iteration will start directly after the target current had been set. This one iteration ensures that the most current state of the boolean variable "Stop intern" will be used to decide which of two possible cases shall be executed. The case "true" will be executed if "Stop intern" reports a boolean "true". This indicates that the button "Stop ramp" was pressed while the VI "Set_terminal_current_to_pers_current" was active. The VI "Set_psu_to_hold" will be called, to initiate a clean rampdown of the power supply unit.

The VI "Set_psu_to_set" will be called afterwards, which is followed by a while loop, that lasts until the SubVI "Current" reports a value between $\pm 0,005$. The case ends by calling the SubVI "Persist Current" which outputs the current persistent current of the magnet and a boolean "false" into the VI "Create_Protokol" which adds a entry into the protocol file.(figure C.13)
The VI "Switch_Heater" gets called with the argument "on", if the boolean variable "stop intern" reports "false". This indicates that the ramp was executed without any interruption until this point. The SubVI "PSU Action" is called using the argument "Ramp to set" to start the ramping of the magnet. The following while loop checks the current current inside the magnet and ends if either the reported valus is within ± 0.0005 of the set target and the reported voltage is between $\pm 0.0095 \times$ "target current" or "stop intern" reports a boolean "false". The indicator "ramping magnet" is lit as long as the loop is active. The VI "Switch_Heater" gets called with the argument "off" immediately after this loop, followed by the VI "Set_psu_to_hold" to initiate a clean rampdown of the power supply units terminals. This rampdown of the PSU gets initiated by calling the SubVI "PSU Action" using the argument "Ramp to Zero", which is followed by a while loop. This loop is active until the value, that the SubVI "Current" reports, is within ± 0.005. The LED "ramping terminals only" is lit until the loop ends. This case finishes by calling the VI "Create_Protokol" using a boolean "false" and the last measured current inside the magnet. (figure C.9). The error line is handed to a error handler at the end of the ramp case.

The Clamp loop consist of a event structure with two cases and the calling of the boolean variables "stop all" and "stop intern". The loop will be stopped, if any of the two boolean variables report a boolean "true".
The two possible events are a timeout case (figure C.5) and a case that gets triggered if the Clamp button gets pressed. (figures C.6 to C.8)
The timeout case gets triggered if the clamp button was not pressed for one second. It checks the status of the internal clamp of the power supply using the SubVI "PSU Action" and set the button Clamped/Unclamped on the front panel accordingly. The boolean variable Clamp" will be set to true, if the SubVI "PSU Action" reports "Hold", "Ramp to Set" or "Ramp to Zero".
The second case gets triggered if the button "Clamp" gets pressed. The value of the variable "ramps activ?" decides which case inside the event structure will be triggered. The main error line will be handed to the error handler at the end of the loop, if the variable is set to "true". The status of the internal clamp will not be changed, due to the fact that a ramp is active. (figure C.8) The status of the boolean variable "Clamp" chooses the inner case that shall be executed if the variable "ramps activ?" reports "false". The SubVI "PSU Action" will get called with the constant "Clamp output", in the case that "Clamp" reports "false". A following loop checks the status of the power supply using the SubVI "PSU Action" until it reports "Clamp output" and will than hand the error line to a error handler. This case will clamp the terminals of the power supply and change the "Clamp/Unclamp" button on the front panel to the "Clamped" state. It is not possible to perform raps in this state. (figure C.6)
The same happens if the variable "Clamp" reports "true", but instate of "Clamp output" will "Hold" be transmitted via the SubVI "PSU Action". This case allows ramps to be performed, the button "Clamp/Unclamp" will light up green. (figure C.7)

The connection between the PC and the power supply will be terminated after the main loop ends using the SubVI "Mercury Close". In parallel to that will the indicator "connection ready” be set to false. The program ends after the error line terminates into a error handler. (figure C.4)

C.1.2 Frontpanel

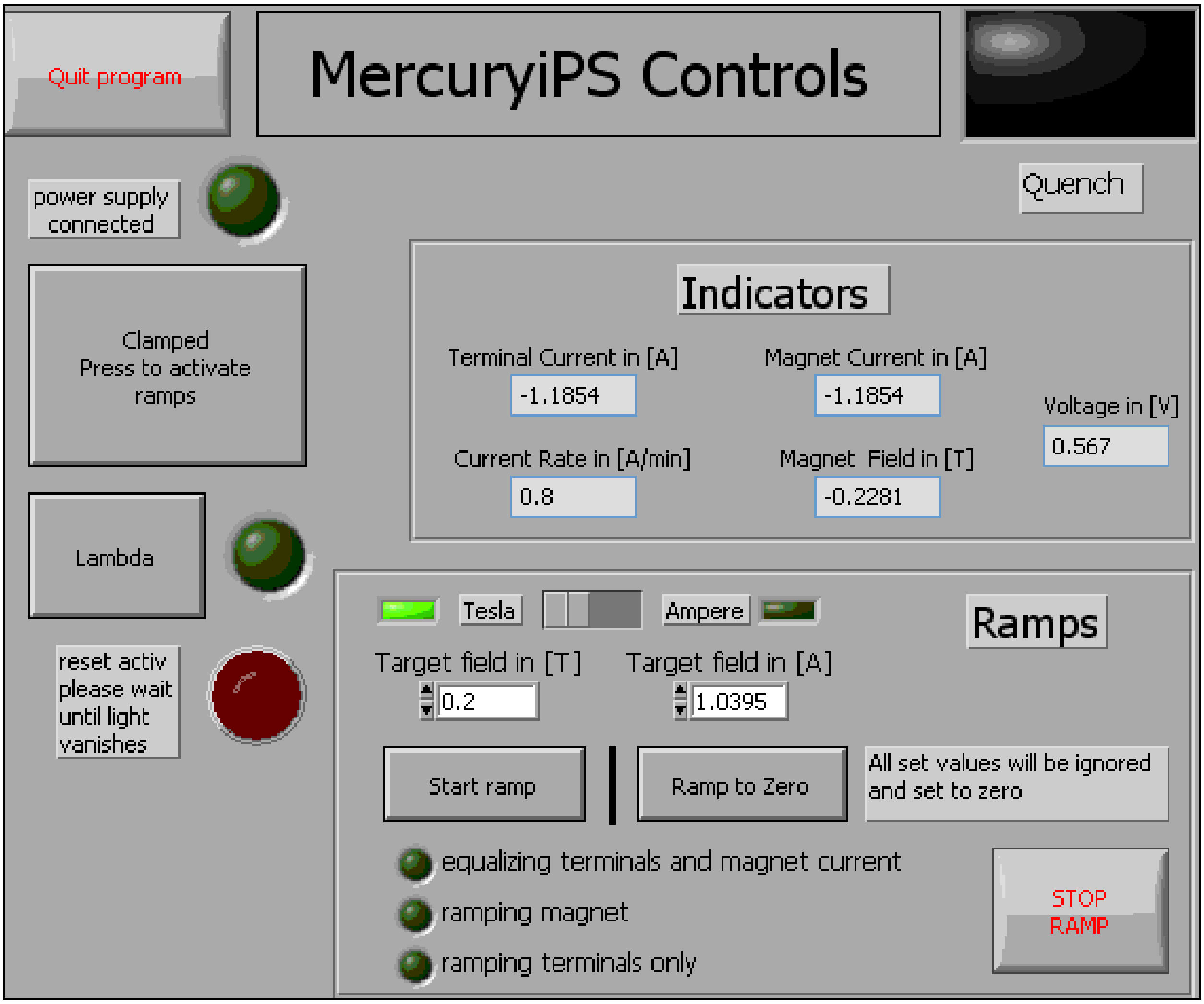

Terminal Current in [A] -1.1854

Magnet Current in [A] -1.1854

Voltage in [V] 0.567

Current Rate in [A/min] 0.8

Magnet Field in [T] -0.2281

Target field in [T] 0.2

Target field in [A] 1.0395

All set values will be ignored and set to zero

Figure C.1: GUI of the implemented MercuryiPS_Controls program.

C.1.3 Blockdiagramms

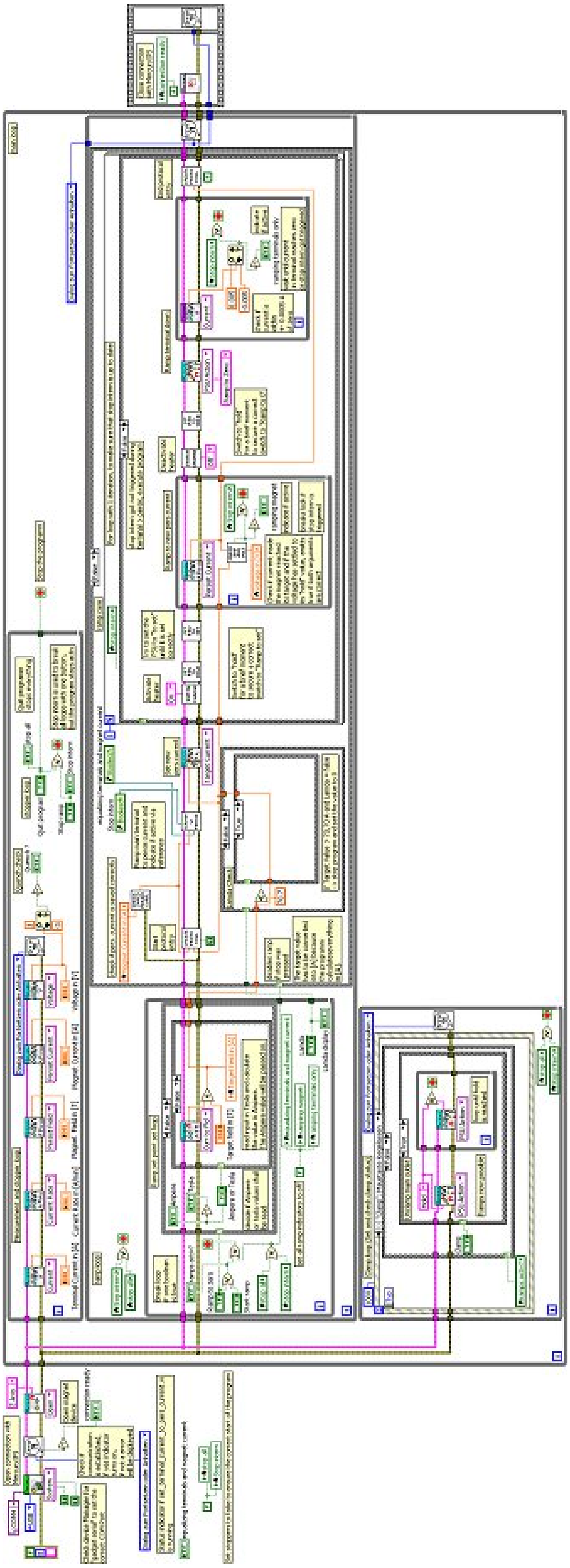

Figure C.2: Overview of the blockdiagramm of MercuryiPS_Controlls

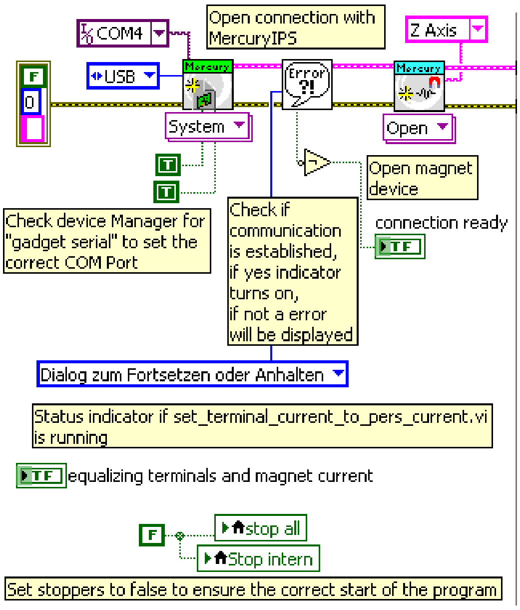

Open connection with MercuryIPS

Check device Manager for "gadget serial" to set the correct COM Port

Check if communication is established, if yes indicator turns on, if not a error will be displayed

Open magnet device

connection ready

Dialog zum Fortsetzen oder Anhalten

Status indicator if set_terminal_current_to_pers_current.vi is running

equalizing terminals and magnet current

Set stoppers to false to ensure the correct start of the program

Figure C.3: Part of the blockdiagramm of MercuryiPS_Controlls displaying the initialisation of the connection between power supply and PC.

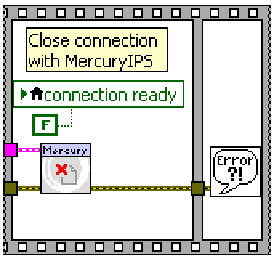

Close connection with MercuryIPS

Figure C.4: Part of the blockdiagramm of MercuryiPS_Controlls displaying the closing of the connection between power supply and PC.

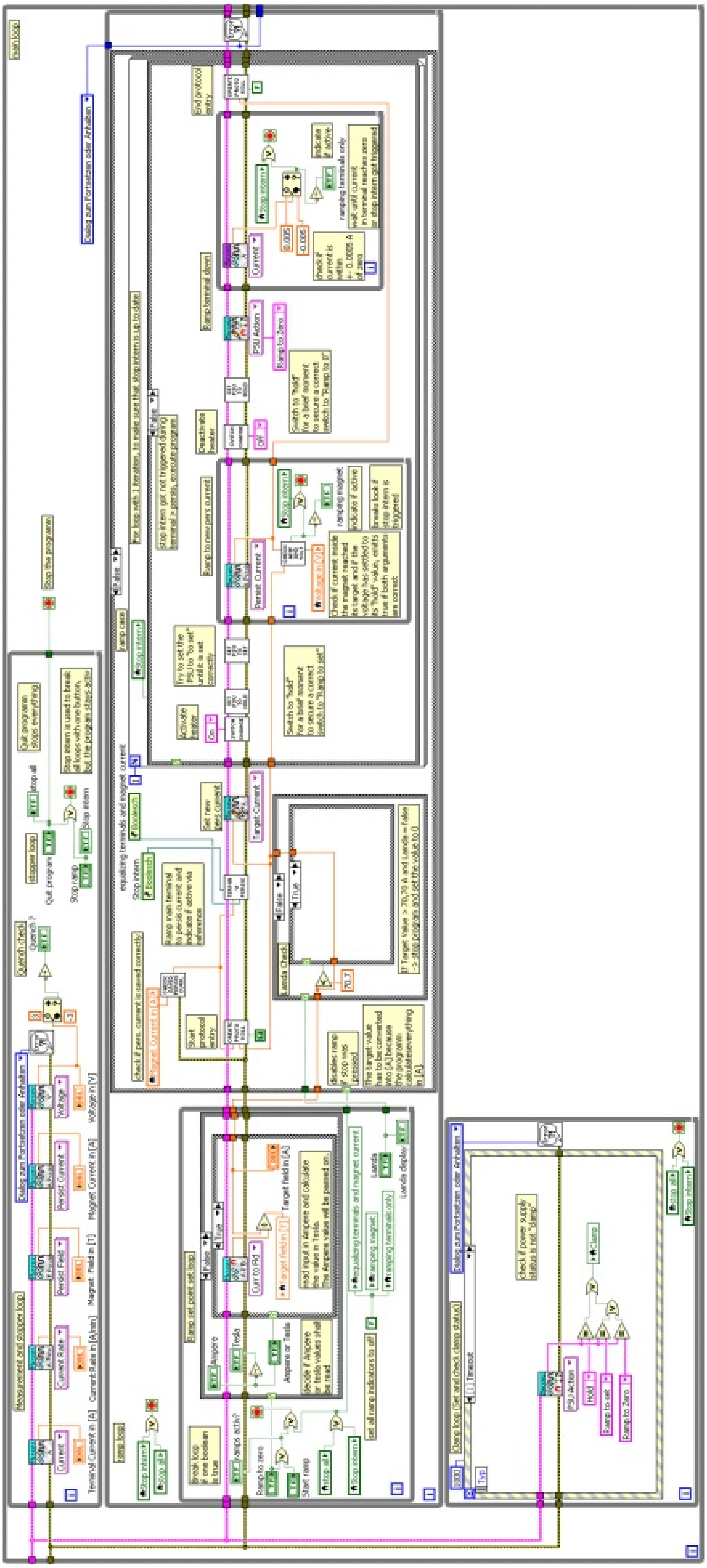

Figure C.5: Part of the blockdiagramm of MercuryiPS_Controlls especially displaying the clamp loop in its timeout state.

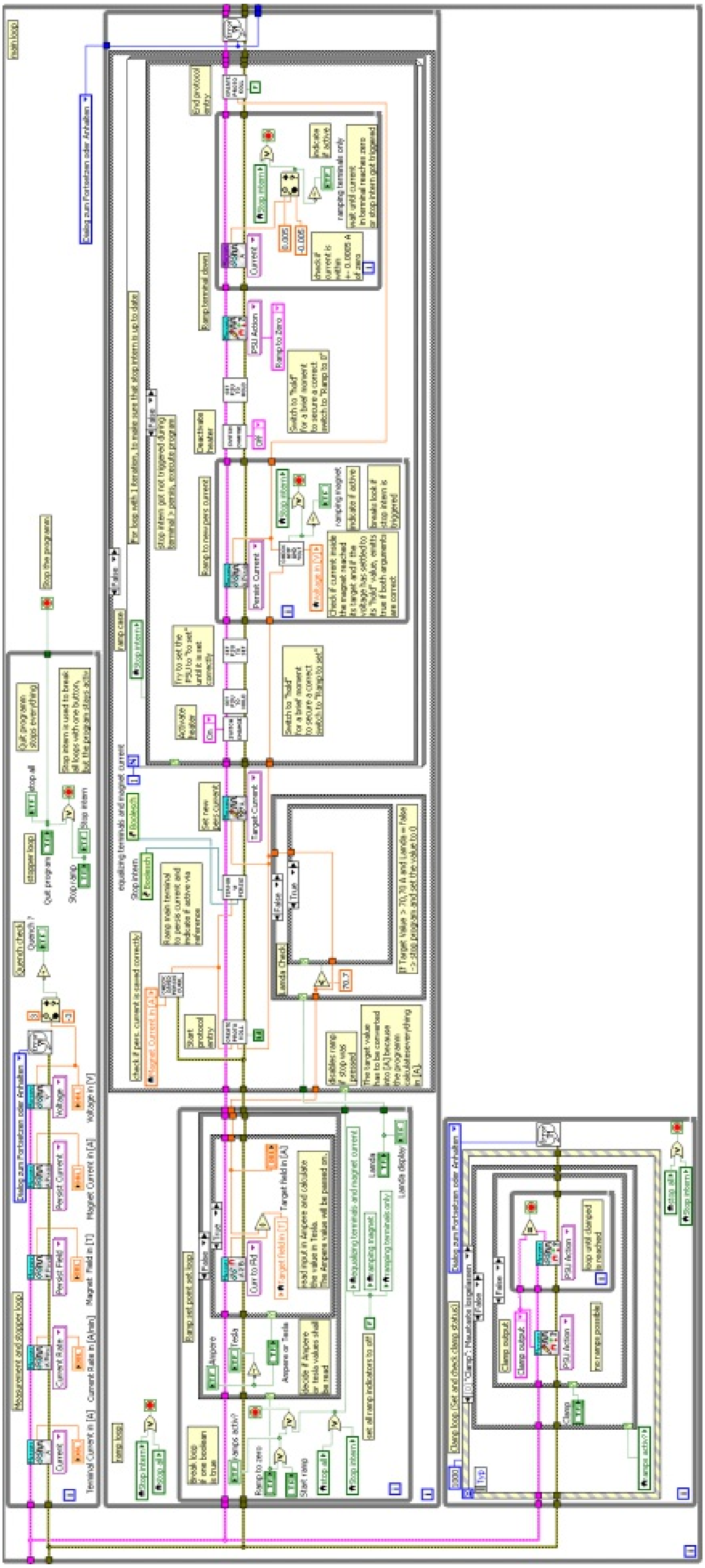

Figure C.6: Part of the blockdiagramm of MercuryiPS_Controlls especially displaying the clamp loop activating the clamp.

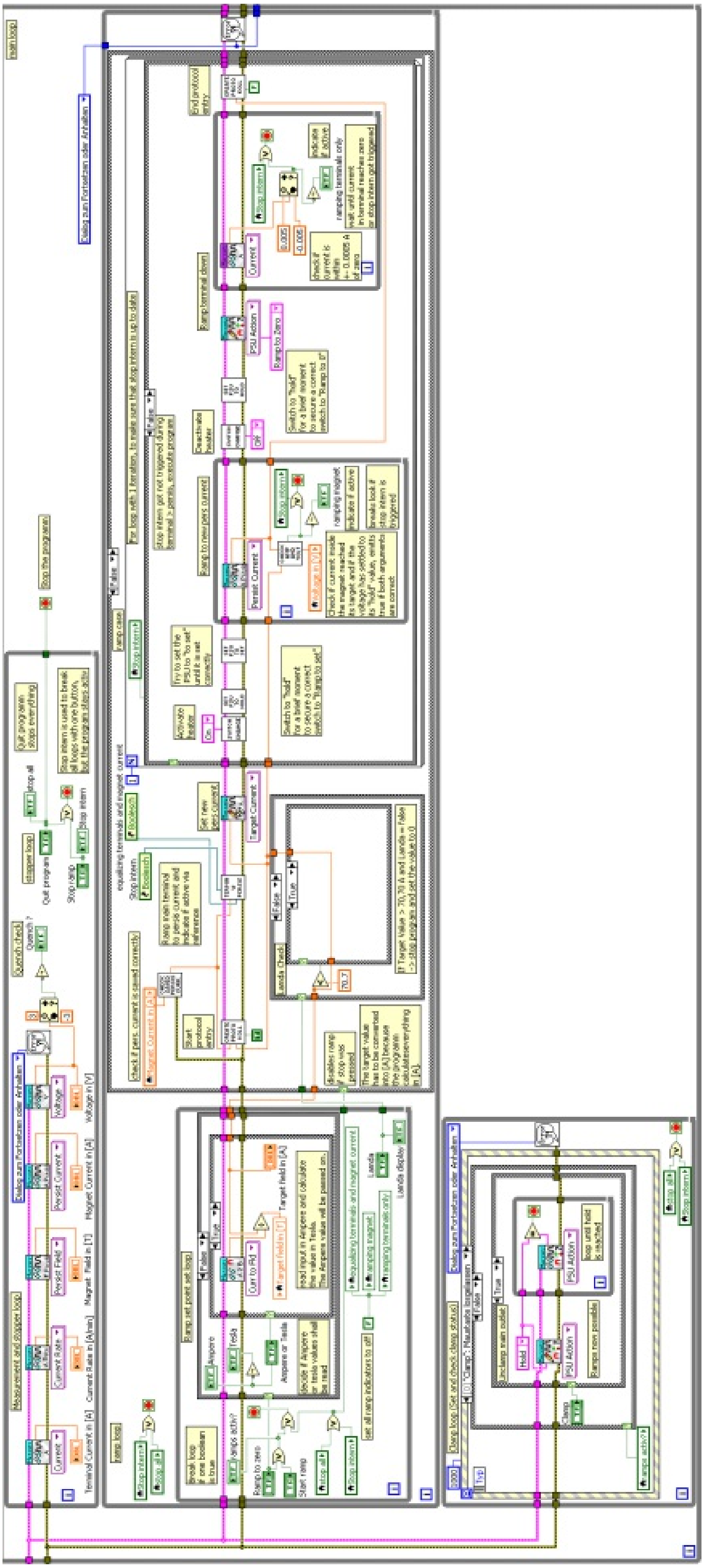

Figure C.7: Part of the blockdiagramm of MercuryiPS_Controlls especially displaying the clamp loop deactivating the clamp.

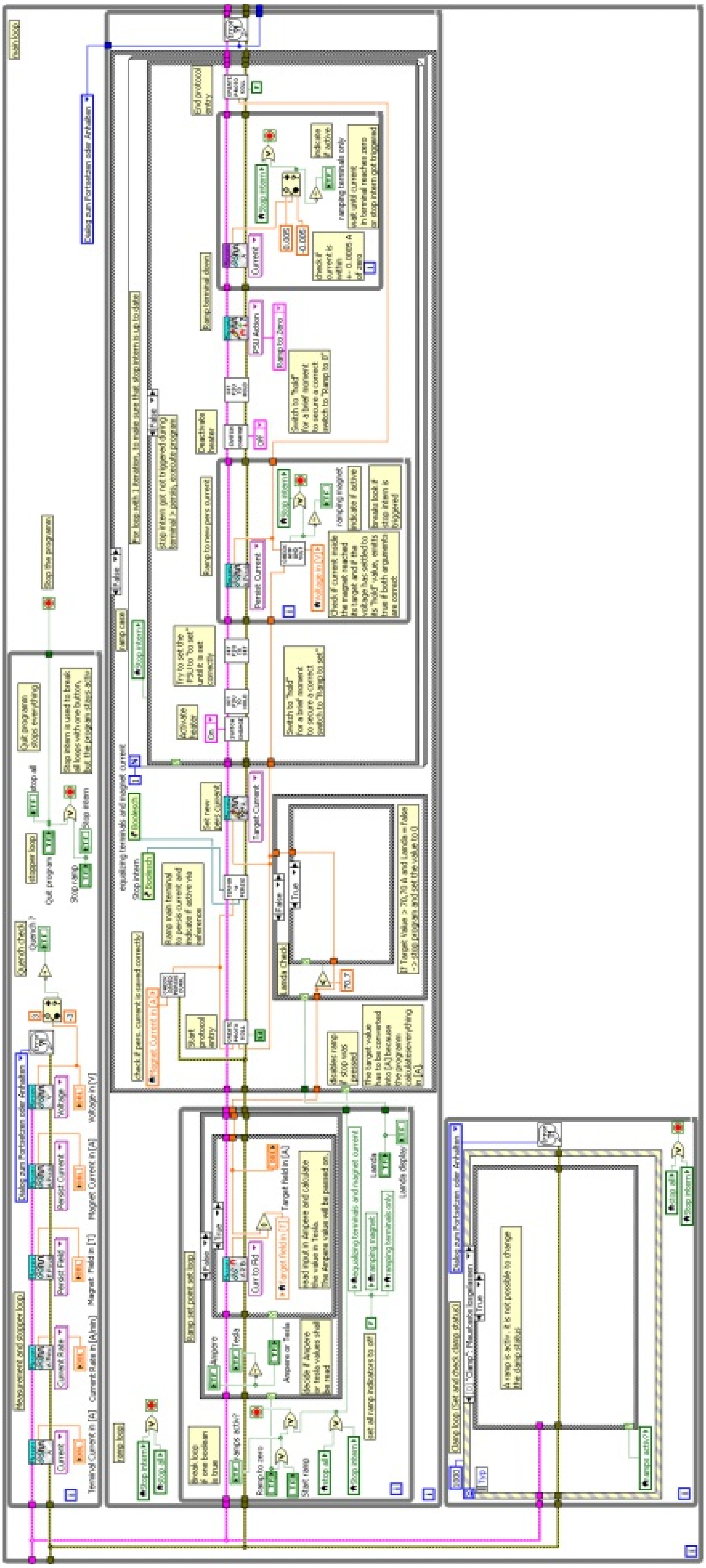

Figure C.8: Part of the blockdiagramm of MercuryiPS_Controlls especially displaying the clamp loop in its locked state.

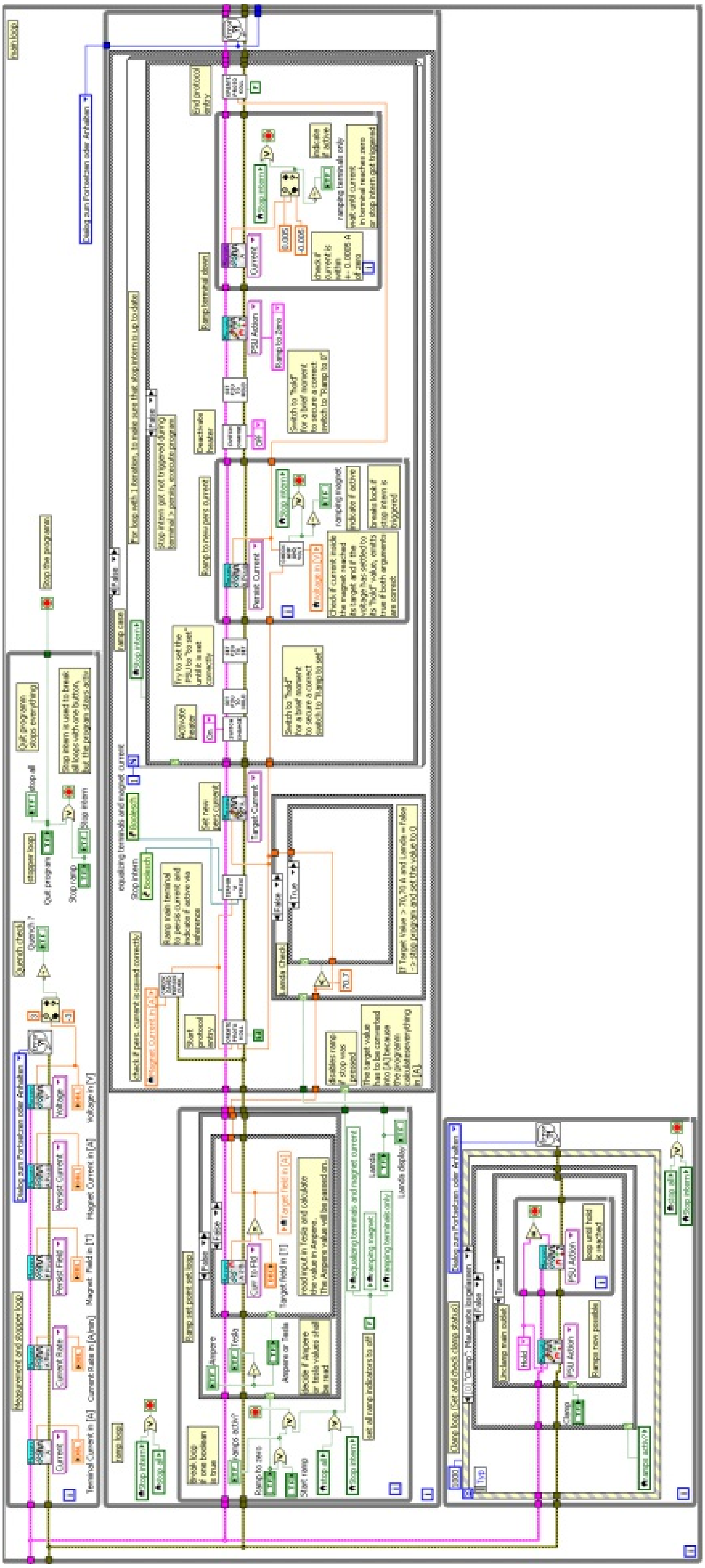

Figure C.9: Part of the blockdiagramm of MercuryiPS_Controlls especially displaying the ramp loop performing a ramp without interruption.

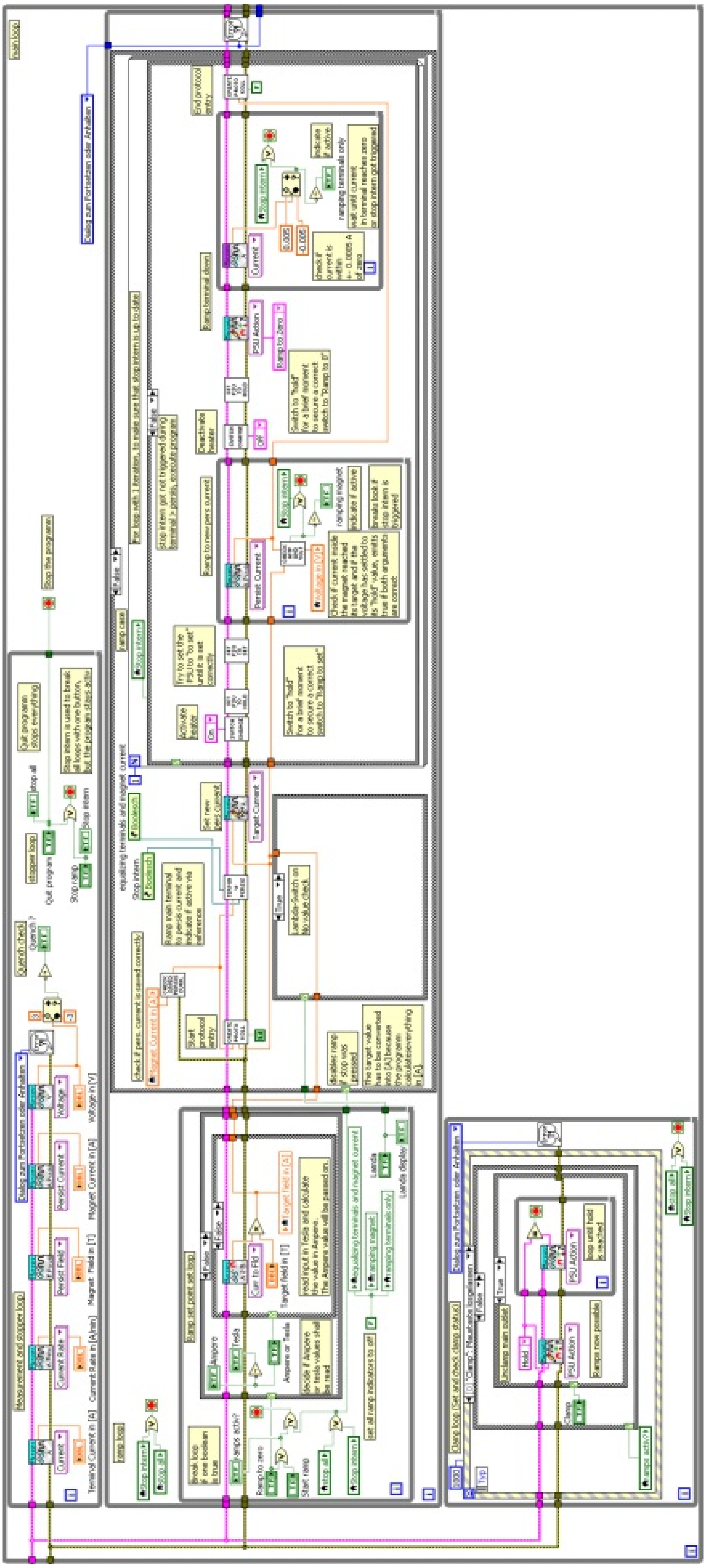

Figure C.10: Part of the blockdiagramm of MercuryiPS_Controlls especially displaying the lambda check if the button lambda is pressed.

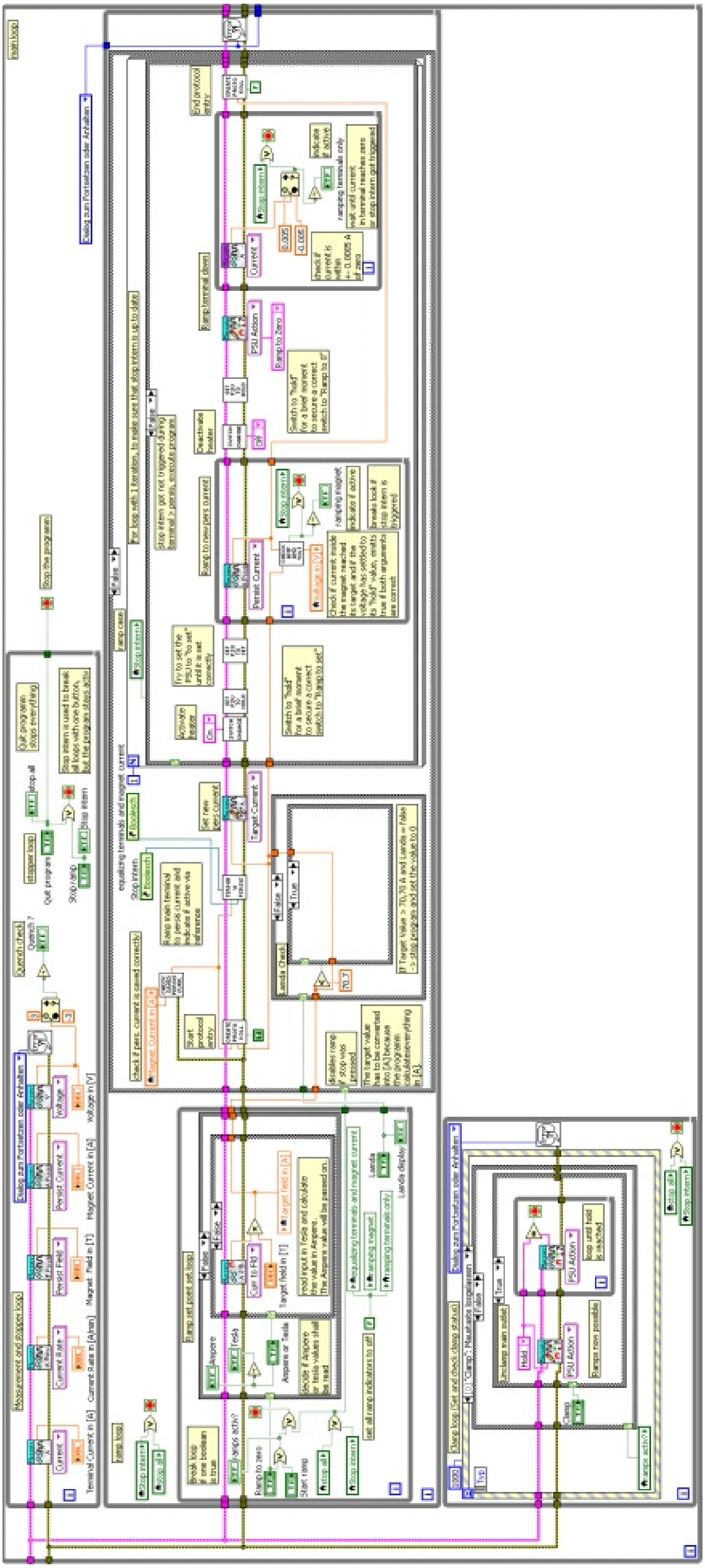

Figure C.11: Part of the blockdiagramm of MercuryiPS_Controlls especially displaying the lambda check if the button lambda is not pressed and the new set point is below 70,7 Ampere.

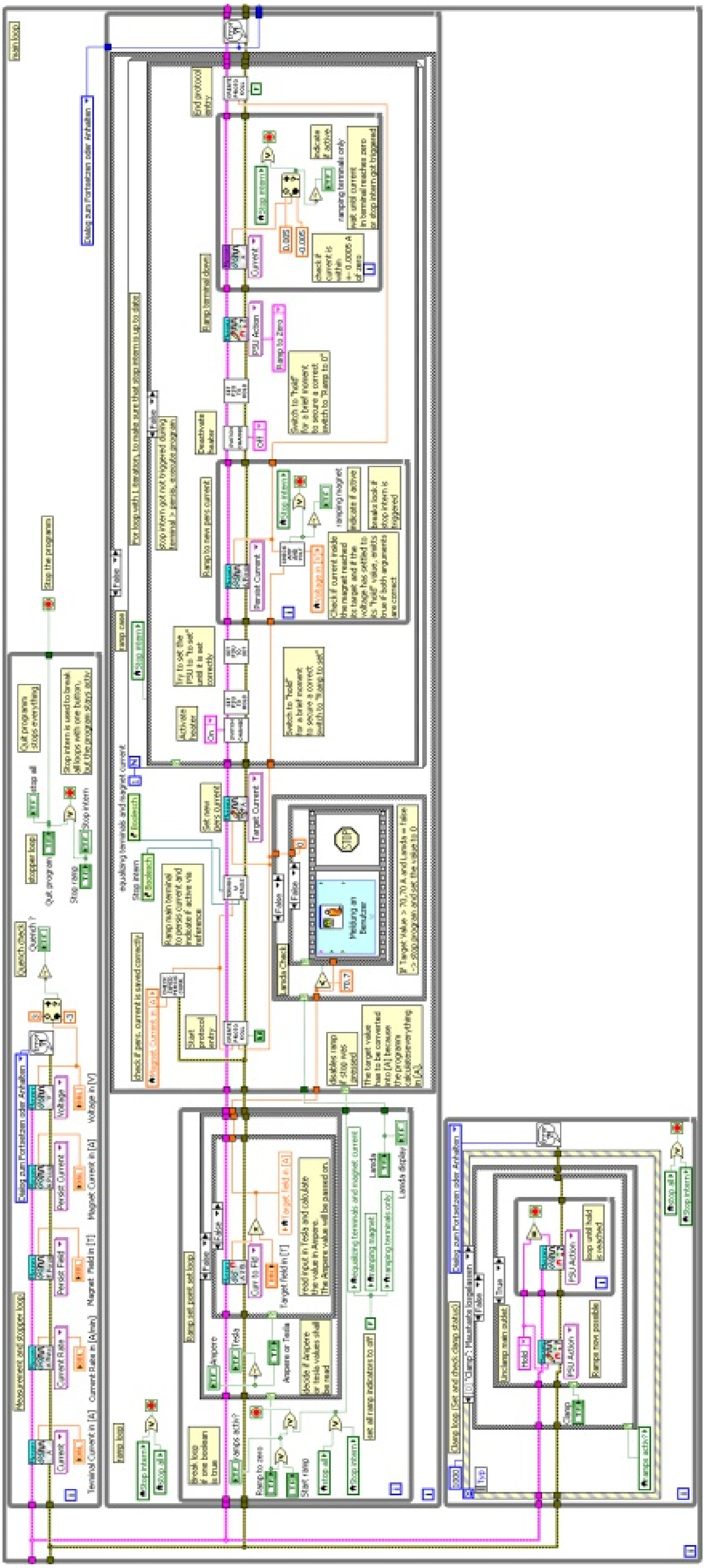

Figure C.12: Part of the blockdiagramm of MercuryiPS_Controlls especially displaying the lambda check if the button lambda is not pressed but the new set point is above 70,7 Ampere.

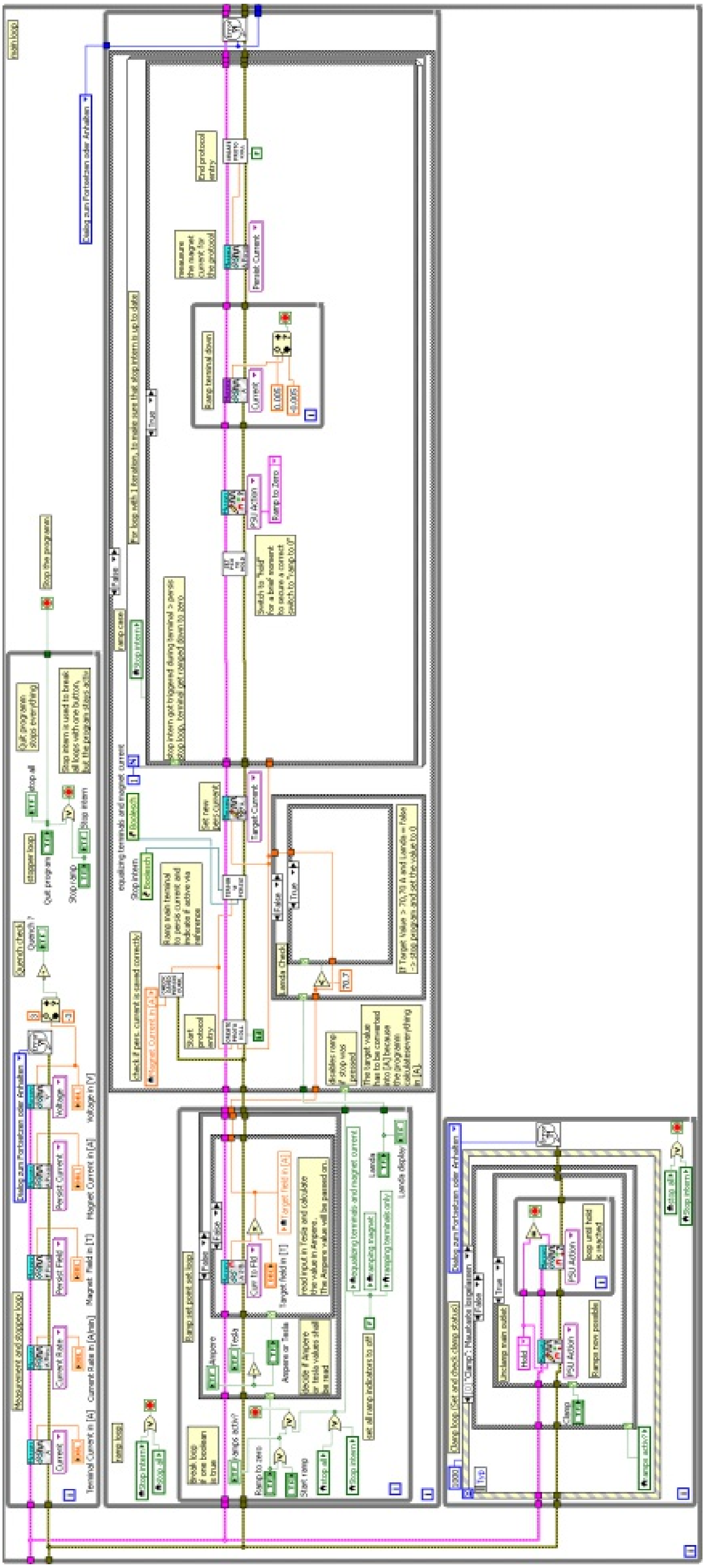

Figure C.13: Part of the blockdiagramm of MercuryiPS_Controlls especially displaying the ramp loop performing a ramp interrupted during the equalisation of the terminal and the magnet current.

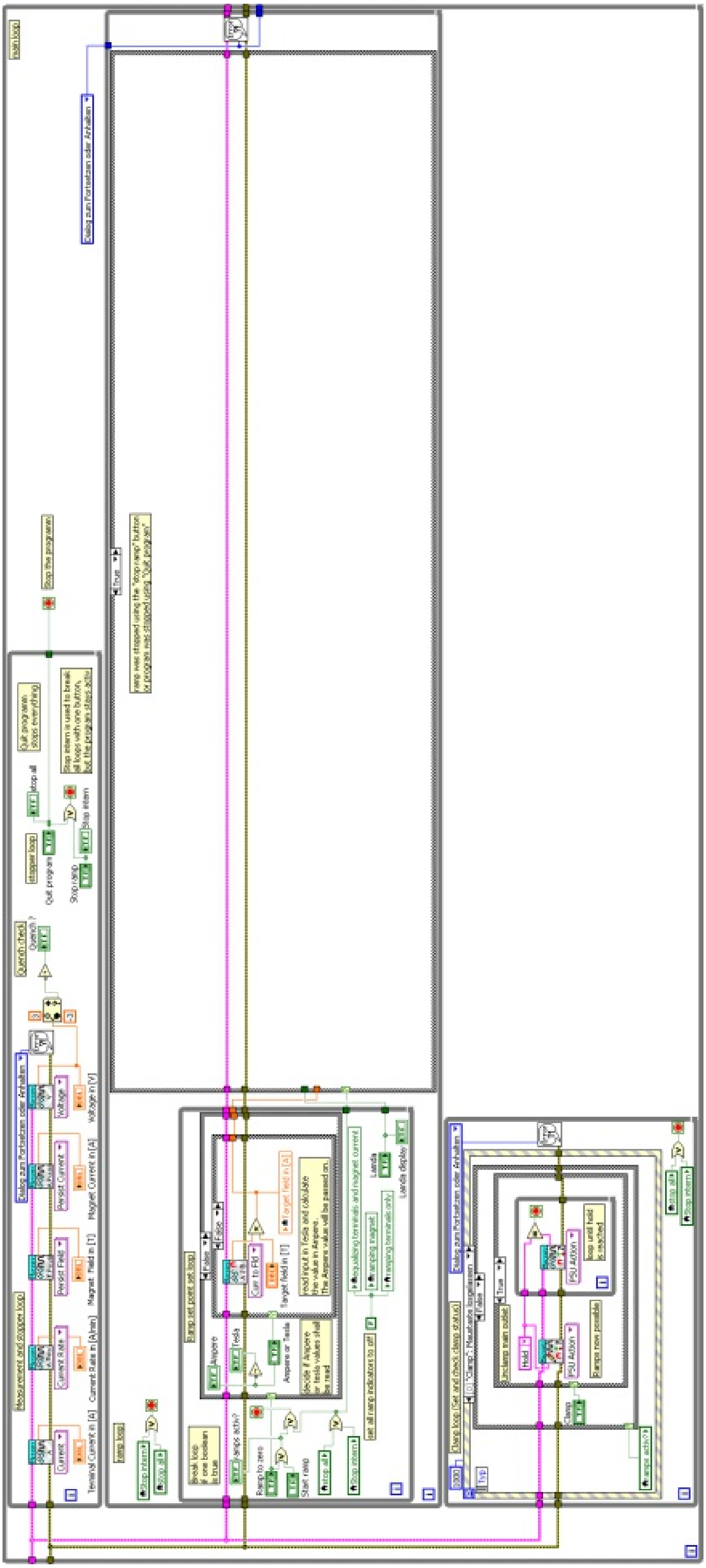

Figure C.14: Part of the blockdiagramm of MercuryiPS_Controlls especially displaying the ramp loop after "Stop ramp" was pressed.

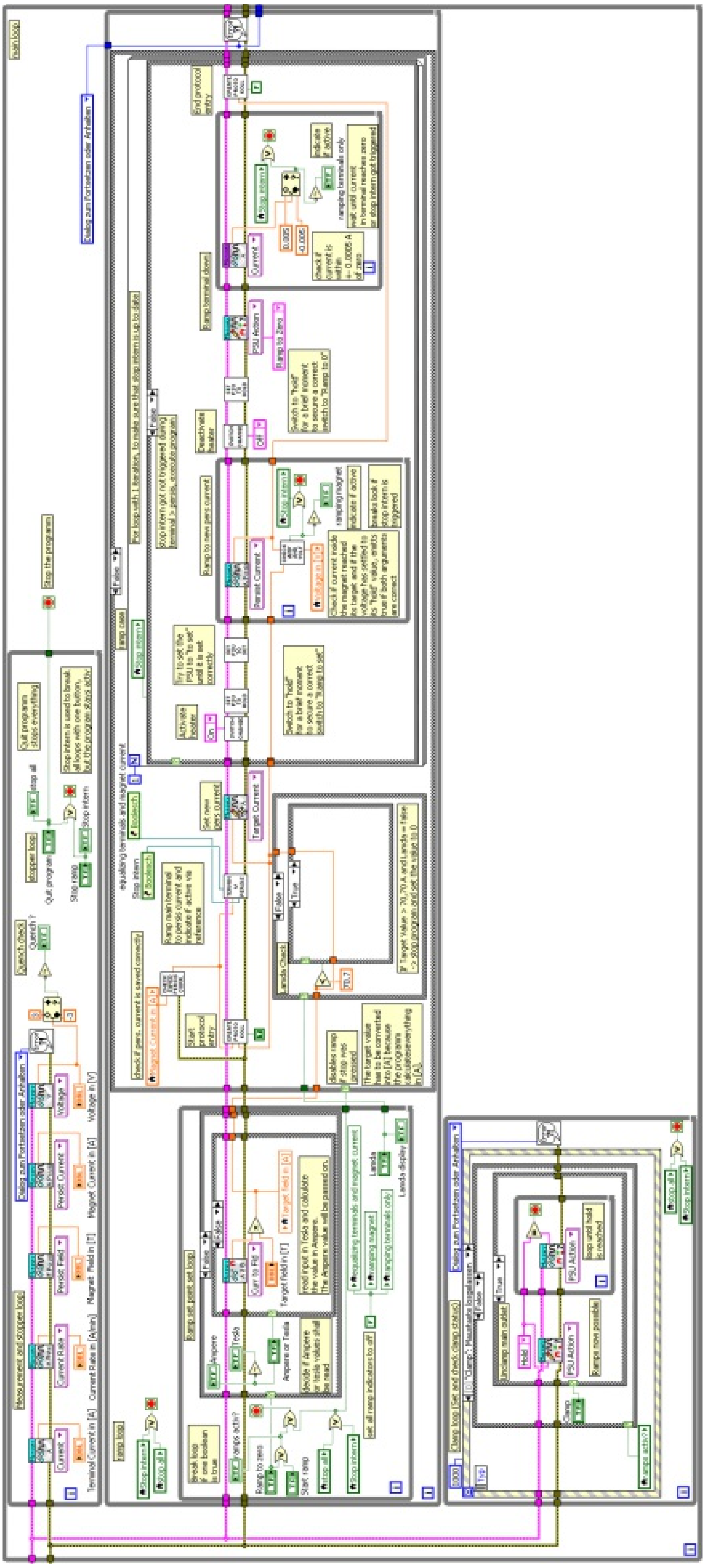

Figure C.15: Part of the blockdiagramm of MercuryiPS_Controlls especially displaying the ramp loop waiting for a new set point in Tesla.

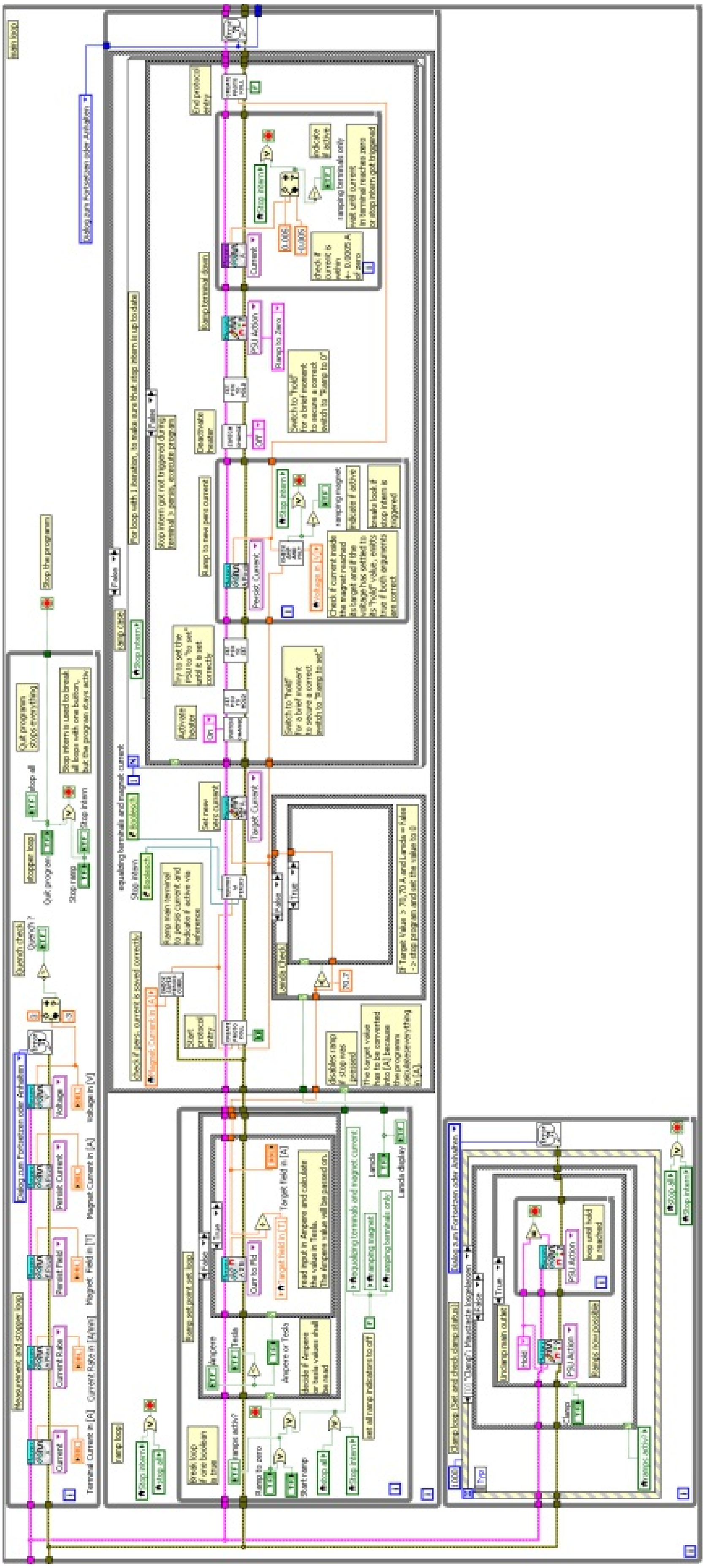

Figure C.16: Part of the blockdiagramm of MercuryiPS_Controlls especially displaying the ramp loop waiting for a new set point in Ampere.

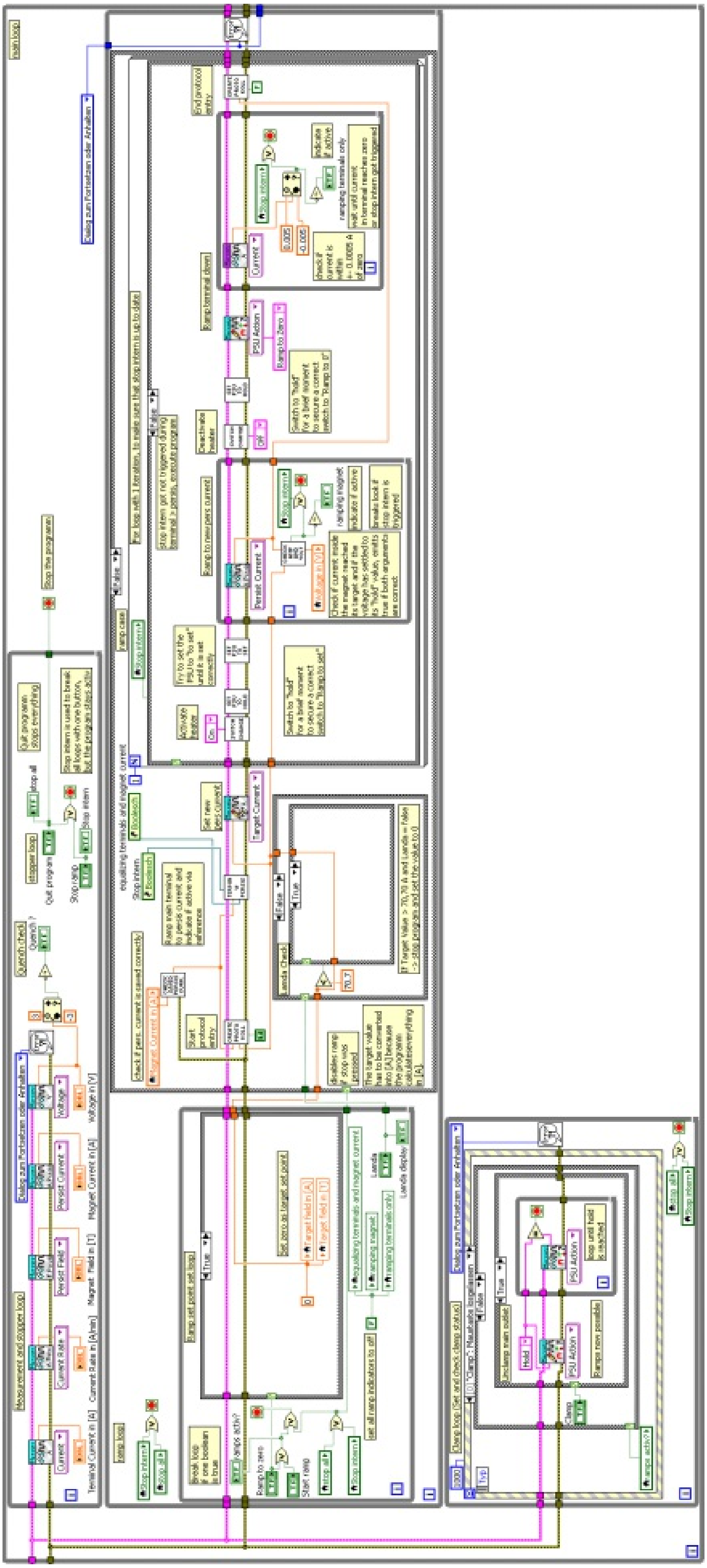

Figure C.17: Part of the blockdiagramm of MercuryiPS_Controlls especially displaying the ramp loop setting the set point to zero.

C.2 Switch_Heater_changer

C.2.1 Description

The program "Switch_Heater_changer" changes the state of the switch heater according to the state provided by the input and waits until the switching finished.

Three inputs are required to run this VI correctly. "Mercury Reference In" contains all important information about the PSU in use, "Error in" contains all previous occurred errors and "Switch Heater Status" the desired status of the Switch heater.
These inputs are fed into the SubVI "Heater Status", that changes the status of the Switch heater according the value provided by "Switch Heater Status". The following while loop checks the status of the heater using the read version of the SubVI "Heater Status" and compares this value with the input in "Switch Heater Status", until these values are identical. The program ends by handing all occurred errors into the output "error out" and the Mercury Reference container into "Mercury Reference out".

C.2.2 Frontpanel

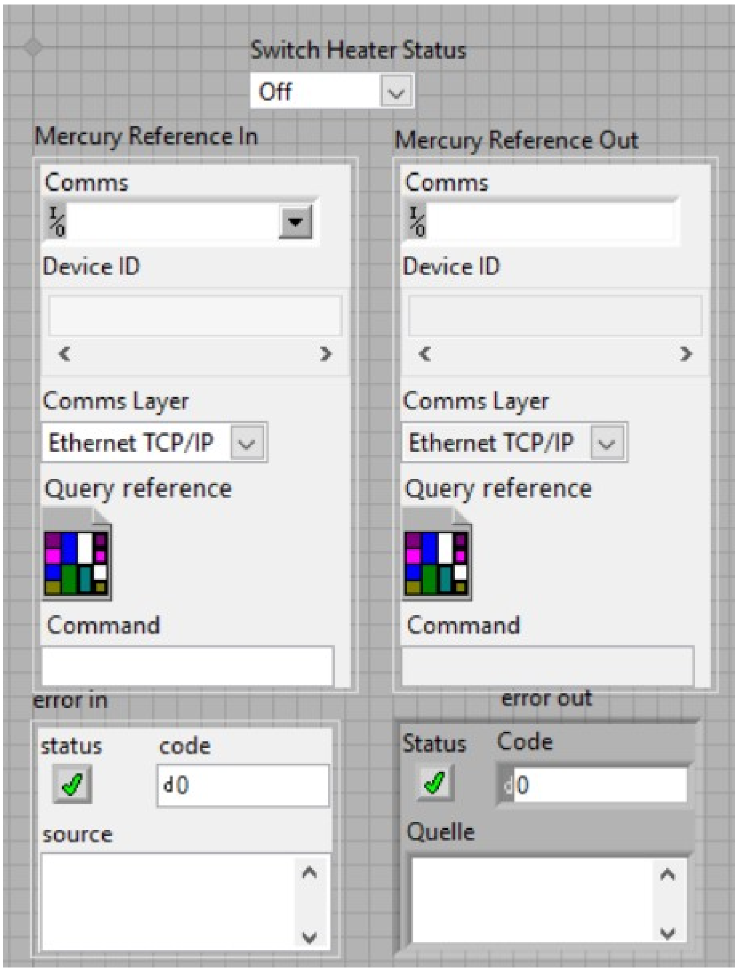

Switch Heater Status: Off

Comms Layer: Ethernet TCP/IP

Comms Layer: Ethernet TCP/IP

code: d0

Code: 0

Figure C.18: GUI of the implemented switch_heater_changer program.

C.2.3 Blockdiagramm

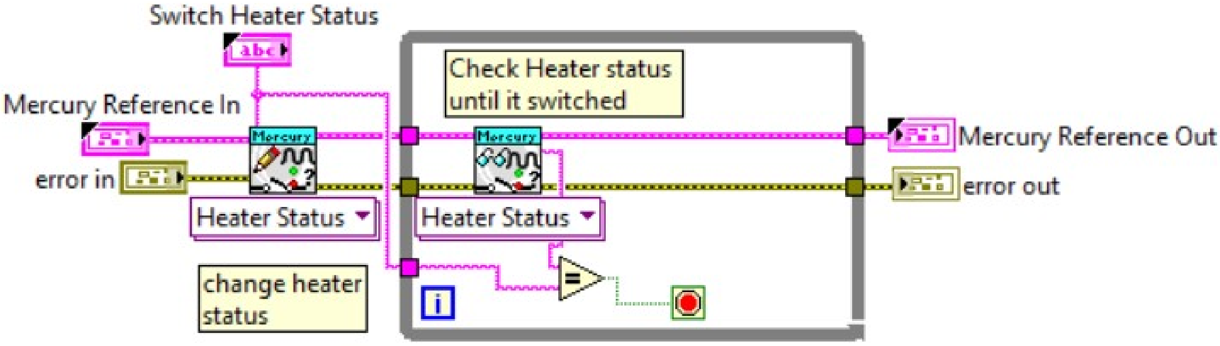

Figure C.19: Blockdiagramm of Switch_Heater_changer.

C.3 Set_terminal_current_to_pers_current

C.3.1 Description

The program "Set_terminal_current_to_pers_current" equalizes the current at the main terminal output of the PSU with the persistent current of the magnet.

Five inputs are required to run this VI correctly. "Mercury Reference In" contains all important information about the PSU in use, "Error in" contains all previous occurred errors, "Persist Current" the last measured persistent current of the magnet and the two references "stop intern" and "Reference if running".
These values are fed into the SubVI "Target Current", which sets the new set point of the PSU to the last measured persistent current. The SubVI "Heater Status" reads the current status of the switch heater and compares the output with the constant "OFF". The Boolean output of this comparison decides the case of the following structure.
The SubVI "PSU Action", with the attribute "Ramp to set" is started if its output is "true" (Figure: C.21). If the heater is activated and the comparison lead to a boolean "false", the VI "Switch_Heater_changer" gets started to deactivate the Switch heater. The SubVI "PSU Action", with the attribute "Ramp to set" starts afterwards. (Figure: C.22) The following while loop measures the current persistent current in the magnet and compares it with the set point. The loop ends if they are within ±0.0005 of each other and the voltage reported by the SubVI "Voltage" is between $\pm 0.0095 \times$ pers current or the boolean reference of "stop intern" reports "true".The Reference "Reference if active" will report a boolean true while the loop is active.
The program ends by handing all occurred errors into the output "error out" and the Mercury Reference container into "Mercury Reference out".

C.3.2 Frontpanel

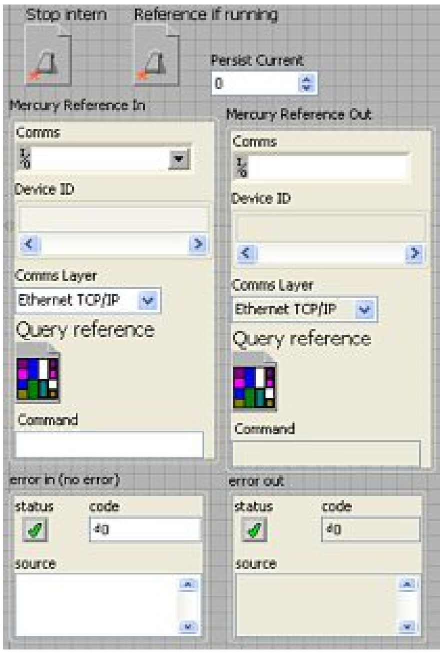

Persist Current 0

Comms Layer Ethernet TCP/IP

Comms Layer Ethernet TCP/IP

code 0

code 0

Figure C.20: GUI of the implemented set_terminal_current_to_pers_current program

C.3.3 Blockdiagramms

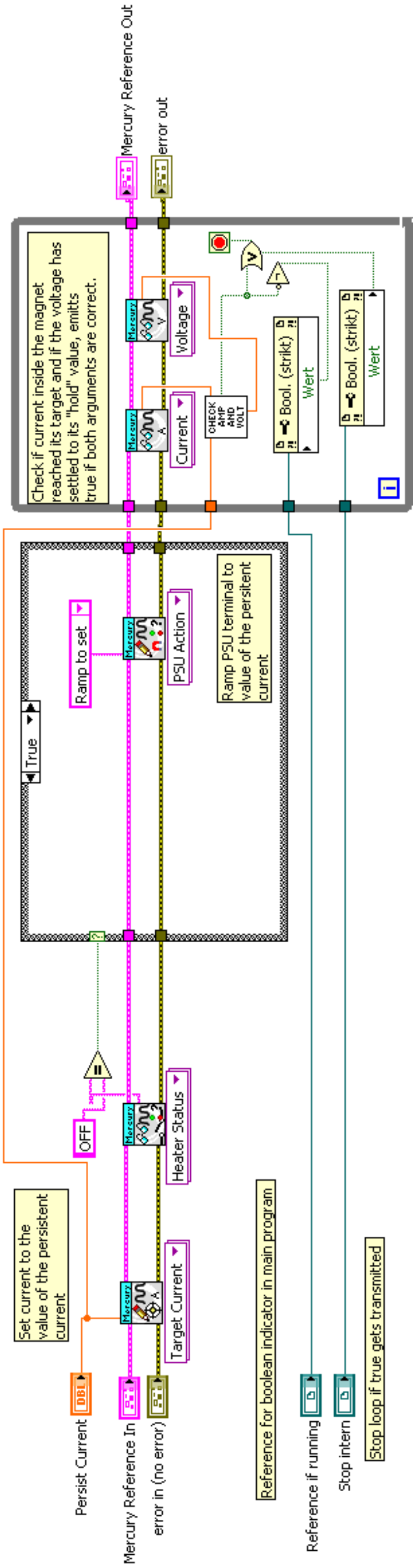

Figure C.21: Blockdiagramm of Set_terminal_current_to_pers_current, where the switch heater was already deactivated.

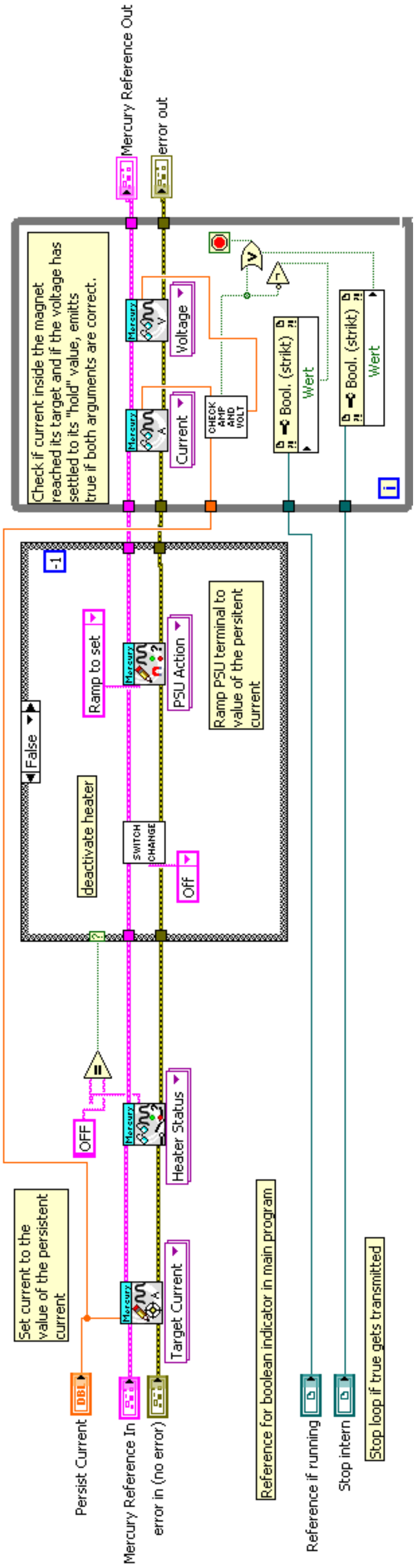

Figure C.22: Blockdiagramm of Set_terminal_current_to_pers_current, where the switch heater is still running at program start.

C.4 Create_Protokol

C.4.1 Description

The program "Create_Protokol" creates a protocol entry of a ramp. It either indicates a start of a ramp with the starting and ending persistent current of the magnet or the finishing of a ramp with the ending persitent current.

Five inputs are required to run this VI correctly. "Mercury Reference In" contains all important information about the PSU in use, "Error in" contains all previous occurred errors, "Start value" contains the current persistent current in Ampere, "End value" the new set current in Ampere and the Boolean switch "Start/Finish of ramp" that changes the entry according to a start or end of a ramp.
The main two inputs "Mercury Reference in" and "error in" split into two parallel executed lines. The upper line read the date and time of the PSU using the SubVI's "Date" and "Time" and combines them into one string separated by a white space, the lower line reads the "current to field"-factor out of the PSU using the SubVI's "Open Device" and "Curr to Fid".
The inputs "Start value" and "end value" divide up into two paths each. One set gets directly converted into a string, the other one gets divided by the current to field factor, to convert the Ampere values into Tesla values. Each string gets converted into a decimal number with four places behind the comma. These values get fed into the case structure including the string containing Date and time.
The SubVI "Open\Create\Replace File" get started in parallel to this, using the attributes "write only", "open or create" and the path "Datenpfad (Dialog verwenden)". This SubVI opens or creates the file located in "Datenpfad".
The standard value is "C:\MB\MercuryiPS\Protokol.txt"
This is followed by the SubVI "Set File Position", with the attribute "end", to add data to the end of the file.
The state of the case structure gets decided by the value of the Boolean input "Start/Finish of ramp". If it reports "false" (Figure C.25) a string of the form "Date Time: Finished at *end value*A (*converted end value*T) \n" gets created.
The string has the form "Date Time: Start ramping from *start value*A (*converted start value*T) to *end value*A (*converted end value*T) \n" if "true" is transmitted.(Figure C.24)
The chosen string gets writen into the protocol file using the SubVI "Write to Text File".
The program ends by closing the protocol file using the SubVI "Close File", and by handing all occurred errors into the output "error out" and the Mercury Reference container into "Mercury Reference out".

C.4.2 Frontpanel

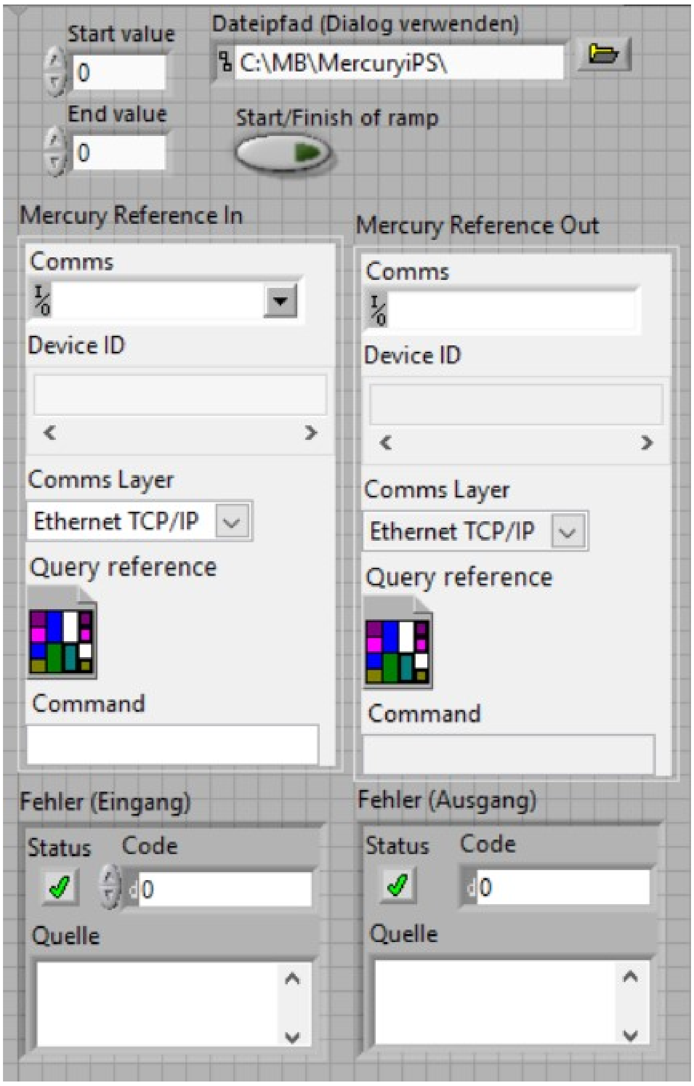

Start value 0

End value 0

Dateipfad (Dialog verwenden) C:\MB\MercuryiPS\

Start/Finish of ramp

Comms Layer Ethernet TCP/IP

Comms Layer Ethernet TCP/IP

Code 0

Code 0

Figure C.23: GUI of the implemented create_Protokol program.

C.4.3 Blockdiagramms

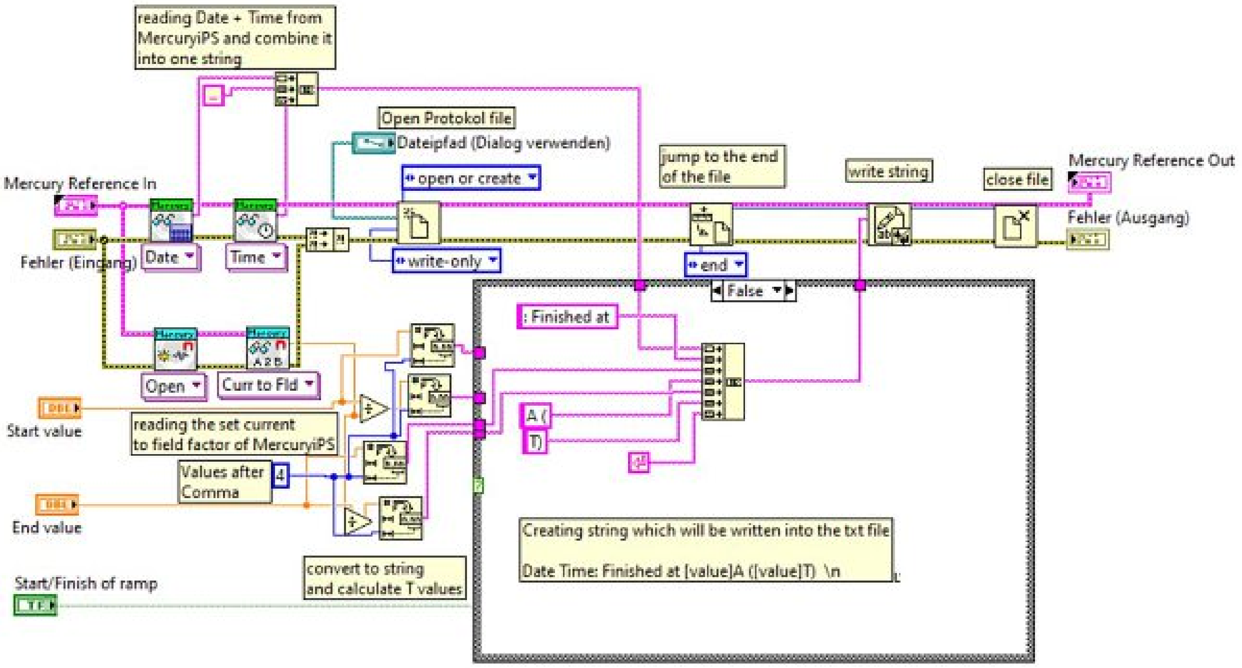

Figure C.24: Blockdiagramm of create_Protokol. The Boolean input was set to false, which represents a finished ramp.

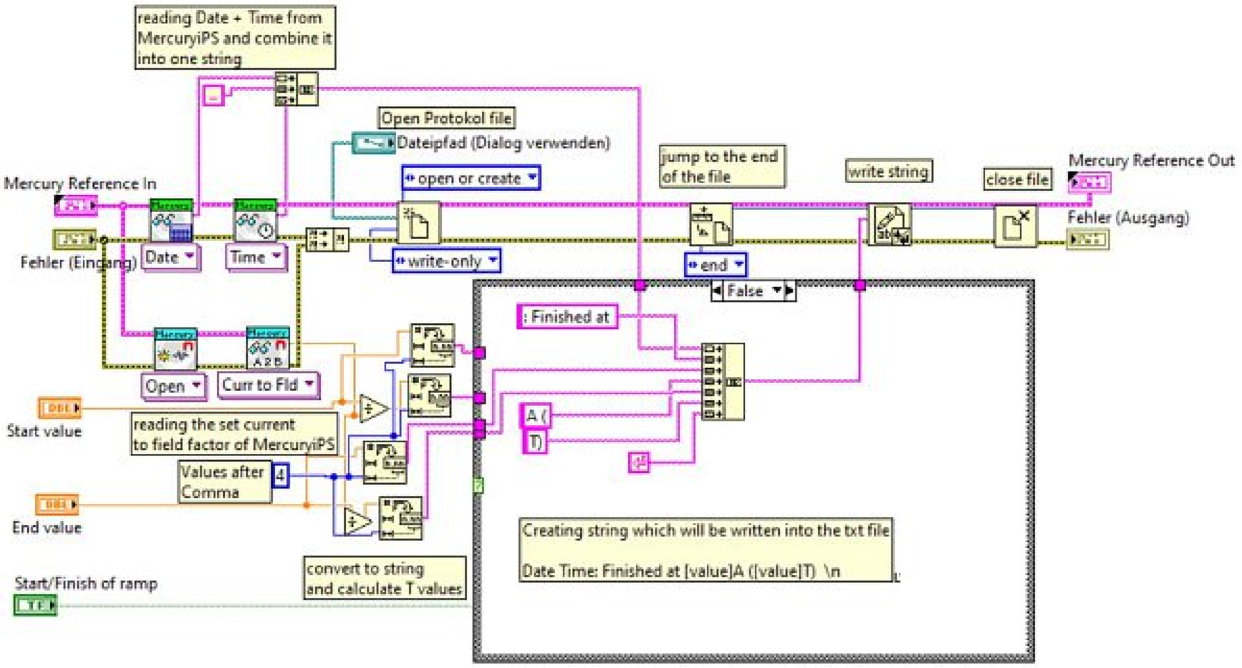

Figure C.25: Blockdiagramm of create_Protokol. The Boolean input was set to true, which represents a starting ramp.

C.5 Set_psu_to_hold

C.5.1 Description

The program "Set_psu_to_hold", changes the state of the MercuryiPS unit to "hold" and ensures that that switch has been completed before it ends.

Two inputs are required to run this VI correctly. "Mercury Reference In" contains all important information about the PSU in use and "Error in" contains all previous occurred errors. The SubVI "PSU Action" gets called using the constant "hold". This is followed by a while loop, which lasts until the SubVI "PSU Action" reports "hold". The program ends by handing all occurred errors into the output "error out" and the Mercury Reference container into "Mercury Reference out".

C.5.2 Frontpanel

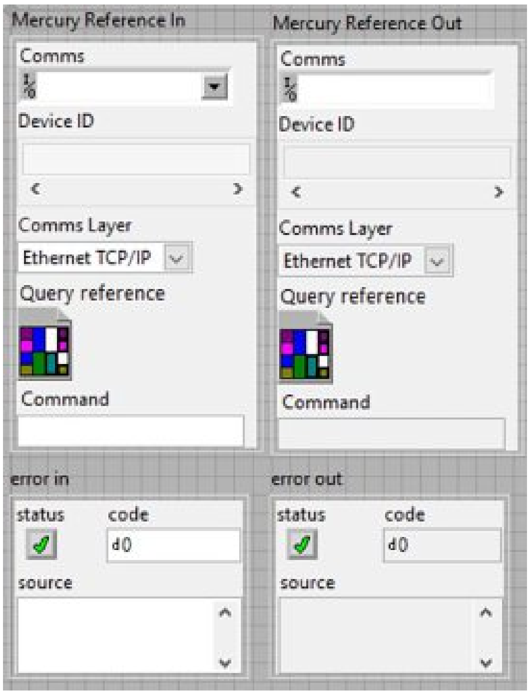

Mercury Reference In
Comms
Device ID
Comms Layer: Ethernet TCP/IP
Query reference
Command

Mercury Reference Out
Comms
Device ID
Comms Layer: Ethernet TCP/IP
Query reference
Command

error in
status ✓ code d0
source

error out
status ✓ code d0
source

Figure C.26: GUI of the implemented Set_psu_to_hold program.

C.5.3 Blockdiagramm

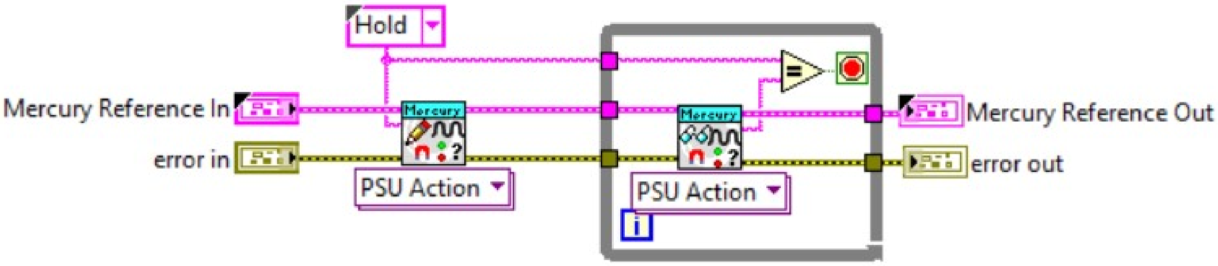

Figure C.27: Blockdiagramm of Set_psu_to_hold.

C.6 Set_psu_to_set

C.6.1 Description

The program "Set_psu_to_set", changes the state of the MercuryiPS unit to "Ramp to set" and ensures that that switch has been completed before it ends.

Two inputs are required to run this VI correctly. "Mercury Reference In" contains all important information about the PSU in use and "Error in" contains all previous occurred errors. The constant "Ramp to set" and the two input wires tunnel into a while loop. This loop uses the SubVI "PSU Action" in write and in read mode, to set the power supply in the state "Ramp to set" and to check if the mode has switched. The loop lasts until the read variant of "PSU Action" reports "Ramp to set". The program ends by handing all occurred errors into the output "error out" and the Mercury Reference container into "Mercury Reference out".

C.6.2 Frontpanel

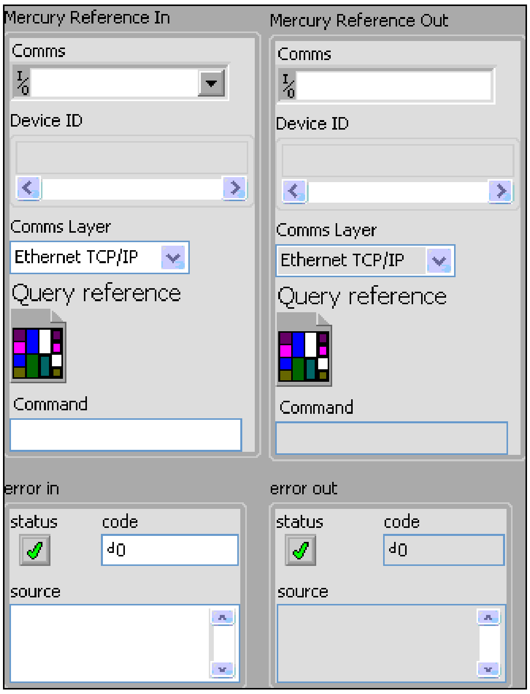

Figure C.28: GUI of the implemented Set_psu_to_set program.

C.6.3 Blockdiagramm

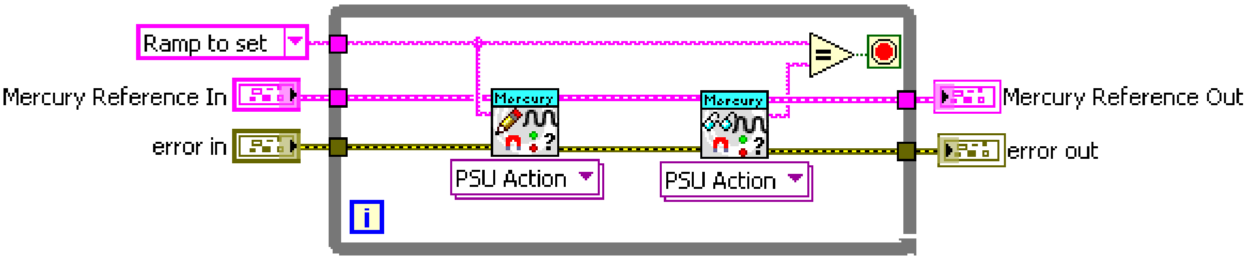

Figure C.29: Blockdiagramm of Set_psu_to_set.

C.7 Read_protocol

C.7.1 Description

The program "Read_protocol", reads the protocol file of the MercuryiPS unit and reports the last saved current inside the magnet.

Two input is required to run this VI correctly. "Datenpfad" contains the path of the protocol file and "Error in" contains all previous occurred errors. The standard value "C:\MB\MercuryiPS\Protokol.txt" will be used if no input is required at Datenpfad". The program opens the file provided by "Datenpfad", jump to the last line inside the file and read the six characters between the 19th and 13th character, counting from the end of the line. This string will be converted into a floating point number and written onto the variable "last measured pers current", which is one of the outputs of this VI. The program ends closing the file and handing all occurred errors into the output "error out".

C.7.2 Frontpanel

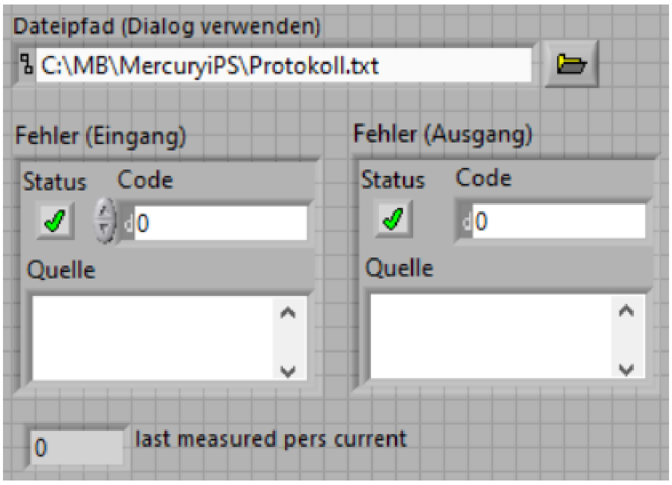

Dateipfad (Dialog verwenden)
C:\MB\MercuryiPS\Protokoll.txt

Fehler (Eingang)
Status ✓ Code 0
Quelle

Fehler (Ausgang)
Status ✓ Code 0
Quelle

0 last measured pers current

Figure C.30: GUI of the implemented Read_Protokol program.

C.7.3 Blockdiagramm

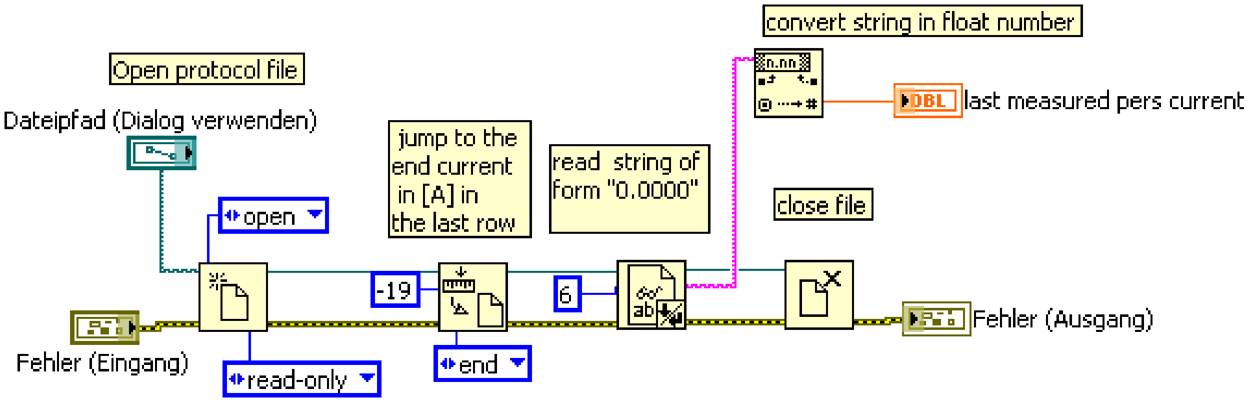

Figure C.31: Blockdiagramm of Read_Protokol.

C.8 check_saved_persis_current

C.8.1 Description

The program "check_saved_persis_current", uses the VI "Read_protocol" and a given input to compare the last saved values of the persitant current of the magnet on the computer and inside the MercuryiPS unit. A popup window appears if they differ by more than ±0.0005, asking the user to verify which of these values is correct.

Two input are required to run this VI correctly. "Persis current input" contains the value of the persistent current measured by the power supply unit and "Error in" contains all previous occurred errors. The VI "Read_Protocol" gets called and its output will be compared with the variable "Persis current input". The following case structure will execute the "false" case if they differ by more than ±0.0005. This case will create a popup window with two buttons, that explains the User that the two compared values differ and show these values. The user has the option to declare one of the two values as correct. This value will be written onto the output "Peris Current output", using a true/false structure. (figure C.33)
The value of "Persis current input" will be written directly onto "Persis current output", if the comparison of the two values report that they are within ±0.0005. (figure C.34)

C.8.2 Frontpanel

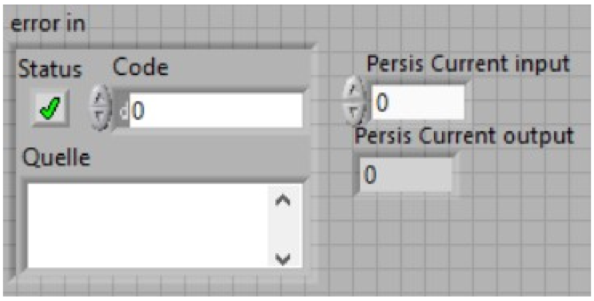

error in

Status ✓ Code 0

Quelle

Persis Current input 0

Persis Current output 0

Figure C.32: GUI of the implemented check_saved_persis_current program.

C.8.3 Blockdiagramms

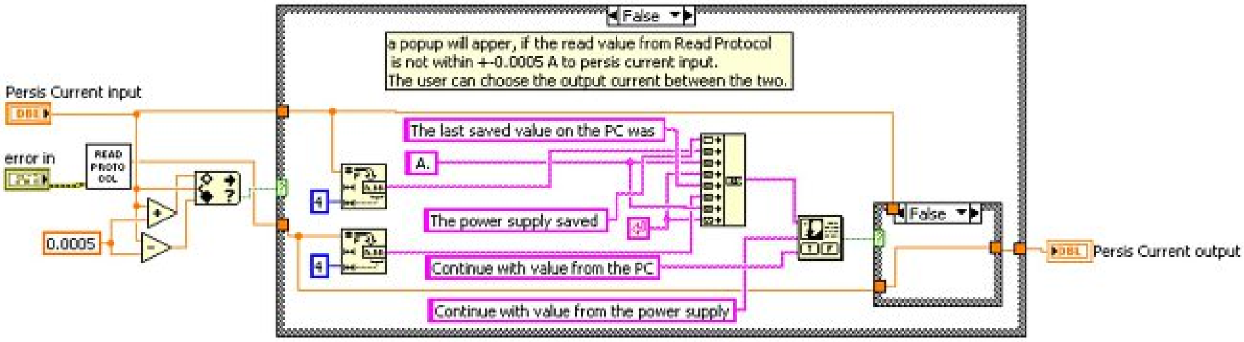

Figure C.33: Blockdiagramm of check_saved_persis_current. The saved persis. current and the current value at the psu are not within ±0.0005 A.

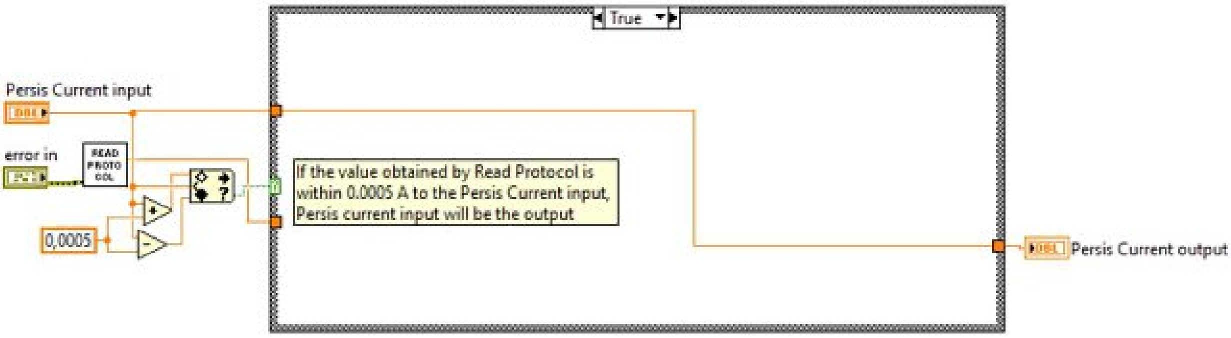

Figure C.34: Blockdiagramm of check_saved_persis_current. The saved persis. current and the current value at the psu are within ±0.0005 A.

C.9 Check_Amp_and_Volt

C.9.1 Description

The program "Check_Amp_and_Volt" determines if the MercuryiPS unit has already reached a set target current and if the voltage at the terminals is below a certain value.

Three inputs are required to run this VI correctly. "Target current" contains the target current of a ramp performed by the MercuryiPS power supply, "persis current" contains the momentary current of either the magnet, if the terminals and the magnet are ramping, or of the terminals, if only the terminals are ramping, and "Voltage" contains the voltage at the terminals. The program is divided into two parts. The first parts checks if the reported value of "persis current" is within the value of "target current" ±0.0005. A boolean "true" gets transmitted if the statement is correct.
The second part of the program checks if the reported value of "Voltage" is within a given range. This range is defined as either ±"target current" × 0.0095 or ±0.1, whichever is greater. A boolean "true" is reported if the value of "Voltage" is within this range.
The output of program is the result of a logical AND of the two boolean outputs of the two parts. This value is written into the boolean variable "Target reached".

C.9.2 Frontpanel

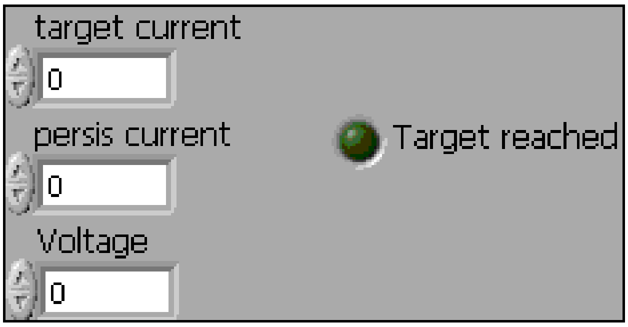
target current
0
persis current
0
Voltage
0
Target reached

Figure C.35: GUI of the implemented Check_Amp_and_Volt program.

C.9.3 Blockdiagramms

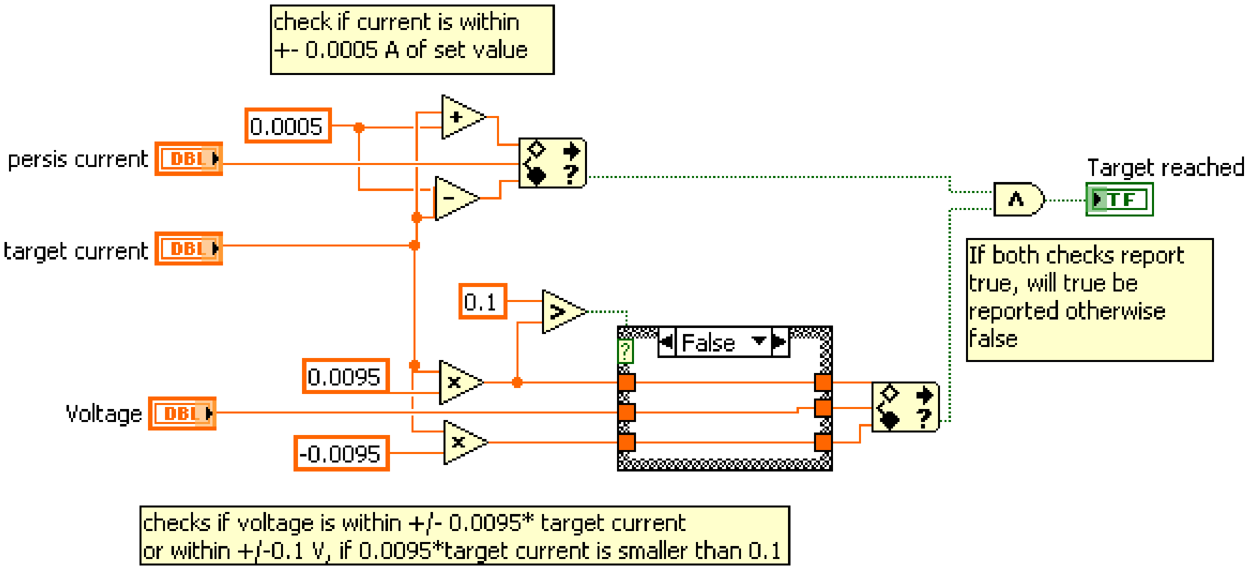

Figure C.36: Blockdiagramm of Check_Amp_and_Volt. Lead resistance × target current > 0.1 Volt.

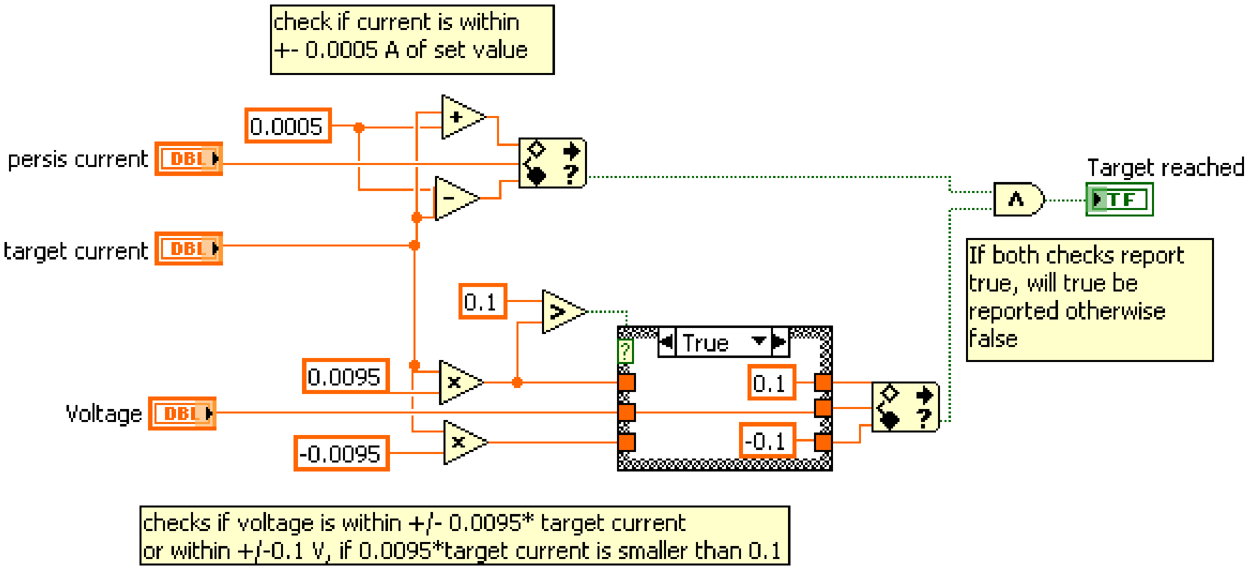

Figure C.37: Blockdiagramm of Check_Amp_and_Volt. Lead resistance × target current < 0.1 Volt.

C.10 Wissoft_Flanken_spiegeln

C.10.1 Description

The program "Wissoft_Flanken_spiegeln" reads a data file provided by Wissoft2003 and inverts the sequence of the data points from 1 to 512 and 513 to 1024.

Two input are required to run this VI correctly. "file path" contains the path to the file provided by Wissoft2003 and "Error in" contains all previous occurred errors. The file located in "file path" gets opened and read into the text array "text input". The file gets closed after this. Parallel to this will a new file be created, using the name of the old file but with the attachment "_Flanken_spiegel". The first line will be copied directly into the new file. A for loop writes the first 512 lines in inverted order into the new file. The last value in the array "text input" needs to be formatted before it can be written into the new file. The correct value will be written into the new file while the rest of the string inside will be stored for later use. A For loop writes the lines 513 to 1024 from the array into the new file backwards. Afterwards will the stored part of the string be attached to the 514th element of the array "text input" and written into the new file. The program ends by closing the new file and providing the path to the new file as output, as well as all occurred errors in the output "Error write".

C.10.2 Frontpanel

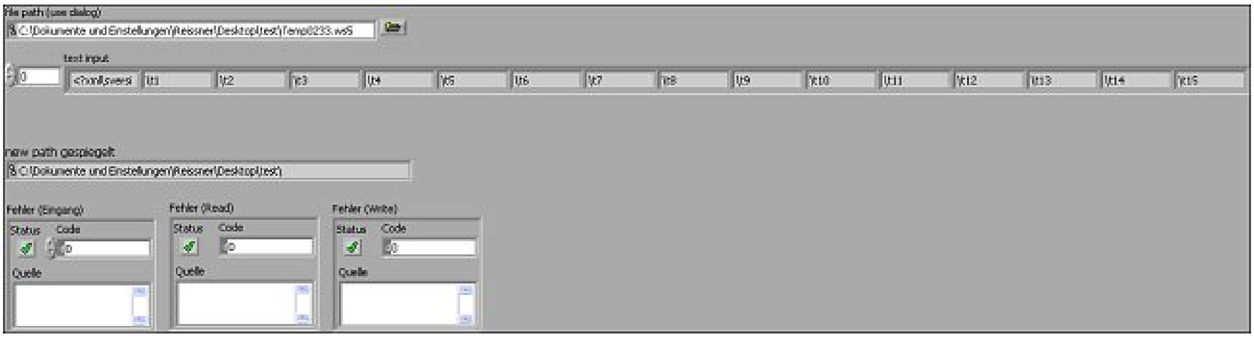

file path (use dialog): C:\Dokumente und Einstellungen\Reissner\Desktop\test\Temp0233.ws5

text input: 0 <?xml versi \t1 \t2 \t3 \t4 \t5 \t6 \t7 \t8 \t9 \t10 \t11 \t12 \t13 \t14 \t15

new path gespiegelt: C:\Dokumente und Einstellungen\Reissner\Desktop\test\

Fehler (Eingang): Status ✓ Code 0

Fehler (Read): Status ✓ Code 0

Fehler (Write): Status ✓ Code 0

Figure C.38: GUI of the implemented Wissoft_Flanken_spiegeln program.

C.10.3 Blockdiagramm

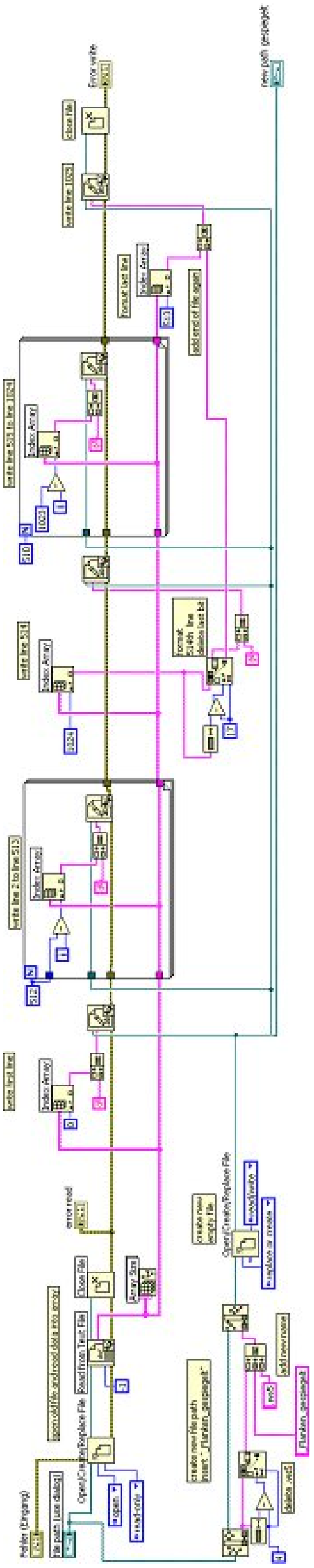

Figure C.39: Blockdiagramm of Wissoft_Flanken_spiegeln.

References

[1] P. Rogl, V. Romaka, J. Bursik, H. Michor, M. Reissner, G. Giester, and V. Homolova, "Structure and properties of a novel boride (V0.92Fe0.08)2FeB2 with partially ordered U3Si2-type," *Journal of Alloys and Compounds*, vol. 746, pp. 638–647, may 2018.

[2] L. May, ed., *An introduction to Mössbauer Spectroscopy*. Washington: Plenum Press New York London, 1971.

[3] P. Gütlich, R. Link, and A. Trautwein, *Mössbauer Spectroscopy an Transition Metal Cemistry*. Berlin, Heidelberg, New York: Springer Berlin Heidelberg, 1978.

[4] V. Weisskopf and E. Wigner, "Über die natürliche Linienbreite in der Strahlung des harmonischen Oszillators," *Zeitschrift für Physik*, vol. 65, pp. 18–29, nov 1930.

[5] M. Bartelmann, B. Feuerbacher, T. Krüger, D. Lüst, A. Rebhan, A. Wipf, M. Bartelmann, B. Feuerbacher, T. Krüger, D. Lüst, A. Rebhan, and A. Wipf, "Eindimensionale Quantensysteme," in *Theoretische Physik*, p. 865, Springer Berlin Heidelberg, 2014.

[6] H. Wegener, *Der Mössbauereffekt und seine Anwendung in Physik und Chemie*. Mannheim: Bibliographisches Institut AG, 1965.

[7] D. A. Shirley, "Application and interpretation of isomer shifts," *Reviews of Modern Physics*, vol. 36, no. 1, pp. 339–351, 1964.

[8] A. Abragam, *The principles of Nuclear Magnetism*. Clarendon: London - Oxford: Oxford University Press, 1961.

[9] T. Viegers, *Thesis*. PhD thesis, Nijmegen, Netherlands, 1976.

[10] A. Gedikli, H. Winkler, and E. Gerdau, "Goldanskii Karyagin effect at Mössbauer E2 transtions," *Zeitschrift für Physik*, vol. 267, p. 61, 1974.

[11] R. L. Mössbauer, "Kernresonanzfluoreszenz von Gammastrahlung in Ir191," *Zeitschrift für Physik*, vol. 151, pp. 124–143, apr 1958.

[12] S. Margulies and J. R. Ehrman, "Transmission and line broadening of resonance radiation incident on a resonance absorber," *Nuclear Instruments and Methods*, vol. 12, no. C, pp. 131–137, 1961.

[13] F. J. Lynch, R. E. Holland, and M. Hamermesh, "Time dependence of resonantly filtered gamma rays from Fe57," *Physical Review*, vol. 120, no. 2, pp. 513–520, 1960.

[14] E. Parthè, L. Gelato, B. Chabot, M. Penzo, K. Censual, and G. R, "TYPIX - Standardized Data and Crystal Chemical Characterization of Inorganic structure Types 1994," vol. 20, p. 138, Berlin-Heidelberg: Springer-Verlag, 1987.

[15] M. Mörth, *Temperaturabhängige Mössbauer Spektroskopie*. Bachelor thesis, TU Wien, 2017.

[16] Oxford Instruments, "OPERATING MANUAL - 13.6/15T Cryomagnetic system for Mössbauerstudies," 1985.

[17] Oxford Instruments, “SUPERCONDUCTING MAGNET OPERATING MANUAL - Magnet Type: HIghfield Solenoid C13,6/15.45.13x,” 1985.

[18] Dr. Zoltán Klencsár, “MossWinn 4.0i Manual,” 2019.

[19] R. W. Grant, “Mössbauer spectroscopy in magnetism characterization of magnetically-ordered compounds,” in *Mössbauer Spectroscopy* (U. Gonser, ed.), p. 97, Berlin, Heidelberg: Springer Berlin Heidelberg, 1975.

[20] S. Mørup and E. Both, “Interpretation of Mössbauer spectra with broadened lines,” *Nuclear Instruments and Methods*, vol. 124, pp. 445–448, mar 1975.

[21] R. Waldi and R. Waldi, “Messung und Stichprobe,” in *Statistische Datenanalyse*, p. 82, Berlin, Heidelberg: Springer Berlin Heidelberg, 2015.

[22] M. Reissner, “Mössbauer Spectroscopy in External Magnetic Fields,” in *Modern Mössbauer Spectroscopy* (Y. Yoshida and G. Langouche, eds.), pp. 381–444, Singapore: Springer, Singapore, 2021.

[23] E. Petrovský and A. Kapička, “On determination of the Curie point from thermomagnetic curves,” *Journal of Geophysical Research: Solid Earth*, vol. 111, dec 2006.

[24] Y. Yoshida and G. Langouche, eds., *Modern Mössbauer Spectroscopy*, vol. 137 of *Topics in Applied Physics*. Singapore: Springer Singapore, 2021.

[25] Oxford Instruments NanoScience, “Mercury iPS Power Supply for Superconducting Magnets - Operators Manual,” 2015.